

DISCOVERY OF ALLOSTERIC MODULATORS OF THE A₃ ADENOSINE
RECEPTOR FOR TREATMENT OF CHRONIC DISEASES

by

Lucas Brett Fallot

Dissertation submitted to the Faculty of the
Molecular and Cell Biology Graduate Program
Uniformed Services University of the Health Sciences
In partial fulfillment of the requirements for the degree of
Doctor of Philosophy 2022

Distribution Statement

Distribution A: Public Release.

The views presented here are those of the author and are not to be construed as official or reflecting the views of the Uniformed Services University of the Health Sciences, the Department of Defense or the U.S. Government.



UNIFORMED SERVICES UNIVERSITY OF THE HEALTH SCIENCES

SCHOOL OF MEDICINE GRADUATE PROGRAMS

Graduate Education Office (A 1045), 4301 Jones Bridge Road, Bethesda, MD 20814



**APPROVAL OF THE DOCTORAL DISSERTATION IN THE MOLECULAR AND
CELL BIOLOGY GRADUATE PROGRAM**

Title of Dissertation: "DISCOVERY OF ALLOSTERIC MODULATORS OF THE A3 ADENOSINE
RECEPTOR FOR TREATMENT OF CHRONIC DISEASES"

Name of Candidate: Lucas Fallot
Doctor of Philosophy Degree

DISSERTATION AND ABSTRACT APPROVED:

[Redacted Signature]

DATE:

3/23/2022

Dr. Kathleen Pratt
DEPARTMENT OF MEDICINE
Committee Chair

[Redacted Signature]

3/23/2022

Dr. Kenneth A. Jacobson
LBC/NIH/NIDDK
Dissertation Advisor

PAZGIER.MARZENA Digitally signed by
.E.1549058660 PAZGIER.MARZENA.E.1549058660
Date: 2022.03.23 13:48:21 -04'00'

3/23/2022

Dr. Marzena Pazgier
DEPARTMENT OF MEDICINE
Committee Member

[Redacted Signature]

3/23/2022

Dr. David A. Grahame
DEPARTMENT OF BIOCHEMISTRY & MOLECULAR BIOLOGY
Committee Member

[Redacted Signature]

3/23/2022

Dr. Brian Cox
DEPARTMENT OF PHARMACOLOGY & MOLECULAR THERAPEUTICS
Committee Member

[Redacted Signature]

3-11-22

Dr. Jurgen Wess
LBC/NIH/NIDDK
Committee Member

ACKNOWLEDGMENTS

First and foremost, I must thank Dr. Kenneth Jacobson for not hanging up the phone when I cold-called him in December 2016, inquiring about a possible research opportunity supporting my Ph.D. Thank you for not only accepting me but waiting two and a half years for my arrival. I am honored to have worked on such an incredible project. Thank you for sharing your wealth of knowledge and life's work with me. What I thought would solely entail synthesizing a library of derivatives evolved into studying a sophisticated and well-orchestrated application of a medicinal chemistry team-of-teams approach to drug discovery.

I am beyond grateful for the collaborative efforts of Dr. John Auchampach and my fellow doctorate candidate, Courtney Fisher. Your work greatly enhanced my understanding of the preclinical testing of drug libraries. I could not have done this research without your invaluable contributions.

Thank you to my fellow scientists of the Molecular Recognition Section of the National Institute of Diabetes and Digestive and Kidney Diseases (NIDDK)—most notably Drs. Rama Suresh, Young-Hwan Jung, Zhiwei Wen, Dilip Tosh, Zhanguo Gao, Kiran Toti, and Veronica Salmaso. I greatly appreciate your willingness to teach and help me throughout my time in the laboratory. The size of your collective brain trust is incredible, but the size of each of your hearts is volumes larger. Thank you, Drs. John Lloyd and Robert O'Connor of NIDDK for all the mass spectra and NMR spectra analyses, respectively. Thank you to Dr. Steven Dudas and Beth Kaufman for keeping me

well supplied with the materials to get the job done—you would make great Army logisticians.

I appreciate my fellow Uniformed Services University (USU) cohort—challenges are better experienced with others than alone. Thank you for being so supportive during our shared time together. Thank you to the staff and faculty of USU—especially my committee—for helping me better understand molecular and cell biology. I couldn't have asked for a better academic program to complement my medicinal chemistry research efforts.

Lastly, thank you to the staff and faculty of the Chemistry and Life Science Department of the United States Military Academy. It is a great honor to obtain my Ph.D. and continue teaching and mentoring our future Army leaders.

DEDICATION

I want to dedicate this work to my wife and kids—Laura, Autumn, and Preston. Thank you for your continued support of my academic and military careers. None of what I do would be possible without you. I love you.

COPYRIGHT STATEMENT

The author hereby certifies that the use of any copyrighted material in the dissertation manuscript entitled: Discovery of Allosteric Modulators of the A₃ Adenosine Receptor for Treatment of Chronic Diseases is appropriately acknowledged and, beyond brief excerpts, is with the permission of the copyright owner.

[Signature]

A large black rectangular box redacting the signature of the author.

Lucas Brett Fallot

Date: 02/28/2022

DISCLAIMER

The views presented here are those of the author and are not to be construed as official or reflecting the views of the Uniformed Services University of Health Sciences, the Department of Defense, or the U.S. Government. References to non-Federal entities or products do not constitute or imply a Department of Defense or Uniformed Services University of the Health Sciences endorsement. Neither I nor my family members have a financial interest in any commercial product, service, or organization providing financial support for this research. The study was undertaken under full accreditation by the Association for Assessment and Accreditation of Laboratory Animal Care (AAALAC) International and approved by the Institutional Animal Ethics Committee (IAEC), JRF.

ABSTRACT

Discovery of Allosteric Modulators of the A₃ Adenosine Receptor for the Treatment of Chronic Diseases

Lucas Brett Fallot, Doctor of Philosophy, 2022

Thesis directed by: Kenneth A. Jacobson, Ph.D.; Adjunct Professor, Department of Anatomy, Physiology, and Genetics

Positive allosteric modulators (PAMs) of G protein-coupled receptors (GPCRs) bind to topographically distinct sites from orthosteric agonists, causing receptor conformational changes that increase agonist affinity, potency, and/or efficacy. *1H*-imidazo[4,5-*c*]quinolin-4-amine derivatives were identified as A₃ adenosine receptor (A₃AR) PAMs. Here, we introduce a 6-step synthesis applied to four groups of *1H*-imidazo[4,5-*c*]quinolin-4-amine derivatives to explore structure-activity relationships and pharmacokinetics. We show the ability to fine-tune both 2-cycloalkyl and open ring derivatives as competitive antagonists and/or allosteric modulators. These activities were separated pharmacologically using chimeric mouse/human A₃ARs to show the PAM binding region likely to occur at a hydrophobic site on the A₃AR cytosolic interface distinct from the orthosteric site. 2-Cyclononyl-*N*-(3,4-dichlorophenyl) **20** (1 μM) derivative increased the A₃AR agonist potency two-fold in [³⁵S]GTPγS binding, as well as E_{max} (242%). 2-(Heptan-4-yl)-*N*-(3,4-dichlorophenyl) **2**, 2-(hept-4-en-1-yl)-*N*-(3,4-

dichlorophenyl) **10**, and 2-(heptan-4-yl)-*N*-(4-iodophenyl) **31** (1 μ M) derivatives were highly efficacious (E_{\max} = 216%, 241% and, 223%, respectively). Although hydrophobic and having low permeability and high plasma protein binding, derivative **10** was orally bioavailable in the rat. The derivatives tested lacked high-affinity off-target binding to forty-five other membrane proteins. Furthermore, we demonstrated a route for radioiodination at the *para*-position of a 4-phenylamino substituent to prepare a radioligand for allosteric site binding. Herein, we advanced the allosteric approach to developing drugs for A₃AR activation that are potentially event- and site-specific in action.

TABLE OF CONTENTS

LIST OF TABLES	xiii
LIST OF FIGURES	xiv
CHAPTER 1: Introduction	1
GPCRs as Therapeutic Drug Targets	1
Therapeutic Possibilities of Targeting the A ₃ AR.....	1
Types of Allosteric Modulators	2
Positive Allosteric Modulators Over Orthosteric Ligands.....	2
Research Objectives, Central Hypothesis, and Specific Aims	4
Specific Aim 1	4
Specific Aim 2	5
Specific Aim 3	5
Scope of the Study	6
CHAPTER 2: Literature Review	7
Molecular Characterization of the A ₃ AR.....	7
Intracellular Signaling of the A ₃ AR.....	8
Inhibition of Cyclic AMP and the Wnt Signaling Pathway.....	8
Phospholipase C Pathway	9
RhoA and Phospholipase D Pathway	9
ERK/p38/JNK MAPK Signaling Pathway	10
PI3K β /AKT Signaling Pathway.....	10
A ₃ AR Agonists in Clinical Trials.....	11
A ₃ AR Antagonists in Clinical Trials.....	12
Four Heterocyclic A ₃ AR PAM Classes	12
3-(2-Pyridinyl)isoquinoline A ₃ AR PAMs.....	13
Amiloride A ₃ AR PAMs	16
1 <i>H</i> -Imidazo[4,5- <i>c</i>]quinolin-4-amine A ₃ AR PAMs.....	18
DU124183.....	18
LUF6000	22
<i>In Vivo</i> Results of LUF6000.....	26
2,4-Disubstituted Quinoline A ₃ AR PAMs.....	27
<i>In Vivo</i> Results of LUF6096.....	28
Species Differences of Ligand Binding to the A ₃ AR	28
Known Locations of GPCR Allosteric Binding Sites.....	32
9-Step Synthesis Protocol of 1 <i>H</i> -Imidazo[4,5- <i>c</i>]quinolin-4-amine Derivatives.....	36
CHAPTER 3: Methodology.....	39
Ligand Structure-Guided Design Approach	39
Design Rationale for Groups of Derivatives.....	41
Hydrophobic Alkyl and Cycloalkyl Derivatives.....	42

Bridged Derivatives	43
Derivatives with Hydrophilic Substitutions.....	45
4-Substituted-phenylamino Derivatives.....	45
Experimental Procedures	46
General.....	46
Synthesis of Commercially Unavailable Carboxylic Acids.....	49
Synthesis of 5,5,5-Trifluoro-2-(3,3,3-trifluoropropyl)pentanoic Acid.....	49
Synthesis of Cyclononane and Cyclodecane Carboxylic Acids.....	50
Synthesis of ((1R,2R,4R)- & (1S,2S,4S)-Bicyclo[2.2.2]oct-5-ene Carboxylic Acid	50
6-Step Synthesis Protocol for 1 <i>H</i> -Imidazo-[4,5- <i>c</i>]quinolin-4-amine Derivatives	51
Preparation of 3-Nitroquinoline-2,4-diol – Step 1	51
Preparation of 2,4-Dichloro-3-nitroquinoline – Step 2	52
Preparation of 2-Chloro-3-nitroquinolin-4-amine – Step 3.....	52
Preparation of 2-Chloroquinoline-3,4-diamine – Step 4.....	52
General Procedure A. for 2-Substituted-4-chloro-1 <i>H</i> -imidazo[4,5- <i>c</i>]quinoline – Step 5.....	53
General Procedure B. for 2-Substituted-4-chloro-1 <i>H</i> -imidazo[4,5- <i>c</i>]quinoline – Step 5.....	53
General Procedure C. for 2-Substituted- <i>N</i> -(3,4-dichlorophenyl)-1 <i>H</i> -imidazo[4,5- <i>c</i>]quinolin-4-amine – Step 6	54
General Procedure D. for 2-Substituted- <i>N</i> -(3,4-dichlorophenyl)-1 <i>H</i> -imidazo[4,5- <i>c</i>]quinolin-4-amine – Step 6	54
General Procedure E. for 2-Substituted- <i>N</i> -(phenyl-substituted)-1 <i>H</i> -imidazo[4,5- <i>c</i>]quinolin-4-amines – Step 6.....	55
Synthesis Protocols for Derivatives from Step-6 1 <i>H</i> -Imidazo[4,5- <i>c</i>]quinolin-4-amine Derivatives	56
Procedure for the Synthesis of 2-((1R,4r,7S)-Bicyclo[5.1.0]octan-4-yl)- <i>N</i> -(3,4-dichlorophenyl)-1 <i>H</i> -imidazo[4,5- <i>c</i>]quinolin-4-amine – Compound 20	56
Procedure for the Synthesis of 2-((1R,4s,7S)- & 2-(1R,4r,7S)-8-Oxabicyclo[5.1.0]octan-4-yl)- <i>N</i> -(3,4-dichlorophenyl)-1 <i>H</i> -imidazo[4,5- <i>c</i>]quinolin-4-amine – Compounds 22 and 23	56
Procedure for the Synthesis of (R)- & (S)-4-(4-((3,4-Dichlorophenyl)amino)-1 <i>H</i> -imidazo[4,5- <i>c</i>]quinolin-2-yl)cycloheptan-1-one – Compound 24	57
Procedure for the Synthesis of (1R,4S)-, (1S,4R)-, & (1R,4R)-, (1S,4S)-4-(4-((3,4-Dichlorophenyl)amino)-1 <i>H</i> -imidazo[4,5- <i>c</i>]quinolin-2-yl)cycloheptan-1-ol – Compounds 25 and 26	58
Procedure for the Synthesis of Methyl (E)- & (Z)-3-(4-((2-cyclohexyl-1 <i>H</i> -imidazo[4,5- <i>c</i>]quinolin-4-yl)amino)phenyl)acrylate – Compound 29	58
Procedure for the Synthesis of 2-Cyclohexyl- <i>N</i> -(4-((5-Chlorothiophen-2-yl)ethynyl)phenyl)-1-1 <i>H</i> -imidazo[4,5- <i>c</i>]quinolin-4-amine – Compound 30	59
Procedure for the Synthesis of 2-(Heptan-4-yl)- <i>N</i> -(4-(trialkylstannyl)phenyl)-1 <i>H</i> -imidazo[4,5- <i>c</i>]quinolin-4-amine – Compounds 32 and 33	59
Effects of Modulators on Agonist Binding to hA ₃ AR Studies	60
Studies of Receptor Activation using [³⁵ S]GTPγS Binding	60
Chimeric Receptor Studies	60

Off-Target Binding Studies.....	60
Pharmacokinetic Studies.....	61
CHAPTER 4: Results	62
Synthesis of Derivatives	62
6-Step Synthesis Protocol for 1 <i>H</i> -Imidazo[4,5- <i>c</i>]quinolin-4-amine Derivatives	62
Kinetic Binding Study Results.....	75
Single-point Dissociation Assay Results	75
Single-point Equilibrium Binding Assay Results.....	77
Results of Receptor Activation Measured by [³⁵ S]GTPγS Binding	79
Chimeric Receptor Study Results	84
Chimeric A ₃ AR Radioligand Binding Studies.....	84
Activation of Chimeric Receptors Studied with [³⁵ S]GTPγS Binding	85
Off-Target Binding Results.....	87
Pharmacokinetic Study Results.....	89
<i>In Vitro</i> Pharmacokinetic Study Results.....	89
<i>In Vivo</i> Pharmacokinetic Study Results.....	91
CHAPTER 5: Discussion.....	94
Synthesis and Purification of Derivatives.....	94
SAR of 1 <i>H</i> -Imidazo[4,5- <i>c</i>]quinolin-4-amine Derivatives	96
SAR Evaluation of 2-Alkyl and 2-Cycloalkyl Substituted 1 <i>H</i> -Imidazo[4,5- <i>c</i>]quinolin-4-amine Derivative Library.....	97
Competitive Antagonism vs. Allosteric Modulation	98
Fine Tuning of Modulator Effects	100
SAR Evaluation of 2-Bicyclo Substituted 1 <i>H</i> -Imidazo[4,5- <i>c</i>]quinolin-4-amine Derivative Library.....	100
SAR Evaluation of a Hydrophilic Substituted 1 <i>H</i> -Imidazo[4,5- <i>c</i>]quinolin-4-amine Derivative Library.....	102
SAR Evaluation of <i>para</i> -Phenylamino Substituted 1 <i>H</i> -Imidazo[4,5- <i>c</i>]quinolin-4-amine Derivative Library.....	105
Evaluation of Chimeric Receptor Results.....	106
Evaluation of ADMET Baseline.....	109
Other PAM Formulation and Administration Methods.....	110
Other Design Decisions Based on ADMET Parameters of Compound 10	112
Potential Allosteric Binding Site Radioligand.....	116
Possible Animal Disease Models for Follow-on Preclinical Studies.....	118
CHAPTER 6: Conclusion.....	121
Summary of A ₃ AR PAM Investigation	121
Appendix A: Compound NMR Spectra.....	123
Appendix B: Compound Mass Spectra and Elemental Analysis.....	164
Appendix C: Compound HPLC Purity	194

Appendix D: Kinetic Binding Assay Methods	202
HEK 293 Cell Line Maintenance.....	202
Membrane Preparation.....	202
Single-Point Dissociation Binding Assays	203
Single-Point Equilibrium Binding Assays	203
Appendix E: GTP γ S Binding Method for Measuring Receptor Activation	204
[³⁵ S]GTP γ S Binding Assays	204
Appendix F: Chimeric Receptor Methods	205
Creation of Stable HEK 293 Cell Lines Expressing WT and Chimeric A ₃ ARs.....	205
Chimeric Receptor Sequences	205
Chimera Receptor [³⁵ S]GTP γ S Binding Assays	206
Appendix G: ADMET Methods.....	207
<i>In Vivo</i> Experiments to Measure Drug Metabolism and Pharmacokinetic Properties	207
<i>In Vitro</i> Assays to Measure Drug Metabolism and Pharmacokinetic Properties.....	208
Plasma Stability	208
HepG2 Cytotoxicity	209
Human Ether-a-go-go Related Gene.....	209
CYP Inhibition	210
Microsomal Stability Assays	210
Caco-2 Permeability Assay.....	211
pION Solubility.....	211
Plasma Protein Binding.....	211
Stability in Gastrointestinal Tract.....	212
Appendix H: Results Chapter Tables.....	213
REFERENCES	218

LIST OF TABLES

Table 1. Hydrophobic alkyl and cycloalkyl substitutions at the 2 position of the 1 <i>H</i> -imidazo[4,5- <i>c</i>]quinolin-4-amine scaffold to investigate fine-tuning of the allosteric enhancement by PAM derivatives	68
Table 2. Bridged bicyclic substitutions to investigate the effects of rigid ring systems on the allosteric enhancement of the PAM derivatives	70
Table 3. Introduction of oxygen-containing functional groups to compound 10 to investigate effects of hydrophilic moieties on the allosteric enhancement of PAM derivatives	72
Table 4. Introduction of various functionalities in the 4 position of the phenylamino group to investigate allosteric tolerance/enhancement of PAM derivatives.....	74
Table 5. Precursor 4 position substituted phenylamino 1 <i>H</i> -imidazo[4,5- <i>c</i>]quinolin-4-amine derivatives for the preparation of a ¹²⁵ I radioligand.....	75
Table 6. Off-target analyses of select PAM derivatives with forty-five other receptors, transporters, and channels.....	88
Table 7. <i>In vitro</i> pharmacokinetic parameters of compound 10	90
Table 8. Caco-2 permeability results of compound 10	91
Table 9. <i>In vivo</i> pharmacokinetic parameters of compound 10 in Wistar rats	92
Table 10. <i>In vivo</i> experimental outline using Wistar rats	207
Table 11. Effect of PAM derivatives on the dissociation of [¹²⁵ I]I-AB-MECA using hA ₃ ARs	213
Table 12. Effect of PAM derivatives on equilibrium binding of [¹²⁵ I]I-AB-MECA at the hA ₃ AR.....	214
Table 13. Effect of alkyl and cycloalkyl PAM derivatives on [³⁵ S]GTPγS binding induced by Cl-IB-MECA using WT hA ₃ ARs	215
Table 14. Effect of bridged PAM derivatives on [³⁵ S]GTPγS binding induced by Cl-IB-MECA using WT hA ₃ ARs.....	215
Table 15. Effect of PAM derivatives with hydrophilic substitutions on [³⁵ S]GTPγS binding induced by Cl-IB-MECA using WT hA ₃ ARs	215
Table 16. Effect of <i>para</i> -phenylamino substituted PAM derivatives on [³⁵ S]GTPγS binding induced by Cl-IB-MECA using WT hA ₃ ARs	216
Table 17. Effect of compound 31 on [³⁵ S]GTPγS binding induced by Cl-IB-MECA using WT hA ₃ ARs.....	216
Table 18. Effect of compound 8 on dissociation rate of [¹²⁵ I]I-AB-MECA using WT and chimeric A ₃ ARs	216
Table 19. Effect of compound 5 on [³⁵ S]GTPγS binding induced by Cl-IB-MECA using WT and chimeric A ₃ ARs	216
Table 20. Effect of compound 8 on [³⁵ S]GTPγS binding induced by Cl-IB-MECA using WT and chimeric A ₃ ARs	217

LIST OF FIGURES

Figure 1. Human A ₃ adenosine receptor	7
Figure 2. A ₃ AR-mediated signaling pathways.....	8
Figure 3. A ₃ AR agonists IB-MECA and Cl-IB-MECA.....	11
Figure 4. A ₃ AR antagonist FM101	12
Figure 5. Four Heterocyclic A ₃ AR PAM Classes.....	13
Figure 6. Effects of VUF5455 on the dissociation of [¹²⁵ I]-AB-MECA from hA ₃ AR expressed in HEK 293 cells	14
Figure 7. Effect of VUF5455 on cAMP production in HEK 293 cells overexpressing hA ₃ AR in the presence of the competitive antagonist MRS1220.....	15
Figure 8. MRS1220 is a competitive hA ₃ AR antagonist used to block allosteric modulator binding at the orthosteric site.....	15
Figure 9. VUF5455 dissociation experiment shows it does not slow down radioligand dissociation for rat A ₁ AR, providing an example of A ₃ AR selectivity over other AR subtypes.....	16
Figure 10. Effect of HMA on forskolin-stimulated cAMP production by Cl-IB-MECA in CHO cells expressing the hA ₃ AR.....	17
Figure 11. Effects of DU124183 on the dissociation of [¹²⁵ I]-AB-MECA from hA ₃ AR expressed in CHO cells.....	19
Figure 12. Concentration-response curve for slowing the dissociation of [¹²⁵ I]-AB-MECA by DU124183.....	20
Figure 13. Concentration-response curve showing DU124183 competition for [¹²⁵ I]-AB- MECA binding to membranes from CHO cells expressing hA ₃ AR.....	21
Figure 14. Effect of DU124183 on Cl-IB-MECA inhibition of forskolin-stimulated cAMP production in CHO cells expressing hA ₃ AR.....	21
Figure 15. Effects of 1 <i>H</i> -imidazo[4,5- <i>c</i>]quinolin-4-amine PAMs with increasing cycloalkyl ring size on the dissociation of [¹²⁵ I]-AB-MECA from hA ₃ AR	23
Figure 16. SAR data shows fine-tuning of A ₃ AR allosteric effects with different 2 position substitutions on the 1 <i>H</i> -imidazo[4,5- <i>c</i>]quinolin-4-amine scaffold.....	24
Figure 17. Comparison between DU124183 and LUF6000 on % inhibition of cAMP production by CHO cells overexpressing A ₃ AR	25
Figure 18. Effect of LUF6000 or LUF6096 on Cl-IB-MECA-induced [³⁵ S]GTPγS binding in assays with HEK 293 cell membranes expressing human, dog, rabbit, or mouse A ₃ AR	29
Figure 19. Effects of LUF6000 and LUF6096 on the dissociation of [¹²⁵ I]-AB-MECA binding to HEK 293 cell membranes expressing human, dog, rabbit, and mouse A ₃ ARs	30
Figure 20. Sequence identities (%) between AR subtypes from different species	31
Figure 21. Effect of LUF6096 on Cl-IB-MECA on [³⁵ S]GTPγS binding and [¹²⁵ I]-AB- MECA binding with HEK 293 cells expressing WT hA ₃ AR and the mutant mEL1- hA ₃ AR.....	32
Figure 22. Rhodopsin-based molecular model of A ₃ AR displays the defined docking mode of Cl-IB-MECA and a possible allosteric binding site for VUF5455 on TM 7 based on mutagenesis results	33

Figure 23. Using the SMD computational method, a theoretical model of the ternary complex between adenosine, LUF6000, and the hA ₃ AR	34
Figure 24. Diversity of the binding sites of synthetic allosteric modulators across Class A GPCRs.....	34
Figure 25. Examples of three different allosteric binding sites of Class A GPCRs	35
Figure 26. 3.2 Å resolution cryo-EM structure showing representative regions from the MIPS521-ADO-A1R-Gi2 complex	36
Figure 27. Previously published 9-step synthesis protocol of 1 <i>H</i> -imidazo[4,5- <i>c</i>]quinolin-4-amine derivatives.....	37
Figure 28. Ligand structure-guided design approach for A ₃ AR PAMs; an iterative preclinical drug discovery process.....	39
Figure 29. Comparative effects of LUF6000 on [³⁵ S]GTPγS binding induced by Cl-IB-MECA and adenosine using HEK 293 cells expressing hA ₃ ARs.....	40
Figure 30. 2- <i>n</i> -pentyl- <i>N</i> -(3,4-dichlorophenyl)-1 <i>H</i> -imidazo[4,5- <i>c</i>]quinolin-4-amine.....	42
Figure 31. 2-(1-Adamantyl)- <i>N</i> -(3,4-dichlorophenyl)-1 <i>H</i> -imidazo[4,5- <i>c</i>]quinolin-4-amine	44
Figure 32. Hydrophilic moieties of previous 1 <i>H</i> -imidazo[4,5- <i>c</i>]quinolin-4-amine derivatives that reduced allosteric enhancement of PAM derivatives	45
Figure 33. Tolerated 4-substituted-phenylamino substituents in 1 <i>H</i> -imidazo[4,5- <i>c</i>]quinolin-4-amine as A ₃ AR PAMs	46
Figure 34. 6-step synthesis protocol for 1 <i>H</i> -imidazo[4,5- <i>c</i>]quinolin-4-amine derivatives	62
Figure 35. Examples of 2-(<i>para</i> -substituted-phenyl)-4-phenyl-1 <i>H</i> -imidazo[4,5- <i>c</i>]quinoline derivatives.....	63
Figure 36. Creation of an acyl imidazolium electrophile to facilitate the substitution reaction between the vicinal diamine and the carboxylic acid	64
Figure 37. Palladium-catalyzed amination reaction cycle for general procedures C & D	65
Figure 38. Synthesis scheme for 5,5,5-trifluoro-2-(3,3,3-trifluoropropyl)pentanoic acid for compound 3	66
Figure 39. Synthesis of cyclononane and cyclodecanecarboxylic acids for compounds 12 and 13	67
Figure 40. Cyclopropanation reaction of compound 10 to form compound 20	71
Figure 41. Synthesis of (1 <i>R</i> ,2 <i>R</i> ,4 <i>R</i>)- & (1 <i>S</i> ,2 <i>S</i> ,4 <i>S</i>)-bicyclo[2.2.2]oct-5-ene carboxylic acid for compound 21	71
Figure 42. Oxidation reactions of compound 10 to produce derivatives with hydrophilic substitutions.	73
Figure 43. Effect of PAM derivatives on dissociation of [¹²⁵ I]I-AB-MECA using hA ₃ ARs	76
Figure 44. Effect of PAM derivatives on equilibrium binding of [¹²⁵ I]I-AB-MECA at the hA ₃ AR.....	78
Figure 45. Effect of alkyl- and cycloalkyl-substituted PAM derivatives on hA ₃ AR activation by Cl-IB-MECA as determined in [³⁵ S]GTPγS binding.	80
Figure 46. Effect of bridged PAM derivatives on hA ₃ AR activation by Cl-IB-MECA determined using [³⁵ S]GTPγS binding.....	82
Figure 47. Effect of PAM derivatives bearing hydrophilic substituents on [³⁵ S]GTPγS binding induced by Cl-IB-MECA using hA ₃ ARs.....	83

Figure 48. Effect of <i>para</i> -phenylamino substituted PAM derivatives on [³⁵ S]GTPγS binding induced by Cl-IB-MECA using hA ₃ ARs.....	83
Figure 49. Effect of compound 31 on [³⁵ S]GTPγS binding, indicating hA ₃ AR activation by Cl-IB-MECA.....	84
Figure 50. Effect of compound 8 on dissociation rate of [¹²⁵ I]I-AB-MECA using WT and chimeric A ₃ ARs	85
Figure 51. Effect of compound 5 on [³⁵ S]GTPγS binding induced by Cl-IB-MECA using WT and chimeric A ₃ ARs	86
Figure 52. Effect of compound 8 on [³⁵ S]GTPγS binding induced by Cl-IB-MECA using WT and chimeric A ₃ ARs.	87
Figure 53. Mean plasma concentrations of compound 10 in Wistar rats vs. multiple timepoints.....	92
Figure 54. <i>t</i> BuXPhosphine oxide by-product from step-6 general procedures C & D.....	95
Figure 55. Proposed 2-(cyclonon-5-en-1-yl)- <i>N</i> -(3,4-dichlorophenyl)-1 <i>H</i> -imidazo[4,5- <i>c</i>]quinolin-4-amine derivative to be synthesized for a hydrophilic carbonyl substitution.....	103
Figure 56. Creation of MRS7422 prodrug through the succinylation of Cl-IB-MECA	104
Figure 57. Bitopic ligand VCP746 for the A ₁ AR	114

CHAPTER 1: Introduction

GPCRS AS THERAPEUTIC DRUG TARGETS

Developing bioavailable and selective small molecules for cell-surface receptors to influence intracellular effectors and second messengers is a widely-used therapeutic strategy (17). G protein-coupled receptors (GPCRs) are the largest class of cell-surface receptors (23). Since the start of the 21st century, 35% of Food and Drug Administration (FDA) approved therapeutic drugs have targeted GPCRs (59). None of those approved drugs targeting GPCRs have been for the A₃ adenosine receptor (A₃AR). The A₃AR is one of four adenosine receptor (AR) subtypes of the superfamily of G protein-coupled cell-surface seven-transmembrane receptors. A₁, A_{2A}, and A_{2B} are the other AR subtypes.

Although there are no FDA-approved A₃AR drugs, there is much ongoing preclinical research in developing lead drug candidates as agonists, antagonists, and allosteric modulators for this receptor (32). In fact, among compounds of publicly disclosed structure, there are two A₃AR agonists (Figure 3) and one antagonist (Figure 4) in clinical trials. There are currently no A₃AR allosteric modulators of publicly disclosed structures enrolled in a clinical trial. This study aims to synthesize and characterize the structure-activity relationships (SAR) of A₃AR allosteric modulators and determine their potential pharmaceutical impact.

THERAPEUTIC POSSIBILITIES OF TARGETING THE A₃AR

ARs are an appealing receptor family for drug development. Adenosine is responsible for regulating many physiological and pathophysiological conditions that promote the protection against stress to an organ and the repair of tissue (14; 40; 71).

Among the beneficial roles of adenosine acting at four subtypes of ARs, activation of the G_i -coupled A_3AR is associated with attenuating chronic neuropathic pain, heart and brain ischemic preconditioning, and anti-inflammatory effects—without serious cardiovascular side effects (39; 64; 71). The A_3AR is the only AR subtype overexpressed in immune and cancer cells, adding to its potential as a possible therapeutic target (15).

TYPES OF ALLOSTERIC MODULATORS

Allosteric modulators bind to topographically distinct binding sites from the orthosteric binding site and can exert their effects through conformational changes different from orthosteric agonists (16). Various types of allosteric modulators differ in their pharmacological effects on the receptors. Positive allosteric modulators (PAMs) improve agonist affinity, potency, and/or efficacy, while negative allosteric modulators (NAMs) do the opposite.

Allosteric modulators can induce a characteristic functional response without agonists, i.e., ago-PAMs. It is possible for PAMs to bind to the orthosteric site additionally and not be fully selective for the allosteric binding site, which can create a competing pharmacological effect on the receptor, mainly if the PAM also binds as an orthosteric antagonist, i.e., a competitive antagonist (52; 56).

POSITIVE ALLOSTERIC MODULATORS OVER ORTHOSTERIC LIGANDS

There are valid reasons to develop PAMs over orthosteric agonists as therapeutic agents. The A_3AR is broadly distributed in many tissue types throughout the body, leading to unwanted side effects of systemically administered orthosteric agonists. The hallmark advantage of PAMs over orthosteric ligands is that they are event- and site-specific in action (23). Because adenosine is endogenously elevated in response to

localized signals within the body, a pure PAM will enhance the protective function of adenosine only when and where it is elevated (78), highly reducing the risk of side effects. For example, directly acting agonists for the ionotropic γ -aminobutyric acid (GABA) receptor cause adverse side effects when administered. Diazepam, a PAM, is safely used to enhance the endogenous neurotransmitter GABA through an allosteric site on the GABA_A receptor (46). This suggests that using a PAM might be safer than a synthetic orthosteric agonist and improve its therapeutic profile (56).

A second advantage of studying PAMs over orthosteric ligands is the possibility of achieving highly selective PAMs for the A₃AR over other AR subtypes. The PAM allosteric binding sites of the AR subtypes—thought to be located in discrete domains of the receptor protein—are not highly conserved, making it easier to develop subtype-selective PAMs, which is not true for the orthosteric binding sites common to all the AR subtypes, located in the center of the transmembrane (TM) domain helical bundle (75).

Developing PAMs that penetrate the blood-brain barrier (BBB) would be more effective in activating an AR in the central nervous system (CNS). AR agonists have multiple potential pharmaceutical applications in the CNS (39), but current A₃AR orthosteric agonists, mainly nucleosides, tend to have low BBB permeability, typically 1–2% free passage (41; 72; 96).

Lastly, it might be possible to create biased allosteric enhancement with the development of PAMs. The binding of modulators causes a receptor conformational change that either positively or negatively influences the binding of the orthosteric ligand, ultimately affecting the activation of the receptor. It is possible to develop individual PAMs to activate distinct A₃AR cell signaling pathways. The A₃AR can

trigger many different intracellular second messengers, such as Ca^{2+} , β -arrestin and inhibit cyclic adenosine monophosphate (cAMP) formation (63).

RESEARCH OBJECTIVES, CENTRAL HYPOTHESIS, AND SPECIFIC AIMS

The main question of our study is: Based on the known SAR of A_3AR PAMs, is it possible to develop a bioavailable, small molecule PAM that is highly selective for the A_3AR and influences the agonist potency, affinity, and/or efficacy at the receptor more than known A_3AR -specific PAMs?

Our central hypothesis was that modifying specific moieties of known allosteric modulators will improve their interaction with the A_3AR allosteric binding site, thus improving the receptor's response to an orthosteric agonist and improving the modulators' pharmacokinetic properties.

There were four primary objectives of this study: 1) to devise a shorter synthesis protocol for *1H*-imidazo[4,5-*c*]quinolin-4-amine PAM derivatives, 2) to synthesize a new *1H*-imidazo[4,5-*c*]quinolin-4-amine PAM derivative series, 3) to determine the SAR of the new series of PAM derivatives, and 4) to obtain a baseline understanding of the absorption, distribution, metabolism, excretion, and toxicity (ADMET) of a potential lead compound from this series of PAM derivatives.

The following specific aims tested our central hypothesis and realized our primary objectives:

Specific Aim 1

The first specific aim dealt with synthesizing focused libraries of allosteric modulators, centered on distinct molecular scaffolds predominantly informed by SAR and determining their influence on agonist binding kinetics. Two single-point radioligand

binding assays—ligand dissociation and equilibrium binding—characterized the binding kinetics of these allosteric modulators using membranes prepared from HEK 293 cells expressing human A₃AR (hA₃AR). These assays determined if the allosteric modulators are positive or negative modulators of orthosteric ligand binding.

Specific Aim 2

The second specific aim was to determine the SARs of A₃AR allosteric modulators. We measured the effects of the modulators on A₃AR-mediated G protein activation using a [³⁵S]GTPγS binding assay, determining the potency of an A₃AR agonist (concentration of half-maximal activation, EC₅₀) and its maximal efficacy (E_{max}). The Psychoactive Drug Screening Program (PDSP) determined interactions with other proteins. Selected compounds were used for mouse/human chimeric A₃AR studies to help elucidate the location of the allosteric binding site.

Specific Aim 3

The third specific aim was to determine structure-pharmacological relationships (SPR) of A₃AR allosteric modulators. We chose a chemical lead that was the most potent, specific, and selective A₃AR modulator to assess the pharmacological and ADMET properties *in vivo* and *in vitro*. *In vivo*, we evaluated its concentration in plasma samples after administering oral gavage (p.o.) of three different doses and one intravenous (i.v.) dose in Wistar rats. Multiple *in vitro* assays assessed drug metabolism and pharmacokinetics (DMPK): plasma stability, HepG2 cytotoxicity, human ether-a-go-go-related gene (hERG) potassium channel inhibition, cytochrome P450 inhibition, microsomal stability, pION solubility, plasma protein binding, and chemical stability in simulated gastric and intestinal fluids.

SCOPE OF THE STUDY

This study focused on the preclinical design, synthesis, and characterization of the 1*H*-imidazo[4,5-*c*]quinolin-4-amine class of A₃AR PAMs. It did not involve any *in vivo* testing in an animal disease model. This study employed a team-of-teams approach to investigate the pharmacological profile of a new series of 1*H*-imidazo[4,5-*c*]quinolin-4-amine derivatives. The Molecular Recognition Section of the National Institute of Diabetes and Digestive and Kidney Diseases (NIDDK) at Bethesda, Maryland, synthesized and characterized the 1*H*-imidazo[4,5-*c*]quinolin-4-amine derivatives. Courtney Fisher and Dr. John A. Auchampach, collaborators in the Department of Pharmacology and Toxicology at the Medical College of Wisconsin, conducted the PAMs' kinetic binding and functional studies. The National Institute of Mental Health (NIMH) PDSP (Dr. Bryan Roth, University of North Carolina, Chapel Hill, NC) conducted the PAMs' off-target binding studies. JRF India of JRF Global (Gujarat, India) completed the *in vivo* and *in vitro* ADMET experiments. Altogether, this study was a comprehensive medicinal chemistry investigation to develop a therapeutic A₃AR PAM further.

CHAPTER 2: Literature Review

MOLECULAR CHARACTERIZATION OF THE A₃AR

The A₃AR protein consists of 318 amino acid residues and is encoded on human chromosome 1p21–p13, having two exon coding regions separated by one 2.4 kb intron on the A₃AR gene (4; 43; 82; 125). The protein consists of seven α -helical transmembrane domains connected by three extracellular loops and three intracellular loops with the N-terminus in the extracellular space and the C-terminus in the cytoplasm (Figure 1) (81). Helix-8 and the C-terminal region of the protein have multiple serine and threonine residues, some of which may be phosphorylated to induce receptor desensitization and internalization (86).

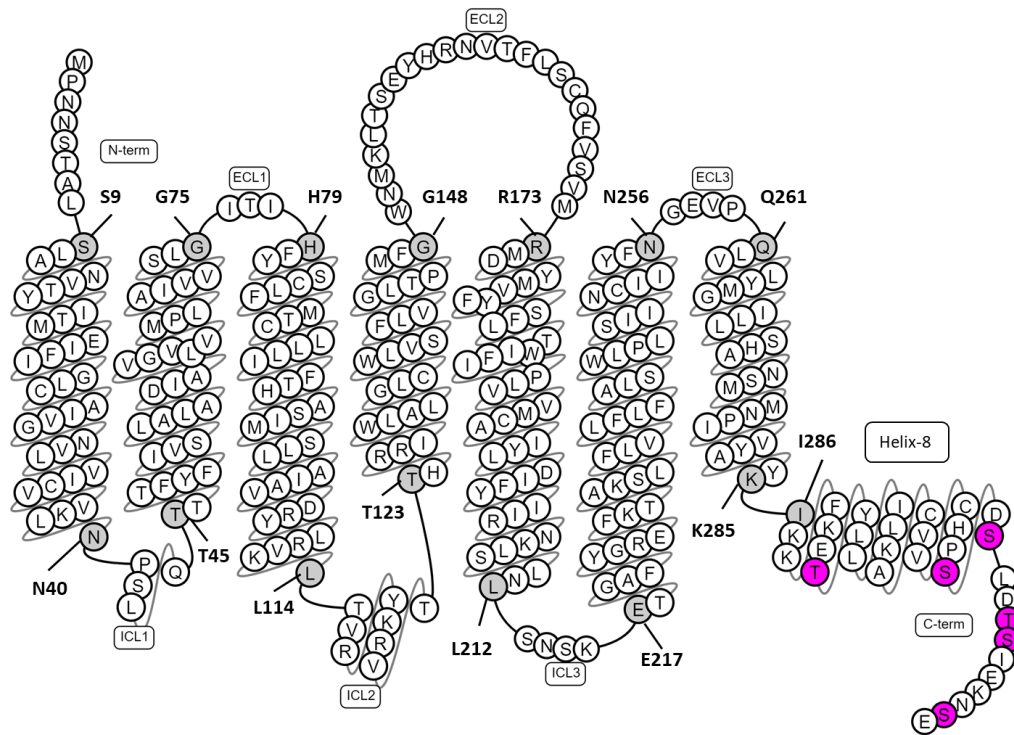


Figure 1. Human A₃ adenosine receptor (81)

INTRACELLULAR SIGNALING OF THE A₃AR

The A₃AR can activate multiple cell signaling pathways (Figure 2), depending on species and cell/tissue type (14; 15; 53).

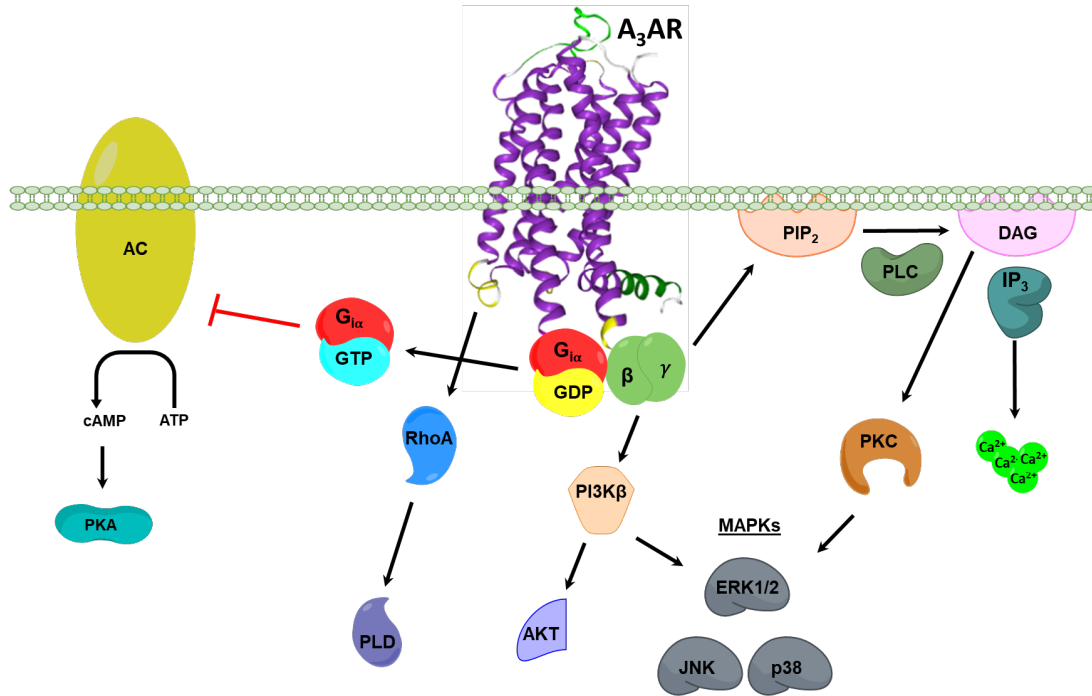


Figure 2. A₃AR-mediated signaling pathways. The A₃AR can influence the activity of many intracellular effector proteins, second messengers, and enzymes of various signaling pathways: 1) inhibition of cAMP and Wnt signaling, 2) phospholipase C (PLC), 3) RhoA and phospholipase D (PLD), 4) extracellular signal-regulated kinase (ERK)/p38/Jun N-terminal kinase (JNK) mitogen-activated protein kinases (MAPK), 5) phosphatidylinositol 3-kinase β (PI3K β)/protein kinase B (PKB or Akt) (87).

Inhibition of Cyclic AMP and the Wnt Signaling Pathway

After binding an agonist, for example, *N*⁶-(3-iodobenzyl)-5'-*N*-methyl carboxamido adenosine (IB-MECA, structure shown in Figure 3), the A₃AR can activate the G_i heterotrimeric guanine nucleotide-binding protein. Following activation, the GTP-bound G _{α} subunit dissociates from G _{$\beta\gamma$} and then decreases cAMP by interacting with and

inhibiting the enzyme adenylyl cyclase (AC). In HCT-116 colon carcinoma cells expressing the A₃AR, introduced in nude male Balb/c mice, the A₃AR-decreased cAMP impaired protein kinase A (PKA) activation, which then modulated other proteins of the Wnt pathway, including glycogen synthase kinase 3 β (GSK3 β) and β -catenin; ultimately inhibiting cell cycle genes such as c-myc and cyclin D1 (35; 73).

When B16-F10 melanoma cells were treated with 10 nM of the selective agonist 2-chloro-*N*⁶-(3-iodobenzyl)-5'-*N*-methylcarboxamidoadenosine (Cl-IB-MECA, structure shown in Figure 3), there was an increase of tumor cells paused in the G₀/G₁ phase and a decrease of cells in the S phase of the cell cycle, pausing telomeric signaling (34).

Phospholipase C Pathway

The free G $\beta\gamma$ subunit can activate PLC and increase the intracellular Ca²⁺ concentration (33; 62). PLC is activated in rat brain preparations treated with agonists, IB-MECA or Cl-IB-MECA, indicated by the increased production of inositol phosphates (InsPs) produced from the hydrolysis of PIP₂ by PLC (1). The increased amount of InsPs leads to the mobilization of Ca²⁺ (124).

Adenosine and other adenosine agonists are known to potentiate the release of inflammatory mediators like β -hexosaminidase from rodent basophilic and mast cells in response to the presence of antigens (91). This effect has been demonstrated to be mediated by the A₃AR.

RhoA and Phospholipase D Pathway

Released adenosine can precondition the heart and prevent cell death during ischemic events, thus reducing infarction size (80). The A₃AR can activate the

monomeric G protein RhoA, which directly couples to PLD (RhoA-PLD1), leading to the cytoprotection of cardiomyocytes (78; 120).

ERK/p38/JNK MAPK Signaling Pathway

ERK1/2 is involved in the signal transduction pathway responsible for proliferation and differentiation in human fetal astrocytes (84). The A₃AR can activate a MAPK cascade involving MAPK kinase kinase (c-RAF), MAPK kinase (MEK), and then MAPK ERK, a cascade initiated by PKC or PI3K β (26; 57; 97). It is possible that signaling through this cascade in GPCRs is enhanced by β -arrestin, which acts as a scaffold protein, though no definitive results show this with the A₃AR (26). Activated ERK1/2 can promote the expression of transcription factors involved in cell growth. Human fetal astrocytes treated with 2-chloroadenosine (2-CA), and then a combination of both 2-CA and the MEK inhibitor, PD098059, DNA synthesis occurred in the former but was prevented in the latter (84).

A₃AR stimulation by Cl-IB-MECA in human hypoxic A172 and U87MG glioblastoma cell lines activates ERK1/2 and p38 MAPKs necessary to increase expression of hypoxia-inducible factor-1 and vascular endothelial growth factor (77). Cl-IB-MECA can also stimulate the A₃AR to phosphorylate JNK MAPKs in U87MG human glioblastoma cells, which increases matrix metalloproteinases, a protein linked to extracellular matrix degradation and tumor invasion (54).

PI3K β /AKT Signaling Pathway

In rat basophilic leukemia (RBL)-2H3 mast-like cells expressing the A₃AR, treatment with 10 nM of agonist IB-MECA stimulates the phosphorylation of PKB or Akt (51). The phosphorylation of Akt in this cell type, linked to PI3K β phosphorylation,

is activated by the $G_{\beta\gamma}$ subunit. The activation of this pathway reduces UV-induced apoptosis in the RBL-2H3 mast-like cells and promotes cell survival (51).

A₃AR AGONISTS IN CLINICAL TRIALS

To date, there are two A₃AR agonists in clinical trials, IB-MECA and Cl-IB-MECA, both first discovered in the Jacobson laboratory in the NIDDK of the National Institutes of Health (NIH) (Figure 3).

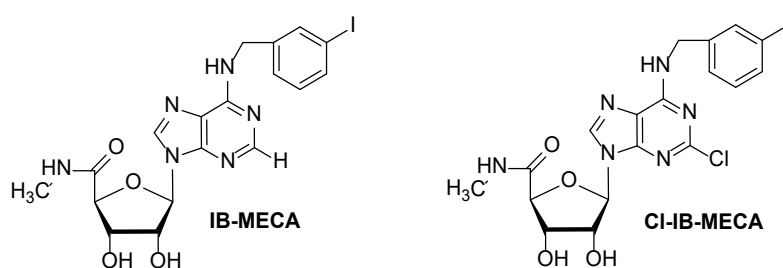


Figure 3. A₃AR agonists IB-MECA and Cl-IB-MECA

IB-MECA, also known as Piclodenoson (CF101), is in Phase III clinical trials for rheumatoid arthritis and psoriasis (22; 36). It is in Phase II clinical trials for the treatment of COVID-19 (58). Cl-IB-MECA, also known as Namodenoson (CF102), is in Phase III clinical trials for chronic hepatitis C, nonalcoholic steatohepatitis, and hepatocellular carcinoma (8; 37; 107). Both compounds are utilized as standard agonists in preclinical concentration-dependent functional response assays for PAMs. An A₃AR PAM of non-disclosed structure but related to acetaminophen, NTM-006 (formerly JNJ-10450232), is in a clinical trial for postoperative (dental) pain (83).

A₃AR ANTAGONISTS IN CLINICAL TRIALS

As of 2021, there is one A₃AR nucleoside antagonist of publicly disclosed structure, FM101 (Figure 4), in Phase I clinical trials to evaluate the safety, tolerability, and pharmacokinetics in healthy subjects for eventual testing in glaucoma patients (113).

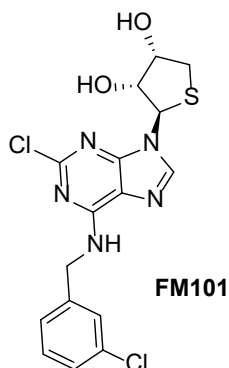


Figure 4. A₃AR antagonist FM101

Park et al. evaluated FM101 as a potential therapeutic for glaucoma and hepatitis in a preclinical rat study (88). They reported FM101 to be functionally biased as a partial agonist for G protein-dependent signaling as well as an antagonist for β -arrestin-dependent signaling (88).

Two other A₃AR antagonists in clinical trials, PBF-677 and PBF-1650, for ulcerative colitis and psoriasis, respectively, have non-disclosed structures (102; 103).

FOUR HETEROCYCLIC A₃AR PAM CLASSES

There are four reported classes of heterocyclic compounds to act as A₃AR PAMs (Figure 5): amiloride, represented by 5-(*N,N*-hexamethylene)amiloride (HMA); 3-(2-pyridinyl) isoquinolines, represented by VUF5455; 1*H*-imidazo[4,5-*c*]quinolin-4-amines,

represented by both DU124183 and LUF6000; and 2,4-disubstituted quinolines, represented by LUF6096 (48; 52; 56; 60).

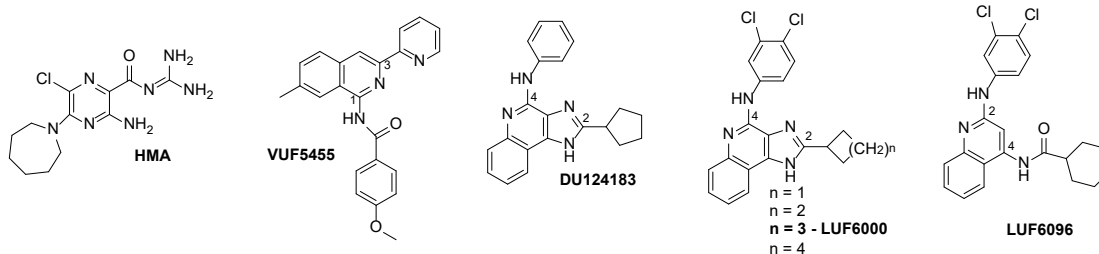


Figure 5. Four Heterocyclic A₃AR PAM Classes

3-(2-Pyridinyl)isoquinoline A₃AR PAMs

In 2001, Gao et al. of the Jacobson laboratory were the first to characterize A₃AR modulation, identifying the 3-(2-pyridinyl)isoquinoline class of compounds as A₃AR allosteric modulators (49). They first studied the effect of the 3-(2-pyridinyl)isoquinoline derivatives on agonist dissociation and forskolin-stimulated cAMP production. The VUF5455 derivative was selected for these experiments because it had the highest K_i value or lowest competitive binding at the orthosteric binding site compared to all the compounds in this class of possible PAMs.

As shown in Figure 6, VUF5455 greatly slowed the dissociation rate of the radioligand, [¹²⁵I]N⁶-(4-amino-3-iodobenzyl)adenosine-5'-N-methyl-uronamide ([¹²⁵I]I-AB-MECA), compared to the control, more so when the enhancer concentration was 10 μ M ($k_{-1} = 0.024 \pm 0.003 \text{ min}^{-1}$) versus 3 μ M ($k_{-1} = 0.031 \pm 0.003 \text{ min}^{-1}$) (49).

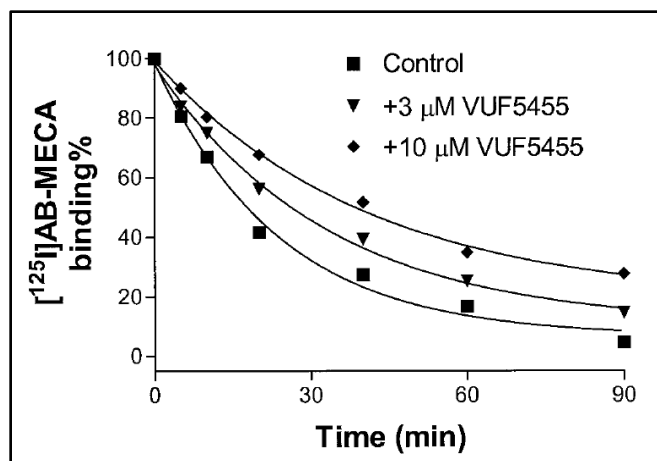


Figure 6. Effects of VUF5455 on the dissociation of [¹²⁵I]AB-MECA from hA₃AR expressed in HEK 293 cells. [¹²⁵I]AB-MECA (0.15 nM) was incubated with membranes expressing hA₃AR for 1 h at 37 °C in a total assay volume of 100 μL. Nonspecific binding was measured at the same time by the addition of 30 μM NECA before incubation. Dissociation was initiated by adding 30 μM NECA with or without VUF5455 at the end of incubation. The incubations were stopped by filtration through GF/B filters on a Brandel cell harvester after the times indicated. The retentate's radioactivity was determined by liquid scintillation spectrometry (n=3) (49).

Gao et al. showed that cAMP production was significantly reduced in the presence of VUF5455 compared to the agonist alone, thus confirming VUF5455 to be a PAM (Figure 7) (49).

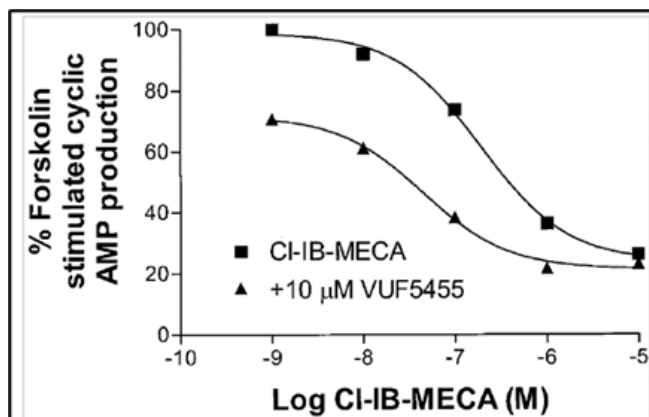


Figure 7. Effect of VUF5455 on cAMP production in HEK 293 cells overexpressing hA₃AR in the presence of the competitive antagonist MRS1220. HEK 293 cells expressing recombinant hA₃AR were treated with test compounds and incubated for 15 min at 37 °C after 10 μM of forskolin was added to stimulate cAMP levels. The reaction was stopped by the addition of 1 mL of 0.1 M HCl. Cellular debris was removed by centrifugation (10,000 x g) for 5 min. cAMP levels measured using a Bio-kinetics reader. The use of MRS1220 (100 nM) overcame the competitive effect of VUF5455 for the orthosteric binding site. 10 μM rolipram and 3 U/mL adenosine deaminase (ADA) were added to all experiments (n=3) (49).

The EC₅₀ of Cl-IB-MECA in cAMP inhibition was 232 ± 67 nM, and 72.5 ± 18.4 nM in the presence of 10 μM of VUF5455, i.e., a three-fold increase in agonist potency compared to control. 100 nM of the competitive hA₃AR antagonist MRS1220 (Figure 8) was used in the functional assay to block VUF5455 binding at the A₃AR orthosteric site because this family of allosteric modulators can act as competitive inhibitors.

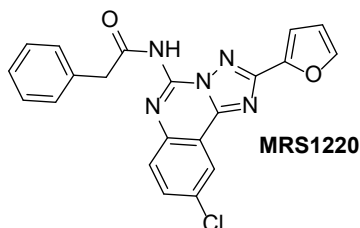


Figure 8. MRS1220 is a competitive hA₃AR antagonist used to block allosteric modulator binding at the orthosteric site

The Jacobson laboratory also showed the PAM to have high A₃AR selectivity over other AR subtypes. The group conducted a dissociation experiment to show that VUF5455 does not slow the dissociation rate of an A₁AR radioligand (Figure 9) (49), indicative of the selectivity of VUF5455 for the A₃AR over the A₁AR.

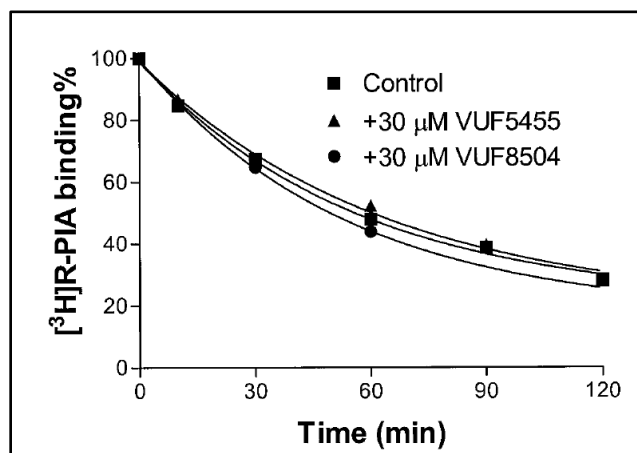


Figure 9. VUF5455 dissociation experiment shows it does not slow down radioligand dissociation for rat A₁AR, providing an example of A₃AR selectivity over other AR subtypes. [³H]R-PIA (1 nM) was incubated for 1 h with rat forebrain membranes expressing A₁ARs at 37 °C for 90 min with Tris-HCl buffer (50 mM) in a total assay volume of 400 μL (pH 7.7). The addition of N⁶-cyclopentyladenosine (CPA) (10 μM) initiated dissociation with or without the tested compound (n=3). Nonspecific binding was determined using 10 μM CPA. Samples were filtered after incubation at the specified time points, and radioactivity was determined in the retentate (49).

Despite the ability of this compound to act as a PAM, VUF5455 still showed competitive binding properties as an A₃AR antagonist, thus complicating its use as a pure PAM.

Amiloride A₃AR PAMs

In a 2003 publication, Gao et al. of the Jacobson laboratory characterized the diuretic amiloride as a PAM for antagonist binding and agonist binding at the A₃AR,

following its identification as an allosteric modulator of antagonist binding to the A_{2A}AR (44; 48). In the antagonist binding studies utilizing a tritiated radioligand, [³H]PSB-11, the amiloride analog HMA increased the antagonist dissociation rate most effectively. Furthermore, in the agonist binding study using the radio-iodinated agonist, [¹²⁵I]I-AB-MECA, HMA proved to be the most potent allosteric modulator, reducing the radioligand dissociation rate with $k_{-1} = 0.031 \pm 0.006 \text{ min}^{-1}$ (48).

Following the A₃AR radioligand binding studies in the presence of amiloride derivatives, the functional effects of the amiloride derivatives on forskolin-stimulated cAMP production, more specifically, HMA, was measured (Figure 10) (48).

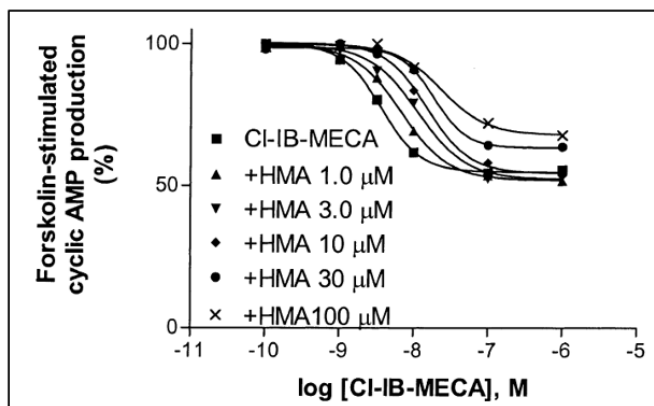


Figure 10. Effect of HMA on forskolin-stimulated (10μM) cAMP production by 10 μM CI-IB-MECA in CHO cells expressing the hA₃AR. CHO cells expressing recombinant hA₃AR treated with test compound and 10 μM rolipram and 3 U/mL of ADA were incubated for 45 min. Cells were treated with 10 μM forskolin to stimulate cAMP levels and incubated for an additional 15 min. The reaction was stopped with the addition of 0.1 M HCl. cAMP production was measured using a competitive protein-binding method. PKA was incubated with [³H]cAMP in K₂HPO₄/EDTA buffer, 20 μL of cell lysate, and 30 μL of 1 M HCl or 50 μL of cAMP solution. Bound radioactivity on washed Whatman GF/C filters was measured by liquid scintillation spectrometry (n=3) (48).

Compared to results in the presence of the agonist alone, the forskolin-stimulated cAMP production was noticeably increased in the presence of HMA in a concentration-dependent manner. This is the opposite of what would be expected of a PAM, which would be predicted to decrease cAMP production compared to the agonist alone. The allosteric modulator reduced the maximal agonist efficacy. It caused a rightward shift of the agonist concentration-response curve, indicating that it takes greater concentrations of the agonist in the presence of an allosteric modulator to achieve the same effect at lower concentrations of the agonist alone. Thus, the allosteric modulator HMA acted more like a NAM (48).

1H-Imidazo[4,5-c]quinolin-4-amine A₃AR PAMs

The *1H*-imidazo[4,5-*c*]quinolin-4-amines were first developed and tested as antagonists of the A₁AR and the A₂AR; they showed a low nanomolar affinity for the A₁AR (118).

DU124183

While screening multiple compounds as possible allosteric modulators in 2002, Gao et al. of the Jacobson laboratory identified DU124183, a *1H*-imidazo[4,5-*c*]quinolin-4-amine, as a compound that enhances agonist binding and function at the A₃AR (47). In binding studies, DU124183 considerably slowed the dissociation of the radioligand [¹²⁵I]I-AB-MECA, initiated by the addition of 3 μM Cl-IB-MECA, compared to control (Figure 11) (47).

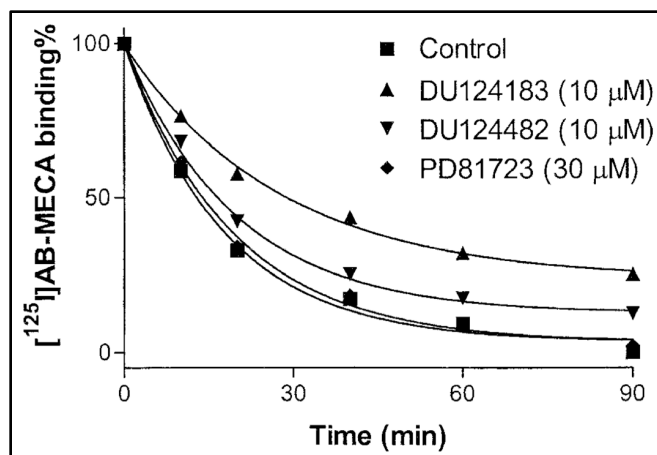


Figure 11. Effects of DU124183 on the dissociation of [¹²⁵I]I-AB-MECA from hA₃AR expressed in CHO cells. [¹²⁵I]I-AB-MECA (1.0 nM) was incubated with cell membranes expressing hA₃AR for 1 h at 25 °C in a total assay volume of 100 μL. Nonspecific binding was determined by adding CI-IB-MECA (3 μM) to cell membranes under the same conditions. Dissociation was initiated by adding CI-IB-MECA (3 μM) with or without test compounds after the 1-hr incubation. The dissociation reactions were stopped by filtration through a Whatman GF/B filter. Bound radioactivity was measured after washing using a γ-counter (n=3) (47).

The dissociation rate of the radioligand alone was $k_{-1} = 0.056 \pm 0.008 \text{ min}^{-1}$ and $k_{-1} = 0.030 \pm 0.006 \text{ min}^{-1}$ in the presence of 10 μM of DU124183. To further show the positive allosteric enhancement capabilities of DU124183, Gao et al. conducted a study that entailed generating a concentration-response curve where membranes of CHO cells expressing hA₃AR were incubated with a fixed amount of agonist radioligand and different concentrations of DU124183. Figure 12 shows the percentage of radioligand bound to hA₃ARs increased as the concentration of DU124183 increased (47).

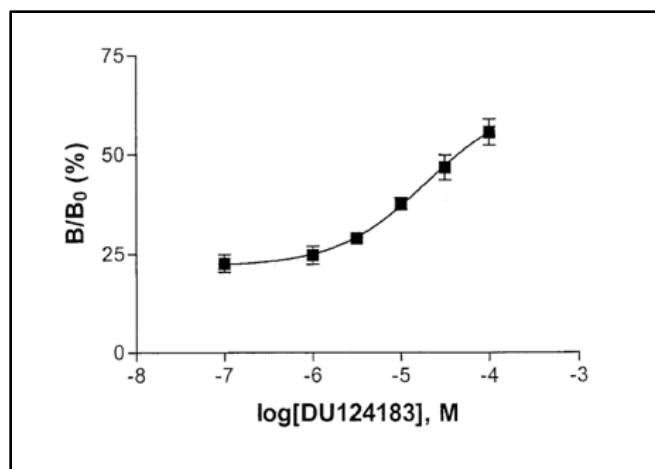


Figure 12. Concentration-response curve for slowing the dissociation of [¹²⁵I]-AB-MECA by DU124183. [¹²⁵I]-AB-MECA (1.0 nM) was incubated with CHO cell membranes expressing hA₃AR for 60 min at 25 °C with or without Cl-IB-MECA (3 μM) for specific and nonspecific binding determination. Cl-IB-MECA (3 μM) was added simultaneously with vehicle or various concentrations of the test compound following the incubation, which was stopped after 45 min by filtration through a Whatman GF/B filter. Bound radioactivity was measured using a γ-counter (n =3). B/B₀ is the percentage of radioligand bound to the hA₃AR (47).

In further studies to understand the biological activity of DU124183, Gao et al. tested the ability of this compound to act as a competitive antagonist to [¹²⁵I]-AB-MECA (Figure 13) (47). As the concentration of DU124183 increased, the binding of the radioligand to the orthosteric binding site decreased; thus, DU124183 also acts as a competitive orthosteric ligand, an undesirable characteristic of an allosteric modulator.

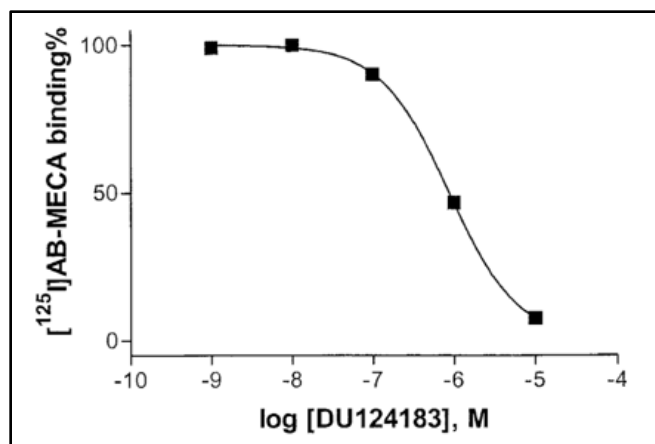


Figure 13. Concentration-response curve showing DU124183 competition for [¹²⁵I]I-AB-MECA (1 nM) binding to membranes from CHO cells expressing hA₃AR. Competitive binding of DU124183 was determined similar to the procedure used in Figure 11 (n=3) (47).

DU124183 potentiated A₃AR function in response to the agonist CI-IB-MECA by decreasing the amount of cAMP produced at its negative plateau at high agonist concentrations (Figure 14) (47).

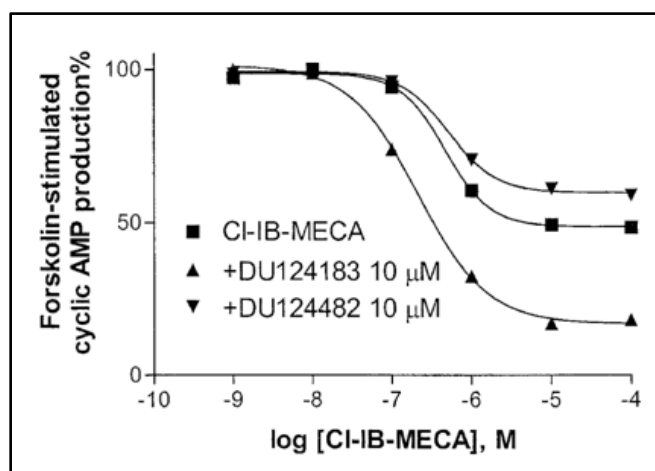


Figure 14. Effect of DU124183 on CI-IB-MECA inhibition of forskolin-stimulated (10 μM) cAMP production in CHO cells expressing hA₃AR. The use of MRS1220 (100 nM) overcame the competitive effect of DU124183 for the orthosteric binding site. 10 μM rolipram and 3 U/mL ADA were added to each experiment (n=3). cAMP levels were stimulated with 10 μM of

forskolin. cAMP production measured similar to the procedure used in Figure 10 (47).

Typically, PAMs should cause a leftward shift in the concentration-response curve compared to the agonist alone, increasing the agonist potency. This phenomenon might not be seen in functional assays where PAMs also act as a competitive antagonist. cAMP assays were conducted with MRS1220 to overwhelm the antagonistic activities of DU124183 to ensure this competitive antagonist effect would not obscure results. DU124183 with MRS1220 substantially reduced the cAMP production compared to Cl-IB-MECA alone, showing 84% inhibition compared to 53%, respectively (47). Despite this increase in efficacy, there was a 100-fold decrease in agonist potency in the presence of DU124183 and MRS1220.

LUF6000

Following the study of DU124183, Göblyös of the IJzerman laboratory (Leiden, Netherlands), in conjunction with the Jacobson laboratory, continued the PAM investigation of 1*H*-imidazo[4,5-*c*]quinolin-4-amines with 2 position and 4-amino position substitutions (56). They found that LUF6000, with 3,4-dichlorophenyl at the 4-amino position and the cyclohexyl ring at the 2 position, improved dissociation binding and functional efficacy in assays but did not improve agonist potency. This compound also moderately competitively displaced the radioligand [¹²⁵I]I-AB-MECA on CHO cells expressing A₁AR and A₃AR, proving to slightly compete with the orthosteric binding site.

A binding dissociation study varying functionality at the 2 position determined that the dissociation rate gradually decreased as the 2 position substituent increased in

size from hydrogen to cycloalkyl groups, such as cyclohexyl. In Figure 15, *N*-(3,4-dichlorophenyl)-1*H*-imidazo[4,5-*c*]quinolin-4-amine with a hydrogen at the 2 position (2-*H*) slowed the dissociation of the agonist radioligand the least, $k_{-1} = 0.061 \pm 0.006 \text{ min}^{-1}$ (56). There was a substantial decrease in the dissociation rate seen with cyclobutyl and cyclohexyl substitutions at the 2 position, $k_{-1} = 0.038 \pm 0.004 \text{ min}^{-1}$ and $k_{-1} = 0.036 \pm 0.005 \text{ min}^{-1}$, respectively.

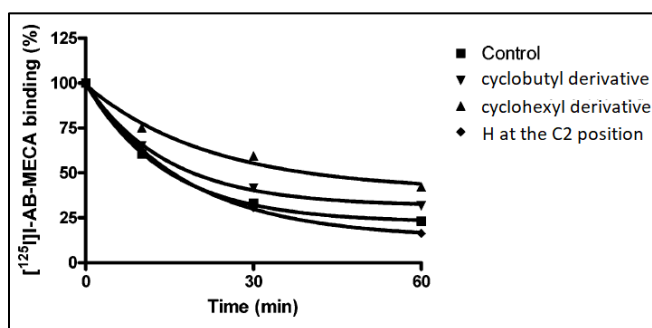


Figure 15. Effects of 1*H*-imidazo[4,5-*c*]quinolin-4-amine PAMs with increasing cycloalkyl ring size on the dissociation of [¹²⁵I]I-AB-MECA from hA₃AR. 20 μg of membranes were pre-incubated at 25 °C for 60 min with [¹²⁵I]I-AB-MECA (0.5 nM) in a total volume of 100 μL of Tris-HCl buffer containing 10 mM MgCl₂, and 1 nM EDTA. Dissociation started with the addition of Cl-IB-MECA (3 μM) with or without the allosteric modulators. The time course of dissociation was measured by rapid filtration at specific time intervals. Nonspecific binding was measured by incubating cell membranes under the same conditions with Cl-IB-MECA (3 μM). Reactions were terminated by filtration through Whatman GF/B filters. Retentate radioactivity on washed filters was measured using a Beckman 5500 γ-counter (56).

The SAR determined from dissociation studies and the percent cAMP inhibition results verified the possibility of fine-tuning the receptor response to an agonist based on changing functional groups on the central scaffold of the PAMs (Figure 16) (50).

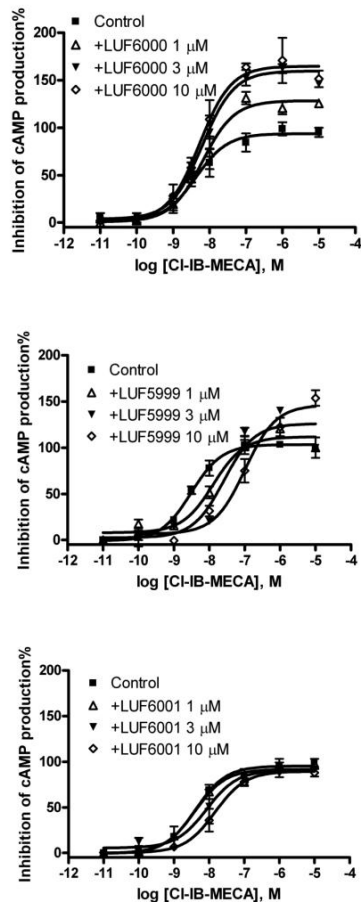


Figure 16. SAR data shows fine-tuning of A_3AR allosteric effects with different 2 position substitutions on the 1*H*-imidazo[4,5-*c*]quinolin-4-amine scaffold. Concentration-response curves illustrate the allosteric effect on Cl-IB-MECA inhibition of forskolin-stimulated cAMP production. Cells were incubated for 20 min with LUF6000, LUF5999, or LUF6001 before adding Cl-IB-MECA. Experiments and measurements of cAMP accumulation were conducted similarly to experimental procedures described in Figure 10 (n=3) (50).

The different substitutions at the 2 position of the 1*H*-imidazo[4,5-*c*]quinolin-4-amine derivatives are presumed to favor various conformational changes of the A_3AR in the presence of the agonist, allowing for different functional results. The 2-H derivative in Figure 16, LUF6001, decreased A_3AR potency and efficacy of Cl-IB-MECA. The cyclobutyl derivative, LUF5999, increased efficacy but reduced potency. Compared to

LUF6001 and LUF5999, the cyclohexyl derivative, LUF6000, increased the efficacy without changing potency.

Gao et al. showed that LUF6000 could be functionally biased and influence A₃AR cell signaling of multiple pathways differently, a concept called biased allosteric enhancement (50; 63). LUF6000 influenced cAMP inhibition more than β-arrestin recruitment. In comparison, there was modest Ca²⁺ mobilization and hyperpolarization. There was no influence on ERK1/2 phosphorylation.

Compared to DU124183, LUF6000 induced a more significant decrease in cAMP production (Figure 17) (56).

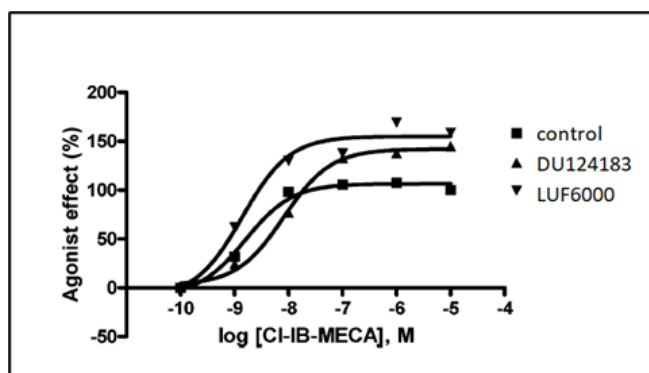


Figure 17. Comparison between 10 μM of DU124183 and 10 μM LUF6000 on % inhibition of cAMP production by CHO cells overexpressing A₃AR. Assay procedures were similar to those described in Figure 10 (56).

Significantly, LUF6000 and many other similar PAMs, unlike PAMs VUF5455 and DU124183, only weakly inhibited orthosteric ligand binding. Weak competitive antagonism is a significant advantage to consider in developing PAMs and selective pharmacological probes of the A₃AR allosteric binding site.

In Vivo Results of LUF6000

A reduction of cytokines in the cellular environment indicates an anti-inflammatory effect. For reduction of cytokines, important inflammatory transcription factors and associated protein concentrations must decrease, most notably nuclear factor kappa B (NF κ B), tumor necrosis factor-alpha (TNF- α), signal transducer, and activator of transcription 1 (STAT1) and Janus kinase 2 (JAK2). In a 2014 study, Cohen et al. showed that LUF6000 could enhance the anti-inflammatory effects of adenosine in three *in vivo* experimental animal models: 1) adjuvant-induced arthritis (AIA) in rats, 2) monoiodoacetate (MIA)-induced osteoarthritis (OA) in rats, and 3) concanavalin A (Con-A)-induced liver inflammation in mice (21).

In the AIA rat model, compared to the control experiment using agonist alone, the presence of LUF6000 significantly reduced the clinical pain score observed (21). This experiment showed LUF6000 downregulating NF- κ B and the upstream signaling proteins: PI3K, IKK, and I κ B in peripheral mononuclear blood cells from the rats (21).

In the MIA-induced OA rat model, the presence of LUF6000 enhanced the efficacy of the endogenous mediator adenosine and reduced knee swelling and edema (21). In this experiment, LUF6000 reduced concentration levels of JAK2 and STAT1—a different mechanism to induce inflammation compared to NF- κ B—in treated rats compared to the untreated control rats.

A third experiment studied the effects of LUF6000 on reducing liver inflammation in a Con-A-induced hepatitis mouse model. Administration of LUF6000 reduced the formation of the enzymes serum glutamic oxaloacetic transaminase and

serum glutamic-pyruvic transaminase, which were produced in liver inflammation in a concentration-dependent manner (21).

In a separate study, Can-Fite BioPharma Ltd. conducted preclinical tests of LUF6000 (CF602) and found it improves erectile dysfunction in a diabetic rat model (<https://www.canfite.com/category/CF602>, accessed on 22 October 2021).

2,4-Disubstituted Quinoline A₃AR PAMs

In 2009, Heitman et al. of the IJzerman laboratory reported a new class of A₃AR PAMs, the 2,4-disubstituted quinolines, which are modified from the 1*H*-imidazo[4,5-*c*]quinolin-4-amine scaffold (60). Instead of having an imidazo heterocycle fused to the quinoline structure, the 2,4-disubstituted family of quinoline derivatives has an amide group at the 4 position. The purpose of exploring this class of PAMs was to attempt to make PAMs like LUF6000 in the 1*H*-imidazo[4,5-*c*]quinolin-4-amine family, but with little to no competitive binding at the A₃AR orthosteric site.

Heitman et al. conducted experiments comparing the effects of LUF6096 and LUF6000 in dissociation studies and the percent inhibition of cAMP production. In the dissociation studies, LUF6000 slowed the dissociation rate of [¹²⁵I]I-AB-MECA more than LUF6096. The k_{-1} for the radioligand in the presence of LUF6000 was $0.029 \pm 0.014 \text{ min}^{-1}$, and the k_{-1} in the presence of LUF6096 was $0.035 \pm 0.008 \text{ min}^{-1}$ (60).

LUF6000 enhanced the inhibition of cAMP accumulation more than LUF6096, but LUF6096 significantly increased the potency of CI-IB-MECA compared to LUF6000, having an EC₅₀ of 9 nM compared to an EC₅₀ of 22 nM in the presence of LUF6000 (60).

When comparing results from equilibrium displacement assays with [¹²⁵I]-AB-MECA on membranes of CHO cells expressing the hA₁AR or the hA₃AR, LUF6096 displaced the radioligand less on both AR subtypes, making it less competitive for the orthosteric site than LUF6000.

In Vivo Results of LUF6096

In a 2011 publication, Du et al. of the Auchampach laboratory showed that LUF6096 reduced infarction size as a percentage of an area at risk in a dog ischemia/reperfusion model (29). Group I represented dogs administered 1 mL of a DMSO/saline vehicle, and Group II represented dogs administered 0.5 mg/kg of LUF6096. Both groups were administered their respective compounds twice, once before ischemia and the second before reperfusion. Group III represented dogs administered LUF6096 once, 1 mg/kg intravenously immediately before reperfusion. LUF6096 in Groups II and III reduced infarction size by 50%.

Unfortunately, LUF6096 showed a short plasma half-life ($t_{1/2}$) of 7.60 min in pharmacokinetic (PK) studies (29). Although the dissociation and *in vitro* and *in vivo* functional data are promising, structural modifications are required to improve the PK characteristics of the 2,4-disubstituted quinolines.

SPECIES DIFFERENCES OF LIGAND BINDING TO THE A₃AR

Du et al. of the Auchampach laboratory reported in 2018 that there are pronounced pharmacological differences between the A₃AR in primates compared to lower species, such as mouse and rat, that could hinder the assessment of potential PAMs when using a non-primate animal model (30). In their effects on [³⁵S]GTP γ S binding, LUF6000 and LUF6096 both increased the efficacy and lowered potency of CI-IB-

MECA in HEK 293 cells expressing human, rabbit, and dog A₃ARs (Figure 18) (30).

There was no effect of the PAMs at the mouse A₃AR (mA₃AR) (not shown), except for a small enhancing effect of LUF6000 in enriched (P2) membranes.

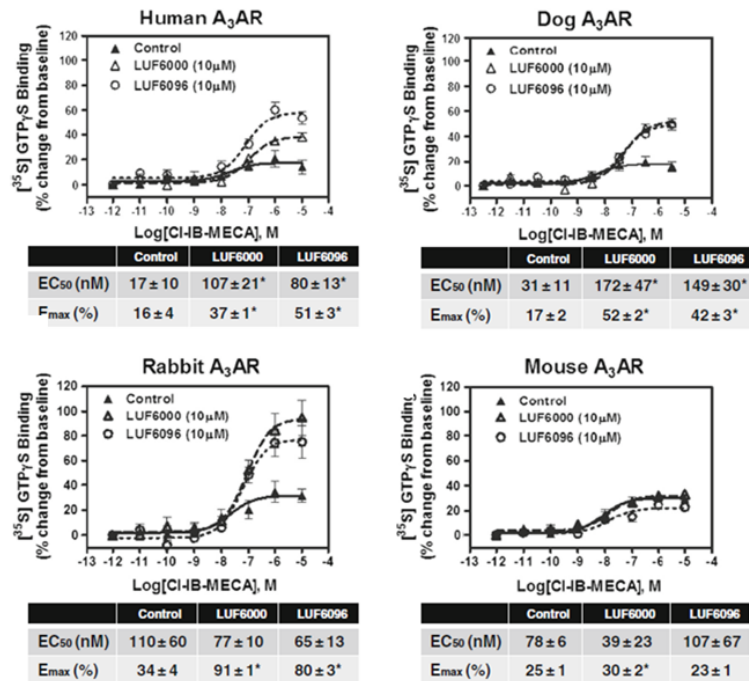


Figure 18. Effect of 10 μ M LUF6000 or LUF6096 on CI-IB-MECA-induced [³⁵S]GTP γ S binding in assays with HEK 293 cell membranes expressing human, dog, rabbit, or mouse A₃AR. [³⁵S]GTP γ S (0.1 nM) and CI-IB-MECA were incubated with a membrane suspension (5 μ g protein 2 h, room temperature). Before initiating the assays, the membrane solutions were preincubated with the modulators for 30 min. Reactions were stopped by rapid filtration through Whatman GF/B filters. The retentate was washed, and radioactivity was measured by liquid scintillation spectrometry. Non-specific binding of [³⁵S]GTP γ S was measured in the presence of 10 μ M unlabeled GTP γ S. Tables summarized the EC₅₀ and E_{max} values, and the mean \pm SEM (n=3). * P < 0.05 versus control by one-way ANOVA followed by post hoc analysis by a student's t-test for unpaired data with the Bonferroni correction (30).

Du et al. characterized [¹²⁵I]I-AB-MECA binding in HEK 293 cell membranes expressing human, dog, rabbit, and mouse A₃AR to explore further the influence of the

allosteric enhancer on the effects of the orthosteric ligand. In these assays, LUF6000 and LUF6096 slowed the dissociation rate of the orthosteric ligand from the human and dog A₃AR, but not the rabbit and mouse (Figure 19) (30).

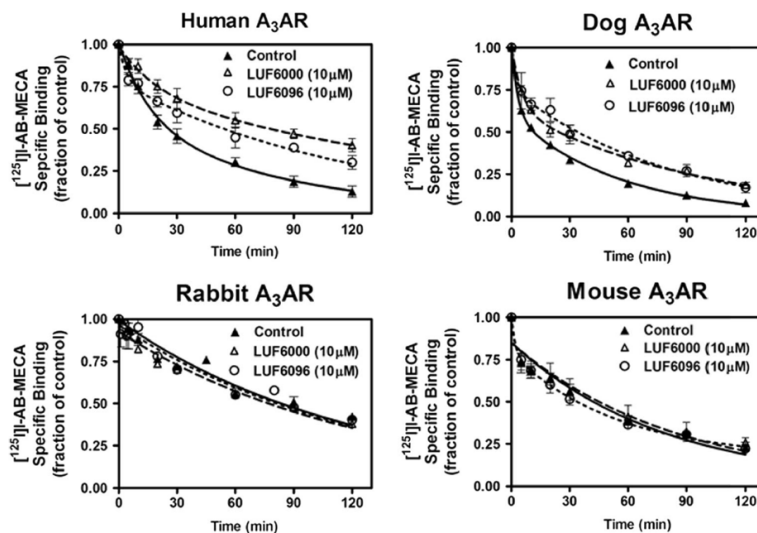


Figure 19. Effects of LUF6000 and LUF6096 on the dissociation of [¹²⁵I]I-AB-MECA binding to HEK 293 cell membranes expressing human, dog, rabbit, and mouse A₃ARs. [¹²⁵I]I-AB-MECA (~ 0.3 nM) incubated with membranes (50 µg) for 2 h at room temperature. Dissociation was initiated by adding 100 µM NECA mixed with either vehicle or modulator. Displayed is the fraction of specific binding at various intervals after the addition of NECA. Non-specific binding was determined by incubation in the presence of 100 µM NECA. Reactions were stopped at times indicated by rapid filtration through Whatman GF/C filters. Bound radioactivity was measured using a γ-counter. Data fitting was to a two-phase exponential decay model (n=3) (30).

Figure 20 compares sequence identities between the human AR subtypes to the AR subtypes of other species (30), indicating low sequence identity between the rat, mouse, and rabbit A₃ARs compared to the hA₃AR.

Human vs.	A ₁	A _{2A}	A _{2B}	A ₃
Rat	97	93	91	77
Mouse	97	93	93	77
Rabbit	97	–	–	78
Dog	98	95	95	91
Sheep	–	–	–	90
Guinea pig	98	–	–	–
Horse	–	94	–	–
Chick	88	–	72	–

Figure 20. Sequence identities (%) between AR subtypes from different species. Rat (77%), mouse (77%), and rabbit (78%) A₃AR have low sequence identities compared to the hA₃AR (69).

In comparative sequence analysis, Du et al. found that four amino acids were conserved in extracellular loop 1 (ECL1) of the human, dog, and rabbit A₃AR. In the mouse and rat, the sequence is different from the human, dog, and rabbit ECL1. Based on this observation and the fact that some receptors, like the muscarinic acetylcholine receptors (mAChR), have allosteric binding sites in the extracellular loops, Du et al. conducted studies with the enhancers utilizing HEK 293 cells expressing a chimeric form of the human and mouse A₃ARs designated mEL1-hA₃AR (30). The purpose of this study was to elucidate if the differences of amino acid residues in ECL1 are the reason for the pharmacological differences seen among the wild-type (WT) receptors. In the mutant mEL1-hA₃AR, the ECL1 region was changed to the mouse sequence (76Q-V-K-M-H80).

In [³⁵S]GTPγS binding assays, LUF6096 potentiated the activation of [³⁵S]GTPγS in the cells expressing WT hA₃AR and the mEL1-hA₃AR. In the [¹²⁵I]I-AB-MECA binding assays, LUF6096 slowed the dissociation of [¹²⁵I]I-AB-MECA in the WT hA₃AR and mEL1-hA₃AR expressing cells (Figure 21) (30). These results suggest that the

allosteric binding site is not necessarily located in the ECL1. The amino acid sequence differences of the ECL1 are not responsible for the differing results between the species.

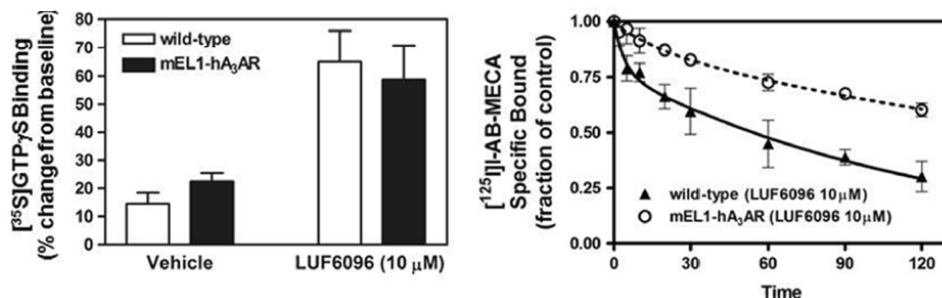


Figure 21. Effect of 10 μM LUF6096 on 10 μM of Cl-IB-MECA on $[^{35}\text{S}]\text{GTP}\gamma\text{S}$ binding and $[^{125}\text{I}]\text{-AB-MECA}$ binding with HEK 293 cells expressing WT hA₃AR and the mutant mEL1-hA₃AR. $[^{35}\text{S}]\text{GTP}\gamma\text{S}$ binding and $[^{125}\text{I}]\text{-AB-MECA}$ binding assays were conducted as in Figures 18 and 19, respectively (n=3) (30).

KNOWN LOCATIONS OF GPCR ALLOSTERIC BINDING SITES

Conformational flexibility of the A₃AR protein has confounded attempts to determine an A₃AR X-ray structure (K. Jacobson, personal communication). There is no reported X-ray crystallographic structure of an A₃AR. Therefore, the exact location of the allosteric binding site and how the PAM orients itself in the receptor are not known.

In 2003, Gao et al. published a site-directed mutagenesis study that explored the effects of three allosteric modulators—HMA, DU1241283, and VUF5455—on the radioligand $[^{125}\text{I}]\text{-AB-MECA}$ dissociation kinetics (45). The authors found that the mutations F182A and N274A completely abolished allosteric enhancement by all three modulators. Figure 22 shows a rhodopsin-based A₃AR molecular model, in which agonist Cl-IB-MECA interacts with TMs 3 (yellow), 5 (cyan), and 6 (blue). Above the putative agonist binding site, the PAM VUF5455 located near TM 7 (purple) acts as a lid on the

orthosteric pocket, suggesting that the allosteric binding site might be in the extracellular loops of the receptor (45).

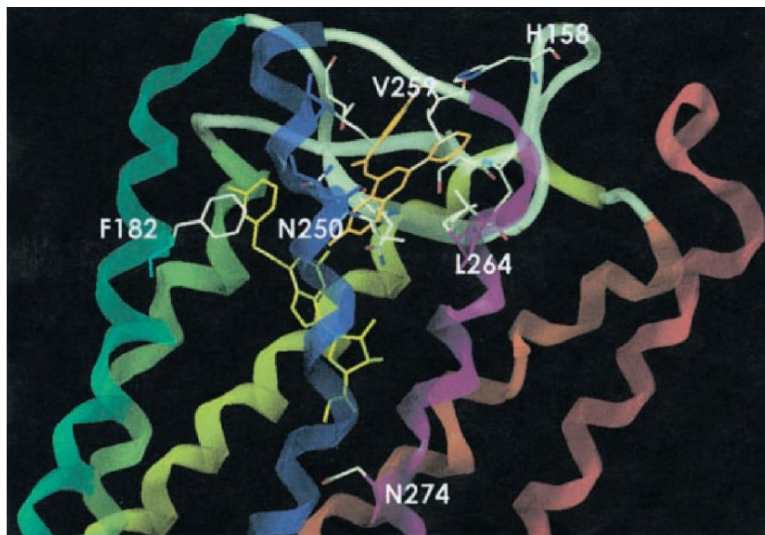


Figure 22. Rhodopsin-based molecular model of A₃AR displays the defined docking mode of CI-IB-MECA (colored according to atom type) and a possible allosteric binding site for VUF5455 (orange) on TM 7 (purple) based on mutagenesis results. Displayed are the secondary structures of each TM. Different colored ribbons represent TMs 1, 2, 3, 4, 5, 6, and 7 with red, orange, yellow, green, cyan, blue, and purple colors, respectively. Residues near the allosteric modulator and F182 and N274 residues are necessary for the allosteric action of VUF5455 (45).

In this molecular model, mutations F182A (located on TM 5, cyan), and N274A (located on TM 3, yellow), are not near the proposed allosteric binding site of VUF5455. The mutational changes could cause conformational changes that promote the interaction of the PAM with the receptor via an indirect allosteric fashion.

Most recently, Ciancetta et al. analyzed the possible interactions of LUF6000 with the hA₃AR using the Supervised Molecular Dynamics (SMD) computational method (20). Like Gao et al., they proposed proximity of a possible PAM LUF6000 binding site to the adenosine bound to the hA₃AR (Figure 23) (20).

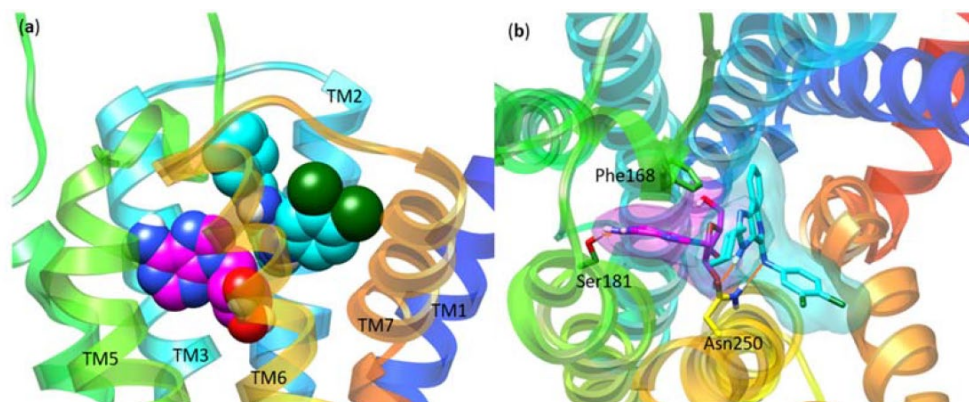


Figure 23. Using the SMD computational method, a theoretical model of the ternary complex between adenosine, LUF6000, and the hA₃AR. (a) side view, (b) top view (20).

These theoretical models notwithstanding, the exact location of the A₃AR PAM binding site is still unknown. The location of Class A Rhodopsin-like GPCR allosteric binding sites could be in regions of the extracellular space, within the transmembrane helical bundle, or on its periphery, or in the intracellular space at the cytosolic interface, in other words, at various sites throughout the receptor (Figure 24) (111).

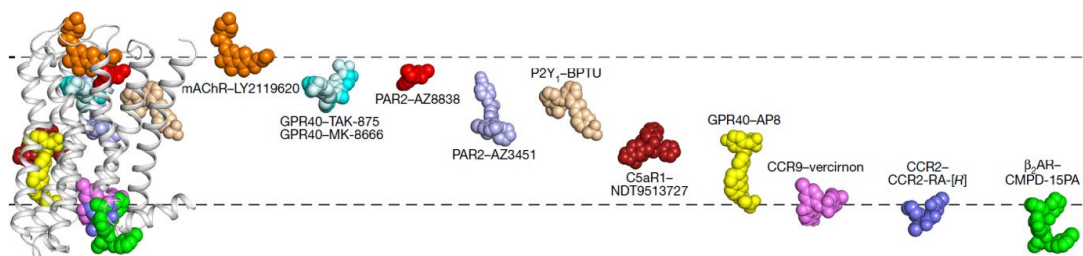


Figure 24. Diversity of the binding sites of synthetic allosteric modulators across Class A GPCRs. The left shows various chemical structures of allosteric modulators (colored) bound to a general form of class A GPCRs (gray). To the right are the same allosteric modulators shown in position on their respective receptors: mAChR (orange), G protein-coupled receptor 40 (GPR40 – teal/off-white/yellow), protease-activated receptor 2 (PAR2 – red/violet), purinergic P2Y₁ receptor (P2Y₁ – beige), complement component 5a receptor 1 (C5aR1 – brown), chemokine (CC motif) receptors 2 and 9

(CCR2/9 – purple/magenta) and β_2 adrenergic receptor (β_2 AR – green). Dashed lines indicate the lipid bilayer boundaries (111).

In the cocrystal of the M_2 mAChR and PAM, LY2119620, the allosteric binding site is in the extracellular region (Figure 25) (119). The ago-PAM AP8 binds to the TM region of the Free Fatty Acid (FFA) Receptor 1 cocrystal. Compound-15 is an example of an allosteric modulator with an intracellular binding site of the cocrystal with the β_2 AR.

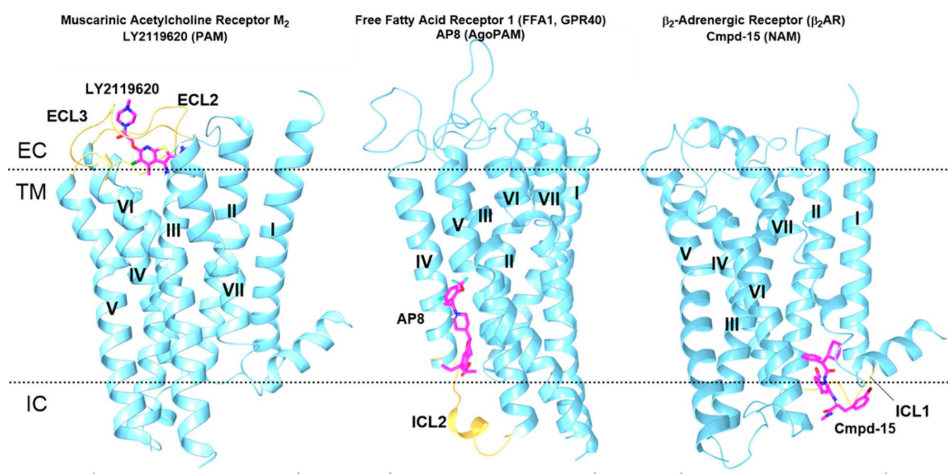


Figure 25. Examples of three different allosteric binding sites of Class A GPCRs. The representative class A allosteric modulators (magenta stick models) are bound to various and distinct sites in their respective cocrystal structure. LY2119620 (left) bound to the extracellular site of the M_2 mAChR; AP8 (center) found in the transmembrane region of the FFA1; Cmpd-15 (right) bound to an intracellular binding site on the β_2 AR (119).

Although obtaining an X-ray crystallographic structure of the A_3 AR bound to a PAM remains elusive, the use of new technologies like cryogenic electron microscopy (cryo-EM) might be helpful to determine an A_3 AR-PAM 3D structure in the future (111; 121). Draper-Joyce et al. reported a 3.2 Å resolution cryo-EM structure of the A_1 AR in a complex with the heterotrimeric G_{i2} protein, adenosine, and PAM MIPS521 (MIPS521-ADO- A_1 R- G_{i2}) (Figure 26) (28).

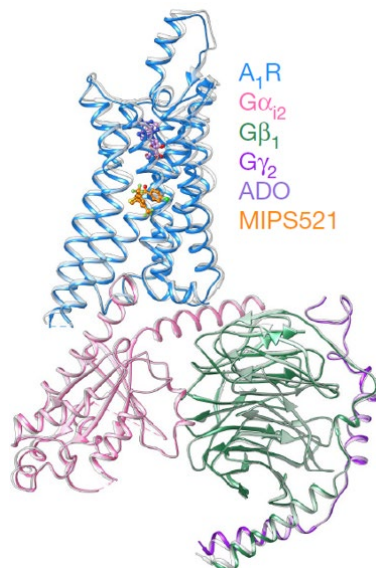


Figure 26. 3.2 Å resolution cryo-EM structure showing representative regions from the MIPS521-ADO-A1R-Gi2 complex. The MIPS521-ADO-A1R-Gi2 complex in color and the ADO-A1R-Gi2 complex in gray are superimposed, both derived from cryo-EM electron density maps (28).

9-STEP SYNTHESIS PROTOCOL OF 1*H*-IMIDAZO[4,5-*C*]QUINOLIN-4-AMINE DERIVATIVES

Göblyös et al. published a 9-step synthesis protocol to study the SAR of 1*H*-imidazo[4,5-*c*]quinolin-4-amine derivatives (Figure 27) (56). Kim et al. used the same synthetic route to synthesize other 1*H*-imidazo[4,5-*c*]quinolin-4-amine derivatives in a 2009 study (68).

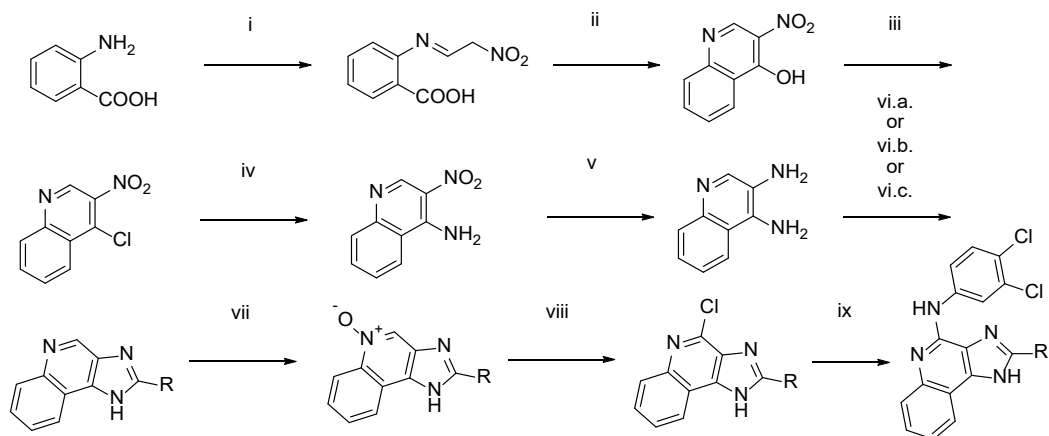


Figure 27. Previously published 9-step synthesis protocol of 1*H*-imidazo[4,5-*c*]quinolin-4-amine derivatives. Reagents and conditions: (i) HCl, HON=CHCH₂NO₂, 55 °C, 89%; (ii) (CH₃CO)₂O, CH₃COOK, 100 °C, 49%; (iii) POCl₃, 81%; (iv) NH₃, 70 °C, 95%; (v) H₂/Pd, 98%; (vi) (a) polyphosphoric acid (PPA), RCOOH, 100 °C, 38-63% (b) trimethyl orthoformate, HCOOH, reflux, 81%, (c) 1. R-COCl, 2. NaOH, 41-44%; (vii) 3-chloroperoxybenzoic acid, reflux, 14-92%; (viii) POCl₃, 100 °C, 26-97%; (ix) RNH₂, microwave, 120 °C, 15-74% (56).

The first step (i) of this synthesis protocol is a condensation reaction between anthranilic acid hydrochloride and 2-nitroacetaldehyde oxime to provide 2-(2-nitroethylideneamino)benzoic acid. In the second step (ii), acetic anhydride with potassium acetate dehydrated 2-(2-nitroethylideneamino)benzoic acid to provide 3-nitro-4-hydroxyquinoline. In the third step (iii), a chlorination reaction of 3-nitrohydroxyquinoline is an aromatic substitution reaction with phosphorous oxychloride to replace the hydroxyl group with a chloride ion to provide 3-nitro-4-chloroquinoline. The fourth step (iv) is an amination reaction of 3-nitro-4-chloroquinoline with ammonia to provide 3-nitro-4-aminoquinoline. This compound was then reduced in the fifth step (v) using hydrogen gas with a 10% palladium on charcoal catalyst.

Göblyös' lab used three different reaction conditions for the sixth step imidazole ring formation, i.e., cyclization of the vicinal diamine. The first method (vi.a.) used polyphosphoric acid with the appropriate carboxylic acid. The second method (vi.b.) used trimethyl orthoformate in formic acid with the appropriate carboxylic acid, and the third method (vi.c.) used an acyl chloride to condense with the diamine followed by a base-assisted intramolecular condensation reaction with sodium hydroxide for the final ring closure.

The ensuing imidazoquinoline compounds were then oxidized using 3-chloroperoxybenzoic acid to make 5-oxide imidazoquinoline compounds (vii). The 4-chloroquinoline amines were then made by reacting the 5-oxides with phosphorous oxychloride (viii). The final products were created by reacting the 4-chloro compounds with the appropriate aniline in ethanol in the microwave (ix).

Although Göblyös and Kim were successful in synthesizing 1*H*-imidazo[4,5-*c*]quinoline amine derivatives using the 9-step synthesis protocol, this study devised a shorter 6-step synthetic route that is more efficient, obtaining high yields with each general step, thus improving the scalability of this class of derivatives (Figure 34). Not only will these derivatives go through additional studies to determine if they possess PAM characteristics comparable to or better than LUF6000, but they will also help facilitate the location of the A₃AR allosteric binding site.

CHAPTER 3: Methodology

LIGAND STRUCTURE-GUIDED DESIGN APPROACH

The development of new allosteric modulators for the A₃AR relied on a ligand structure-guided design approach (Figure 28). Although it is possible to make modeling predictions for the hA₃AR using its close homolog, the hA_{2A}AR (20), these predictions do not reach the confidence level needed for design decisions for allosteric compounds. Instead, empirical SAR and PK data inform design decisions.

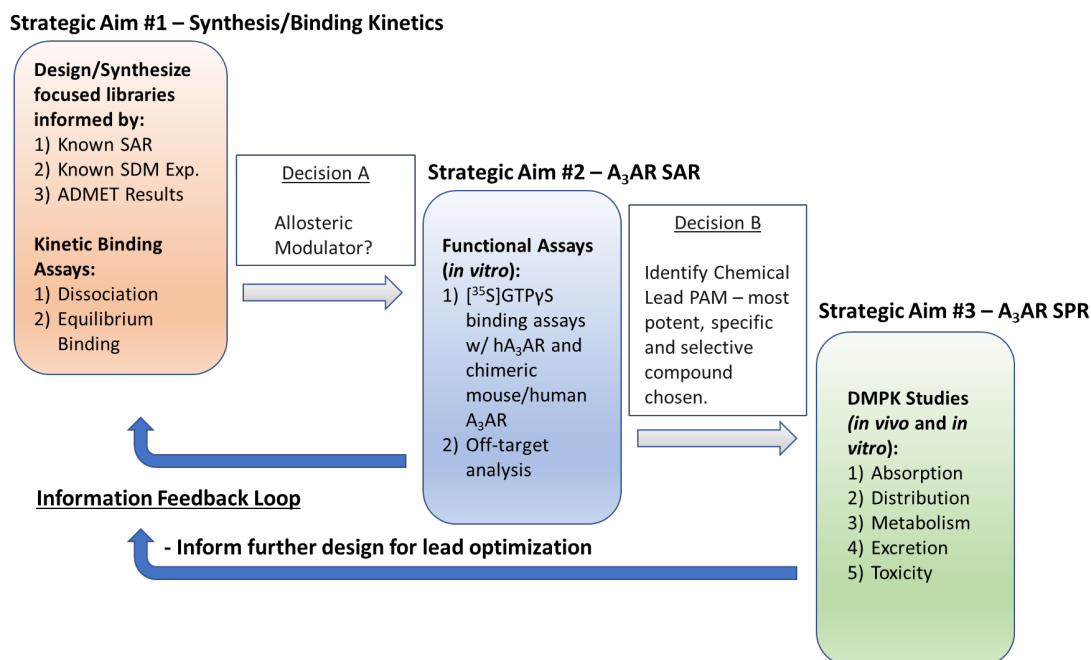


Figure 28. Ligand structure-guided design approach for A₃AR PAMs; an iterative preclinical drug discovery process

Specifically, design decisions for new compounds originated from known SAR and ADMET data from previous investigations involving the 1*H*-imidazo[4,5-*c*]quinolin-4-amine family of derivatives (56; 68). Two single-point kinetic assays: ligand

dissociation, and equilibrium binding, using the [¹²⁵I]I-AB-MECA radioligand, initially tested the binding kinetics of each modulator. Subsequently, each compound was characterized in a functional [³⁵S]GTPγS binding assay, measuring the level of G protein activation, a receptor-mediated event following agonist occupation of the GPCR.

[³⁵S]GTPγS binding assays were conducted with the synthetic agonist, Cl-IB-MECA, instead of adenosine. It is essential to recognize that the activity of PAMs may, in some cases, be probe-dependent (14; 18), i.e., they may vary when combined with different synthetic agonists. Probe-dependency implies that the enhancement of Cl-IB-MECA by a given A₃AR PAM might not be equivalent to their enhancing effects of the native agonist adenosine.

Although LUF6000 potentiates adenosine E_{max} at the A₃AR similarly to Cl-IB-MECA (Figure 29), we used the synthetic agonist in the [³⁵S]GTPγS binding assays because it is more selective for the A₃AR over other AR subtypes than adenosine.

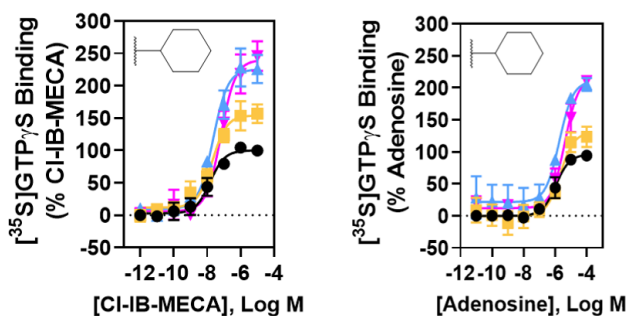


Figure 29. Comparative effects of LUF6000 on [³⁵S]GTPγS binding induced by Cl-IB-MECA and adenosine using HEK 293 cells expressing hA₃ARs. 1 μM LUF6000, Cl-IB-MECA (n=3) had E_{max} 225 ± 10% and EC₅₀ 23 nM and adenosine (n=6) had E_{max} of 211 ± 18% and EC₅₀ of 2 μM. Assay procedures were similar to those described in Figure 18.¹

¹ Data is unpublished and generated by Courtney Fisher and Dr. John Auchampach, Department of Pharmacology and Toxicology of the Medical College of Wisconsin. Data received 1/19/2022 by email communication.

Another reason for using a synthetic agonist instead of adenosine is to have better control over the agonist concentration in each assay. The adenosine concentration would be variable due to its ubiquitous presence in cells and membrane preparations. The variable adenosine concentration would introduce experimental error and decrease [³⁵S]GTPγS data accuracy and precision, ultimately affecting conclusions.

We chose structurally distinct compounds that enhanced agonist binding and G protein activation better than LUF6000 for DMPK studies. The development of PAMs is an iterative process, and we based follow-on design decisions on cumulative SAR and ADMET data from previously synthesized derivatives, thereby working as an information feedback loop. Once the first library of derivatives was complete and initial SAR data reported, all experimental phases—synthesis, radioligand binding, and ADMET studies—were done concurrently.

Design Rationale for Groups of Derivatives

The Jacobson laboratory synthesized four libraries of derivatives to investigate the potential of the 1*H*-imidazo[4,5-*c*]quinolin-4-amine derivatives as therapeutic allosteric drugs. The first three libraries of analogues incorporated the 4-(3,4-dichlorophenylamino) substitution. In previous studies, this 4-amino substitution increased the PAM activity according to agonist efficacy and dissociation kinetics compared to other haloaryl groups (3,5- and 2,4-dichlorophenyl derivatives) (56). At the 2 position, compounds in the first library have hydrophobic alkyl and cycloalkyl moieties (Results, Table 1); compounds in the second library have bridged bicyclic substitutions (Results, Table 2), and compounds in the third library have hydrophilic substitutions of a cycloheptyl ring (Results, Table 3).

Compounds in the fourth library have a cyclohexyl ring at the 2 position, with different *para*-substitutions at the 4-arylamino position (Results, Table 4).

Hydrophobic Alkyl and Cycloalkyl Derivatives

As part of strategic aims 1 & 2, a sub-hypothesis to our central hypothesis was that 1*H*-imidazo[4,5-*c*]quinolin-4-amine derivatives with hydrophobic alkyl groups larger than hydrogen or more considerable cycloalkyl ring modifications at the 2 position would improve [¹²⁵I]I-AB-MECA binding to the A₃AR. They could also enhance the potency and maximal efficacy of the Cl-IB-MECA agonist compared to the modulatory effects of LUF6000.

In 2006, Göblyös et al. published a study investigating the allosteric effects of 1*H*-imidazo[4,5-*c*]quinolin-4-amine derivatives (56). One of these agents was a derivative with an *n*-pentyl substitution at the 2 position (Figure 30) (56).

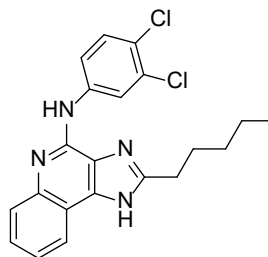


Figure 30. 2-*n*-pentyl-*N*-(3,4-dichlorophenyl)-1*H*-imidazo[4,5-*c*]quinolin-4-amine

In a cAMP inhibition assay, the 2-*n*-pentyl-*N*-(3,4-dichlorophenyl) derivative did not enhance maximal agonist efficacy (102% efficacy when compared to 100% for the agonist alone) (56). When comparing the percent of the bound radioligand [¹²⁵I]I-AB-MECA remaining at a fixed time after addition of unlabeled agonist, the 2-*n*-pentyl-*N*-

(3,4-dichlorophenyl) derivative showed a slightly slower dissociation rate (116% compared to the agonist radioligand alone as 100%). Although this effect was modest, exploring other alkyl derivatives at the 2 position was of potential interest. Therefore, we synthesized 2-alkyl-substituted-*N*-(3,4-dichlorophenyl)-1*H*-imidazo[4,5-*c*]quinolin-4-amine derivatives with propyl and heptan-4-yl substitutions at the 2 position to investigate their allosteric activity compared to that of the 2-*n*-pentyl-*N*-(3,4-dichlorophenyl)-1*H*-imidazo[4,5-*c*]quinolin-4-amine derivative.

The Jacobson laboratory also investigated various sized cycloalkyl substitutions from cyclobutyl to cycloheptyl at the 2 position (56; 68). Because these derivatives showed a pattern of slower agonist dissociation kinetics and increased functional efficacy, we synthesized derivatives with increased ring size from cyclopropyl to cyclododecyl to investigate the effect of the increased cycloalkyl ring size on the functional efficacy of the representative orthosteric agonist Cl-IB-MECA.

In both 2-alkyl and 2-cycloalkyl series, two allosteric modulators were fluorinated—by replacing a -CH₃ with a -CF₃—to produce a bioisostere with improved potency and/or increased metabolic stability (76). It might be possible for fluorinated compounds to be ¹⁸F-labeled imaging tracers for positron emission tomography (PET)—if the affinity of the modulator for the allosteric binding site were sufficiently high and the compounds would not act as competitive antagonists at the orthosteric binding site (13).

Bridged Derivatives

Moreover, Kim et al. of the Jacobson laboratory investigated various bridged substitutions at the 2 position (68). Many of these agents led to increased functional

efficacy and slower dissociation kinetics of the orthosteric agonist. One derivative, 2-(1-adamantyl)-*N*-(3,4-dichlorophenyl)-1*H*-imidazo[4,5-*c*]quinolin-4-amine (Figure 31), a tricyclic compound with a cyclohexyl base structure, had the slowest dissociation kinetics and the highest efficacy characteristics within the group. These results are possible due to two factors: the ring size and the rigidity provided by bridging the ring system.

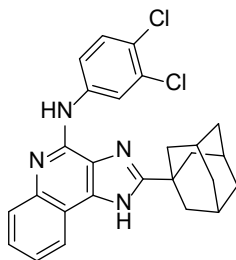


Figure 31. 2-(1-Adamantyl)-*N*-(3,4-dichlorophenyl)-1*H*-imidazo[4,5-*c*]quinolin-4-amine

A second sub-hypothesis in support of strategic aims 1 and 2 was that 1*H*-imidazo[4,5-*c*]quinolin-4-amine derivatives with bridged modifications at the 2 position would improve [¹²⁵I]I-AB-MECA binding parameters at the A₃AR as well as improve potency and maximal efficacy of agonist Cl-IB-MECA, compared to the modulatory effects of LUF6000. For this reason, we synthesized 2 position substituted derivatives with bridged bicycloalkyl groups of various sizes to investigate their modulatory effects further. For example, cyclopropanation of larger cycloalkenyl rings has proven beneficial in other medicinal chemistry investigations, often improving small molecule potency, receptor subtype selectivity, solubility, etc. (110).

Derivatives with Hydrophilic Substitutions

In 2009, Kim et al. investigated the allosteric effect of a tetrahydropyran substitution and multiple piperidine substitutions at the 2 position of the 1*H*-imidazo[4,5-*c*]quinolin-4-amine scaffold (Figure 32) (68). Unfortunately, these hydrophilic nitrogen and oxygen substitutions reduced the allosteric enhancement of this PAM scaffold (68).

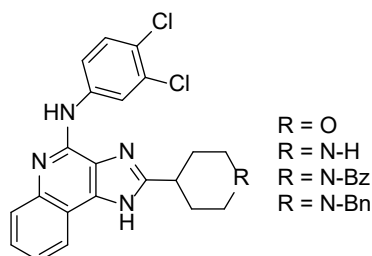


Figure 32. Hydrophilic moieties of previous 1*H*-imidazo[4,5-*c*]quinolin-4-amine derivatives that reduced allosteric enhancement of PAM derivatives

We continued to investigate additional derivatives with reduced lipophilicity by installing different functional groups with oxygen on a cycloheptyl ring: oxirane, alcohol, and carbonyl. These derivatives retained the *N*-(3,4-dichlorophenyl) substitution. A third sub-hypothesis supporting all strategic aims was that 1*H*-imidazo[4,5-*c*]quinolin-4-amine derivatives with hydrophilic modifications at the 2 position would maintain their allosteric enhancement and increase the water solubility of this family of PAMs.

4-Substituted-phenylamino Derivatives

Kim et al. also investigated other halogen and non-halogen *ortho*-, *meta*- and *para*- substitutions of the phenylamino group, i.e., fluoro, cyano, and alkoxy (68). None of these compounds showed better properties than LUF6000 in dissociation kinetic studies and functional efficacy assays, but this work did prove the toleration of various

halogenated substitutions. Notably, 4-methyl, 4-methoxy, and 4-chloro substituted phenylamino derivatives showed promising allosteric enhancement results for dissociation kinetics and functional efficacy (Figure 33) (56).

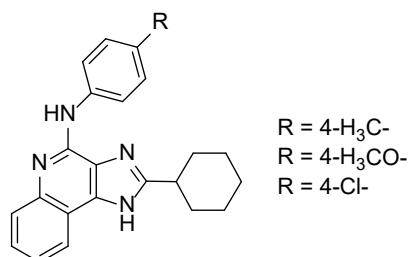


Figure 33. Tolerated 4-substituted-phenylamino substituents in 1H-imidazo[4,5-c]quinolin-4-amine as A₃AR PAMs

Therefore, a fourth sub-hypothesis in support of strategic aims 1 and 2 was that 1H-imidazo[4,5-c]quinolin-4-amine derivatives with 4 position substitutions of the phenylamino group would improve [¹²⁵I]I-AB-MECA binding parameters at the A₃AR as well as improve the potency and maximal efficacy of Cl-IB-MECA as an agonist in [³⁵S]GTPγS binding assays, compared to the modulatory effects of LUF6000.

Experimental Procedures

General

All glassware and stir bars were oven-dried before use in a reaction. All reactions were conducted in a ventilated hood. Pyrophoric reagents were handled and administered under a nitrogen gas atmosphere to reactions in an evacuated oven-dried glass round bottom. All final compounds were stored at 38 °C in a parafilm sealed vial.

All solvents used were of anhydrous grade, requiring no purification. The following commercial compounds were supplied by the following suppliers: quinoline-

2,4-diol, *N,N,N',N'*-tetramethylchloroformamidinium hexafluorophosphate (TCFH), PPA, ethyl 2-cyanoacetate, 3-bromo-1,1,1-trifluoropropane, tetrabutylammonium bromide (TBAB), cyclohexa-1,3-diene, methyl acrylate, cyclodecanone, cycloundecanone, bicyclo[1.1.1]pentane-1-carboxylic acid, methyl acrylate, *p*-bromoaniline, *p*-iodoaniline, 3,4-dichloroaniline, palladium (II) acetate (Pd(OAc)₂), tris(dibenzylideneacetone) dipalladium(0) (Pd₂(dba)₃), bis(triphenylphosphine)palladium (II) dichloride (PdCl₂(PPh₃)₂) and *t*BuXPhos were purchased from Sigma-Aldrich (St. Louis, MO); all solvents, carboxylic acids, and other reagents not stated hereafter, were purchased from Sigma-Aldrich; bicyclo[3.3.1]nonane-1-carboxylic acid was purchased from Chemspace US (Monmouth Junction, NJ); (1*R*,3*S*,5*S*)-bicyclo[3.3.1]nonane-3-carboxylic acid was purchased from AstaTech (Bristol, PA); cyclohept-4-ene carboxylic acid was purchased from Ambeed (Arlington Heights, IL); bicyclo[2.2.1]heptane-1-carboxylic acid was purchased from Enamine (Kyiv, Ukraine). All reagents used were of commercial grade.

NMR spectra were recorded on a Bruker 400 MHz spectrometer at 25 °C under an optimized parameter setting for each sample (Appendix A). For compounds **2**, **5**, **10** – **14**, and **16** – **33**, ¹H NMR chemical shifts were measured relative to the residual solvent peak of 7.26 ppm for CDCl₃ or CDCl₃/CD₃OD. For compounds **3** and **15**, ¹H NMR chemical shifts were measured to the residual solvent peak of 2.5 ppm for DMSO-*d*₆. For compound **1**, ¹H NMR chemical shifts were measured to the residual solvent peak of 3.34 ppm for CD₃OD. For compounds **4**, ¹H NMR chemical shifts were measured to the residual solvent peak of 1.94 for CD₃CN. ¹H NMR chemical shifts were measured relative to tetramethylsilane at 0.00 ppm in CDCl₃ and the residual water peak at 3.30 ppm in CD₃OD. ¹⁹F NMR spectra were recorded for derivatives **3**, **4**, and **12** – **15**.

Suggested NMR peak assignments of some target compounds are shown in Appendix A and are based on 2D COSY and 1D NOE experiments.²

Analytical thin-layer chromatography (TLC) was performed on 0.2 mm silica-coated sheets with an F254 indicator (Sigma-Aldrich). TLC visualization of the products was aided using UV light or by staining with a solution of potassium permanganate (1.5 g of KMnO_4 , 10 g K_2CO_3 , and 1.25 mL 10% NaOH in 200 mL water). Column chromatography was performed on 230-400 mesh silica gel (pore size of 60 Å, Sigma-Aldrich).

Accurate mass data were obtained using a Xevo G2-XS QToF mass spectrometer (Waters, Milford, MA, Refer to Appendix B). The instrument was operated in a positive ion-electron spray ionization (ESI) mode (resolution of 25,000). The ESI capillary voltage was 2.8 kV, and the desolvation temperature was 280 °C. Accurate masses were determined using trifluoroacetic acid (TFA) sodium salt as an internal standard. The liquid chromatography system was a Waters Acquity Ultra Performance Liquid Chromatography I-Class. Solvent A was 100% water, and solvent B was an 80:20 mixture of acetonitrile (ACN):MeOH with 0.1% TFA and 0.2% formic acid added. The column was a ProSwift RP-4H 1x50 mm monolithic (ThermoFisher, Waltham, MA). The LC gradient was 0% B to 100% B in 10 min at a flow rate of 0.250 mL per min. Accurate mass high-resolution LC/ESI/MS at the Mass Spectrometry Facility, NIDDK, NIH.³

² Assignment of proton peaks to differentiate between stereoisomers was performed by Dr. Robert O'Connor, NMR technician of NIDDK, NIH, building 8A.

³ Mass spectra and elemental analyses were obtained by Dr. John Lloyd in the Mass Spec Facility of NIDDK, NIH in building 8A. Write-up of mass spectrometry procedures provided by Dr. John Lloyd on 9/24/2021 by email.

The purity of compounds was determined using Reversed-Phase High Pressure Liquid Chromatography (RP-HPLC), carried out with an Agilent 1100 Series HPLC equipped with an Agilent Eclipse 5 μm XDB-C18 analytical column (250 \times 4.6 mm; Agilent Technologies Inc, Palo Alto, CA, USA). The mobile phase was a linear gradient solvent system, 10 mM TEAA (triethylammonium acetate):CH₃CN from 50:50 to 0:100 in 20 minutes, and then with 100% CH₃CN for 5 minutes; the flow rate was 1.0 mL min. Peaks were detected by UV absorption with a diode array detector at 210, 230, 254, and 280 nm. Most derivatives tested for biological activity showed >95% purity (Refer to Appendix C).

Synthesis of Commercially Unavailable Carboxylic Acids

Synthesis of 5,5,5-Trifluoro-2-(3,3,3-trifluoropropyl)pentanoic Acid

In a 50 mL round bottom flask equipped with a stir bar were added ethyl 2-cyanoacetate (0.91 mL, 8.54 mmol, 1.0 equiv), 3-bromo-1,1,1-trifluoropropane (2.0 mL, 18.8 mmol, 2.2 equiv), potassium carbonate (2.48 g, 17.9 mmol, 2.1 equiv) and 21 mL of DMF (~0.4 M). The reaction mixture was flushed with N₂ and stirred at 60 °C for 48 h. The reaction mixture was cooled to room temperature. The solvent was removed under reduced pressure by rotary evaporation to obtain a crude residue as a mixture of ethyl 5,5,5-trifluoropentanoate and ethyl 2-cyano-5,5,5-trifluoro-2-(3,3,3-trifluoropropyl)pentanoate. The residue (1.37 g, 4.49 mmol, 1.0 equiv) was dissolved in aqueous NaOH (21 mL, ~9.0 g, 225 mmol, 50 equiv), and TBAB (303 mg, ~21 mol %) was added to the flask. The reaction mixture was stirred under reflux at 90 °C for 36 h. 1 M aqueous HCl was added to the reaction mixture until pH 7. The mixture was extracted with ethyl acetate, and the organic layer was washed with water. The organic layer was dried over

MgSO₄, filtered, and the solvent evaporated *in vacuo* to provide the product as a black-brown oil, distilled under a high vacuum at 170-180 °C to afford the black-brown crude product.

Synthesis of Cyclononane and Cyclodecane Carboxylic Acids

General method: The appropriate cyclic ketone (1.25 mmol, 1.0 equiv), *N*-bromosuccinimide (1.40 mmol, 1.0-1.1 equiv), and *p*-toluenesulfonic acid (0.13 mmol, 10 mol %) was added to 5 mL of dichloromethane in a 15 mL round bottom flask. The reaction mixture was stirred at room temperature for 16 h. The solvent was removed under reduced pressure by rotary evaporation to obtain a residue. The residue was dissolved in 10% ethyl acetate in hexane and then passed through a short silica plug. The filtrate was concentrated by rotary evaporation to obtain the α -brominated cyclic ketone as an oily residue, which was used for the next step without further purification.

In a 25 mL round bottom flask, the crude α -brominated cyclic ketone (0.43 mmol) and sodium methoxide (232 mg, 4.3 mmol) were dissolved in 8 mL of methanol. The reaction mixture was stirred overnight and then refluxed for 30 min. 1 M HCl was added to the reaction mixture until pH ~7. The reaction mixture was diluted with water (10 mL) and extracted with ethyl acetate (2x20 mL). The organic layer was separated, dried over MgSO₄, filtered, and concentrated by rotary evaporation to get a crude product. Purification by silica gel chromatography using a 20% ethyl acetate in hexane eluent system provides white solid products with ~27% yield.

Synthesis of ((1R,2R,4R)- & (1S,2S,4S)-Bicyclo[2.2.2]oct-5-ene Carboxylic Acid

Toluene (2 mL) was added to a 15 mL glass pressure tube containing 1,3-cyclohexadiene (0.50 mL, 5.2 mmol, 1.0 equiv) and methyl acrylate (0.52 mL, 5.78

mmol, 1.1 equiv). The solution was purged with N₂ (g) and then sealed. The reaction mixture was stirred at 180 °C for 20 h. The reaction mixture was cooled to room temperature, and the solvent evaporated by rotary evaporation to afford the mixture of *endo* and *exo* isomers as a clear oil. The racemic *endo* product (carboxylate methyl ester) was isolated as a clear oil (402 mg, 49% yield) by silica gel chromatography using 5% ethyl acetate in hexane as the eluent system.

The *endo* carboxylate methyl ester (80.0 mg, 0.48 mmol) was dissolved in 5 mL of methanol and 5 mL of an aqueous NaOH solution (1.5 M) in a 25 mL round bottom flask. The reaction mixture was stirred at room temperature for 1 h. 1M HCl was added to the reaction mixture until pH 7. The reaction mixture was diluted with water (10 mL) and extracted with ethyl acetate (2x20 mL). The organic layer was separated, dried over MgSO₄, filtered, and concentrated by rotary evaporation to obtain the desired carboxylic acid.

6-Step Synthesis Protocol for 1H-Imidazo-[4,5-c]quinolin-4-amine Derivatives

Preparation of 3-Nitroquinoline-2,4-diol – Step 1

Quinoline-2,4-diol (2.0 g, 12.41 mmol) was added to 12 mL of concentrated nitric acid in a 50 mL round bottom flask. The reaction mixture was stirred for 10 min at room temperature and heated in an oil bath at 75 °C for 15 min. The reaction mixture was cooled to room temperature and poured on a crushed ice-water mixture to obtain a precipitate. The suspension was filtered, and the solid was washed with cold water and dried to get the product as a yellow solid (2.43 g, 95% yield).

Preparation of 2,4-Dichloro-3-nitroquinoline – Step 2

3-Nitroquinoline-2,4-diol (2.0 g, 9.7 mmol) was added to 17 mL of phenylphosphonic dichloride in a 50 mL round bottom flask. The flask was fitted with a condenser and placed in an oil bath at 135 °C for 3 h. The reaction mixture was cooled to room temperature, poured slowly on a crushed ice-water mixture, and stirred vigorously to obtain the light brown clay-like precipitate. The mixture was filtered using a fritted funnel, and the precipitate was washed with cold water and dried under air to afford the product as an orange solid (2.05 g, 87% yield).

Preparation of 2-Chloro-3-nitroquinolin-4-amine – Step 3

2,4-Dichloro-3-nitroquinoline (2.0 g, 8.0 mmol) and 28% aqueous ammonia (6 mL, 19.0 equiv) were added to 20 mL of acetonitrile in a 100 mL glass pressure vessel. The mixture was stirred at 50 °C for 6 to 7 h. The reaction mixture was diluted with water (20 mL) and extracted with a mixture of ethyl acetate and methanol (95:5, 2x50 mL). The organic layer was separated, dried over MgSO₄, filtered, and concentrated by rotary evaporation to obtain the product as a yellow solid (1.7 g, 97% yield).

Preparation of 2-Chloroquinoline-3,4-diamine – Step 4

To a 100 mL sealed vessel, 2-chloro-3-nitroquinolin-4-amine (2.0 g, 9.0 mmol, 1.0 equiv), 30 ml of EtOH:H₂O (4:1), concentrated hydrochloric acid (10 mL, 406 mmol, 45.0 equiv) and Fe powder (2.5 g, 45 mmol, 5.0 equiv) were added, and the reaction mixture was stirred at 75 °C for 3 h. The reaction mixture was cooled to room temperature and filtered through a short silica-plug, and the plug was washed with EtOH:H₂O (95:5, 20 mL). The combined filtrate was neutralized with aqueous NaOH/KOH until pH ~7.0, and the product was extracted with a mixture of ethyl acetate

and methanol (95:5, 2x100 mL). The organic layer was separated, dried over MgSO₄, filtered, and concentrated by rotary evaporation, leaving a residue. The residue was purified by silica chromatography with 2% methanol in dichloromethane as an eluent to obtain the product as a brown solid (1.2 g, 70% yield).

General Procedure A. for 2-Substituted-4-chloro-1H-imidazo[4,5-c]quinoline – Step 5

General Method: 2.0 g PPA (per 50 mg of 2-chloroquinoline-3,4-diamine) was weighed in a 5 mL round bottom flask. 2-Chloroquinoline-3,4-diamine (1.0 equiv) and the appropriate carboxylic acid (1.2 equiv) were added to the round bottom flask. The reaction mixture was stirred at 120 °C for 5 h. The reaction mixture was quenched by pouring on a crushed ice-water mixture. The ice-water mixture was neutralized with K₂CO₃ (2 M) until pH 8-9 under stirring. The reaction mixture was extracted with ethyl acetate and then washed with water and brine several times. The organic layer was dried over MgSO₄, filtered, and the solvent removed by rotary evaporation to obtain the crude product, which was purified by silica column to obtain the 1H-imidazo[4,5-c]quinoline derivative with 15-25% ethyl acetate in hexane as the eluent system.

General Procedure B. for 2-Substituted-4-chloro-1H-imidazo[4,5-c]quinoline – Step 5

General Method: The appropriate carboxylic acid (1.4 equiv) and *N*-methyl imidazole (3.5 equiv) were added to 4 mL acetonitrile in a 15 mL round bottom flask with stirring, followed by 2-chloroquinoline-3,4-diamine (1.0 equiv) and TCFH (1.5 equiv). The reaction mixture was stirred at 60 °C for 5 h. The cooled reaction mixture was treated with ethyl acetate, and the organic layer was washed with brine (3X). The organic layer was dried over MgSO₄, filtered, transferred to a 50 mL round bottom flask, and the solvent evaporated by a rotary evaporator. A 1:1 solution of aqueous NaOH (15.0

equiv of NaOH in 10 mL of H₂O):methanol (10 mL) was added with stirring. The reaction mixture was refluxed at 90 °C for 3 h. The cooled reaction mixture was treated with ethyl acetate, and the organic layer was washed with brine (3X) followed by water (3X). The organic layer was dried over MgSO₄, evaporated *in vacuo*, and the resulting residue was used in the final reaction step without further purification.

General Procedure C. for 2-Substituted-N-(3,4-dichlorophenyl)-1H-imidazo[4,5-c]quinolin-4-amine – Step 6

General Method: An oven-dried 10 mL round bottom flask (cooled to room temperature under nitrogen) equipped with a stir bar was charged with the appropriate 2-substituted-4-chloro-1H-imidazo[4,5-c]quinoline derivative (1.0 equiv), 3,4-dichloroaniline (1.5 equiv), Pd₂(dba)₃ (5-20 mol %), *t*BuXPhos (20-40 mol %), and sodium butoxide (1.5–2.0 equiv). The flask was evacuated for 2 min and backfilled with nitrogen. Dioxane (0.1-0.2 M) was added via syringe, and the reaction mixture was flushed/purged with nitrogen for 5 min while stirring. The reaction mixture was stirred at preheated oil bath (95-100 °C) under nitrogen for 16-24 h. Subsequently, the reaction mixture was cooled to room temperature and diluted with EtOAc (5 mL). The solution was then filtered through a silica plug. The filtrate was concentrated by rotary evaporation to obtain the crude product, purified by a silica column with 10-25% ethyl acetate in hexane as the eluent system to obtain the product. Some of the products were further purified by preparative RP-HPLC.

General Procedure D. for 2-Substituted-N-(3,4-dichlorophenyl)-1H-imidazo[4,5-c]quinolin-4-amine – Step 6

General Method: An oven-dried 10 mL round bottom flask (cooled to room temperature under nitrogen) equipped with a stir bar were added Pd(OAc)₂ (1 mol %),

*t*BuXPhos (3 mol %), and H₂O (40 mol %) and dissolved in 1.0 mL of dry 1,4-dioxane. The solution was degassed with N₂ (g) for 15 min and allowed to stir at 80 °C for 5 min. The appropriate 2-substituted-4-chloro-1*H*-imidazo[4,5-*c*]quinoline derivative (1.0 equiv), 3,4-dichloroaniline (1.2 equiv) and sodium butoxide (2.0 equiv) were dissolved in 3 mL of dry 1,4-dioxane in a separate 25 mL round bottom flask. The reaction mixture in the 25 mL round bottom flask was degassed at room temperature with N₂ (g) for 15 min. The activated catalyst from the 10 mL flask was cooled and then transferred to the 25 mL reaction mixture using a cannula. The 25 mL flask was slightly immersed in a 100 °C oil bath, and the reaction continued for 16 to 20 h. The reaction mixture was diluted with ethyl acetate (5 mL) and filtered through a short silica plug. A rotary evaporator concentrated the filtrate to obtain a residue, which was purified by silica column chromatography with 10% ethyl acetate in hexane as the eluent system to afford the product.

*General Procedure E. for 2-Substituted-N-(phenyl-substituted)-1H-imidazo[4,5-*c*]quinolin-4-amines – Step 6*

The appropriate 4-chloro-2-substituted-1*H*-imidazo[4,5-*c*]quinoline starting material (0.05 mmol, 1.0 equiv) and the respective halogenated aniline compound (0.15 mmol, 3.0 equiv) were added to 1 mL of ethanol in a 2.0 to 5.0 mL microwaveable vial. The reaction contents were degassed with N₂ (g) for 15 min, and the reaction was set up in an Initiator microwave reactor (Biotage, Charlotte, NC) at 130 °C for 6 h. The reaction mixture was filtered through a silica plug. The filtrate was evaporated *in vacuo*, and the product was purified by flash chromatography with 15% ethyl acetate in a hexane eluent system.

Synthesis Protocols for Derivatives from Step-6 1H-Imidazo[4,5-c]quinolin-4-amine Derivatives

Procedure for the Synthesis of 2-((1R,4r,7S)-Bicyclo[5.1.0]octan-4-yl)-N-(3,4-dichlorophenyl)-1H-imidazo[4,5-c]quinolin-4-amine – Compound 20

2-(Cyclohept-4-en-1-yl)-N-(3,4-dichlorophenyl)-1H-imidazo[4,5-c]quinolin-4-amine (30 mg, 0.07 mmol) was added to 1 mL of dichloromethane in a 10 mL round bottom flask. The reaction mixture was cooled to 0 °C and degassed with N₂ (g) for 15 min. Diethyl zinc (249 µL, 0.25 mmol) was slowly added to the reaction vessel, followed by the slow addition of diiodomethane (29 µL, 0.35 mmol). The reaction mixture was stirred at 0 °C for 30 min, and then the silicone stopper was replaced with a plastic stopper and wrapped with parafilm. The reaction reacted at room temperature overnight. Saturated aqueous ammonium chloride (0.5 mL) was added to the reaction vessel, and the reaction continued to stir for 30 min. The product was extracted with ethyl acetate, and the organic layer was washed with water and brine. The organic layer was dried over magnesium sulfate, filtered, and concentrated by a rotary evaporator to obtain a residue, purified by flash chromatography using 15% ethyl acetate in a hexane eluent system to provide the product as a white solid (4 mg, 13% yield).

Procedure for the Synthesis of 2-((1R,4s,7S)- & 2-(1R,4r,7S)-8-Oxabicyclo[5.1.0]octan-4-yl)-N-(3,4-dichlorophenyl)-1H-imidazo[4,5-c]quinolin-4-amine – Compounds 22 and 23

meta-chloroperoxybenzoic acid (*m*-CPBA) (17 mg, 0.10 mmol, 2.0 equiv.) was added to a 10 mL round bottom flask containing a solution of 2-(cyclohept-4-en-1-yl)-N-(3,4-dichlorophenyl)-1H-imidazo[4,5-c]quinolin-4-amine (21 mg, 0.05 mmol) in dichloromethane (2 mL). The reaction mixture was stirred at room temperature for 3 h.

Once the starting material disappeared via TLC, 1 mL of acetone and 1 mL of 10% aqueous sodium bicarbonate were added, and the mixture was allowed to stir for 30 min. The product was extracted with ethyl acetate, and the organic layer was washed with water and brine. The organic layer was dried using magnesium sulfate and filtered, and a rotary evaporator evaporated the solvent to obtain a crude residue. The residue was first purified by flash chromatography using a 30% acetone in hexane eluent system, followed by a second flash chromatography column using a 0.75-1.0% methanol in dichloromethane eluent system to provide compounds **22** (2 mg, 6% yield) and **23** (4 mg, 12% yield) as red solids.

Procedure for the Synthesis of (R)- & (S)-4-(4-((3,4-Dichlorophenyl)amino)-1H-imidazo[4,5-c]quinolin-2-yl)cycloheptan-1-one – Compound 24

To a 10 mL round bottom flask containing a solution of (1R,4S)-, (1S,4R)-, (1R,4R)-, & (1S,4S)-4-(4-((3,4-dichlorophenyl)amino)-1H-imidazo[4,5-c]quinolin-2-yl)cycloheptan-1-ol (17 mg, 0.039 mmol) in dichloromethane (1.5 mL) was added one portion of Dess-Martin periodinane (DMP) (25 mg, 0.058 mmol). The reaction mixture was stirred at room temperature until the starting material disappeared (monitored by TLC). The reaction mixture was quenched with saturated aqueous NaHCO₃. The product was extracted with dichloromethane, and the organic layer was washed with water and brine. The organic layer was dried over magnesium sulfate, filtered, and concentrated by rotary evaporator to obtain a crude residue, which was purified by flash chromatography using a 0.75 to 1.0% methanol in dichloromethane eluent system to provide compound **24** (3.9 mg, 23% yield) as a red solid.

Procedure for the Synthesis of (1R,4S)-, (1S,4R)-, & (1R,4R)-, (1S,4S)-4-(4-((3,4-Dichlorophenyl)amino)-1H-imidazo[4,5-c]quinolin-2-yl)cycloheptan-1-ol – Compounds 25 and 26

2-(Cyclohept-4-en-1-yl)-N-(3,4-dichlorophenyl)-1H-imidazo[4,5-c]quinolin-4-amine (20 mg, 0.05 mmol) was added to 0.5 mL of dry tetrahydrofuran in a 25 mL round bottom flask and flushed with N₂ (g). The reaction mixture was cooled to 0 °C, and borane dimethyl sulfide complex solution in 2.0 M THF (47 µL, 0.01 mmol) was added to the reaction vessel. The reaction mixture was stirred for 30 min at 0 °C and then overnight at room temperature. The reaction flask was placed in a 0 °C ice-water bath when all the starting material was consumed. 10% aqueous NaOH (0.5 mL, 0.15 mmol) and H₂O₂ (1 mL, 0.26 mmol) were added successively to the reaction vessel. The reaction mixture reacted at 0 °C for 3 h. The product was extracted with ethyl acetate, and the organic layer was washed with water and brine. The organic layer was dried over magnesium sulfate, filtered, and then evaporated by a rotary evaporator. The crude residue was purified by flash chromatography using a 0.75 to 1.0% methanol in dichloromethane eluent system to provide compounds **25** (1.6 mg, 8% yield) and **26** (2.6 mg, 12% yield) as red solids.

Procedure for the Synthesis of Methyl (E)- & (Z)-3-(4-((2-cyclohexyl-1H-imidazo[4,5-c]quinolin-4-yl)amino)phenyl)acrylate – Compound 29

2-Cyclohexyl-N-(4-bromophenyl)-1H-imidazo[4,5-c]quinolin-4-amine (15 mg, 0.036 mmol), methyl acrylate (9 µL, 0.104 mmol), Pd(OAc)₂ (1 mg, 4.4 µmol), and triethylamine (15 µL, 0.108 mmol) were added successively to 2 mL of dimethylformamide in a 50 mL sealed tube. The reaction mixture was purged with N₂ (g) at room temperature for 30 min and then stirred at 140 °C for 24 h. The product was diluted with ethyl acetate (5 mL) and filtered through a short silica plug. The filtrate was

concentrated by rotary evaporator and then co-evaporated with toluene (2x2 mL) to obtain a crude residue, which was purified by flash chromatography using a 0.75 to 1.0% methanol in dichloromethane solvent system to afford compound **29** (2.8 mg, 18% yield) as a white solid.

Procedure for the Synthesis of 2-Cyclohexyl-N-(4-((5-Chlorothiophen-2-yl)ethynyl)phenyl)-1H-imidazo[4,5-c]quinolin-4-amine – Compound 30

2-Chloro-5-ethynylthiophene (141 mg, 1.06 mmol, 5.0 eq.), 2-cyclohexyl-*N*-(4-iodophenyl)-1*H*-imidazo[4,5-*c*]quinolin-4-amine (100 mg, 0.214 mmol, 1.0 equiv), PdCl₂(PPh₃)₂ (30 mg, 42.8 μmol, 5 mol %), copper (I) iodide (4 mg, 21.4 μmol, 2.5 mol %), and triethylamine (298 μL, 2.14 mmol, 10.0 equiv) were added successively to 4 mL of dry dimethylformamide in a round bottom flask. The reaction mixture was purged with N₂ (g) at room temperature for 30 min and then stirred at 80 °C for 4 h under N₂ (g). The reaction mixture was cooled to room temperature, diluted with ethyl acetate (10 mL), and filtered through a silica plug. The filtrate was concentrated by rotary evaporator and then co-evaporated with toluene (2x3 mL) to obtain a crude residue, which was purified by flash chromatography using a 15% ethyl acetate in hexane eluent system to provide compound **30** (10 mg, 10% yield) as a white solid.

Procedure for the Synthesis of 2-(Heptan-4-yl)-N-(4-(trialkylstannyl)phenyl)-1H-imidazo[4,5-c]quinolin-4-amine – Compounds 32 and 33

General Method: 2-(heptan-4-yl)-*N*-(4-iodophenyl)-1*H*-imidazo[4,5-*c*]quinolin-4-amine (0.10 mmol, 1.0 equiv), PdCl₂(PPh₃)₂ (20 μmol, 20 mol%), hexamethylditin or hexabutylditin (0.5 mmol, 5.0 equiv) were added to 2 mL of 1,4-dioxane in a 10 mL round bottom flask. The reaction mixture was purged with N₂ (g) at room temperature for 30 min and stirred at 70 °C for 2.5 h or until the starting material disappeared (monitored

by TLC). The reaction mixture was cooled to room temperature, diluted with ethyl acetate (10 mL), and filtered through a short silica plug. The filtrate was concentrated by rotary evaporator and then co-evaporated with toluene (2x3 mL) to obtain a crude residue, which was purified by flash chromatography using a 10% ethyl acetate in hexane eluent system to provide compounds **32** (5 mg, 10% yield) and **33** (9 mg, 13% yield) as white solids.

Effects of Modulators on Agonist Binding to hA_3AR Studies

Binding studies were performed by Dr. John Auchampach and Courtney Fisher, a Ph.D. Candidate, in the Department of Pharmacology and Toxicology at the Medical College of Wisconsin. Refer to Appendix D for methods.

Studies of Receptor Activation using [3S]GTP γ S Binding

Studies of agonist-induced increased [3S]GTP γ S binding as a measure of receptor activation were performed by Dr. John Auchampach and Courtney Fisher, a Ph.D. Candidate, in the Department of Pharmacology and Toxicology at the Medical College of Wisconsin. Refer to Appendix E for methods.

Chimeric Receptor Studies

Chimeric receptor studies were performed by Dr. John Auchampach and Courtney Fisher, a Ph.D. Candidate, in the Department of Pharmacology and Toxicology at the Medical College of Wisconsin. Refer to Appendix F for methods.

Off-Target Binding Studies

We thank Dr. Bryan L. Roth (Univ. North Carolina at Chapel Hill) and the NIMH PDSP (Contract # HHSN-271-2008-00025-C) for screening studies. Initially, the

compounds were tested at 10 μ M in a primary screen at forty-five different receptors, transporters, and channels. If the percent of binding inhibition exceeded 50% at any of the targets listed below, a secondary screen of that compound was performed with an entire concentration-response curve (concentrations of 0.1 nM to 10 μ M, in increments of half-integral log values) (11).

Unless noted in the text, no significant interactions (<50% inhibition at 10 μ M) of any of the derivatives were found with the following target proteins (all of these are human unless noted otherwise, and most are GPCRs): 5HT_{1A} (serotonin), 5HT_{1B}, 5HT_{1D}, 5HT_{1E}, 5HT_{2A}, 5HT_{2B}, 5HT_{2C}, 5HT₃, 5HT_{5A}, 5HT₆, 5HT₇, α _{1A} (adrenergic), α _{1B}, α _{1D}, α _{2A}, α _{2B}, α _{2C}, β ₁, β ₂, β ₃, BZP (benzodiazepine) rat brain site, D₁ (dopamine), D₂, D₃, D₄, D₅, delta opioid receptor (DOR), kappa opioid receptor (KOR), GABA_A, H₁ (histamine), H₂, H₃, H₄, M₁ (muscarinic acetylcholine), M₂, M₃, M₄, M₅, mu opioid receptor (MOR), σ ₁ (sigma) , σ ₂, DAT (dopamine transporter), NET (norepinephrine transporter), SERT (serotonin transporter), TSPO (translocator protein). Methods can be found at the following URL:

<https://pdsp.unc.edu/pdspweb/content/PDSP%20Protocols%20II%202013-03-28.pdf>

Pharmacokinetic Studies

In vitro and *in vivo* pharmacokinetic studies were conducted by the Jai Research Foundation (JRF, Gujarat, India). The study was undertaken under full accreditation by the Association for Assessment and Accreditation of Laboratory Animal Care (AAALAC) International and approved by the Institutional Animal Ethics Committee (IAEC), JRF. Refer to Appendix G for methods.

CHAPTER 4: Results

SYNTHESIS OF DERIVATIVES

6-Step Synthesis Protocol for 1*H*-Imidazo[4,5-*c*]quinolin-4-amine Derivatives

This study developed a shorter 6-step synthesis protocol than the previously reported 9-step route to create a new series of 1*H*-imidazo[4,5-*c*]quinolin-4-amine derivatives (Figure 34).

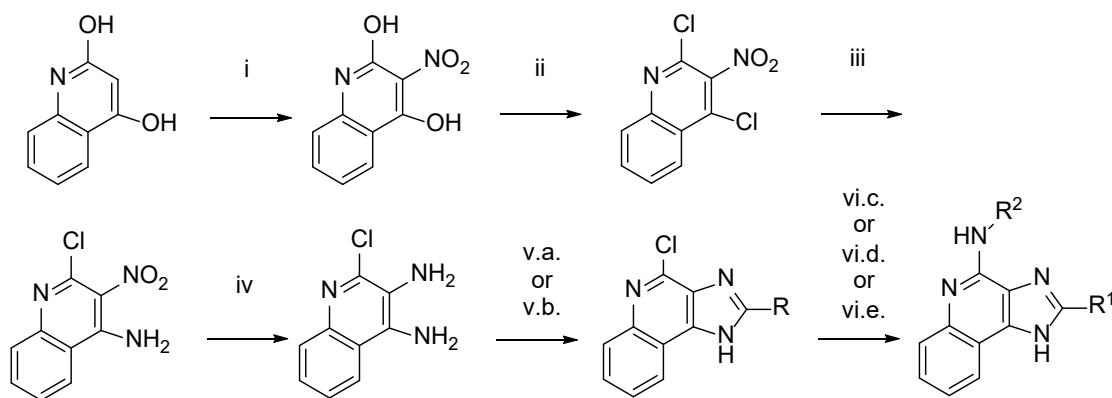


Figure 34. 6-step synthesis protocol for 1*H*-imidazo[4,5-*c*]quinolin-4-amine derivatives. Reagents and conditions: (i) HNO₃, 75 °C, 95%; (ii) PhPOCl₂, 135 °C, 87%; (iii) NH₃:H₂O, CH₃CN, 50 °C, 97%; (iv) Fe powder, HCl, CH₃CH₂OH/H₂O, 75 °C, 70%; (v) a. PPA, R¹-COOH, 120 °C; b. 1.) TCFH, NMI, R¹-COOH, ACN, 60 °C, 2) NaOH, H₂O:MeOH, 90 °C; (vi) c. R²-NH₂, Pd₂(dba)₃, *t*BuXPhos, NaOBu^t, 1,4-dioxane, 100 °C, 5-28%; d. R²-NH₂, Pd(OAc)₂, *t*BuXPhos, NaOBu^t, H₂O, 1,4-dioxane, 100 °C, 2-33%; e. R²-NH₂, ethanol in microwave, 130 °C, 10-61%.

Steps one through four closely followed the synthetic route described by Gao et al. in 2016 to synthesize a library of 2-(*para*-substituted-phenyl)-4-phenyl-1*H*-imidazo[4,5-*c*]quinoline derivatives having a phenyl group at the 4 position instead of the 4-aminophenyl group (Figure 35) (42).

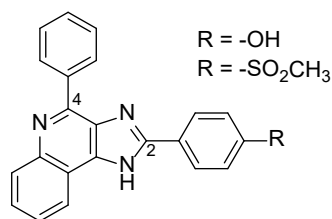


Figure 35. Examples of 2-(*para*-substituted-phenyl)-4-phenyl-1*H*-imidazo[4,5-*c*]quinoline derivatives

In the first step (i), quinoline-2,4-diol was treated with nitric acid to produce 3-nitroquinoline-2,4-diol. In step two, 3-nitroquinoline-2,4-diol was chlorinated with phenylphosphonic dichloride to generate 2,4-dichloro-3-nitroquinoline (ii). This product was aminated with 28% aqueous ammonia in step three to give 2-chloro-3-nitroquinoline-4-amine (iii). In step four, Fe powder and hydrochloric acid reduced the 3-nitro group to an amine, thereby providing the vicinal diamine, 2-chloroquinoline-3,4-diamine (iv) (42).

Two different step-5 reaction protocols cyclized the vicinal diamine with a carboxylic acid.⁴ The first reaction protocol, general procedure A (v.a.), utilized PPA for the initial condensation between 2-chloroquinoline-3,4-diamine and the appropriate carboxylic acid, followed by the cyclization to the imidazole (56). The second reaction protocol was a two-step process (general procedure B) (v.b.), first using TCFH as a coupling agent with *N*-methylimidazole to make an adduct intermediate, which then reacted with the appropriate carboxylic acid to produce an acyl imidazolium electrophile (Figure 36) (12). An amine of the diamine—a weak Lewis base—then performed a nucleophilic attack at the acyl imidazolium's highly partially charged carbonyl carbon to

⁴ Majority of carboxylic acids used in this study were commercially available. The following carboxylic acids were not commercially available and therefore, were synthesized for this study: 5,5,5-trifluoro-2-(3,3,3-trifluoropropyl)pentanoic acid, cyclononancarboxylic acid, cyclodecanocarboxylic acid and (1*R*,2*R*,4*R*)- & (1*S*,2*S*,4*S*)-bicyclo[2.2.2]oct-5-ene carboxylic acid.

make an amide intermediate (not shown). The published method uses room temperature (12). However, we found that heating at 60 °C brought the reaction to completion and increased the yield. The crude amide was subjected to a base-catalyzed cyclization reaction to close the imidazole ring and incorporate a 2 position substitution on the quinoline scaffold.

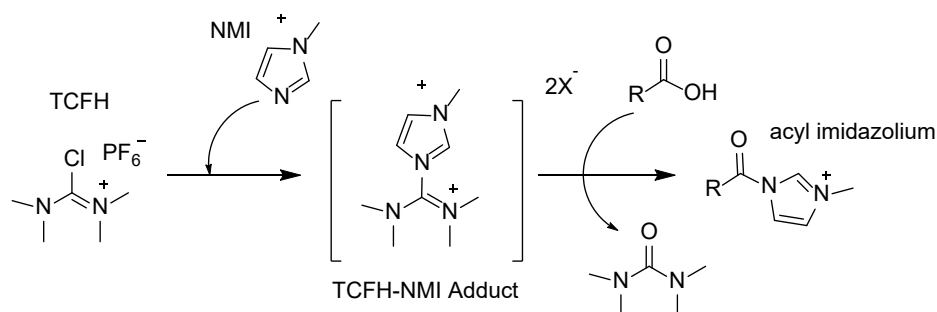


Figure 36. Creation of an acyl imidazolium electrophile to facilitate the substitution reaction between the vicinal diamine and the carboxylic acid (12)

The last step, a C–N cross-coupling reaction, was performed using three different reaction protocols. The first two, general procedures C and D, are palladium-catalyzed amination reactions (Figure 37) (109). The first reaction protocol utilized the palladium catalyst tris(dibenzylideneacetone) dipalladium (0) ($\text{Pd}_2(\text{dba})_3$) (general procedure C – (vi.c.)) (55; 93; 109), while the second used a water-activated palladium acetate ($\text{Pd}(\text{OAc})_2$) catalyst (general procedure D – (vi.d.)) (38; 93).

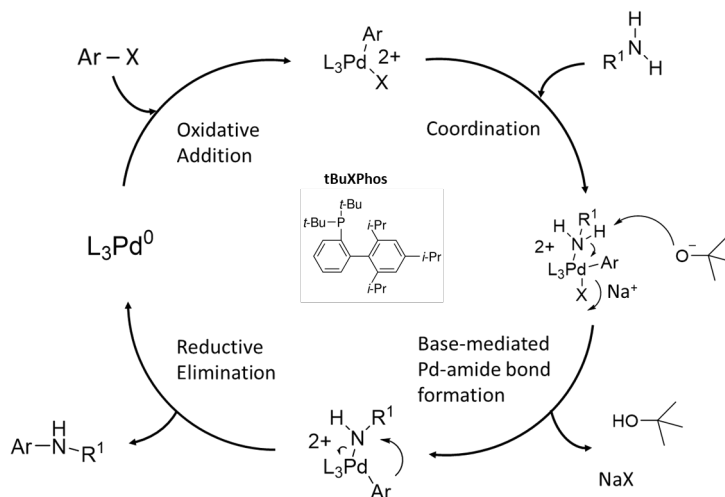


Figure 37. Palladium-catalyzed amination reaction cycle for general procedures C & D. After the catalyst is activated to Pd⁰, the reaction cycle will go through 1) oxidative addition of aryl halide to Pd⁰, 2) coordination of aniline to Pd-complex with aryl halide, 3) base-mediated Pd-amide bond formation, 4) reductive elimination of imidazoquinoline amine from Pd catalyst.

*t*BuXPhos provides electron density to stabilize the reactive L₃Pd⁰ catalyst. The 4-chloroimidazoquinoline step-5 product will undergo an oxidative addition reaction with the palladium catalyst. The respective aniline will then coordinate and bind to the Pd catalyst. Sodium butoxide will initiate the rearrangement of atoms around the Pd catalyst by deprotonating hydrogen from the aniline, which will cause the halide ion to leave. Reductive elimination is the last step in this catalytic cycle that performs the C–N cross-coupling reaction to produce the final product.

The third reaction protocol was a microwave-assisted reaction in ethanol at 130°C to achieve the final 1*H*-imidazo[4,5-*c*]quinolin-4-amine derivative (general procedure E – (vi.e.)) (56).

The first library of PAMs consisted of fifteen derivatives (Table 1). Compounds **1** – **3** have alkyl 2 position substitutions, with compound **3** aiming to investigate the

fluorine effect on the SAR of compound **2** (76). The carboxylic acid for compound **3** was made through enolate chemistry by the deprotonation of ethyl 2-cyanoacetate with potassium carbonate, followed by the S_N2 reaction of the subsequent anion with two equivalents of 3-bromo-1,1,1-trifluoropropane (Figure 38) (79). The ester product obtained underwent a series of base-catalyzed reactions: hydrolysis of the ester to a carboxylic acid, decarboxylation, hydrolysis of the nitrile to an amide, and the hydrolysis of the amide to the final carboxylic acid.

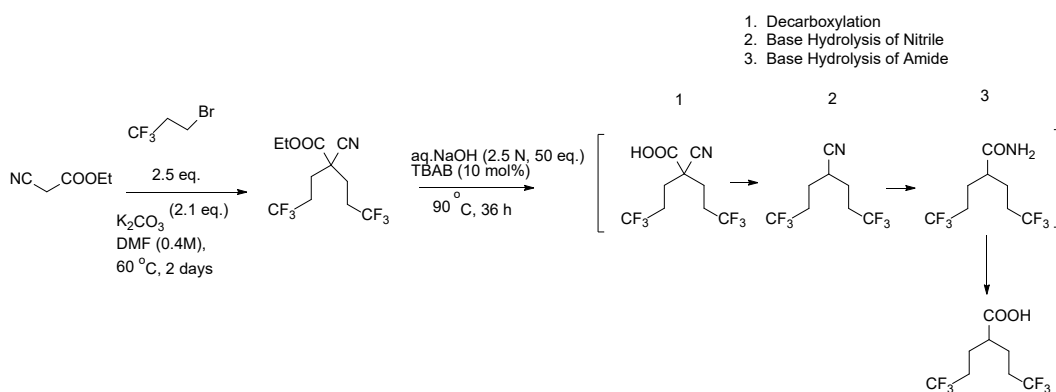


Figure 38. Synthesis scheme for 5,5,5-trifluoro-2-(3,3,3-trifluoropropyl)pentanoic acid for compound **3**

Compound **4** had a similar objective to test the fluorine effect on the SAR of a known PAM, compound **8**, with a trifluoromethyl group at the 4 position of the cyclohexyl ring.

A two-step process synthesized the carboxylic acids for compounds **12** and **13** (Figure 39).

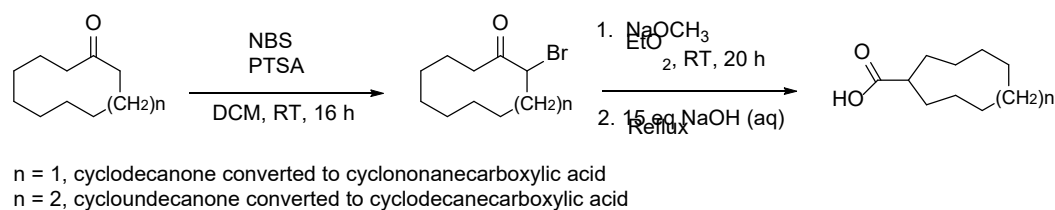
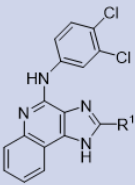
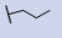
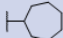
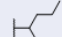
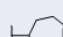
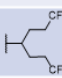
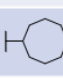
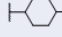
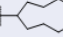

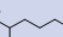

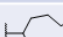





Figure 39. Synthesis of cyclononane and cyclodecanecarboxylic acids for compounds 12 and 13. Two-step process: 1) α -bromination followed by 2) Favorskii ring contraction.

First, an α -bromocycloketone using *N*-bromosuccinimide and *p*-toluenesulfonic acid (PTSA) was formed (98), followed by a Favorskii ring contraction reaction (67; 116); a base-catalyzed rearrangement of the α -bromo-cycloalkylketone compound into a methyl cycloalkyl carboxylate using sodium methoxide in diethyl ether. Methoxide removes an α -hydrogen, allowing free electrons to displace the bromide ion, creating a cyclopropenone intermediate. Methoxide then attacks the carbonyl, initiating the ring contraction and carboxylate formation, reducing the ring by one methylene ($-\text{CH}_2-$) group. The carboxylic acid is formed by refluxing the methyl cycloalkyl carboxylate with sodium hydroxide, followed by the protonation of the carboxylate with 1M HCl.

Table 1. Hydrophobic alkyl and cycloalkyl substitutions at the 2 position of the 1*H*-imidazo[4,5-*c*]quinolin-4-amine scaffold to investigate fine-tuning of the allosteric enhancement by PAM derivatives

	Compound ID		R ¹	Compound		R ¹
	MRS7529	1		MRS3718	9	
	MRS7551	2		MRS7788	10	
	MRS8048	3		MRS7530	11	
	MRS7676	4		MRS7827	12	
	MRS7431	5		MRS7828	13	
	MRS3720	6		MRS7829	14	
	MRS3557	7		MRS7830	15	
	LUF6000	8				

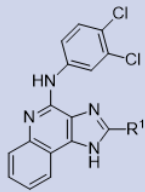
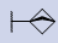
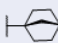

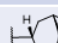


Final compounds **1 – 5** and **10 – 14** were made using the step-6 general procedure C, with a percent yield ranging from 5 to 28%. Compound **15** was synthesized using the step-6 general procedure E for the C–N cross-coupling of the step-5 product to 3,4-dichloroaniline, having a percent yield of 25%.

Compounds **5 – 15** have cycloalkyl ring substitutions at the 2 position of the 1*H*-imidazo[4,5-*c*]quinolin-4-amine scaffold, ranging from cyclopropyl to cyclododecyl. Compounds **6 – 9** are compounds previously reported by the Jacobson laboratory (56). They were included in this study to get a comprehensive understanding of the SAR of a large set of derivatives of various sized hydrophobic rings under the same kinetic binding and functional assay experimental conditions.

Compound **10** is a cyclohept-4-enyl group with a double bond placed at C4 of the cycloheptyl ring. Due to the double bond functionality on the ring at C4, this derivative has a plane of symmetry; therefore, only one isomer is possible. Compounds **1 – 14**, except for compound **10**, went through the step-5 general procedure A. Compound **10** required the alternative cyclization reaction, utilizing the step-5 general procedure B (12). Step-5 general procedure B was exclusively used to make subsequent derivatives—despite it being a two-step protocol—because of the ease of execution compared to using PPA from step-5 general procedure A.

Compounds **16 – 21** consist of various sized bicyclic derivatives at the 2 position (Table 2). Compounds **16 – 18** are quaternary bicyclic derivatives with only one isomer possible, being that they lack a chiral center. Compound **19** is like compound **18** in that both have a cyclooctyl ring with a one-carbon bridge, differing in that the compound **18** bridge creates a quaternary carbon, and the compound **19** bridge creates products with an *endo* and *exo* stereochemical orientation. Compound **19** was formed with the *endo* stereochemistry orientation based on the corresponding carboxylic acid as a commercial starting material with the *endo* stereochemistry orientation.

Table 2. Bridged bicyclic substitutions to investigate the effects of rigid ring systems on the allosteric enhancement of the PAM derivatives

	Compound		R ¹
	MRS7962	16	
	MRS7963	17	
	MRS7964	18	
	MRS7965	19	
	MRS7966	20	
	MRS7974	21	

Compounds **16** – **19** were produced using the step-6 general procedure D, having a percent yield ranging from 2 to 33%. The change in procedure was an attempt to improve the cross-coupling reaction yield with the use of Pd(OAc)₂ rather than the Pd₂(dba)₃ catalyst, with the rationale being that the sizeable dba ligand removed during the activation of the palladium catalyst might sterically hinder the formation of product in the catalytic cycle (93). However, similar yields were obtained for the step-6 general procedures C and D.

In the cyclopropanation reaction of compound **10** to form compound **20**, only the *cis* stereoisomer was produced and isolated, which was confirmed by NMR (Figure 40). The reaction is initiated when the π electrons from the cyclohept-4-enyl ring of compound **10** attack the electrophilic iodomethylzinc iodide carbenoid, formed from diiodomethane and diethylzinc (25).

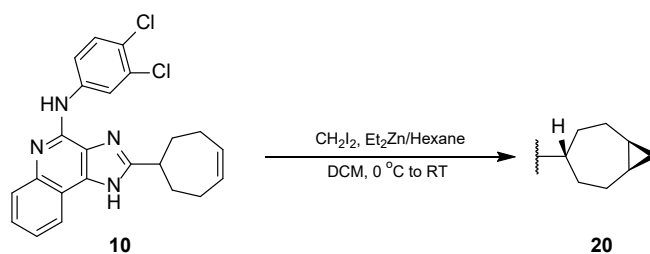


Figure 40. Cyclopropanation reaction of compound 10 to form compound 20

Compound **21** is the only bridged derivative having a two-carbon bridge with a double bond to provide extra rigidity to the ring system. This product resulted from a bicyclic carboxylic acid obtained upon saponification of the methyl ester products formed from a Diels-Alder reaction between 1,3-cyclohexadiene and methyl acrylate (Figure 41) (100; 101).

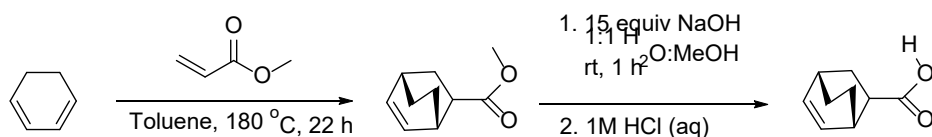
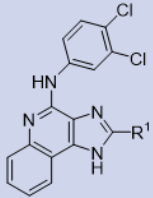
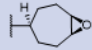
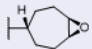
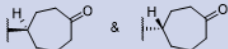

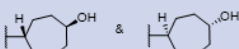


Figure 41. Synthesis of (1R,2R,4R)- & (1S,2S,4S)-bicyclo[2.2.2]oct-5-ene carboxylic acid for compound 21

Two pairs of enantiomers that are diastereoisomers to one another were isolated from the Diels-Alder reaction, the majority being the *endo* enantiomeric pair, likely due to the lower transition state energy favoring the formation of the *endo* over *exo* stereoisomers. Thus, compound **21** is a racemic mixture of *endo* enantiomers.

The double bond of compound **10** allowed for installing hydrophilic oxygen-containing functional groups (Table 3 and Figure 42).

Table 3. Introduction of oxygen-containing functional groups to compound 10 to investigate effects of hydrophilic moieties on the allosteric enhancement of PAM derivatives

	Compound		R ¹
	MRS7969	22	
	MRS7970	23	
	MRS7971	24	
	MRS7972	25	
	MRS7973	26	

Two oxirane compounds, **22** and **23**, were produced in the same epoxidation reaction of compound **10** using *m*-CPBA (**3**). Two diastereomer products were resolved during the purification. Compounds **25** and **26** were made in the same hydroboration-oxidation reaction (**27**); though, only the enantiomeric pairs of the possible alcohols and not each stereoisomer were separable. The enantiomeric pairs are diastereomers to one another and are racemic mixtures. Compound **24** was made from treating a mixture of compounds **25** and **26** with the oxidizing agent, DMP (**9**), producing the racemic carbonyl enantiomers.

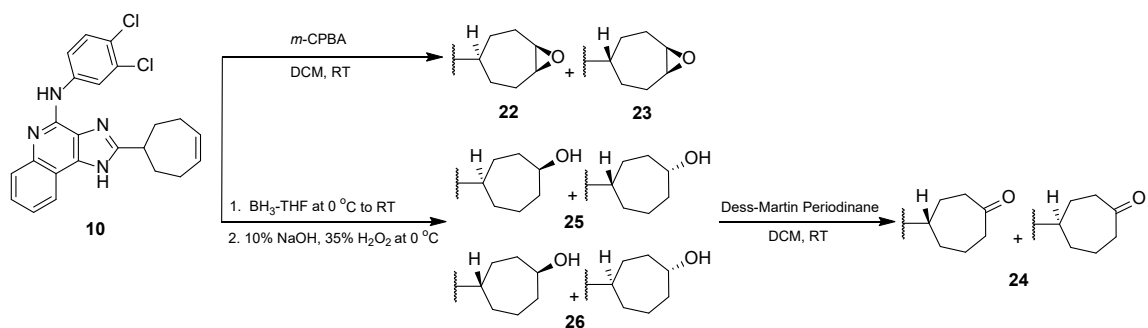
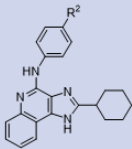

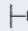
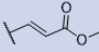
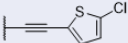


Figure 42. Oxidation reactions of compound 10 to produce derivatives with hydrophilic substitutions. 1) Epoxidation reaction of compound **10** to form compounds **22** and **23**, 6-12%; 2) Hydroboration-oxidation reaction of compound **10** to form compounds **25** and **26**, 8-12%; 3) Oxidation reaction of a mixture of compounds **25** and **26** to form compound **24**, 23%.

Table 4 shows 1*H*-imidazo[4,5-*c*]quinolin-4-amine derivatives with various *para*-substitutions on the 4-phenylamino moiety. Compounds **27** and **28** have 4-iodophenyl and 4-bromophenyl substitutions, respectively. Both were produced using the step-6 general procedure E microwave-assisted reaction between the 4-chloro-2-cyclohexyl-imidazo[4,5-*c*]quinoline amine step-5 product with their respective aniline, *p*-iodoaniline or *p*-bromoaniline, in ethanol. This protocol resulted in fewer by-products than the previous two step-6 reactions, thus simplifying the separation by flash silica gel chromatography. The percent yield using this protocol for compound **27** was 61%, and the percent yield of **28** was 10%.

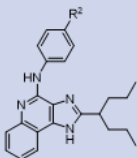

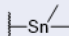
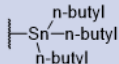
Table 4. Introduction of various functionalities in the 4 position of the phenylamino group to investigate allosteric tolerance/enhancement of PAM derivatives

	Compound		R ²
	MRS7967	27	
	MRS7968	28	
	MRS7975	29	
	MRS8055	30	

Compound **29** is an 80:20 mixture of *E*- and *Z*- isomers, having a methyl acrylate 4 position substitution on the phenylamino moiety, generated from a Heck reaction between compound **28** and methyl acrylate using a Pd(OAc)₂ catalyst (90). Compound **30** has a *para*-(5-chlorothiophen-2-yl)ethynyl substitution, generated from a Sonogashira reaction between compound **27** and 2-chloro-5-ethynylthiophene using a PdCl₂(PPh₃)₂ catalyst (106; 112). A reaction was first attempted using compound **28**, but no product was formed—only with compound **27**, presumably because iodide was the better leaving group.

Compound **31** was produced to make an allosteric biological probe (Table 5). The trimethyl- and tributyl-stannyl derivatives, **32** and **33**, were produced from compound **31** (5) as potential precursors for a radio-iodination reaction to make the ¹²⁵I radioligand (104).

Table 5. Precursor 4 position substituted phenylamino 1*H*-imidazo[4,5-*c*]quinolin-4-amine derivatives for the preparation of a ¹²⁵I radioligand

	Compound		R ²
	MRS8054	31	
	MRS8057	32	
	MRS8061	33	

KINETIC BINDING STUDY RESULTS

Two types of single-point kinetic assays using fixed PAM concentrations—ligand dissociation and equilibrium binding—characterized the allosteric influence of the new derivatives on hA₃AR agonist radioligand binding. The single-point assays also helped facilitate quick design decisions of follow-on derivatives. Dissociation (K_d) and association (K_a) constants cannot be calculated from these experiments because dissociation rate constants (k_{-1}) and association rate constants (k_{+1}) were not derived from multiple time point measurements.

Single-point Dissociation Assay Results

In Figure 43, single-point dissociation assays were conducted to measure the relative influence each derivative had on the dissociation of [¹²⁵I]I-AB-MECA from the hA₃AR after 60 minutes of incubating the A₃AR-overexpressing HEK 293 cell membranes with the competitive antagonist adenosine-5'-*N*-ethylcarboxamide (NECA) (Table 11, Appendix H). The horizontal dotted line represents the control amount of

agonist radioligand remaining bound without an enhancer, 26% of the amount bound at time 0.

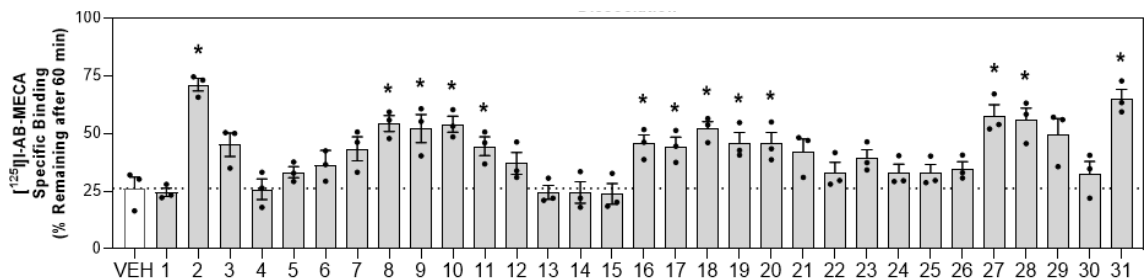


Figure 43. Effect of PAM derivatives (10 μ M) on dissociation of [125 I]I-AB-MECA (0.3 nM) using hA₃ARs. HEK 293 membranes stably overexpressing the hA₃AR were incubated with \sim 0.3 nM [125 I]I-AB-MECA and 10 μ M of the indicated modulator for 3 h. The addition of 100 μ M NECA initiated dissociation. The amount of radioligand remaining after 60 min was measured. Statistical significance was determined by two-tailed paired student's t-test (n=3; * denotes P < 0.05). Data are presented as mean \pm SEM.⁵

Compounds **1** – **4** showed varying results, with compound **2** ((2-heptan-4-yl)/MRS7551) slowing agonist dissociation the most, with 71% of agonist binding remaining. Despite being the hexa-fluoro equivalent of compound **2**, compound **3** did not slow agonist dissociation compared to the control (P-value = 0.958).

Compounds **5** – **15** represent the 2-substitution cycloalkyl ring systems ranging from three to twelve carbons. As the hydrophobic ring system increased from cyclopropyl **5** to cyclooctyl **11**, there was a steady increase in percent agonist remaining bound to the A₃AR compared to the control, with compounds **8** (cyclohexyl) – **11** (cyclooctyl) displaying the most bound, ranging from 45% to 54%. As the ring size

⁵ Data generated from dissociation binding studies is unpublished data. Experiments and raw/processed data were generated by Courtney Fisher and Dr. John Auchampach of the Department of Pharmacology and Toxicology at the Medical College of Wisconsin.

increased from cyclononyl **12** to cyclododecyl **15**, there was no apparent slowing of agonist dissociation compared to the control (P-values = 0.188, 0.786, 0.808, and 0.735, respectively).

Compounds **16** – **21** had bicyclic ring systems of varying sizes. All of these compounds except for compound **21** slowed the agonist dissociation compared to the control. The percent of radioligand remaining bound in the presence of modulators **16** – **20** ranged from 45% to 52%. The compounds with hydrophilic substitutions, **22** – **26**, did not slow radioligand dissociation compared to the control.

Among the *para*-substituted phenyl amino derivatives **27** – **30**, compounds **27** (4-iodophenyl) and **28** (4-bromophenyl) slowed the radioligand dissociation rate the most, with 57% and 56% radioligand remaining, respectively. Compounds **29** (methyl (E)- & (Z)-3-(4-aminophenylacrylate)) and **30** (((5-chlorothiophen-2-yl)ethynyl)phenyl)) did not slow the dissociation rate of the agonist compared to the control (P-values = 0.052 and 0.450, respectively).

Compound **31**, a combination of compounds **2** and **27**, i.e., containing both 2-(heptan-4-yl) and 4-iodophenylamino substitutions, considerably slowed radioligand dissociation with 65% remaining A₃AR-bound.

Single-point Equilibrium Binding Assay Results

Figure 44 shows single-point equilibrium binding assay results, displaying the positive, negative, or neutral percent change from the vehicle of the radioligand in the presence of a fixed concentration (10 μM) of each modulator under equilibrium conditions (Table 12, Appendix H). The radioligand bound was measured at 18 h, which is assumed to be sufficiently long to achieve equilibrium ($k_{on}=k_{off}$) for the A₃AR binding

of [¹²⁵I]I-AB-MECA. Thus, bars above the 0 line represent compounds that positively modulate radioligand binding as PAMs, resulting from a possible increase of agonist affinity for the receptor or an increase in density of binding sites for the agonist. Bars significantly below the 0 line represent a dominant negative modulatory effect on hA₃AR agonist radioligand binding, expressed as % inhibition by the derivative, presumably as an A₃AR orthosteric antagonist.

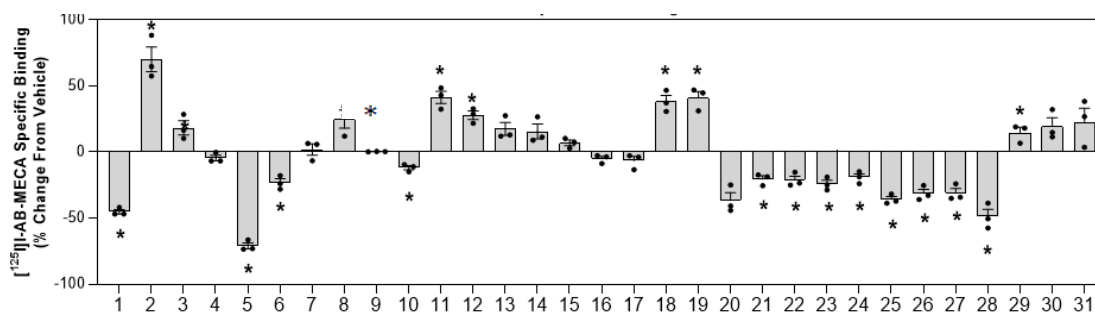


Figure 44. Effect of PAM derivatives (10 μ M) on equilibrium binding of [¹²⁵I]I-AB-MECA (0.3 nM) at the hA₃AR. HEK 293 membranes stably overexpressing the hA₃AR were incubated with \sim 0.3 nM [¹²⁵I]I-AB-MECA and 10 μ M of the indicated modulator for \sim 18 hours to reach equilibrium. The amount of specific binding was determined, and % change from the vehicle was calculated. Statistical significance was determined by two-tailed paired student's t-test (n=3; * denotes P < 0.05). Data are presented as mean \pm SEM.⁶

Comparing compounds **1** – **4**, the propyl derivative **1** decreased agonist equilibrium binding with a -45% change from the vehicle. Compound **2** increased agonist equilibrium binding the most with 70% change from the vehicle.

Of the cycloalkyl 2-substituted derivatives, compound **5** (cyclopropyl) decreased agonist equilibrium binding by -71% compared to the control, and compound **11**

⁶ Data generated from equilibrium binding studies is unpublished data. Experiments and raw/processed data were generated by Courtney Fisher and Dr. John Auchampach of the Department of Pharmacology and Toxicology at the Medical College of Wisconsin.

(cyclooctyl) increased agonist equilibrium binding by 41% compared to the control.

Compounds **7**, **9**, and **13 – 15** had neutral results and did not affect any change in agonist equilibrium binding compared to the control.

Of the bridged compounds **16 – 21**, compounds **18** (2-bicyclo[3.3.1]nonan-1-yl) and **19** (2-(1R,3s,5S)-bicyclo[3.3.1]nonan-3-yl) increased agonist equilibrium binding with 38% and 41% change from vehicle, respectively. Compounds **16** and **17** did not affect radioligand binding, where compounds **20** and **21** decreased agonist equilibrium binding with -37% and -21% change from the vehicle, respectively.

All the derivatives with hydrophilic substitutions, **22 – 26**, decreased equilibrium binding of the radioligand to the A₃AR, with compound **25** having the most significant decrease in agonist equilibrium binding with -36% change from the vehicle when compared to the control.

Of the *para*-substituted phenylamino derivatives, compound **29** increased agonist equilibrium binding the most with a 15% change from the vehicle. Compounds **27** and **28** decreased agonist equilibrium binding with -31% and -49% change from the vehicle, respectively. Compound **31**, 2-heptan-4-yl-*N*-(4-iodophenyl) derivative, did not affect agonist equilibrium binding compared to control.

RESULTS OF RECEPTOR ACTIVATION MEASURED BY [³⁵S]GTP γ S BINDING

In addition to the kinetic binding studies, the ability of each compound to allosterically modulate hA₃AR G protein activation by Cl-IB-MECA was measured using a [³⁵S]GTP γ S functional assay. Concentration-response curves were generated for each compound, including a curve for the control alone and curves for the radioligand with 0.1 μ M, 1.0 μ M, and 10 μ M of the modulator (Figures 45 – 49). For each modulator, EC₅₀,

expressed in nM, and E_{max} , expressed as % efficacy compared to control, values are listed in Tables 13 – 17 of Appendix H.

Figure 45, referencing 1.0 μ M of modulator used in the [35 S]GTP γ S binding

assays for compounds **1 – 15**, compounds **2, 8, 10**, and **12** doubled agonist E_{max} compared to the control (Table 13, Appendix H).

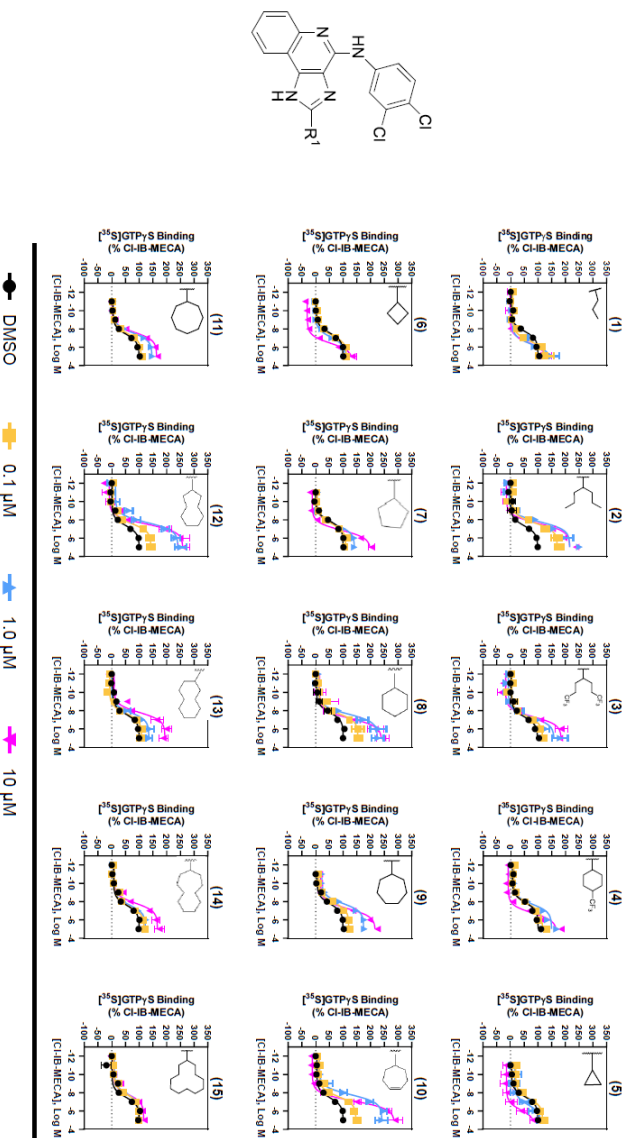


Figure 45. Effect of alkyl- and cycloalkyl-substituted PAM derivatives on hA_3AR activation by Cl-IB-MECA as determined in [35 S]GTP γ S binding. HEK

293 cells were treated with Cl-IB-MECA, modulators, radiolabeled [35 S]GTP γ S, and allowed to incubate for 2 h at room temperature. PSB-603 was added to block $A_{2B}AR$. 1 μ L/mL of ADA was added to degrade endogenous adenosine. Reactions were stopped by rapid filtration through a Whatman GF/B filter. Trapped radioactivity was measured by liquid scintillation spectrometry. Nonspecific binding of [35 S]GTP γ S was measured in the presence of 10 μ M of GTP γ S. Cl-IB-MECA potency and maximal efficacy were measured using 0.1 μ M, 1.0 μ M, and 10 μ M of the modulator. Results were normalized to the Cl-IB-MECA E_{max} value (%) of receptor activation.⁷

⁷ Data generated from WT hA_3AR , WT mA_3AR , and chimera A_3AR [35 S]GTP γ S activation assays is unpublished data. Experiments and raw/processed data were generated by Courtney Fisher and Dr.

There was a two-fold increase in agonist potency in the presence of 1 μ M of compound **12** compared to the agonist alone (P-value = 0.009). EC₅₀ and E_{max} of the radioligand increased in the presence of 1 μ M of compound **5** to compound **8**. As shown in Figure 45, the 1.0 μ M concentration-response curves steadily shift leftward, indicating an increase in potency, and steadily shift upward, indicating an increase in E_{max}. This change is represented by the cyclopropyl to the cyclohexyl 2 position substitutions of the 2-cycloalkyl-*N*-(3,4-dichlorophenyl)-1*H*-imidazo[4,5-*c*]quinolin-4-amine derivatives. As the cycloalkyl ring increased in size from cyclodecyl to cyclododecyl, there was no change in agonist potency but a gradual decrease in its E_{max}. The fluorinated compounds, **3** and **4**, at 1 μ M moderately improved agonist E_{max} but did not influence agonist potency.

Compounds **16** – **20** moderately enhanced [³⁵S]GTP γ S binding in the presence of agonist CI-IB-MECA compared to the control (Figure 46 and Table 14, Appendix H). Of the bicyclic compounds, compound **18**, at 1 μ M, doubled the agonist E_{max} compared to the control but produced no change in agonist potency. Compound **17** was the only bicyclic compound to induce a four-fold decrease in agonist potency at 1 μ M compared to the control (P-value = 0.049). Compound **21** did not influence agonist potency and led to a moderate increase in agonist E_{max} (167%). All bicyclic compounds appear to behave as inverse agonists, and compound **21** at 10 μ M decreased the basal efficacy the most, at the lowest agonist concentration by ~100%.

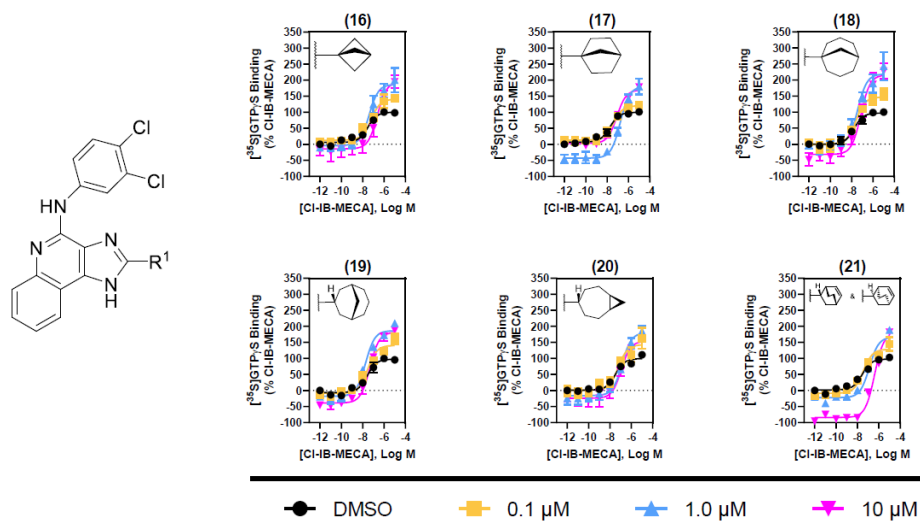


Figure 46. Effect of bridged PAM derivatives on hA₃AR activation by CI-IB-MECA determined using [³⁵S]GTPγS binding. Assay procedures were similar to those described in Figure 45.

Compounds **22** – **26**, derivatives with hydrophilic substitutions, moderately allosterically enhanced [³⁵S]GTPγS binding (Figure 47 and Table 15, Appendix H). However, all the modulators at concentrations of 0.1 μM and 1.0 μM had no significant effect on agonist potency compared to the control. At 1.0 μM, only compounds **23**, **24**, and **26** increased agonist E_{max} compared to the control, ranging from 167% to 186% maximal efficacy of the agonist alone. Like compound **21**, compound **26** behaved as an inverse agonist at 10 μM, decreasing basal efficacy at the lowest agonist concentration by ~50%.

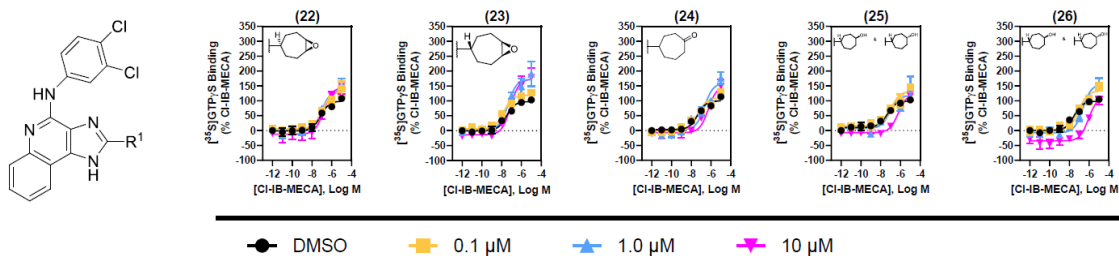


Figure 47. Effect of PAM derivatives bearing hydrophilic substituents on $[^{35}\text{S}]\text{GTP}\gamma\text{S}$ binding induced by Cl-IB-MECA using hA_3ARs . Assay procedures were similar to those described in Figure 45.

Of the *para*-substituted phenylamino derivatives, compounds **27**, **29**, and **30** at 1.0 μM moderately increased agonist efficacy compared to control (Figure 48 and Table 16, Appendix H). At 1 μM , compound **28** doubled the agonist efficacy compared to the control. None of the *para*-substituted phenylamino derivatives influenced agonist potency compared to the control.

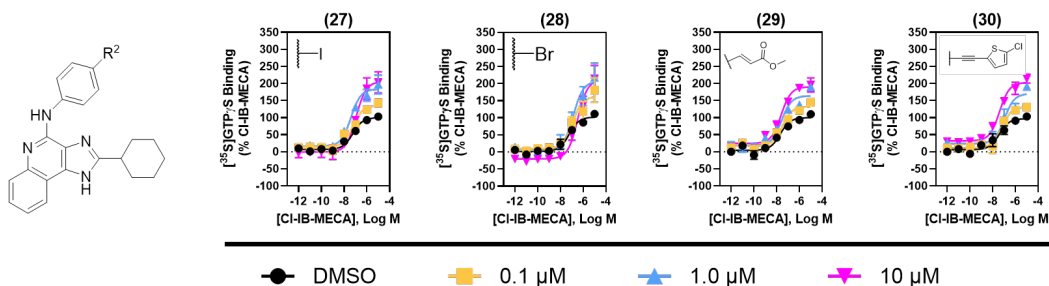


Figure 48. Effect of *para*-phenylamino substituted PAM derivatives on $[^{35}\text{S}]\text{GTP}\gamma\text{S}$ binding induced by Cl-IB-MECA using hA_3ARs . Assay procedures were similar to those described in Figure 45.

Compound **31** was synthesized following the favorable results seen for compounds **2** and **27** on dissociation kinetics and $[^{35}\text{S}]\text{GTP}\gamma\text{S}$ binding (Figure 49 and Table 17, Appendix H). It combines structural features present in compounds **2** and **27**.

Compared to the control at 1 μM , compound **31** did not improve agonist potency but doubled agonist E_{max} compared to the control.

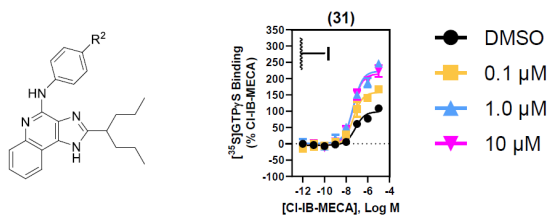


Figure 49. Effect of compound 31 ($R^2 = \text{I}$) on $[^{35}\text{S}]\text{GTP}\gamma\text{S}$ binding, indicating hA_3AR activation by CI-IB-MECA. Assay procedures were similar to those described in Figure 45.

CHIMERIC RECEPTOR STUDY RESULTS

Chimeric A_3AR Radioligand Binding Studies

Radioligand binding studies were conducted with $[^{125}\text{I}]\text{I-AB-MECA}$ in the presence of 10 μM of compound **8** (LUF6000) using human, mouse, mouse $_{\text{Out}}$ /human $_{\text{In}}$ and human $_{\text{Out}}$ /mouse $_{\text{In}}$ A_3AR s (Figure 50 & Table 18, Appendix H). As expected from previous radioligand studies (30), compound **8** slowed the radioligand dissociation from the hA_3AR but not from the mA_3AR . With 10 μM of compound **8** present, it took 97.6 min for half the WT hA_3AR s to dissociate from the radioligand, twice the amount of time compared to the control, taking 39.8 min for half the receptors to dissociate from the radioligand without the enhancer present.

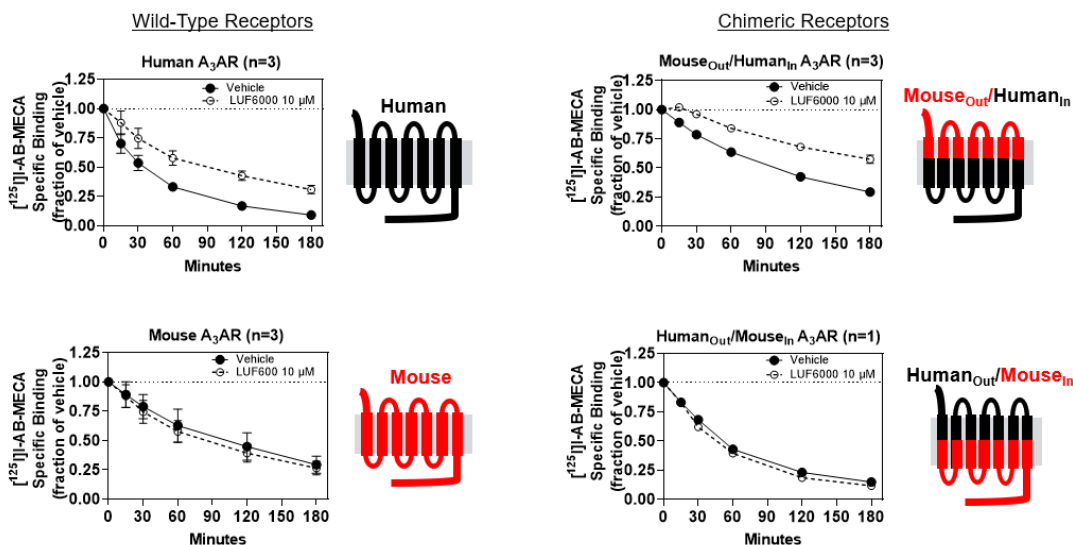


Figure 50. Effect of compound 8 on dissociation rate of [¹²⁵I]I-AB-MECA using WT and chimeric A₃ARs. Assay procedures were similar to those described in Figure 19.

With the mouse_{Out}/human_{In} chimeric receptors, compound **8** slowed the dissociation rate of the radioligand similarly to the dissociation experiments with the WT hA₃AR, doubling the time required for half the receptors incubated with the modulator to dissociate from the radioligand ($t_{1/2} = 208$ min) compared to the receptors without the enhancer ($t_{1/2} = 98.6$ min). Compound **8** did not slow the radioligand dissociation from the human_{Out}/mouse_{In} chimeric receptors.

Activation of Chimeric Receptors Studied with [³⁵S]GTP γ S Binding

The effects of compounds **5** (Figure 51 and Table 19, Appendix H) and **8** (Figure 52 and Table 20, Appendix H) on [³⁵S]GTP γ S binding induced by C1-IB-MECA using WT and chimeric A₃ARs were evaluated. As predicted, compound **5** caused no change to the efficacy of the agonist but elicited a substantial decrease in its potency as the concentration of the modulator increased in [³⁵S]GTP γ S assays with the hA₃AR (Table

19, Appendix H). When compound **5** was incubated with the mA₃AR, little to no change in efficacy or potency of the agonist was noted. Similar to the results of the WT mA₃AR, compound **5** minimally influenced efficacy or potency of the agonist binding to the mouse_{Out}/human_{In} chimeric receptor. Concerning the human_{Out}/mouse_{In} receptor, the enhancer caused similar effects to the hA₃AR, minimally decreasing efficacy and substantially reducing the potency of the agonist as the modulator concentration increased.

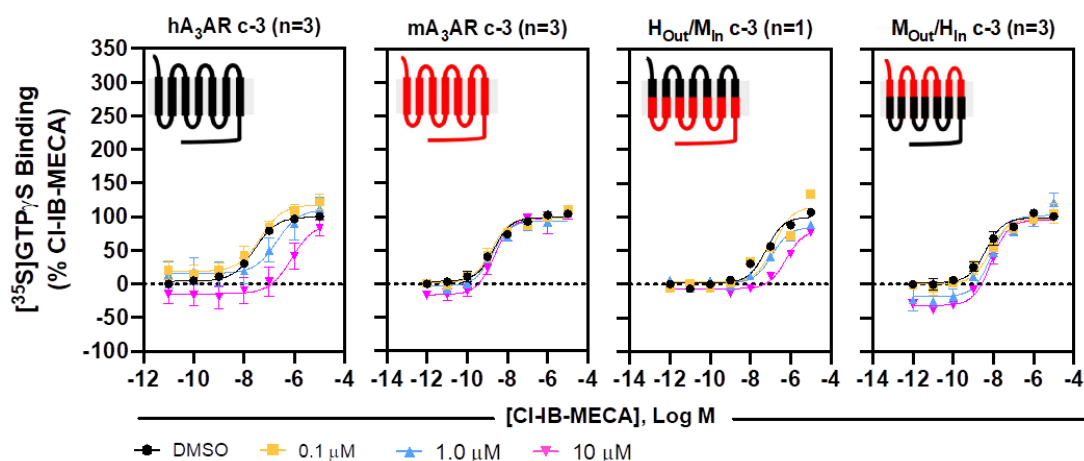


Figure 51. Effect of compound **5 on [³⁵S]GTP_γS binding induced by CI-IB-MECA using WT and chimeric A₃ARs.** Assay procedures were similar to those described in Figure 45.

As expected from prior studies of species differences of the A₃AR (30), compound **8** potentiated the efficacy of CI-IB-MECA in the WT hA₃AR but not the WT mA₃AR. In the mouse_{Out}/human_{In} A₃AR, compound **8** at every concentration potentiated the agonist efficacy, having an E_{max} of 195% with 10 μM of enhancer used. Furthermore, the agonist was 17-fold more potent in the presence of 1.0 μM of modulator compared to the control with the mouse_{Out}/human_{In} chimeric receptors (EC₅₀ = 0.597 ± 0.185 nM, P-

value = 0.0002). In the human_{Out}/mouse_{In} A₃AR, at 10 μ M, compound **8** decreased the potency of the agonist, presumably binding to the orthosteric binding site as a competitive antagonist.

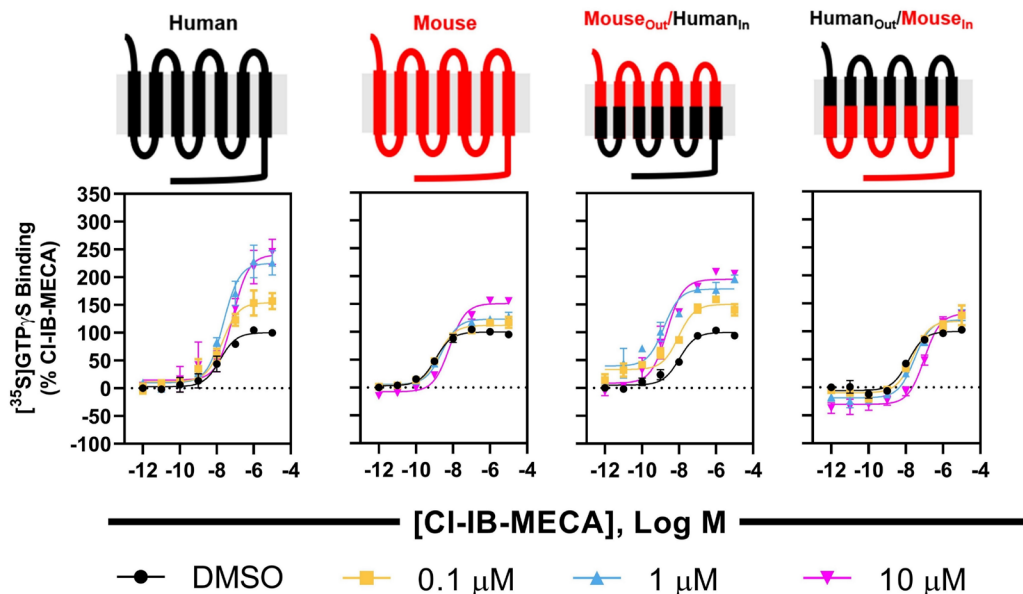


Figure 52. Effect of compound **8** on [³⁵S]GTP γ S binding induced by CI-IB-MECA using WT and chimeric A₃ARs. Assay procedures were similar to those described in Figure 45.

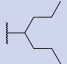
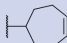
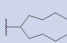
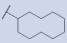
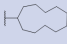


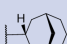
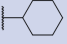
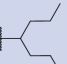
OFF-TARGET BINDING RESULTS

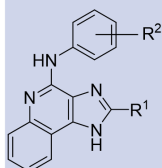
A total of ten derivatives were tested for off-target binding against forty-five other receptors, transporters, and channels (Table 6). Only a few off-target interactions were observed, the lowest K_i being for compound **31** at the translocator protein (TSPO) with K_i = 0.123 μ M. The two 4-iodophenyl derivatives tested, compounds **27** and **31**, were the only derivatives interacting with TSPO.

Most derivatives interacted with one or two sigma receptors, specifically σ_1 and σ_2 . Compound **31** had the lowest K_i observed, 0.891 μ M, among the derivatives

interacting with a sigma receptor. Compound **19** interacted with the most off-target sites: kappa (KOR) and mu (MOR) opioid receptors, σ_1 , σ_2 , dopamine transporter (DAT), and serotonin 5HT_{2B} receptors; interacting most strongly with DAT at $K_i = 0.467 \mu\text{M}$.

Table 6. Off-target analyses of select PAM derivatives with forty-five other receptors, transporters, and channels

	Derivative		Protein	K_i (μM)
	R ¹	R ²		
2		3,4-dichloro	5HT _{2B}	1.36
			σ_1	1.48
			σ_2	1.36
10		3,4-dichloro	σ_1	4.64
			σ_2	0.575
12		3,4-dichloro	σ_1	5.15
			σ_2	0.907
13		3,4-dichloro	σ_2	3.62
14		3,4-dichloro	D ₃	5.28
15		3,4-dichloro	D ₃	7.63
			σ_1	3.02
			σ_2	2.84
18		3,4-dichloro	σ_1	2.34
			σ_2	1.34
19		3,4-dichloro	MOR	7.22
			σ_1	2.42
			σ_2	3.43
			KOR	5.50
			DAT	0.467
			5HT _{2B}	3.25
27		4-iodo	D ₃	0.846
			TSPO	0.427
			σ_2	3.01
31		4-iodo	5HT _{2B}	2.60
			TSPO	0.123
			σ_2	0.891



PHARMACOKINETIC STUDY RESULTS

We chose compound **10**, 2-(cyclohept-4-en-1-yl)-*N*-(3,4-dichlorophenyl)-1*H*-imidazo[4,5-*c*]quinolin-4-amine, as a potent, specific, and selective A₃AR modulator to assess *in vivo* and *in vitro* the pharmacological and ADMET properties.

In Vitro Pharmacokinetic Study Results

In vitro pharmacokinetic parameters of compound **10** are represented in Table 7. When compound **10** was dissolved in simulated intestinal and gastric fluids, 88.1% and 69.1% of the compound remained after two hours, respectively. Among five cytochrome P450 enzymes, compound **10** interacted with CYP1A2 the most strongly, having an IC₅₀ of 6.99 μM, which is comparable to the reference compound miconazole, having an IC₅₀ of 4.55 μM. Compound **10** had an IC₅₀ above 30 μM for all other cytochrome P450 enzymes measured.

Table 7. *In vitro* pharmacokinetic parameters of compound 10

Test	Reference Compound	Compound 10/MRS7788
Simulated intestinal fluid % remaining at 120 min ($t_{1/2}$, min)	n/a	88.1 (573)
Simulated gastric fluid (pH 1.2) % remaining at 120 min ($t_{1/2}$, min)	n/a	69.1 (204)
Plasma stability % remaining at 120 min ($t_{1/2}$, min, 3 species)	n/a	69.7 (159, h); 88.7 (580, r); 83.5 (695, m)
CYP1A2 (IC_{50} , μ M)	Miconazole 4.55	6.99
CYP2C9 (IC_{50} , μ M)	Miconazole 0.38	>30
CYP2C19 (IC_{50} , μ M)	Miconazole 0.00002	>30
CYP2D6 (IC_{50} , μ M)	Miconazole 1.64	>30
CYP3A4 (IC_{50} , μ M)	Miconazole 0.0010	>30
Microsomal stability, % remaining at 120 min ($t_{1/2}$, min, 3 species)	Testosterone 5.44 (15.6, h); 0 (1.43, r); 0 (4.33, m)	81.2 (200, h); 52.1 (70, r); 76.4 (194, m)
Plasma protein binding, % bound (3 species)	n/a	~100 (h); 99.1 (r); ~100 (m)
hERG, IC_{50} (μ M)	n/a	6.06
HepG2 cell toxicity, IC_{50} (μ M)	n/a	>30
Aqueous solubility (pH 7.4, μ g/mL)	n/a	0.39

Compound **10** was the most stable upon incubation with rat plasma, having 88.7% of the compound remaining after 120 min. The longest half-life of compound **10** in plasma was achieved in the mouse plasma at 695 min. This cyclohept-4-enyl derivative was relatively stable in the microsomal assays, having the most degradation with rat microsomes, i.e., 52% of the compound remaining after 120 min. In the microsomal stability assays, compound **10** had a greater % remaining in all species compared to the reference compound testosterone.

In the hERG potassium ion channel inhibition assay, compound **10** displayed an IC_{50} of 6.06 μ M. Compound **10** was not toxic to HepG2 liver cells, having an IC_{50} greater than 30 μ M. In all three species—human, rat, and mouse—compound **10** was strongly bound to plasma protein, with values of ~100%, 99.1%, and ~100%, respectively. The measured solubility of compound **10** determined using the pION buffer (pH 7.4) method was 0.39 μ g/mL, corresponding to 0.92 μ M.

The intestinal permeability of compound **10** was assessed using the Caco-2 cell permeability assay (Table 8). Compound **10** had no measurable permeability (P_{app}) in either apical to basolateral (A-B) and basolateral to apical (B-A) directions. Of the three reference compounds, compound **10** most resembled atenolol, also classified as having low permeability. An efflux ratio was not calculated due to low P_{app} in A to B and B to A. B to A had a relatively large % recovery of 78.0%, which was substantially more than the 48.1% seen for the A to B % recovery.

Table 8. Caco-2 permeability results of compound 10

Compound Name	Average Values					
	P_{app} (10^{-6} cm/sec)		Efflux Ratio	A to B % Recovery	B to A % Recovery	Classification
	A to B	B to A				
MRS7788 / Compound 10	0.00	0.00	NC	48.1	78.0	LOW
Digoxin	0.13	9.96	74.2	82.0	84.2	LOW
Propranolol	28.4	17.6	0.62	74.4	101	HIGH
Atenolol	0.00	0.00	NC	87.8	86.1	LOW

***In Vivo* Pharmacokinetic Study Results**

The baseline *in vivo* pharmacokinetic parameters using compound **10** as a prototype were obtained using male Wistar rats (Table 9). The longest half-life of 2.60 h was upon oral administration of 10 mg/kg of compound **10**, similar to the half-life of 2.38 h seen with the i.v. dose of 0.5 mg/kg compound **10**. 28.7%F and 47.5%F were determined for compound **10**, indicating substantial oral bioavailability. The source of the

discrepancy between the Caco-2 cell results and the moderate bioavailability remains unexplored.

Table 9. *In vivo* pharmacokinetic parameters of compound 10 in Wistar rats

Dose (Route)	C _{max} (ng/mL)	T _{max} (h)	AUC _{0-last} (h* ng/mL)	AUC _{0-∞} (h*ng/mL)	T _{1/2} (h)	MRT _{last} (h)	V _d (mL/kg)	k _{el} (1/h)	F (%)	Cl (mL/h/kg)
0.5 mg/kg (i.v.)	696	0.083	1080	1120	2.38	2.64	1530	0.292	100	447
1 mg/kg (p.o.)	185	2.00	-	-	-	-	-	-	-	-
3 mg/kg (p.o.)	487	2.00	1860	1900	1.29	3.01	2930	0.539	28.7	1580
10 mg/kg (p.o.)	1780	2.00	10,200	10,300	2.60	3.98	3660	0.266	47.5	975

As seen in Figure 53, orally administered 10 mg/kg of compound 10 produced higher plasma concentrations than the other groups during each time measured. All groups of rats orally administered compound 10, i.e., at 1, 3, and 10 mg/kg, achieved the maximum plasma concentration at ~2 h.

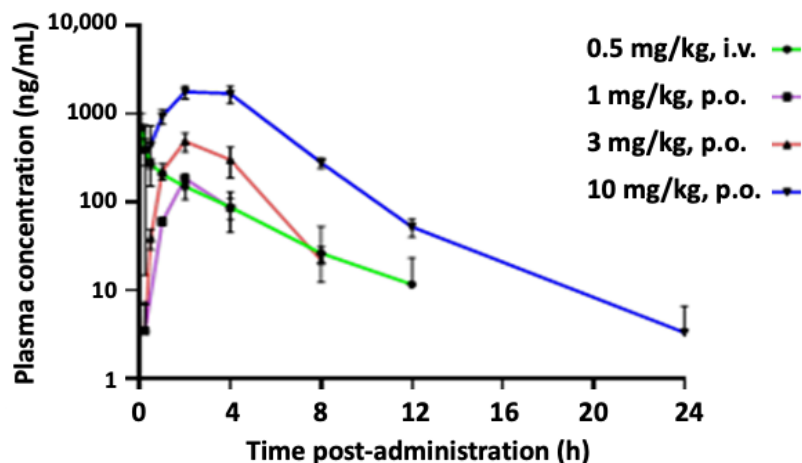


Figure 53. Mean plasma concentrations of compound 10 in Wistar rats vs. multiple timepoints. The dose and administration route are specified above for each of the four groups (three rats in each group).

Rats receiving 3 mg/kg (p.o) had almost double the rate of clearance (1580 mL/(h·kg)) of compound 10 from the plasma compared to rats receiving 10 mg/kg (975

mL/(h·kg)) and roughly three times the rate of clearance compared to rats receiving 0.5 mg/kg, i.v. (447 mL/(h·kg)). Rats receiving 3 mg/kg (p.o.) had double the elimination rate constant, k_{el} , compared to 0.5 mg/kg (i.v.) and 3 mg/kg (p.o.), having ~50% of the remaining compound in the body excreted every hour. Rats receiving 10 mg/kg (p.o.) had the longest mean residence time (MRT)—length of time compound in the system before elimination—3.98 h.

CHAPTER 5: Discussion

This study aimed to develop new allosteric drugs for the A₃AR by synthesizing and characterizing a new series of 1*H*-imidazo[4,5-*c*]quinolin-4-amine derivatives. It extends two previously published studies, making different structural modifications at the 2- and the 4-aminophenyl positions of the 1*H*-imidazo[4,5-*c*]quinolin-4-amine scaffold and characterizing their SAR through various binding and functional assays (56; 68). We evaluated four libraries of modulators to determine their influence on agonist dissociation, affinity, potency, and/or efficacy at the A₃AR compared to reference compound **8**, LUF6000. We used alkene derivative **10** as a representative lead derivative to obtain an ADMET baseline. Experiments with compounds **5** and **8** determined the general location of the allosteric binding site. Collectively, the SAR obtained from this series, the ADMET baseline, and the determination of the general location of the allosteric binding site on the receptor protein will facilitate future 1*H*-imidazo[4,5-*c*]quinolin-4-amine derivative design and drug formulation and administration decisions.

SYNTHESIS AND PURIFICATION OF DERIVATIVES

General procedure B, the two-step process to produce the cyclized 4-chloroimidazoquinolines, proved to be the most effective step-5 reaction. Likewise, general procedure E, the microwave-assisted C–N coupling method, proved to be the most effective step-6 reaction to achieve the final compounds. Concerning step-5 general procedures A and B, despite involving two steps, the reaction mixtures of general procedure B were easier to work with than the highly viscous PPA used in the general procedure A. Also, indicated by TLC, general procedure B had a full conversion of reactants to products for both steps. Although percent yields varied for the step-6 general

procedure E, it did have the highest yield of 61%. This reaction procedure was the ‘greener’ of the three and the easiest to execute as it only required two reactants in ethanol, whereas the two palladium-catalyzed reactions required four to five reactants in 1,4-dioxane.

Purification of the final compounds proved troublesome for various reasons, leading to changes in the step-6 purification procedures and reaction conditions. *t*BuXPhosphine oxide was a by-product of step-6 general procedures C and D (Figure 54), being non-polar, having an R_f of ~0.32 using a 25% ethyl acetate in hexane eluent system. The mass of the starting reagent, *t*BuXPhos, was 424 g/mol, and the mass of the by-product, determined by mass spectrometry, was 440 g/mol, a difference in mass of 16 g/mol, the atomic mass of one oxygen atom. This by-product, an oxidized biaryl monophosphine ligand, was present in all the step-6 general procedures C and D reactions (61).

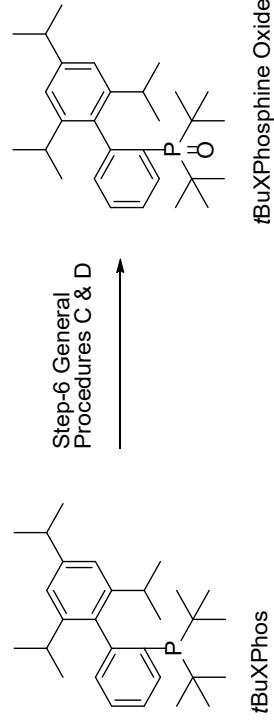


Figure 54. *t*BuXPhosphine oxide by-product from step-6 general procedures C & D

As the alicyclic ring system at C2 increased in size, most notably from cyclononyl to cyclododecyl, the desired product became more difficult to separate—using conventional gravity silica gel column chromatography—from the *t*BuXPhosphine oxide by-product, as the products were of similar polarity to the by-product on TLC. This

complication led to the need to isolate products using RP-HPLC. This purification process solved the issue of separating the final product from the *t*BuXPhosphine oxide by-product. Another issue emerged when purifying compounds **12** – **15** using RP-HPLC; they were too hydrophobic, adsorbing to the C18 column using standard acetonitrile and water eluent system. Changing the RP-HPLC eluent system to an aqueous acetonitrile mixture containing 0.1% trifluoroacetic acid overcame this challenge, transforming the product into a salt that moved readily through the column.

Although RP-HPLC was convenient, it was only practical for small amounts of pure product—roughly 1 to 3 mg. When more significant quantities of the final product were required, for example, 25 mg for ADMET studies, purification by RP-HPLC was not practical, and conventional gravity silica column chromatography was necessary. General procedure E reaction residues were the easiest to purify using this method due to the presence of fewer by-products, which made the purification of palladium-catalyzed procedures complicated by any means.

SAR OF 1*H*-IMIDAZO[4,5-*C*]QUINOLIN-4-AMINE DERIVATIVES

As in past studies, this series of derivatives showed various modulatory effects, with positive, neutral, and slightly negative effects on [¹²⁵I]I-AB-MECA dissociation, and potency and maximal efficacy of Cl-IB-MECA (EC₅₀, and E_{max}) (56). Although the effects of PAMs, in general, are probe-dependent (19, 23), we expect the effects of this series of PAMs on the pharmacology of synthetic agonists [¹²⁵I]I-AB-MECA and Cl-IB-MECA to resemble the effects on endogenous adenosine. Each group of derivatives affected the A₃AR agonist response differently. It is important to note that all the derivatives subjected to off-target analyses—using forty-five other GPCRs, ion channels,

and transporters—had little off-target activity, suggesting that the series of PAMs are generally A₃AR selective. Prior studies with compound **8**, LUF6000, and other members of this PAM family indicate only minimal binding to the orthosteric sites of other AR subtypes. Compound **8** also lacked allosteric effects at other ARs (56; 68).

SAR Evaluation of 2-Alkyl and 2-Cycloalkyl Substituted 1*H*-Imidazo[4,5-*c*]quinolin-4-amine Derivative Library

Prior *n*-pentyl substitutions at the 2 position of the 1*H*-imidazo[4,5-*c*]quinolin-4-amine scaffold with the 3,4-dichlorophenylamino group at the 4 position did not significantly influence agonist binding and maximal efficacy at the receptor in a positive manner (56). At 1 μM, compound **2**, with a 2-heptan-4-yl substitution—originating from valproic acid—did not increase agonist potency compared to the control (P-value = 0.327). Still, it enhanced the agonist E_{max} compared to the control (E_{max} of 216±12%, P-value = <0.0001). This two-fold increase in E_{max} of Cl-IB-MECA at the receptor is comparable to the enhancement by compound **8**. Interestingly, compound **8** has a 2-cyclohexyl ring substitution, and compound **2**, an open-chain 2-heptan-4-yl substitution, have similar functional properties. When evaluating the many rotations of the covalent bonds of the 2-heptan-4-yl substitution, a conformation that closely approximates a cyclohexyl ring shape is possible. However, we cannot draw any conclusions from these two analogues about the conformational requirements of the 2-substituent when receptor-bound. Compound **2** displayed promising characteristics in A₃AR radioligand binding studies. Compound **2** performed the best out of all the derivatives in slowing the agonist radioligand dissociation rate and increasing the specific binding of the agonist to the A₃AR. Explanations of binding results for compound **2** are, first, it competitively inhibited the binding of the agonist the least at the orthosteric binding site. Secondly, the

presence of compound **2** caused positive cooperativity, possibly enhancing the affinity of the agonist for the A₃AR, or increasing the density of available binding sites, as evidenced by the greater amount of radioligand bound to the receptor compared to the control (P-value = 0.02). This derivative showed it is possible to improve agonist binding kinetics and function through increasing the size of acyclic alkyl substitutions at the 2 position.

When evaluating other cycloalkyl derivatives compared to compound **8**, compounds **10** (cyclohept-4-enyl) and **12** (cyclononyl) stand out the most. Compounds **10** and **12** at 1 μM both potentiated the maximal efficacy of the agonist similar to compound **8** (225±10%), having E_{max} values of 241±9% and 242±9%, respectively. Unlike compounds **8** and **10**, compound **12** at 1 μM was the only modulator of this series with statistical significance to increase the potency of the agonist at the receptor by two-fold compared to the control (P-value = 0.009). Compounds **10** and **12** also showed PAM characteristics by slowing the rate of agonist radioligand dissociation from the receptor.

Thus, compound **12** performs like a PAM by more criteria than compound **8**, slowing radioligand dissociation and improving the efficacy and potency of an agonist at the A₃AR.

Competitive Antagonism vs. Allosteric Modulation

When comparing [³⁵S]GTPγS binding results for the 2-cycloalkyl substituted derivatives at a concentration of 1 μM, there is a noticeable increase in agonist EC₅₀ and E_{max} as the ring size increases from the 2-cyclopropyl derivative **5** to the 2-(cyclohept-4-en-1-yl) derivative **10** (Figure 45 & Table 13, Appendix H). Decreasing antagonist and increasing agonist-enhancing activities can also explain this gradual trend. One possible

explanation for these very different activities in the same chemical series is that compounds may bind at two separate sites on the receptor, the antagonist orthosteric site and the PAM binding site, a hypothesis supported by subsequent analysis of chimeric receptors. For compound **5** (2-cyclopropyl), having the smallest ring, only antagonism is observed, suggesting binding to the orthosteric site to inhibit agonist binding, thereby decreasing the agonist's potency and efficacy. The ratio of the orthosteric site to allosteric site binding shifts in favor of the allosteric site from compounds **5** to **10**, apparent in the gradual increases of potency and maximal efficacy as modulator ring size increases. In this library, compounds **10** and **12** act more like true PAMs, with the agonist enhancement being the predominant effect. Thus, their binding to the allosteric site could be more energetically favorable than at the orthosteric site. One possible explanation for this separation of activities is that the orthosteric site could be more sterically limited than the allosteric site around the larger 2-cyclohept-4-enyl and 2-cyclononyl rings. Furthermore, their enhanced performance compared to rings of fewer carbons is possibly due to their ability to adapt to more bioactive conformations at the allosteric site (85).

Increasing the ring size beyond cyclononyl does not lead to allosteric enhancement of the agonist, as seen with compounds **10** and **12**. The cyclodecyl **13** to cyclododecyl **15** substitutions do not improve potency, and their influence on agonist E_{\max} decreases from **13** to **15**. As observed from the concentration-response curves in Figure 45, this suggests that compounds **13** and **14** are interacting minimally with the allosteric site and that compound **15** does not, possibly due to steric hindrance. These functional results corroborate the radioligand binding studies where compounds **13** to **15** do not influence radioligand dissociation and equilibrium binding of the agonist.

The increase in ring size improved potency and efficacy to an optimum of nine carbons, with the allosteric effect diminishing with the ring size of ten and beyond. Altogether, at 1 μ M, the cyclopropyl derivative **5** acted as an antagonist, reducing the potency and efficacy of the agonist, and the cyclononyl derivative **12** worked like a PAM, increasing the potency and efficacy of the agonist.

Fine Tuning of Modulator Effects

As previously mentioned, through ligand dissociation and cAMP inhibition studies, fine-tuning of modulator effects is possible through the structural modifications at the 2 position of the 1*H*-imidazo[4,5-*c*]quinolin-4-amine scaffold with the 3,4-dichlorophenyl group at the 4-amino position (**50**). This study broadened that notion by synthesizing and evaluating the cyclopropyl to cyclododecyl derivatives. Compounds **5** (cyclopropyl) through **7** (cyclopentyl) achieved competitive antagonism to varying degrees. Similarly, compounds **8** (cyclohexyl) through **12** (cyclononyl) achieved allosteric enhancement. Compounds **13** (cyclodecyl) through **15** (cyclododecyl) diminished allosteric enhancement.

SAR Evaluation of 2-Bicyclo Substituted 1*H*-Imidazo[4,5-*c*]quinolin-4-amine Derivative Library

In principle, incorporating a bicyclic ring to allow less conformational freedom, and a bridged PAM approximating a hypothetical receptor-preferred conformation, would increase the potency and efficacy of the agonist compared to the modulatory effects of compound **8**. All bridged modulators at 1 μ M increased efficacy of the agonist, with compounds **16** and **18** – **20** increasing agonist efficacy by approximately two-fold. None of the bicyclic derivatives improved the potency of the agonist compared to the control.

No clear relationship was seen between structure and modulatory effects of the agonist potency and efficacy when evaluating various-sized bicyclic ring derivatives. Bicyclic ring derivatives proved to uniformly act as PAMs by slowing the radioligand dissociation and improving the maximal efficacy of the agonist, but not improving potency. The binding of bridged derivatives between the orthosteric and allosteric binding sites is a possible explanation for no improvement in agonist potency, as was seen with non-bridged cycloalkyl derivatives. Interestingly, compound **21** acted more like compound **5**, a competitive antagonist, significantly decreasing the potency of the agonist in a concentration-dependent manner.

Another phenomenon detected for some of the bicyclic compounds is their ability to act as inverse agonists, fully reversing the basal receptor activation in the absence of agonists (95). These compounds likely shift the receptor conformation from a constitutively active form—to varying degrees—to an entirely inactive state when bound to the orthosteric site of the receptor. Compound **21** acted as an inverse agonist most markedly compared to other bicyclic derivatives—decreasing basal activity by ~100%. It was the most rigid among the bridged derivatives due to the double bond. Increased rigidity could potentially impair the ability of **21** to interact with the allosteric site, as this compound displayed the least modulation of agonist dissociation rate, potency, and efficacy among the bridged derivatives. We noted the inverse agonist activity of **21** and several other derivatives resulting from binding to the orthosteric site. However, the inverse agonism contrasted with the effect of compound **5**, which appears to be a neutral orthosteric antagonist.

Overall, bicyclic substitutions are tolerated, moderately enhancing agonist dissociation and maximal efficacy at 1 μ M. Still, none of the compounds in the bicyclic library influenced agonist pharmacology at the hA₃AR to a greater degree than compound **8**. However, compounds **18** and **19**, two bicyclo[3.3.1]cyclononane diastereomers, did have similar improvements in agonist binding kinetics to compound **8**.

SAR Evaluation of Hydrophilic Substituted 1*H*-Imidazo[4,5-*c*]quinolin-4-amine Derivative Library

We installed different hydrophilic groups on compound **10** to improve PAM water solubility while maintaining enhancement of the agonist dissociation and functional effects at the A₃AR. This group of derivatives with various oxygen substitutions, i.e., oxirane, alcohol, and carbonyl, did not influence agonist potency but had similar improvements in agonist efficacy compared to the bicyclic library of derivatives. These derivatives act as PAMs but with limited cooperativity due to their mediocre radioligand dissociation improvements and reduced agonist specific binding compared to the control (**19**). Although improvements in efficacy compared to the control were moderate, these are positive results compared to the lackluster performance of previously tested polar heterocyclic derivatives (68).

Due to the positive results seen with the hydrophobic cycloalkyl rings compared to their hydrophilic counterparts, would a future hydrophilic substituted derivative benefit from a greater number of carbons in the cycloalkyl ring? The hydrophobic ring is necessary for allosteric enhancement. As demonstrated, polar functional groups can achieve modest improvements in efficacy. Therefore, is it possible to create a derivative where the hydrophobic nature of the ring dominates interactions in the receptor but with a polar moiety that can improve aqueous solubility? Of all the hydrophilic derivatives made

so far, the cis oxirane of compound **23**, the racemic mixture of carbonyls of compound **24**, and the racemic mixture of trans alcohols of compound **26**—proved to be the most promising oxygen-containing functional groups. The most metabolically stable would be the carbonyl, over the alcohol and epoxide, which are very susceptible to metabolic modifications. The following logical cycloalkyl derivative to produce such a derivative would have a 2-cyclonon-5-enyl substitution (Figure 55) to synthesize a racemic carbonyl derivative like compound **24**. Not only this, but a 2-cyclonon-5-enyl substituted derivative might have allosteric enhancing properties alone, as was seen in the improvement of agonist E_{\max} between compounds **9** and **10** (P-value = 0.002).

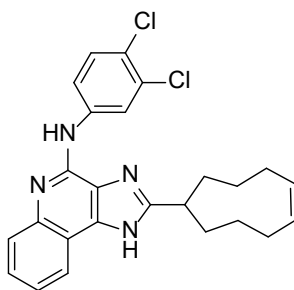


Figure 55. Proposed 2-(cyclonon-5-en-1-yl)-N-(3,4-dichlorophenyl)-1H-imidazo[4,5-c]quinolin-4-amine derivative to be synthesized for a hydrophilic carbonyl substitution

Another alternative to develop a more hydrophilic 1H-imidazo[4,5-c]quinolin-4-amine derivative is to create a prodrug—a charged small molecule, converted to its active form *in vivo* by enzymic activity—from a known derivative with proven results to improve dissociation and potency and/or efficacy of the agonist. Highly selective A₃AR agonists have low aqueous solubility—approximately 1.6 µg/mL for MRS5698 (108). Suresh et al. improved the solubility of both MRS5698 and Cl-IB-MECA through a

succinylation reaction of the 2' and 3' hydroxyl groups of the ribose ring to circumvent the low solubility issue (Figure 56) (108).

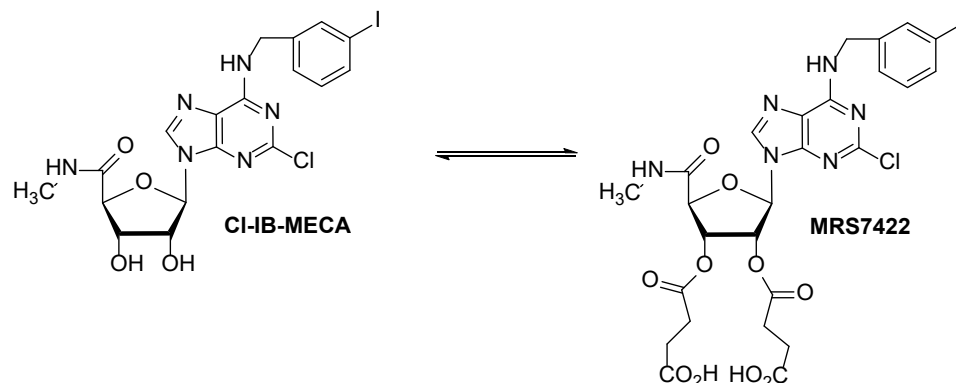


Figure 56. Creation of MRS7422 prodrug through the succinylation of Cl-IB-MECA (108)

The solubility of MRS7422 is 3.0 mg/mL. Exposure to porcine liver esterases reverted the prodrug to Cl-IB-MECA. Using the chronic constriction injury (CCI) mouse model (10), MRS7422 reversed neuropathic pain mice that were administered 1 and 3 $\mu\text{mol/kg}$ by oral gavage (108).

It is essential to continue to develop a more aqueous soluble 1*H*-imidazo[4,5-*c*]quinolin-4-amine derivative because aqueous solubility of compound **10** (MRS7788) was only 0.39 $\mu\text{g/mL}$ or 0.92 μM from *in vitro* PK studies (Table 7). However, none of the analogues produced in this study that performed well have the functional groups typically used for prodrug derivatization of small drug molecules (92). For example, derivatives that possess functional groups, i.e., alcohol, like compounds **25** and **26**, are not suitable for prodrugs because they did not sufficiently allosterically enhance agonist binding and functional effects at the A₃AR.

It might be possible to develop additional *para*-phenylamino 1*H*-imidazo[4,5-*c*]quinolin-4-amine derivatives with functional groups for prodrug derivatization. If one of these derivatives improves the agonist's dissociation, efficacy, and/or potency, they could potentially be transformed into more hydrophilic prodrugs for further *in vitro* and *in vivo* testing.

SAR Evaluation of *para*-Phenylamino Substituted 1*H*-Imidazo[4,5-*c*]quinolin-4-amine Derivative Library

In prior studies, other halogenated phenylamino derivatives and 4-substituted phenylamino derivatives were tolerated and enhanced PAM effects at the receptor (68). Overall, all *para*-phenylamino substitutions were tolerated, none having stellar binding or functional effects compared to compound **8**. These results closely resemble the bicyclic derivatives at 1 μ M of modulator used where potency remained unchanged, and E_{\max} doubled. Compounds **27** and **28**, with the 4-iodo- and 4-bromo-phenylamino substitutions, respectively, had a similar non-optimal influence on potency and efficacy as compounds **29** and **30**. However, they both considerably slowed the dissociation of the radioligand (58% and 56% remaining, respectively) compared to the control (P-values = 0.010 and 0.015, respectively). Although compounds **27** and **28** slowed the radioligand dissociation, they both considerably decreased the specific binding of the agonist for the receptor by -31% and -49% compared to the vehicle (P-values = 0.040 and 0.036, respectively). This means **27** and **28** have mixed binding between the orthosteric and allosteric sites and, relative to the other modulators, inhibited the binding of the radioligand more. Important to note is the substantial increase in agonist E_{\max} at 1 μ M between compounds **27** and **31**, ($184 \pm 9\%$ and $223 \pm 10\%$, P-value = 0.044). This improvement can be attributed to the 2-heptan-4-yl substitution of **31**, improving the interaction of the PAM with the allosteric

binding site, as evidenced by improved specific binding of the radioligand in the equilibrium binding assay.

Interestingly, compound **29**, having a methyl acrylate *para*-phenylamino substitution, slowed radioligand dissociation and had favorable equilibrium binding properties, having low % inhibition binding as a competitive antagonist. These are promising results because **29** has more hydrophilic characteristics than the rest of the library, possessing a polar moiety like compounds in the library with hydrophilic substitutions at the 2 position but on the 4-aminophenyl ring. Of the compounds with hydrophilic substitutions, compound **29** most represents a PAM. A hydrophilic *para*-phenylamino substitution would more likely achieve a hydrophilic PAM, as suggested by the differences in SAR between **29** and the derivatives with hydrophilic substitutions at the 2 position. Altogether, it would be worth investigating other polar *para*-phenylamino substitutions that could improve the binding kinetics and functional effects of the agonist.

EVALUATION OF CHIMERIC RECEPTOR RESULTS

The chimeric receptor studies helped elucidate the general location of the allosteric binding site and provided insight into the competitive antagonist activity of compound **5** and the allosteric enhancement of compound **8**. Convincingly, the SAR from the [³⁵S]GTPγS binding studies substantiates the SAR findings from the chimeric mouse/human receptor studies, identifying an allosteric binding site located in a possibly hydrophobic environment at the receptor cytosolic interface.

The premise of this study originates from the A₃AR species differences described by Auchampach et al., showing that compound **8** potentiated human, dog, and sheep A₃AR activity, but not mouse A₃AR (30). As discussed earlier, the PAMs show mixed

binding at both orthosteric and allosteric sites—compound **5** representing a PAM that favors binding to the orthosteric site and compound **8** representing a PAM that favors binding to the allosteric site. Theoretically, by creating chimeric receptors, variations where either the extracellular or intracellular half of the receptor consisted of hA₃AR or mA₃AR, and vice versa, would allow one to distinguish between these two sites because the allosteric enhancement is nearly absent for mA₃AR. For example, compound **8** and other PAMs should bind to the hA₃AR portion of the chimeric receptors to potentiate agonist efficacy. Any hint of orthosteric antagonism is maintained exclusively in the mA₃AR portion of the chimeric receptors. Studying the effects of various derivatives at other split regions of the mouse/human chimera would be appropriate to pinpoint the regions involved in the allosteric effect.

Compound **8** potentiated the efficacy of the mouse_{Out}/human_{In} A₃AR. However, it lacked enhancing activity at the human_{Out}/mouse_{In} chimera and decreased potency, most likely due to competitive antagonism at the orthosteric binding site. Moreover, compound **8** slowed agonist dissociation from the mouse_{Out}/human_{In} A₃AR but not from the human_{Out}/mouse_{In} A₃AR. These findings were consistent with the location of the allosteric binding site being on the cytosolic side of the receptor.

The intracellular location of the allosteric binding site of the receptor is substantiated further by the SAR of compound **5**, as seen in the chimeric receptor studies. In WT hA₃AR studies, compound **5** behaved similar to competitive antagonists that bind to the A₃AR orthosteric site, which is thought to be in the extracellular half of the transmembrane portion of the receptor. In the chimeric receptor studies, compound **5** decreased potency of Cl-IB-MECA in the human_{Out}/mouse_{In} A₃AR, as was observed in

the WT hA₃AR receptor [³⁵S]GTPγS binding study. In the mouse_{Out}/human_{In} A₃AR chimera, there was no change in potency or efficacy of the agonist, similar to WT mA₃AR results. These results imply compound **5** is a negative modulator of the A₃AR activation by binding to a site different from that responsible for the PAM activity and likely at the canonical orthosteric site.

The SAR obtained for derivatives with hydrophobic and hydrophilic substitutions supports the earlier evidence that the allosteric binding site is on the intracellular side of the A₃AR. Simply, the more hydrophobic derivatives like **2**, **10**, **12**, **19**, and **27** showed allosteric enhancement, whereas the derivatives with hydrophilic substitutions, which would not favor traversing the receptor's intracellular space, did not.

The chimeric receptor studies provided further understanding of the competitive antagonist nature of compound **8**, despite it without a doubt acting like a PAM and potentiating the agonist activity at the A₃AR. In previous studies, compound **8** did not increase potency, just maximal efficacy of the agonist (56; 68). Remarkably, in the mouse_{Out}/human_{In} A₃AR [³⁵S]GTPγS binding results, the potency of the agonist was increased 17-times more than the control, due to the absence of competitive binding to the orthosteric binding site of the mouse portion of the receptor.

We can draw two conclusions from these results. First, this strongly suggests that the positive modulatory activity **8** resides on the cytosolic side of the receptor, and binding of the members of the series at the distinct orthosteric site is responsible for all of the negative modulatory effects. Thus, there is no evidence for NAM activity in this series because the negative modulation disappears in the human_{In}/mouse_{Out} chimera, at which compound **8** enhances agonist potency and efficacy as a pure PAM. We can finally

ascribe these opposing actions of the 1*H*-imidazo[4,5-*c*]quinolin-4-amine scaffold as binding at two separate sites on the receptor.

Secondly, these results also suggest room for improving this class of PAMs through structural modifications to achieve a true PAM that binds only to the allosteric site. Based on the observed differences in agonist EC₅₀ between the WT hA₃AR and mouse_{Out}/human_{In} A₃AR, the chimeric receptor studies can evaluate future PAMs and their relative binding to the orthosteric site vs. the allosteric site. For true PAMs that bind only to the allosteric site, the potency values will be nearly the same between the mouse_{Out}/human_{In} A₃AR and WT hA₃AR in [³⁵S]GTPγS binding studies.

EVALUATION OF ADMET BASELINE

Compound **10** proved to be a lead candidate of the series of PAM derivatives for ADMET studies, displaying favorable allosteric effects on [¹²⁵I]I-AB-MECA dissociation and [³⁵S]GTPγS binding. Overall, this compound proved to be bioavailable, allowing it to be administered orally—despite having low A-B and B-A permeability results.

Compound **10** was not strongly affected by simulated digestive fluids, nor did it interact extensively with important cytochrome P450 enzymes. The concerning ADMET result for this compound was the extremely high % plasma protein binding for all three species tested, attributed to the high affinity of plasma proteins like albumin for hydrophobic compounds like compound **10**. These results could have positive or negative implications. In one regard, high % plasma protein binding of a PAM could provide a reservoir of the compound in the body for prolonged use, as it would release gradually from a bound to unbound state. On the other hand, this could limit the amount of

compound available to traverse to the needed cellular environment for event- and site-specific action, potentially showing no functional results at all.

Other PAM Formulation and Administration Methods

For *in vitro* PK studies, formulation for oral administration consisted of a PAM-DMSO solution mixed with Kollipher El and phosphate buffer saline (PBS). In contrast, the formulation for parenteral administration consisted of a PAM-DMSO solution combined with an aqueous solution of 20% 2-hydroxypropyl- β -cyclodextrin (HPBCD). There are various formulation approaches to optimize the delivery of drugs (7; 24; 70; 89; 99). Other modes of formulation must be considered other than conventional methods used for oral and parenteral administration for this drug class due to the compound's high % plasma protein binding, low permeability, and poor aqueous solubility. Other forms of administration could be considered, like dermal and nasal.

In a preclinical trial, Canfite Pharma—with an undisclosed formulation method—administered compound **8**, LUF6000/CF602, topically to treat erectile dysfunction in a diabetic rat model (<https://www.canfite.com/category/CF602>, accessed on 1 December 2021). This local administration allows for the absorption of the small drug to the cellular environment for event- and site-specific action with the endogenous agonist adenosine.

Other formulation methods developed using nanotechnologies, which utilize low toxicity macromolecules, can improve the drug's ADMET properties (7). Considering the poor aqueous solubility, high % plasma protein binding, and low permeability of compound **10**, this family of PAMs might benefit from a solid dispersion system. In this polymer-based system, a drug, through various intermolecular forces, is stabilized by a

water-soluble carrier or a co-amorphous mixture of two or more small molecular weight compounds that make up a homogenous amorphous system (24).

In vitro, Caco-permeability assays predict *in vivo* human intestinal permeability measurements for passively absorbed potential drugs. There were low Caco-permeability ADMET results for compound **10**— low P_{app} in A to B and B to A. Sandri et al. used nanoparticles like chitosan and *N*-trimethyl chitosan chloride (TMC) to help increase the Caco-permeability of insulin (94). This formulation method might improve the *in vitro* Caco-permeability of compound **10** and its bioavailability due to the improved permeability.

Nanogels are crosslinked polymer nanoparticles ranging in size from 10-100 nm and maintain their structure in an aqueous medium (7). A PAM could be covalently bound to a hydrophilic nanogel and administered through nasal delivery because the A₃AR is on astrocytes and brain and spinal cord neurons (2; 105). Employing this method of drug administration avoids a couple of issues. It allows drugs to be delivered directly to the brain tissue through olfactory neurons, sidestepping the BBB (31). Also, drugs bypass first-pass metabolism.

Even though compound **10** did not interact with many enzymes involved in metabolism, having an IC₅₀ of 6.99 μ M with the P450 enzyme CYP-1A2, nasal delivery of a covalently-bonded PAM with the nanogel could resolve this issue. Furthermore, the nasal administration of the PAM-nanogel could also enable systemic drug delivery through the blood circulation. The hydrophilic nature of the nanogel would help improve the aqueous solubility issue of this family of PAMs and, quite possibly, significantly lower the % plasma protein binding of the PAM.

Solid lipid nanoparticles (SLN) and nanostructured lipid carriers (NLC) might be suitable formulation methods for this family of drugs because of their hydrophobic cores composed of triglycerides mixed with saturated fatty acyl chains and triglycerides with a mixture of unsaturated fatty acyl chains, respectively (89).

A₃AR PAMs can benefit in many ways from SLN and NLC therapeutic drug formulation, aside from encapsulating hydrophobic compounds, thus improving their aqueous solubility. SLNs and NLCs control and extend drug release, target specific cells, and prolong circulation time in the body, improving *in vivo* PK parameters like half-life and MRT. An advantage of NLCs over SLNs is their amorphous structure, limiting the amount of drug expulsion when loading, as experienced with NLCs due to their perfect crystal lipid structure (74). NLCs are colloidal particles ranging in size from 100 to 500 nm. They are typically orally or dermally administered. NLCs are a mixture of solid- and liquid-phase lipids.

A similar concept to NLCs is using co-amorphous formulations of two or more low molecular weight components to create a homogenous amorphous system. This formulation technique makes a co-amorphous drug-excipient blend between the hydrophobic drug and a low molecular weight excipient, e.g., amino acids (24). Spray drying is a method to prepare such amorphous dispersion systems by rapidly evaporating the solvated components to create the amorphous states (99).

Other Design Decisions Based on ADMET Parameters of Compound 10

Design decisions for future 1*H*-imidazo[4,5-*c*]quinolin-4-amine derivatives cannot just be based on known SAR. As experienced from the ADMET studies, the hydrophobic nature of compound **10**, although facilitating the interaction of the ligand

with the hydrophobic allosteric binding site, is causing it to have low permeability and solubility and high % plasma protein binding. The hydrophobic nature of the 2 position substitution is critical for allosteric enhancement of agonist action, possibly hinting at the general orientation of the PAM when it interacts with the intracellular side of the A₃AR. Therefore, we must explore other *para*-phenyl 4-amino position substitutions performing two needed functions: 1) maintain allosteric enhancement of the PAM and 2) provide hydrophilic characteristics to make the drug more water-soluble and less attracted to hydrophobic binding sites on plasma proteins. An effort that can run parallel to developing additional *para*-phenyl 4-amino position substituted derivatives is to develop *para*-phenyl 4-amino position substitutions that could be converted to prodrugs, pending positive allosteric enhancement results, of course.

Another design decision to consider is the synthesis of a bitopic ligand for the A₃AR (66), a compound comprised of allosteric and orthosteric pharmacophores covalently bonded through a linker. For example, Valant et al. created a bitopic ligand, VCP746, for the A₁AR between adenosine and a known PAM, VCP171 (Figure 57) (117).

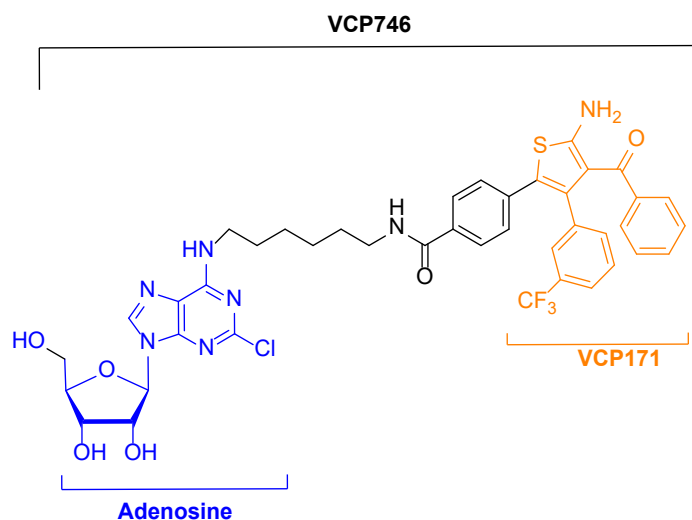


Figure 57. Bitopic ligand VCP746 for the A₁AR (117)

Valant et al. pharmacologically characterized the binding of the ligand. They compared it to other compounds using radioligand binding assays, showing that VCP746 had greater affinity and potency at the A₁AR than other orthosteric comparators (117). They also conducted two functional studies to show the biased agonism of VCP746 (117). Although VCP746 activated both pathways, it favors cAMP inhibition over ERK1/2 phosphorylation.

The group took advantage of allosteric modulation and biased agonism, covalently linking adenosine to a PAM to induce a specific conformational change to the receptor to elicit biased allosteric enhancement signaling favoring a particular pathway. In this study, the group showed the ability of VCP746 to protect A₁AR-expressing cardiomyoblasts and cardiomyocytes from ischemic damage without increasing heart rate, which is a typical side effect of using A₁AR agonists alone (117).

Currently, there are no bitopic ligands for the A₃AR. Could a bitopic ligand be made between adenosine or any other known A₃AR agonists with PAMs generated from

this study? We already know from earlier studies that compound **8**, LUF6000, is a biased modulator for the inhibition of cAMP over other signaling pathways (50). Knowing cycloheptan-4-yl, cyclohept-4-enyl, and cyclononyl 2-substitutions allosterically enhance the agonist at the receptor and are most likely necessary for the interaction of the compound to the hydrophobic intracellular allosteric binding site, the linkage to the agonist should not come from the 2 position of the 1*H*-imidazo[4,5-*c*]quinolin-4-amine scaffold, but from the *para*-phenyl 4-amino position.

Two obstacles exist that make it improbable to develop a pharmacologically active bitopic ligand for the A₃AR. The first obstacle is the relative distance between the extracellular orthosteric binding site and the intracellular allosteric binding site of the A₃AR. The distance between the two would require a long linker between the agonist and allosteric modulator, creating a geometrically matched compound required to transverse to the intracellular portion of the A₃AR. The second obstacle is that the linker would constrain the rotations of the agonist and modulator, making it difficult for them to orientate to their respective binding sites properly.

Design constraints notwithstanding, linking adenosine to a PAM and creating a bitopic ligand could potentially improve the solubility of this class of hydrophobic PAMs. As discussed earlier, MRS7422, the prodrug made from the agonist Cl-IB-MECA, could be a possible candidate to make a bitopic ligand with a 1*H*-imidazo[4,5-*c*]quinolin-4-amine PAM derivative with a cycloheptan-4-yl, cyclohept-4-enyl, or cyclononyl 2 position substitution with linkage at the *para*-phenyl 4-amino position of the enhancer.

POTENTIAL ALLOSTERIC BINDING SITE RADIOLIGAND

[¹²⁵I]I-AB-MECA and [³⁵S]GTP γ S are biological probes that allow the quantification of ligands' interactions with the receptor and their functional activity. [¹²⁵I]I-AB-MECA is used to quantify radioligand-receptor binding kinetics, and [³⁵S]GTP γ S is used to quantify the amount of G protein activated due to the activation of the receptor by the agonist. The development of a radiolabeled allosteric agent would help further the understanding of the A₃AR by monitoring binding events at the allosteric site. For example, equilibrium binding competition assays could measure the relative affinity of other modulators for the allosteric binding site.

[³H]Dimethyl-W84 is a tritium-labeled allosteric modulator radioligand for the M₂ mAChR (115). Tränkle et al. conducted competition assays to measure the inhibition of specific [³H]dimethyl-W84 binding by increasing concentrations of allosteric modulators for the M₂ mAChR (115).

Tränkle et al. reported the affinity of each allosteric modulator for the M₂ mAChR as $\log K_{i, \text{alloster}}$. The higher the $\log K_{i, \text{alloster}}$ value, the higher the affinity of the allosteric modulator for the allosteric binding site on the M₂ mAChR. For the series of PAMs in this study, instead of making a tritiated radioligand, we asked: would it be possible to make a radio-iodinated one?

We synthesized compound **31** due to compounds **2** and **27** slowing the dissociation of [¹²⁵I]I-AB-MECA and improving the functional effects of Cl-IB-MECA. The heptan-4-yl moiety at the 2 position convincingly improved the allosteric enhancement of compound **2**. The 4-iodo-phenylamino substitution of compound **27** was tolerated. With these two substitutions, compound **31** slowed the radioligand dissociation and increased the efficacy of the agonist comparable to compound **8**. The 4-iodo-

phenylamino substitution will allow the synthesis of a radio-iodinated form of the PAM (5). This radio-iodinated form of compound **31** can undergo similar equilibrium binding competition assays as [³H]dimethyl-W84 for the M₂ mAChR to measure the relative affinity of future 1*H*-imidazo-4,5-*c*]quinolin-4-amine PAMs for the allosteric binding site.

As another use for an allosteric radioligand, measuring the amount of allosteric radioligand bound in chimeric receptor studies could help elucidate the location of the allosteric binding site of the A₃AR. Instead of just preparing chimeric halves of hA₃AR and mA₃AR, produce smaller intracellular hA₃AR divisions to narrow down the location of the allosteric binding site. Higher radioligand measurements correspond to more accurately identified hA₃AR protein residues required to interact with the PAM. The more precise pinpointing of the mouse/human A₃AR allosteric binding site along with the use of molecular modeling methods could help elucidate modulator interactions with the receptor and provide critical insight to design more potent and selective modulators in the future.

Compound **31** was converted to two trialkylstannyl derivatives, precursors to radio-iodination, creating a [¹²⁵I]radioligand. The specific binding against a known PAM, like compound **8**, will be determined to assure that it only interacts with the allosteric site of the receptor, assuming there is sufficient specific compared to nonspecific binding. These results will ensure that radioligand measurements will be reliable in competitive binding assays to screen novel PAM derivatives unambiguously for their ability to bind to the A₃AR allosteric site.

POSSIBLE ANIMAL DISEASE MODELS FOR FOLLOW-ON PRECLINICAL STUDIES

Species differences of the A₃AR and the mouse/rat A₃AR unresponsiveness to compound **8**, LUF6000, are the main factors delaying preclinical studies of the 1*H*-imidazo[4,5-*c*]quinolin-4-amine family of PAMs (30). The research community must explore alternative *in vivo* models in light of these issues. Jin et al. conducted *in vivo* studies of the effects of inosine—a metabolite of adenosine and putative weak A₃AR agonist—on the degranulation of mast cells in guinea pigs (65). Auchampach et al. did a similar study in the dog (6). However, when running a protein sequence comparison using the Basic Local Alignment Search Tool (BLAST) between the hA₃AR (homo sapiens, accession AAA16365.1) and the guinea pig A₃AR (*Cavia porcellus*, accession XP_012998623.1), the guinea pig A₃AR had a 75% sequence identity match to the hA₃AR (<https://www.ncbi.nlm.nih.gov>, accessed 12 December 2021), which is lower than the mouse and rat (30). Even though there is low sequence similarity between the human and the guinea pig A₃ARs, and high sequence similarities of the dog and sheep A₃ARs to the hA₃AR (30), different A₃AR species homologues would have to be empirically vetted for PAM activity to determine if a given species would be suitable for determining *in vivo* efficacy in models of inflammation, cancer or neuropathic pain. One cannot assume based on the sequence identity alone whether a particular animal model will work or not.

Yamano et al. evaluated the pharmacological effects of A₃AR agonists and antagonists using A₃AR-humanized (A₃AR^{h/h}) mice and chimeric human/mouse A₃AR mice models (122; 123). The group first attempted to evaluate the activation of the PI3Kγ-dependent signaling pathway in A₃AR^{h/h} mice, where the hA₃AR gene replaced the mA₃AR gene. Although Cl-IB-MECA increased Ca²⁺ mobilization in bone marrow-

derived mast cells (BMMCs) expressing the $A_3AR^{h/h}$, it could not potentiate the release of β -hexosaminidase, nor was it able to phosphorylate PI3K γ and PKB, both needed for mast cell degranulation (123). The group proposed that the lack of phosphorylation of PI3K γ and PKB was due to the activated hA₃AR not correctly interacting with the mouse BMMC G protein effectors responsible for initiating the downstream signaling needed to phosphorylate PI3K γ and PKB.

Due to their previous results with the $A_3AR^{h/h}$, Yamano et al. created mice that expressed chimeric receptors with the mA₃AR sequence in the intracellular space and the hA₃AR in the extracellular space, denoted as $A_3AR^{c/c}$ mice (123). Yamano et al. hypothesized that maintaining the extracellular domains of the hA₃AR but using the mouse intracellular domains will facilitate the coupling of the receptor to the proper G proteins responsible for phosphorylating PI3K γ and PKB. Cl-IB-MECA activation increased Ca²⁺ mobilization, phosphorylation of PI3K γ and PKB, and receptor internalization in BMMCs isolated from the $A_3AR^{c/c}$ mice.

Although Yamano et al. were successful in using a human/mouse A₃AR chimera to evaluate the activation of the PI3K γ -dependent signaling pathway, this was to test the effects of an A₃AR agonist, which we know would bind to the extracellular orthosteric binding site of the hA₃AR portion of the human/mouse A₃AR chimera. If the binding site of the A₃AR PAM exists on the cytosolic side of the hA₃AR, as supported by the mouse_{Out}/human_{In} chimera [³⁵S]GTP γ S activation results of this study, then producing a mouse_{Out}/human_{In} A₃AR chimera might suffer the same consequences of the $A_3AR^{h/h}$ mice study, where the $A_3AR^{h/h}$ receptor did not properly couple to the G proteins and elicit the proper signaling pathway. On the other hand, using a human_{Out}/mouse_{In} A₃AR

chimera would elicit no PAM enhancing effects, as supported by the human_{Out}/mouse_{In} chimera [³⁵S]GTPγS activation results of this study.

Are human/mouse A₃AR chimeras a viable option to test the 1*H*-imidazo[4,5-*c*]quinoline amine PAM derivatives? There is insufficient information to know whether chimeric mouse models are a viable course of action or not. It is conceivable that there is a mouse_{Out}/human_{In} A₃AR construct that encompasses the binding region of the PAM but still has enough intracellular mA₃AR residues to properly couple with the correct G proteins and elicit the proper downstream signaling effects. This gap just might be bridged through further mouse_{Out}/human_{In} A₃AR expressed on HEK 293 GTPγS binding studies, using mouse_{Out}/human_{In} A₃ARs consisting of smaller quadrants of the hA₃AR. This approach, coupled with molecular modeling techniques, might best approximate the actual allosteric binding site for this family of 1*H*-imidazo[4,5-*c*]quinolin-4-amine PAMs. Once the narrowest configuration of intracellular hA₃AR is determined and optimized, the mouse_{Out}/human_{In} A₃AR DNA sequence can be used to make the corresponding recombinant chimeric mouse_{Out}/human_{In} A₃AR mouse model for *in vivo* studies.

CHAPTER 6: Conclusion

SUMMARY OF A₃AR PAM INVESTIGATION

Altogether, this study was a comprehensive medicinal chemistry investigation toward possibly developing a therapeutic A₃AR PAM. We achieved our research objectives by creating a shorter 6-step synthesis protocol for 1*H*-imidazo[4,5-*c*]quinolin-4-amine PAM derivatives, synthesizing a new series of PAM derivatives, determining the SAR of the series of derivatives, and obtaining a baseline ADMET of this family of derivatives.

Although we did not discover a PAM derivative with greater allosteric enhancing capabilities than compound **8**, we did reveal promising 2- and 4-amino substitutions. The heptan-4-yl 2 position substitution slowed agonist dissociation from the A₃AR the most, with both 3,4-dichlorophenyl and 4-iodophenyl substitutions at the 4-amino position. In addition to the 2-heptan-4-yl substitution, the 2-cyclohept-4-enyl and 2-cyclononyl substitutions improved agonist efficacy comparable to the cyclohexyl substitution of compound **8**. The only derivative to increase the potency of the agonist was compound **12** at 1 μ M. Other 2 position substitutions like the bicyclic and hydrophilic did not significantly enhance modulator effects. However, hydrophilic substitution derivative results encourage the synthesis of a more effective water-soluble PAM.

Substantiated through the SAR and ADMET of a member of this family of derivatives, the human/mouse A₃AR chimeric studies show that the allosteric binding site is on the cytosolic interface of the receptor. Fine-tuning of this family of PAMs is achievable, acting as either competitive antagonists or PAMs by binding at the receptor's distinct orthosteric and allosteric binding sites. Varying the ring size at the 2 position of

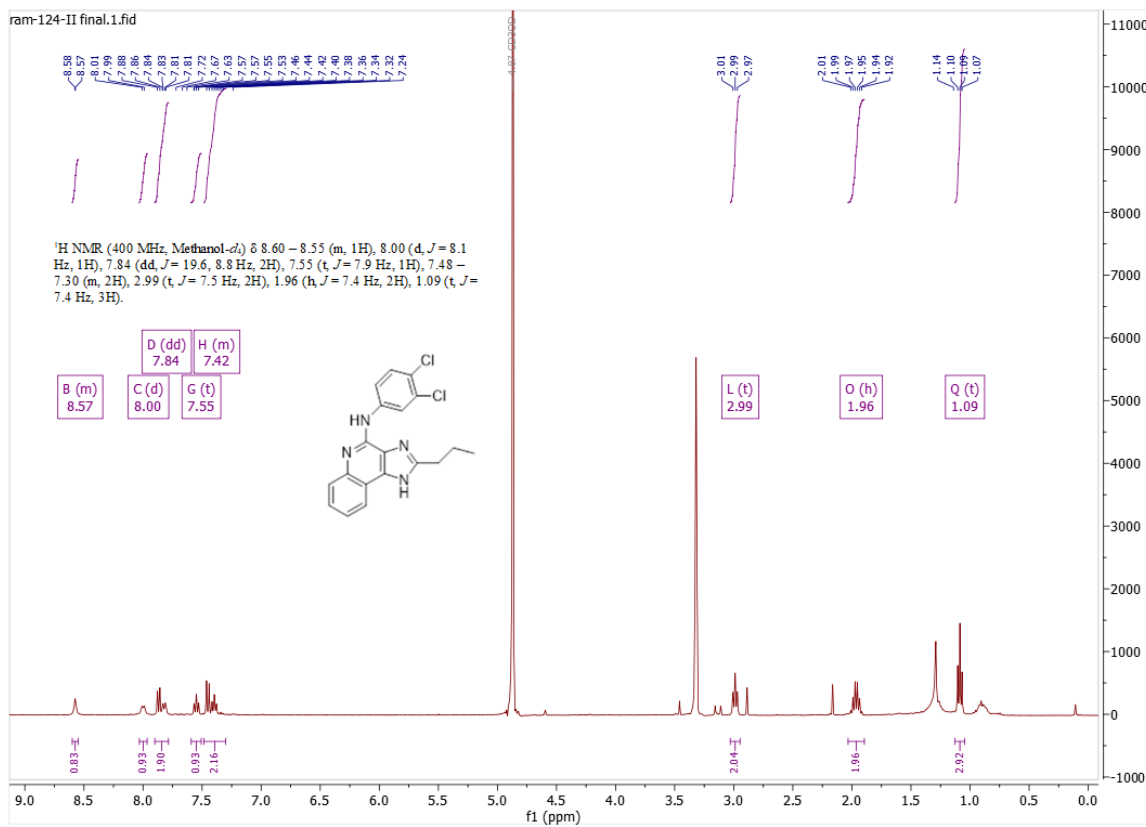
the 1*H*-imidazo[4,5-*c*]quinolin-4-amine scaffold or adding sterically-constraining bridging groups could direct this mix of activities at these two sites.

In vivo studies carried out by our collaborators showed that a member of this family of PAMs was bioavailable, having high % plasma protein binding, low Caco-permeability, and low aqueous solubility. The hydrophobic nature of this family of derivatives suggests possible future improvements in administration/formulation methods of the drug, or the synthesis of a hydrophilic modulator, possibly at the *para*-phenyl 4-amino position.

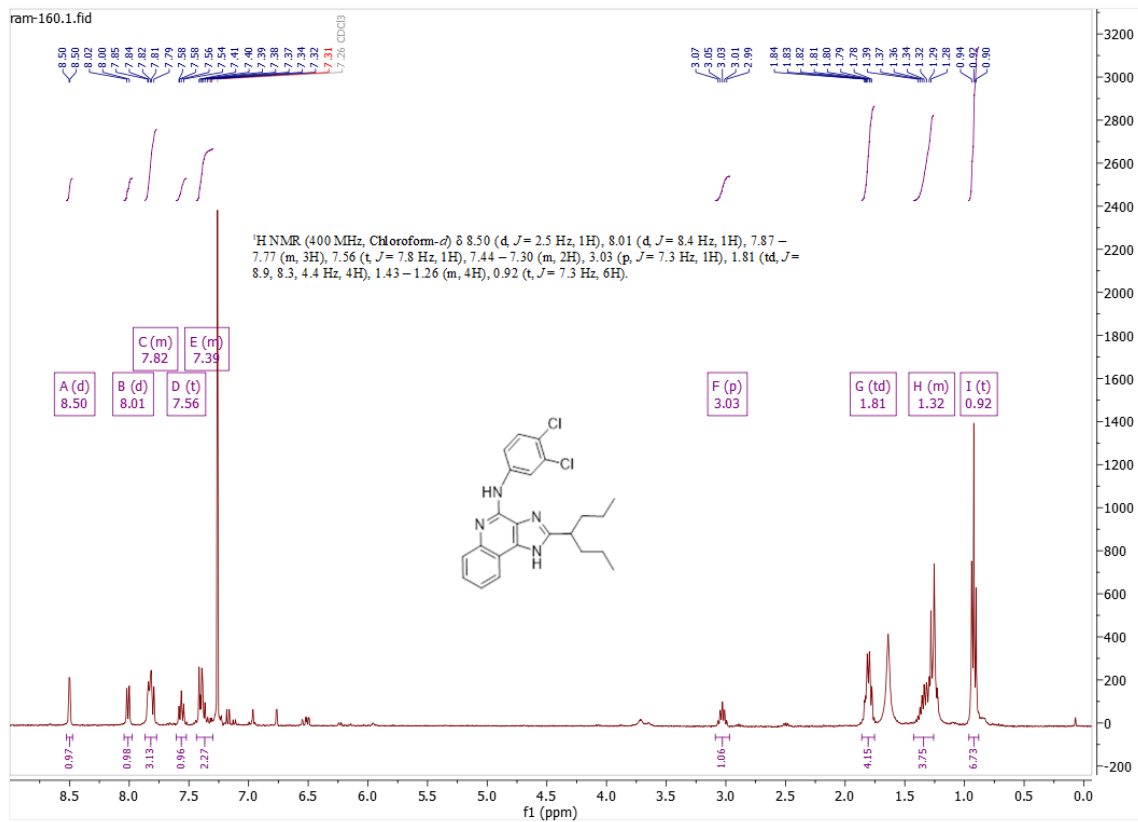
Developing a radioligand specific for the 1*H*-imidazo[4,5-*c*]quinolin-4-amine PAM binding site would significantly aid the SAR of this family of derivatives and their pharmacological characterization. We prepared a precursor for introducing a ¹²⁵I label and plan to perform future labeling studies.

We have developed a promising series of 1*H*-imidazo[4,5-*c*]quinolin-4-amine modulators. Selected compounds will be utilized in future preclinical studies once an animal disease model is identified, thereby furthering the allosteric approach to developing drugs for the A₃AR that are event- and site-specific in action.

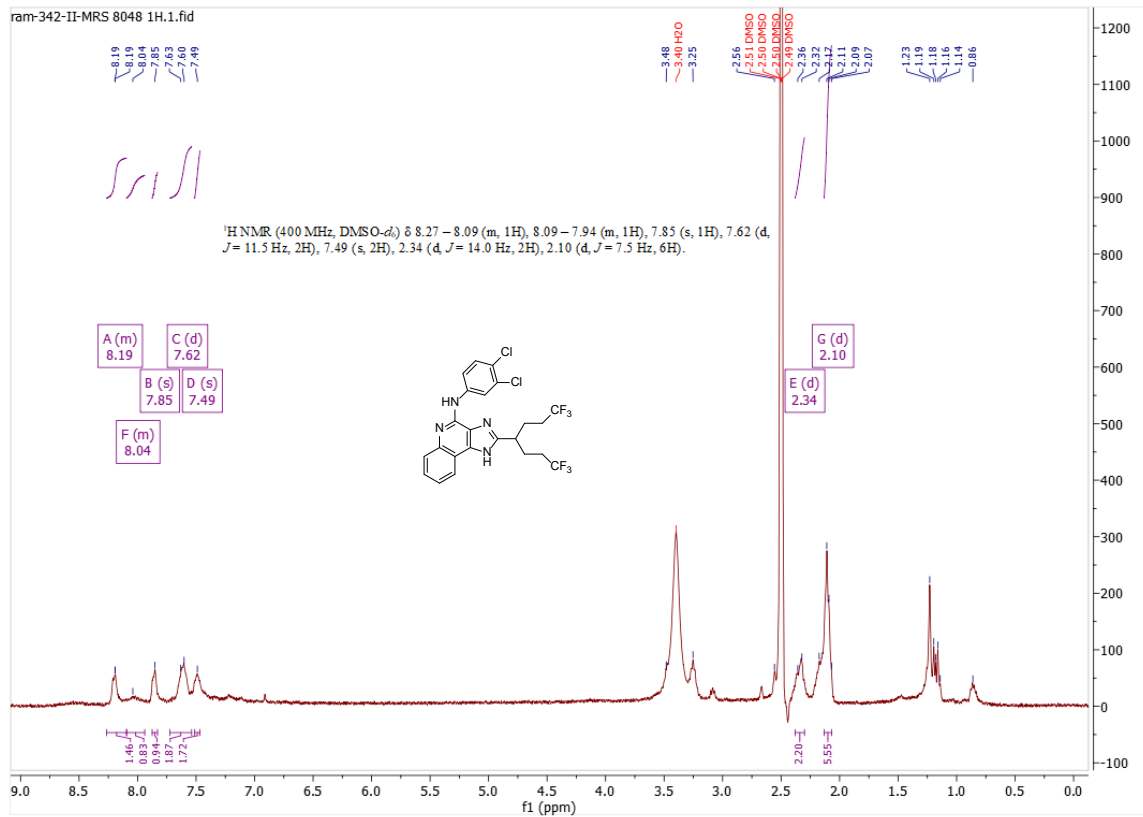
Appendix A: Compound NMR Spectra



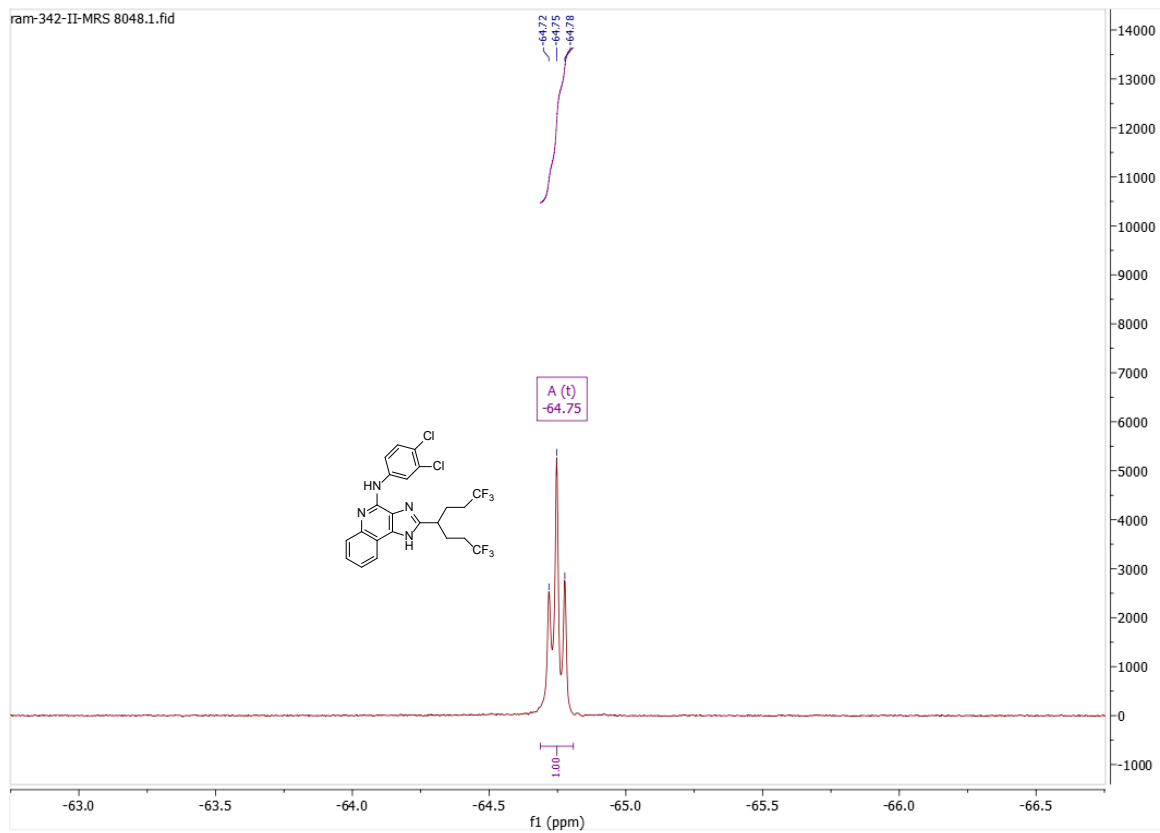
¹H NMR of 2-ethyl-*N*-(3,4-dichlorophenyl)-1*H*-imidazo[4,5-*c*]quinolin-4-amine – Compound **1**



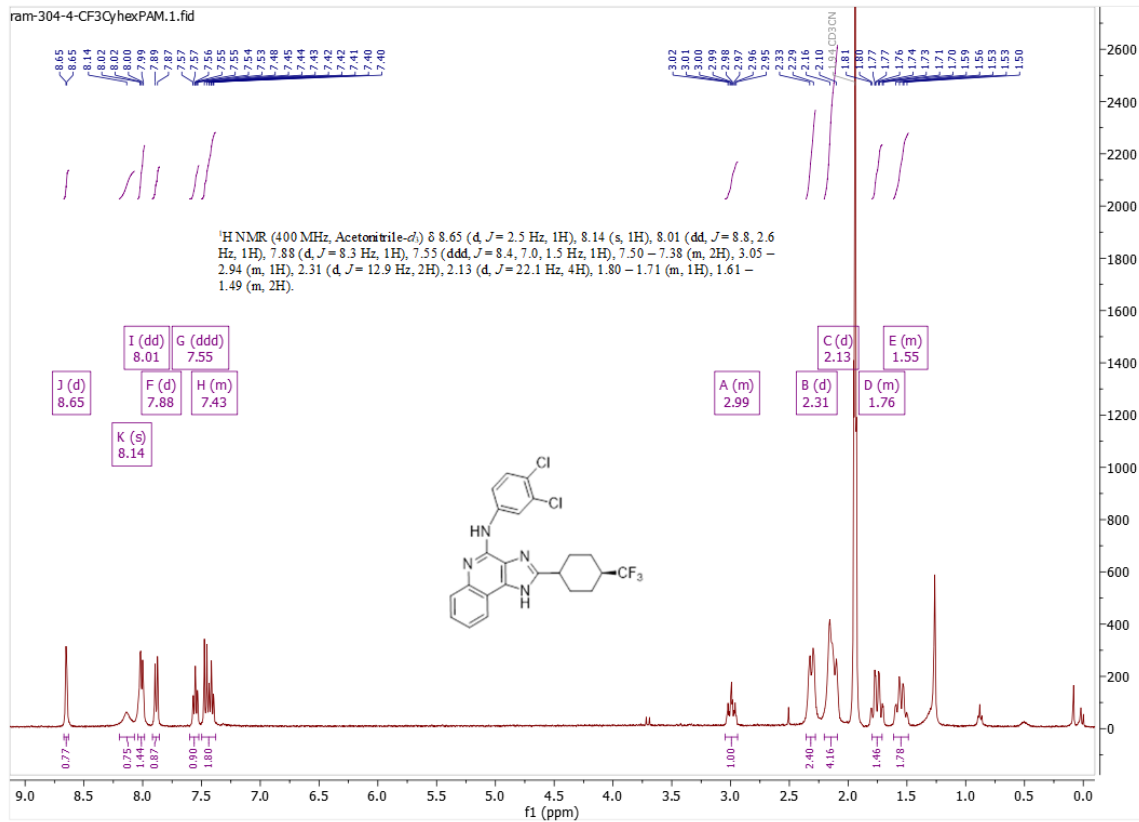
¹H NMR of 2-(heptan-4-yl)-*N*-(3,4-dichlorophenyl)-1*H*-imidazo[4,5-*c*]quinolin-4-amine
– Compound **2**



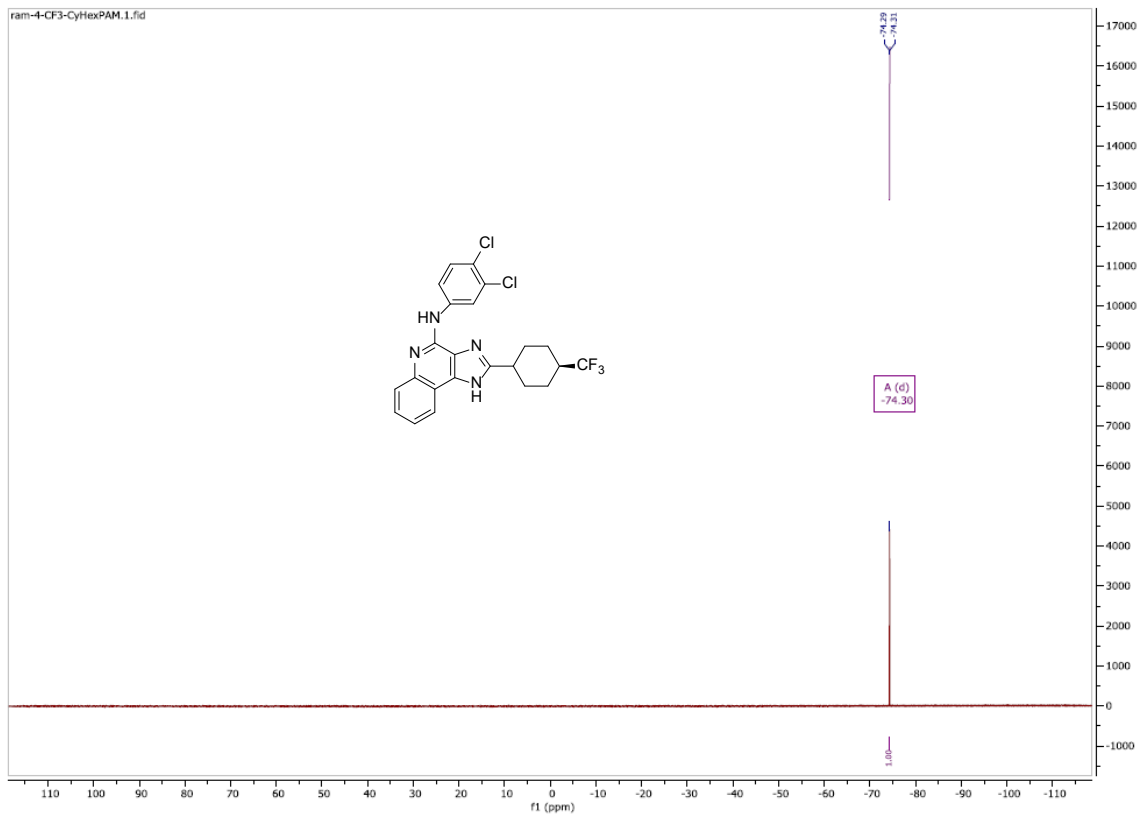
$^1\text{H NMR}$ of 2-(1,1,1,7,7,7-hexafluoroheptan-4-yl)-*N*-(3,4-dichlorophenyl)-1*H*-imidazo[4,5-*c*]quinolin-4-amine – Compound **3**



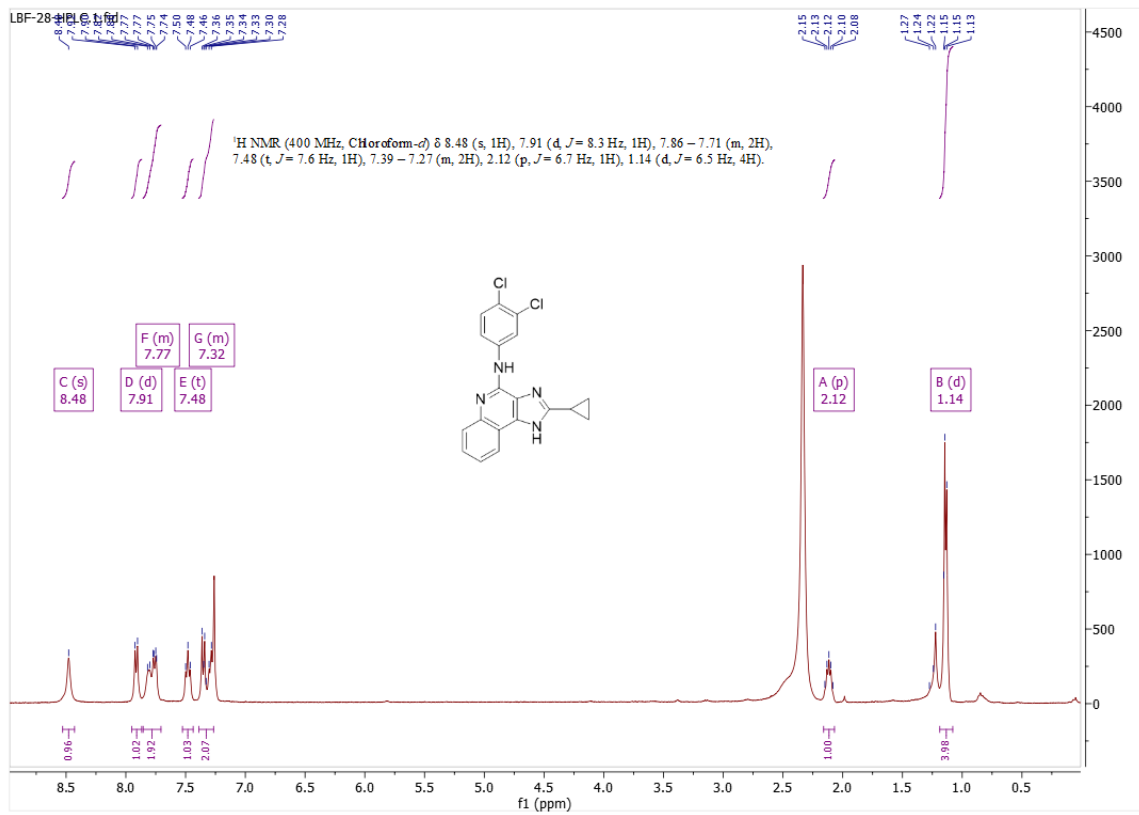
^{19}F NMR of 2-(1,1,1,7,7,7-hexafluoroheptan-4-yl)-*N*-(3,4-dichlorophenyl)-1*H*-imidazo[4,5-*c*]quinolin-4-amine – Compound **3**



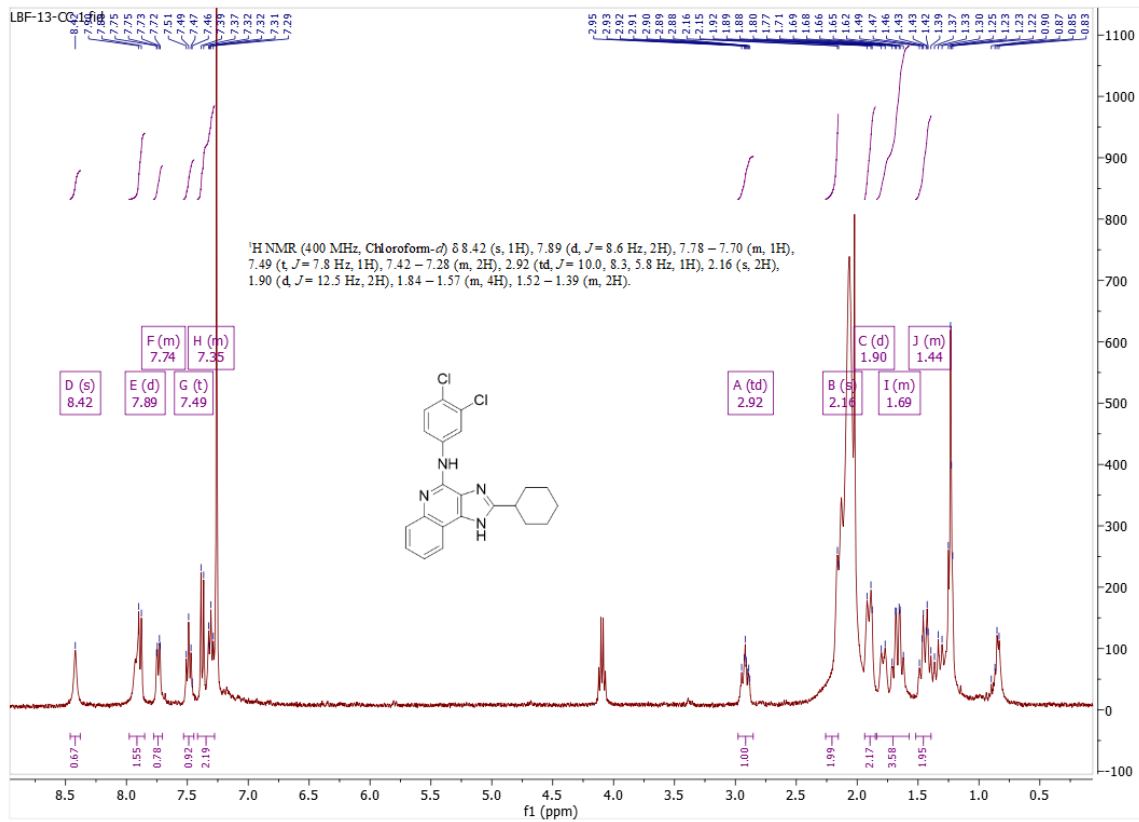
¹H NMR of 2-(4-(trifluoromethyl)cyclohexyl)-*N*-(3,4-dichlorophenyl)-1*H*-imidazo[4,5-*c*]quinolin-4-amine – Compound 4



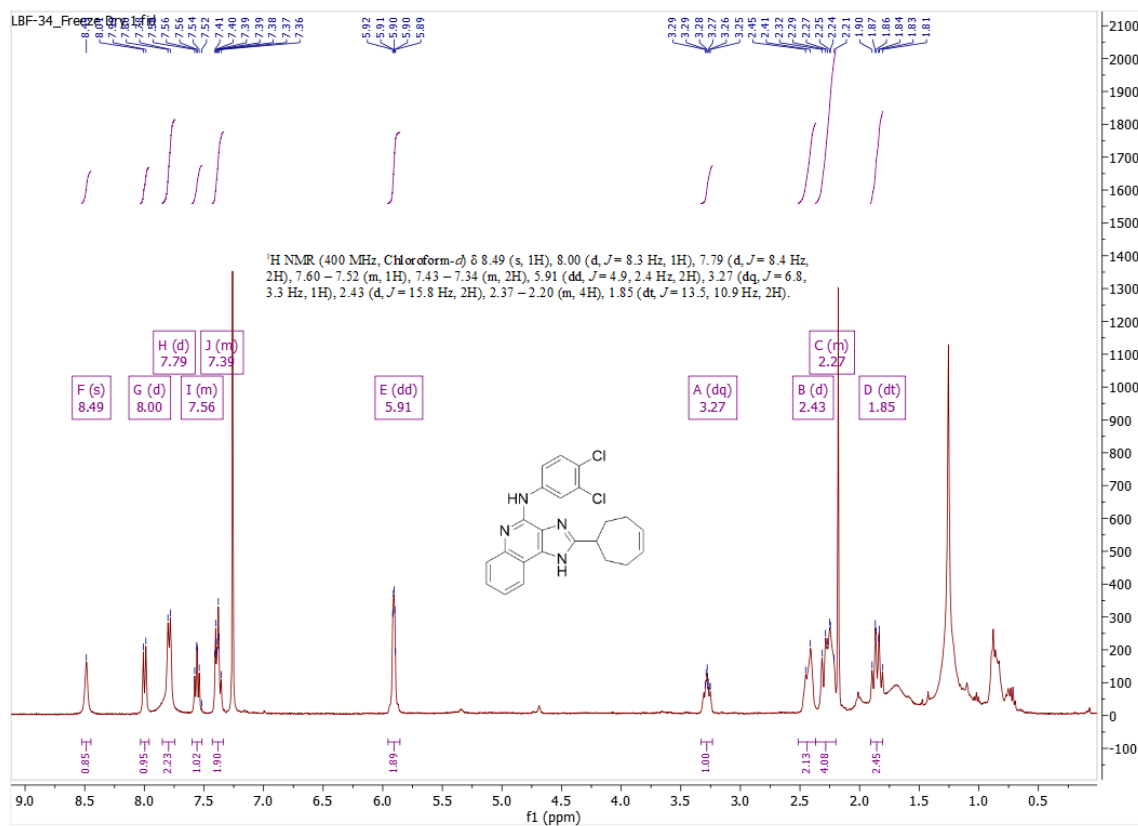
^{19}F NMR of 2-(4-(trifluoromethyl)cyclohexyl)-*N*-(3,4-dichlorophenyl)-1*H*-imidazo[4,5-*c*]quinolin-4-amine – Compound 4



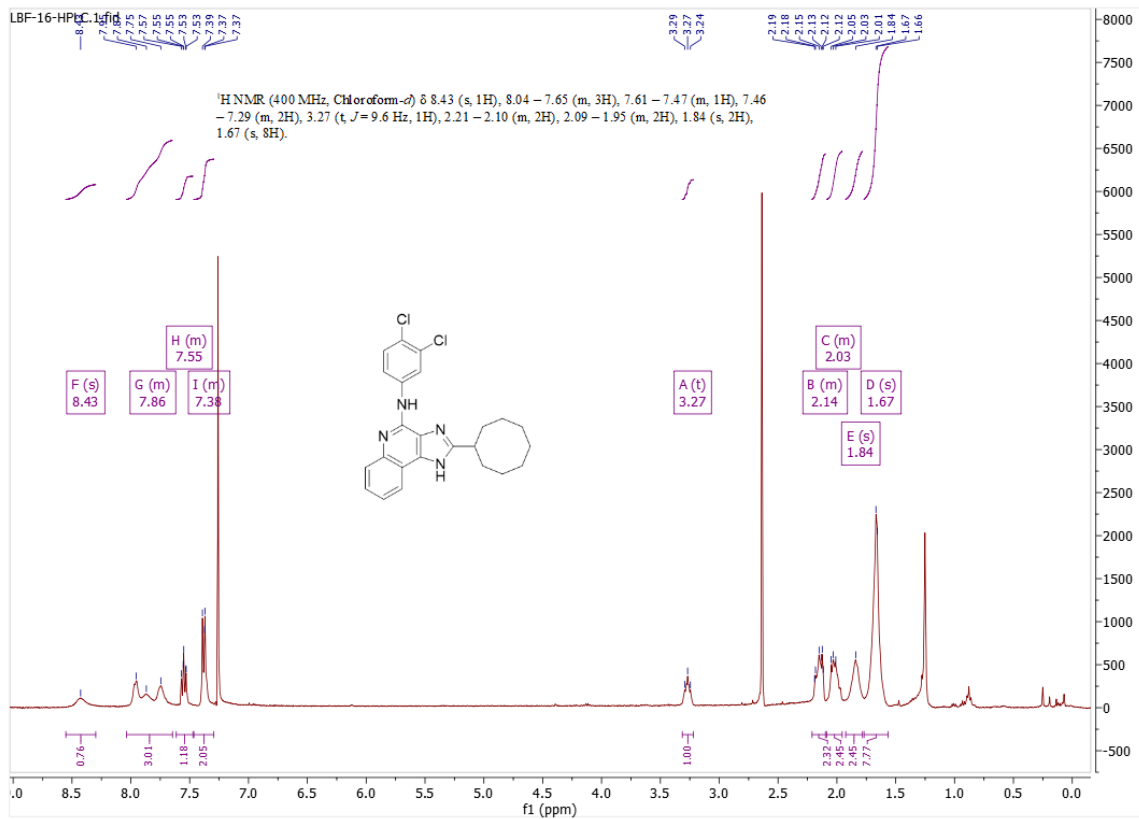
¹H NMR of 2-(cyclopropyl)-*N*-(3,4-dichlorophenyl)-1*H*-imidazo[4,5-*c*]quinolin-4-amine – Compound 5



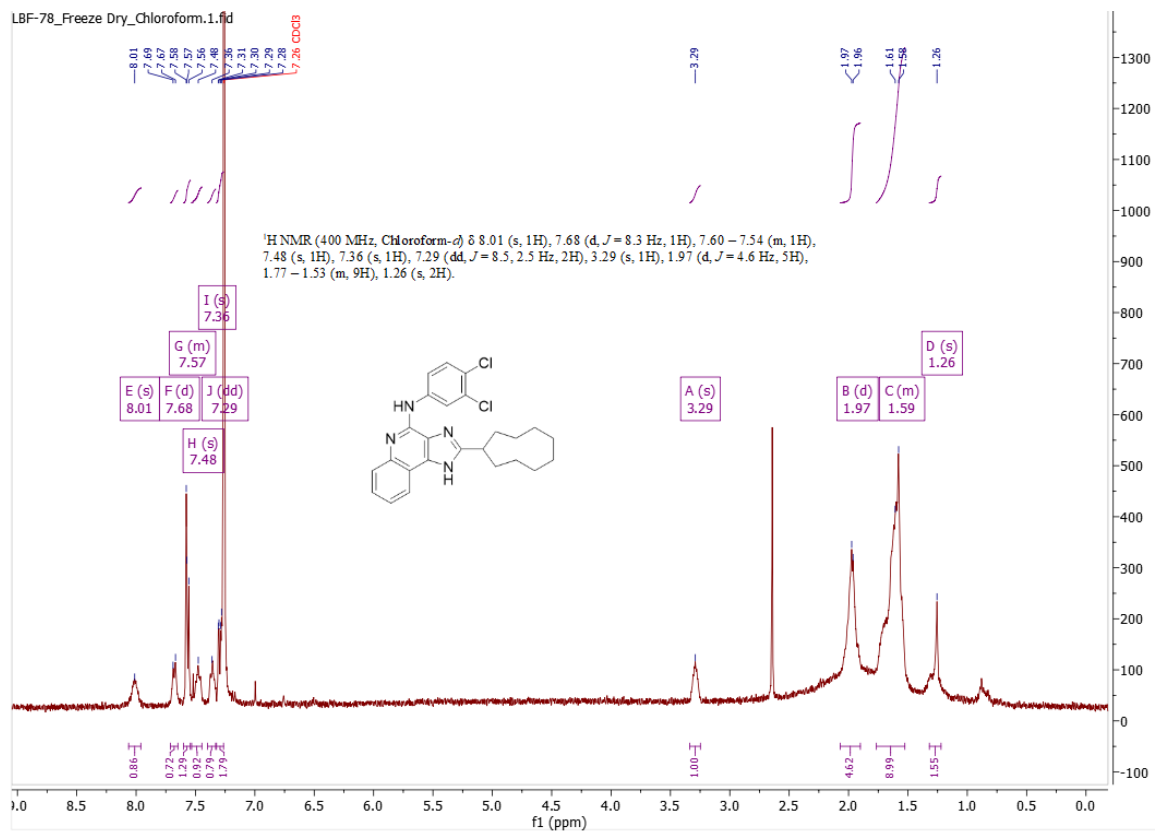
¹H NMR of 2-(cyclohexyl)-*N*-(3,4-dichlorophenyl)-1*H*-imidazo[4,5-*c*]quinolin-4-amine – Compound **8**



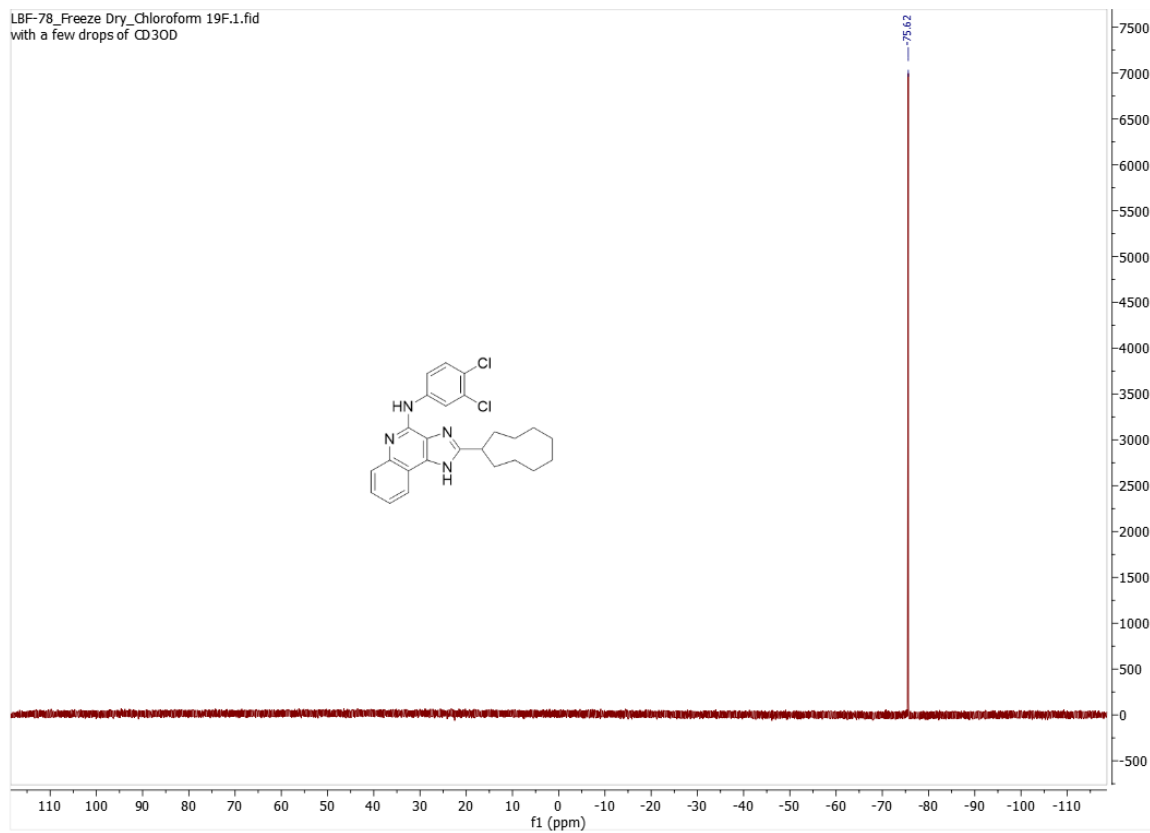
¹H NMR of 2-(cyclohept-4-en-1-yl)-*N*-(3,4-dichlorophenyl)-1*H*-imidazo[4,5-*c*]quinolin-4-amine – Compound **10**



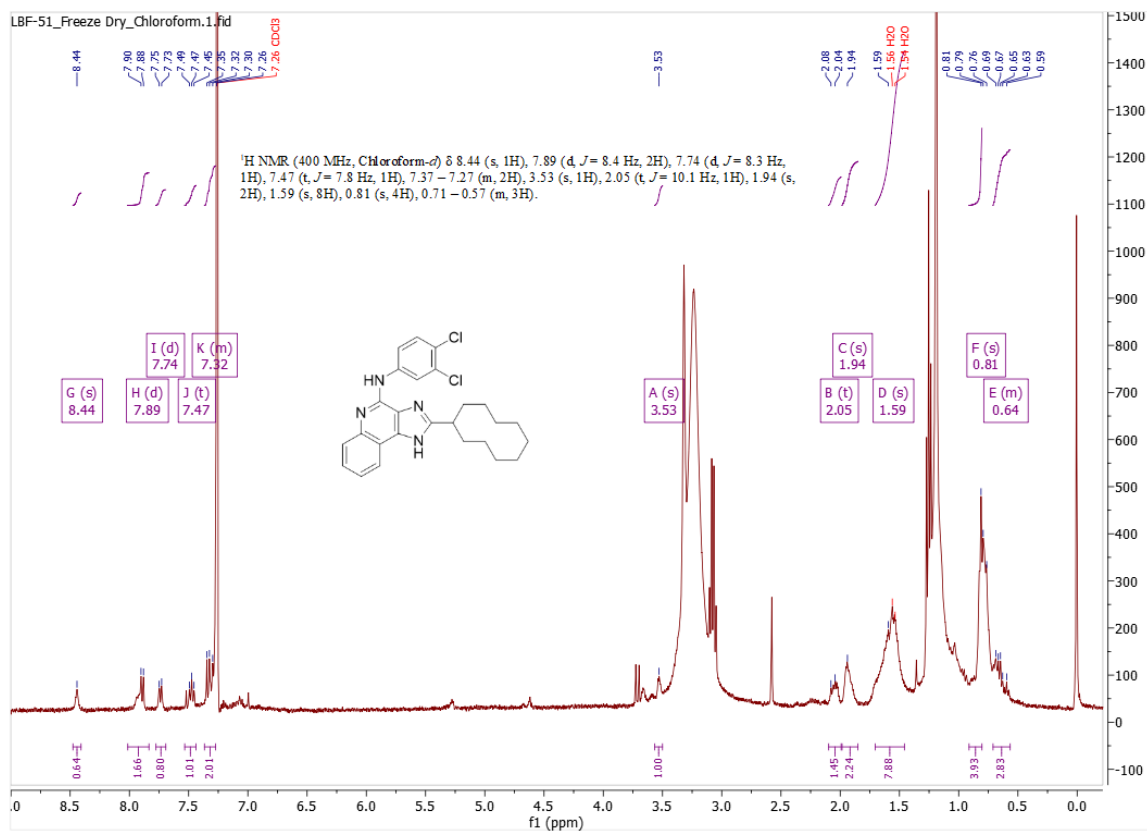
¹H NMR of 2-(cyclooctyl)-*N*-(3,4-dichlorophenyl)-1*H*-imidazo[4,5-*c*]quinolin-4-amine – Compound **11**



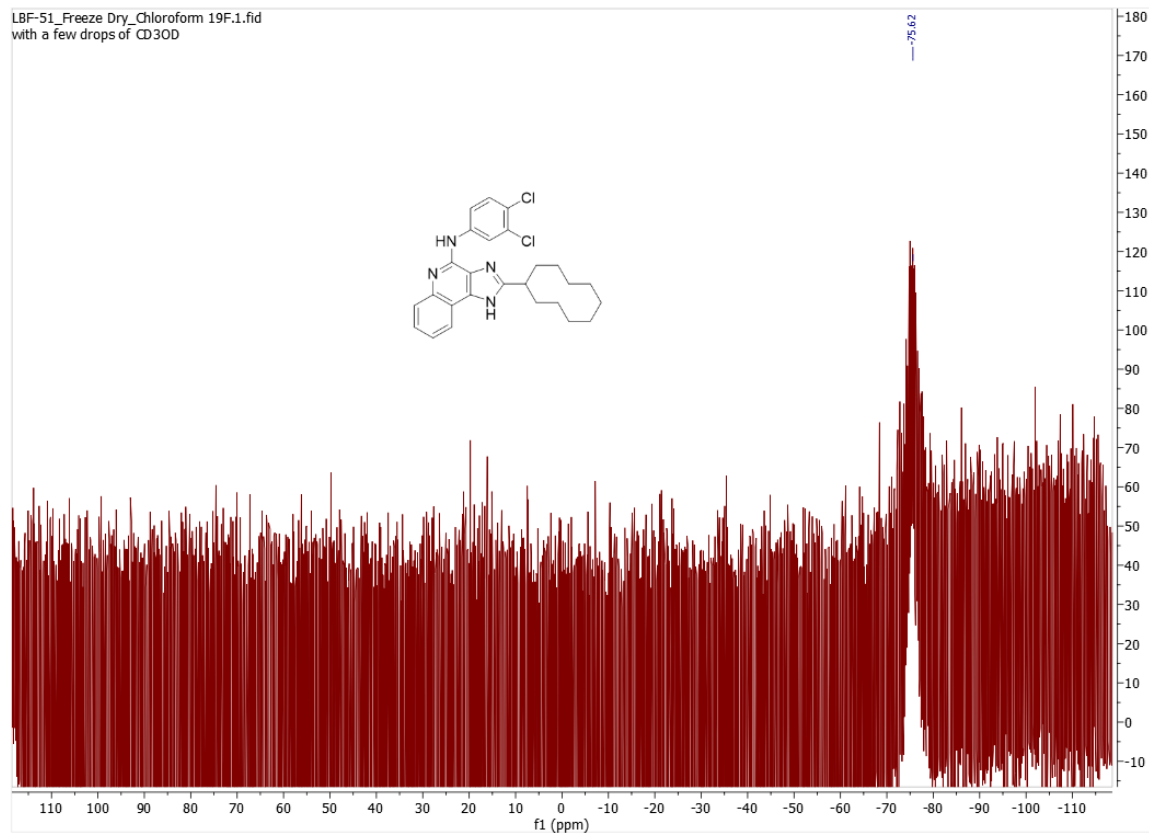
¹H NMR of 2-(cyclononyl)-*N*-(3,4-dichlorophenyl)-1*H*-imidazo[4,5-*c*]quinolin-4-amine – Compound **12**



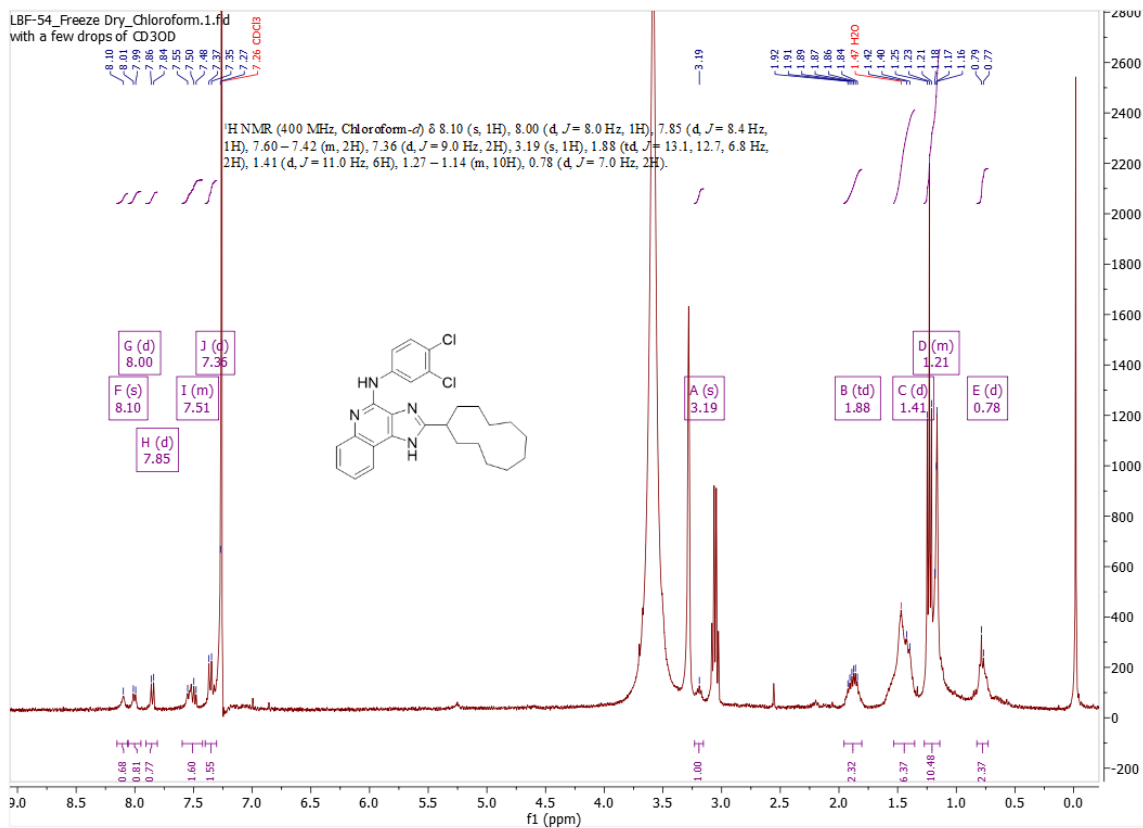
^{19}F NMR of 2-(cyclononyl)-*N*-(3,4-dichlorophenyl)-1*H*-imidazo[4,5-*c*]quinolin-4-amine
– Compound **12**



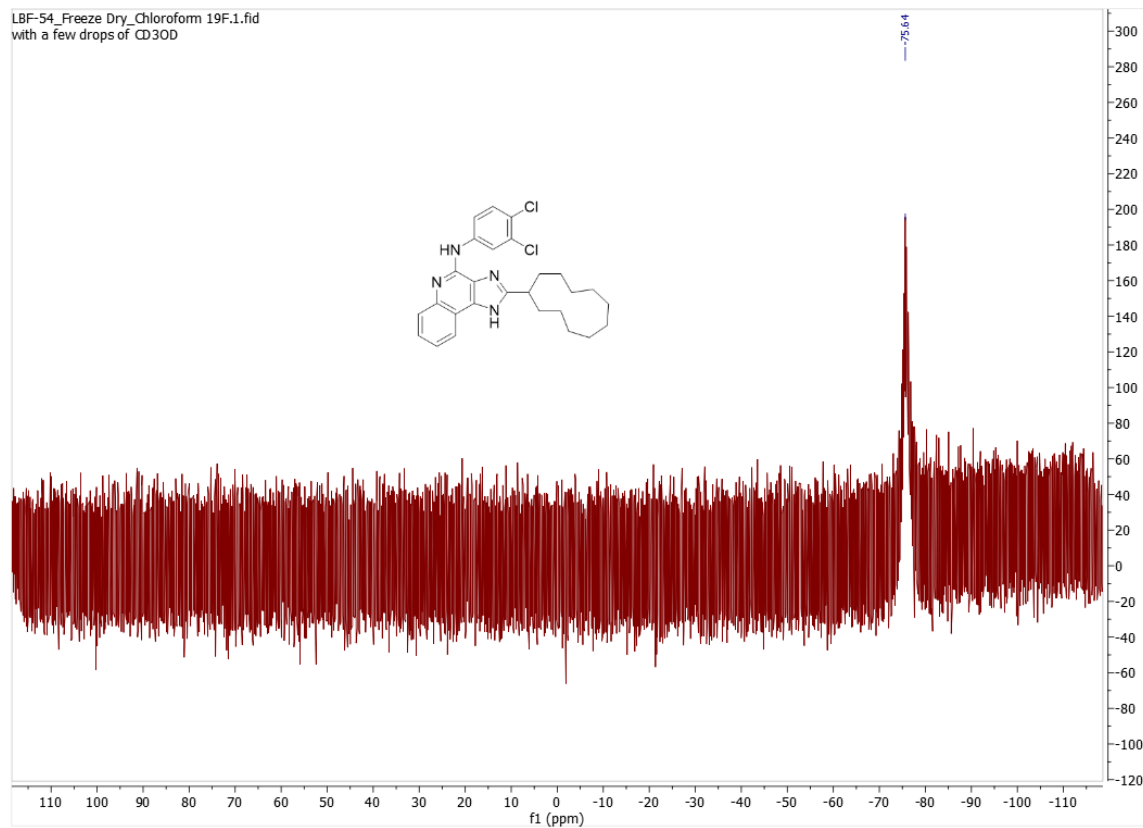
¹H NMR of 2-(cyclodecyl)-*N*-(3,4-dichlorophenyl)-1*H*-imidazo[4,5-*c*]quinolin-4-amine – Compound **13**



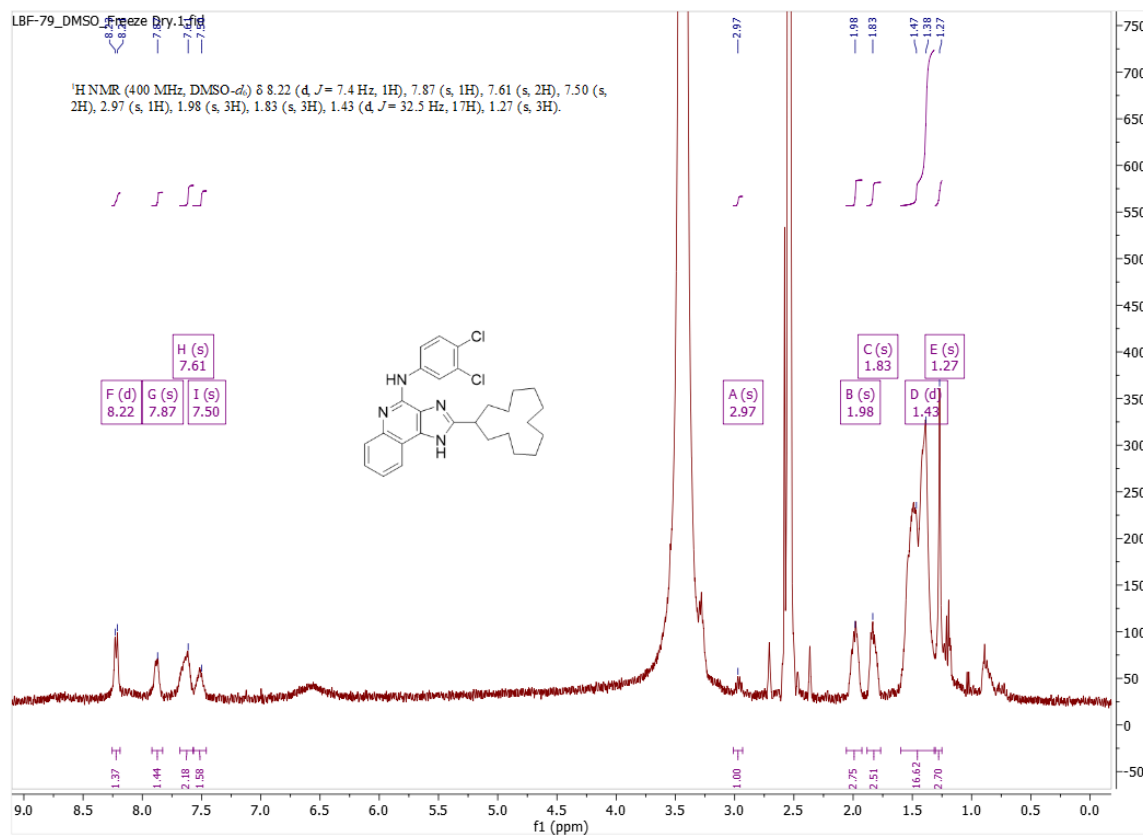
^{19}F NMR of 2-(cyclodecyl)-*N*-(3,4-dichlorophenyl)-1*H*-imidazo[4,5-*c*]quinolin-4-amine
– Compound **13**



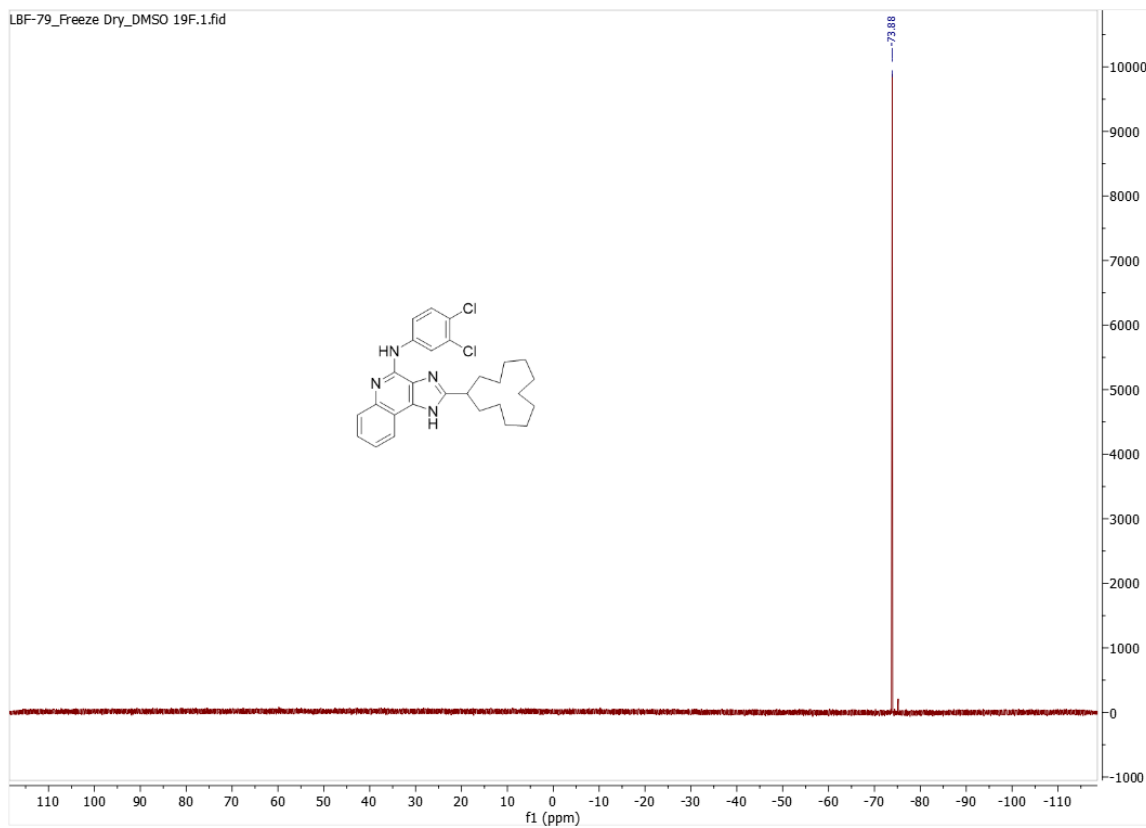
^1H NMR of 2-(cycloundecyl)-*N*-(3,4-dichlorophenyl)-1*H*-imidazo[4,5-*c*]quinolin-4-amine – Compound **14**



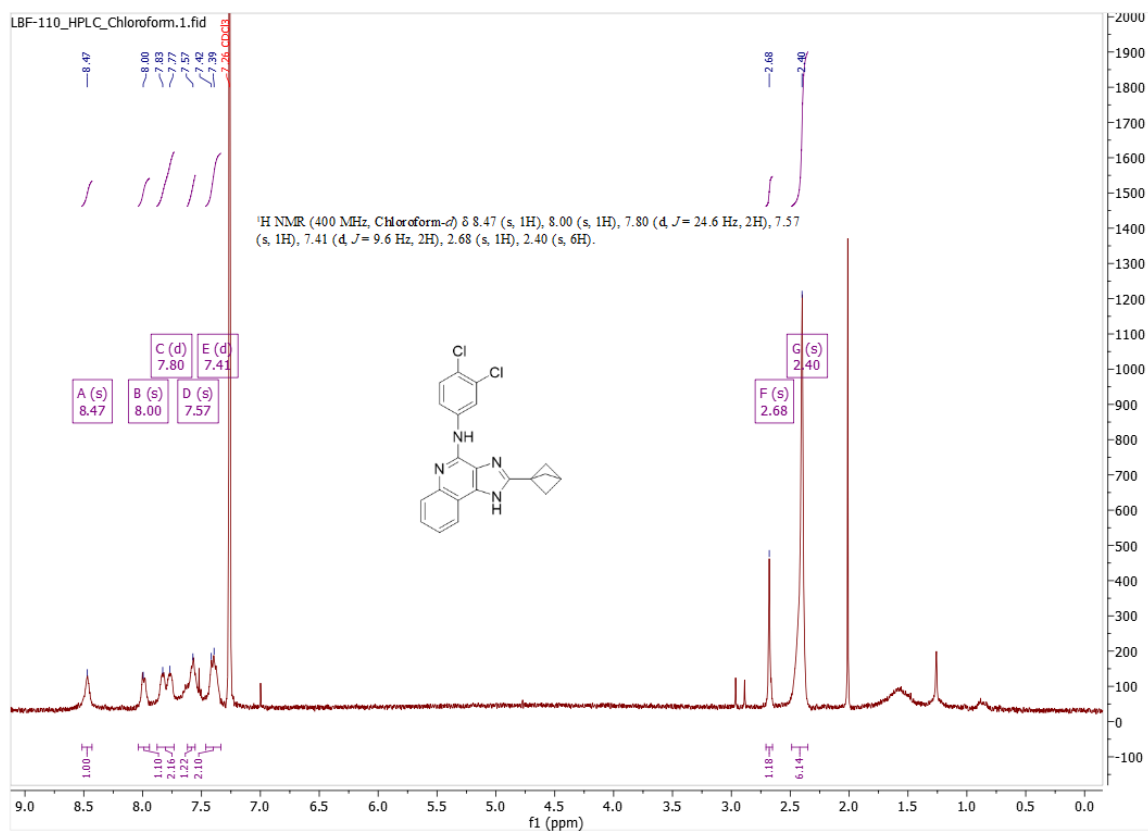
^{19}F NMR of 2-(cycloundecyl)-*N*-(3,4-dichlorophenyl)-1*H*-imidazo[4,5-*c*]quinolin-4-amine – Compound **14**



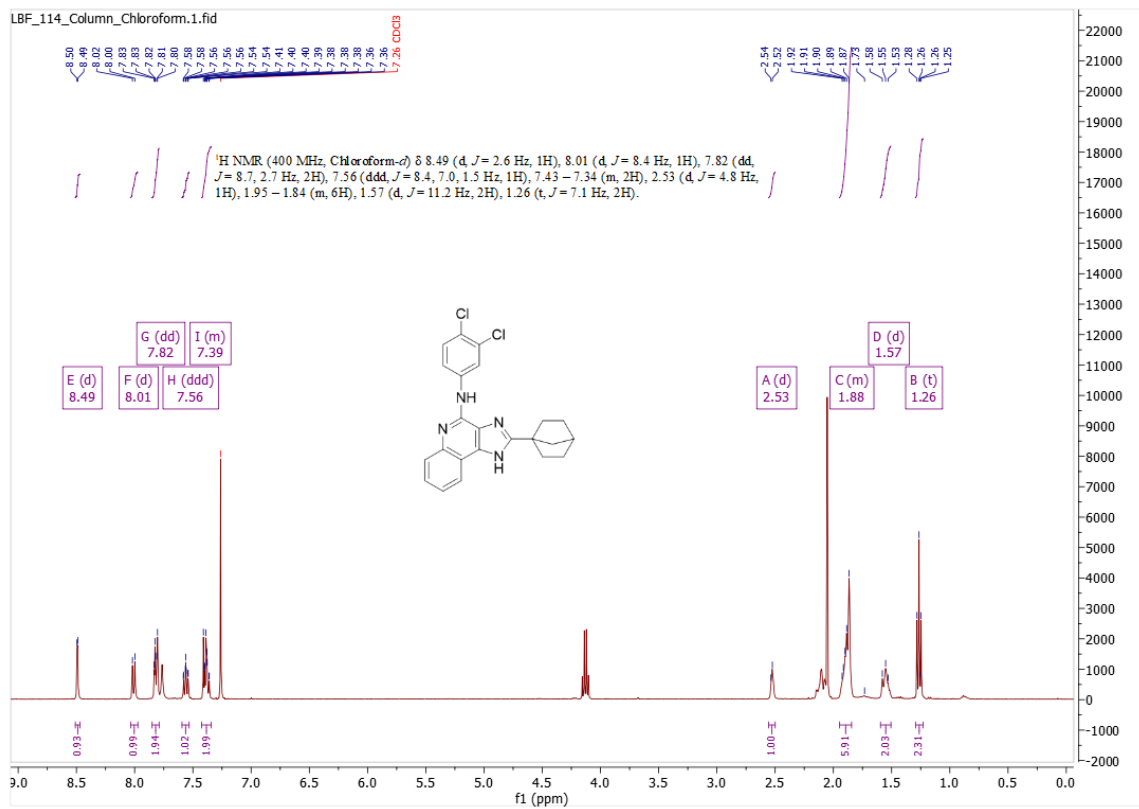
¹H NMR of 2-(cyclododecyl)-*N*-(3,4-dichlorophenyl)-1*H*-imidazo[4,5-*c*]quinolin-4-amine – Compound **15**



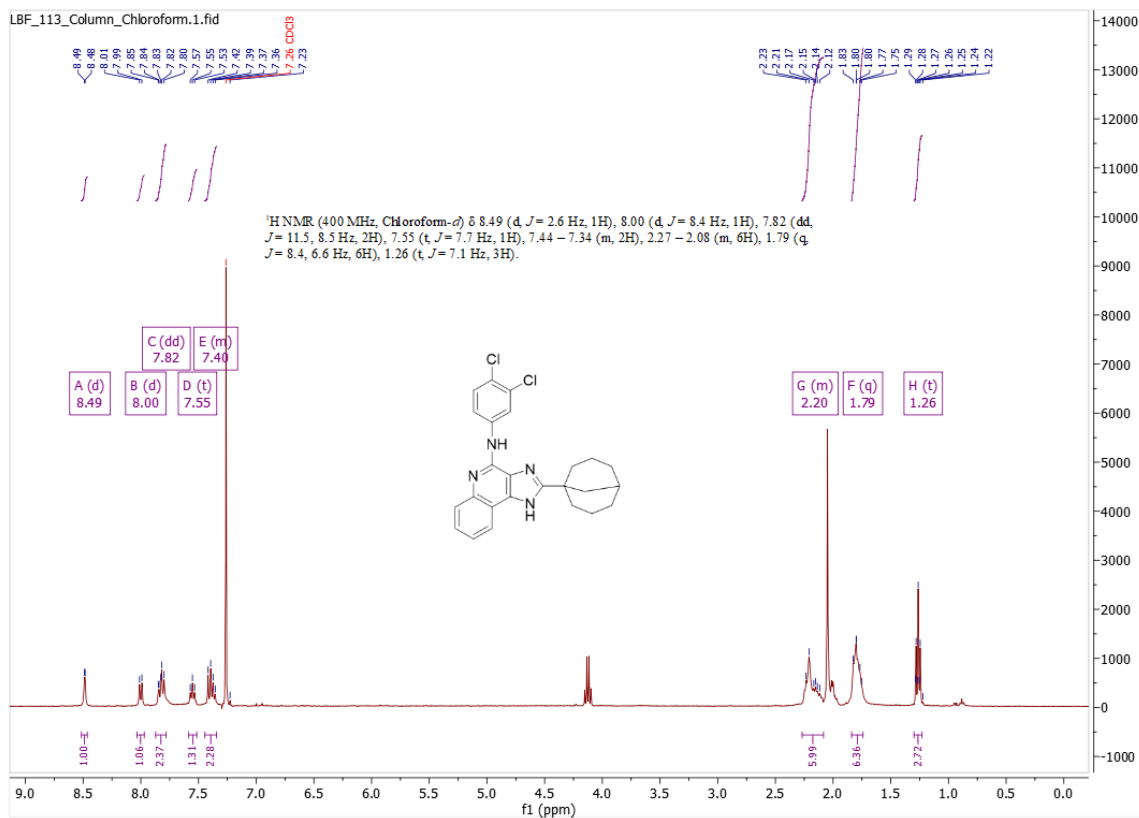
^{19}F NMR of 2-(cyclododecyl)-*N*-(3,4-dichlorophenyl)-1*H*-imidazo[4,5-*c*]quinolin-4-amine – Compound **15**



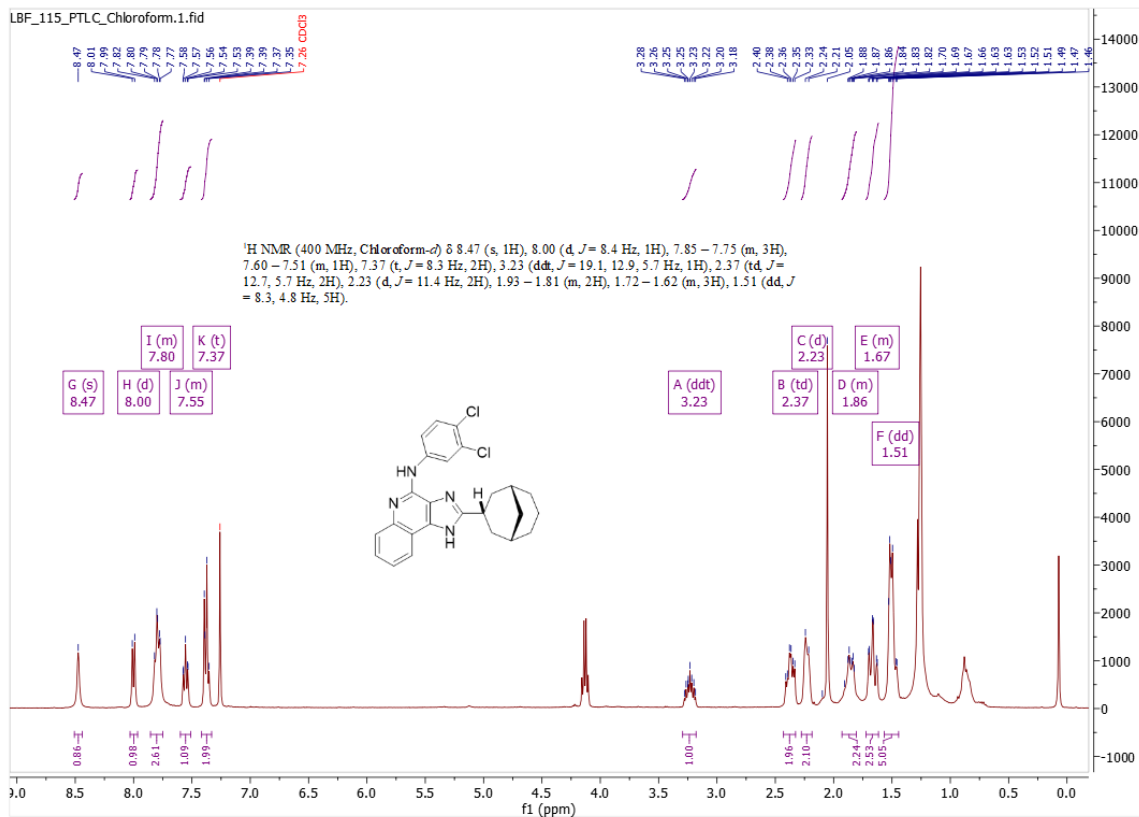
¹H NMR of 2-(bicyclo[1.1.1]heptan-1-yl)-*N*-(3,4-dichlorophenyl)-1*H*-imidazo[4,5-*c*]quinolin-4-amine – Compound **16**



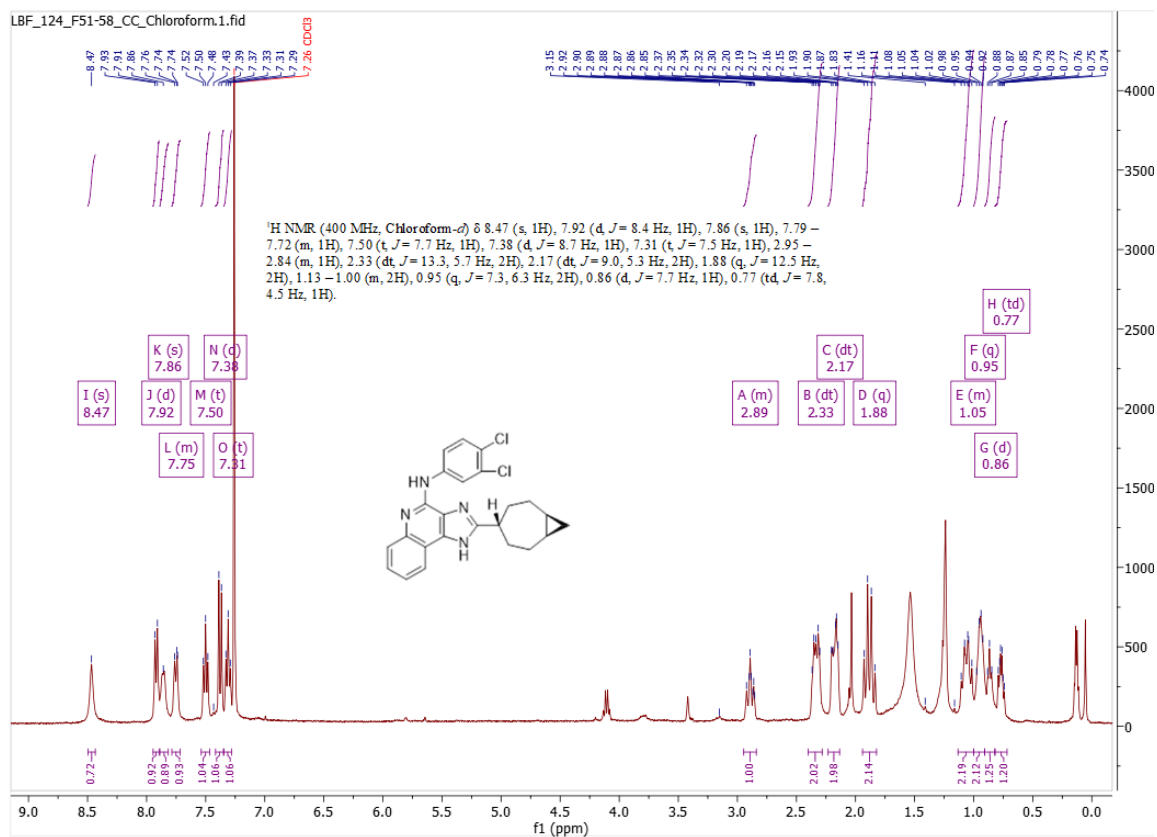
¹H NMR of 2-(bicyclo[2.2.1]heptan-1-yl)-*N*-(3,4-dichlorophenyl)-1*H*-imidazo[4,5-*c*]quinolin-4-amine – Compound **17**



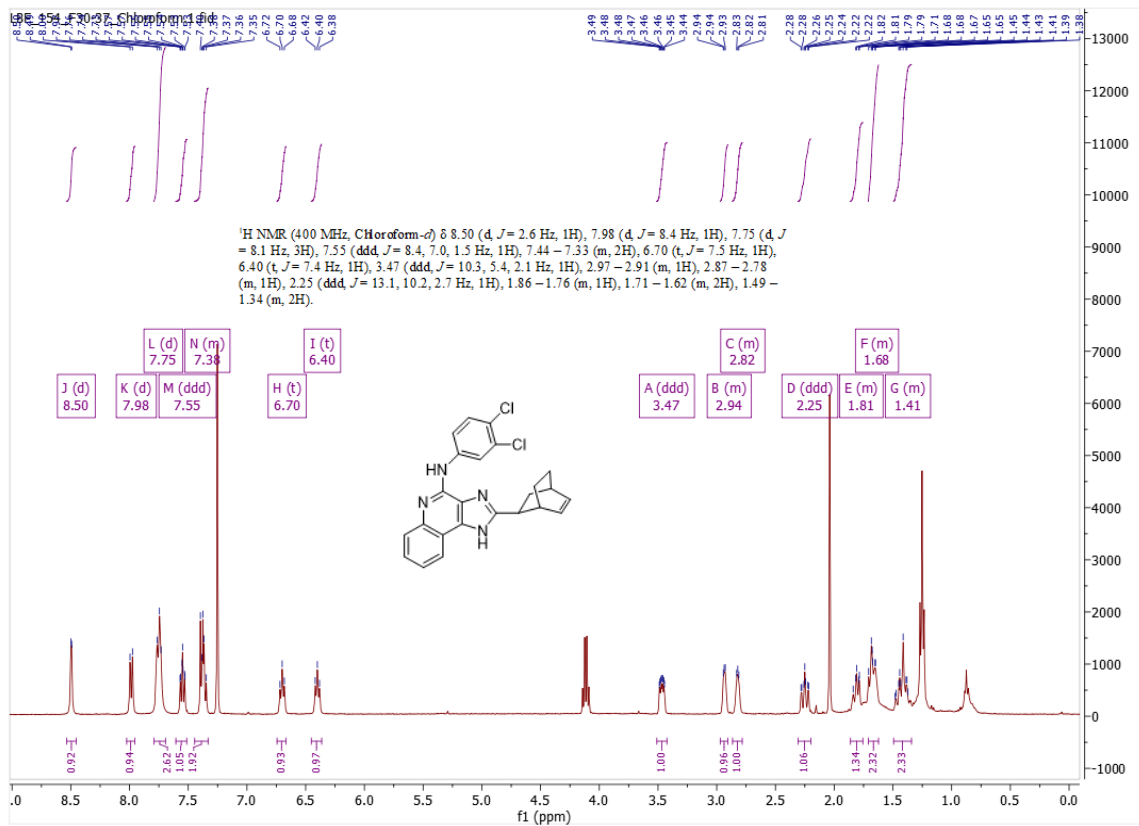
¹H NMR of 2-(bicyclo[3.3.1]nonan-1-yl)-*N*-(3,4-dichlorophenyl)-1*H*-imidazo[4,5-*c*]quinolin-4-amine – Compound **18**



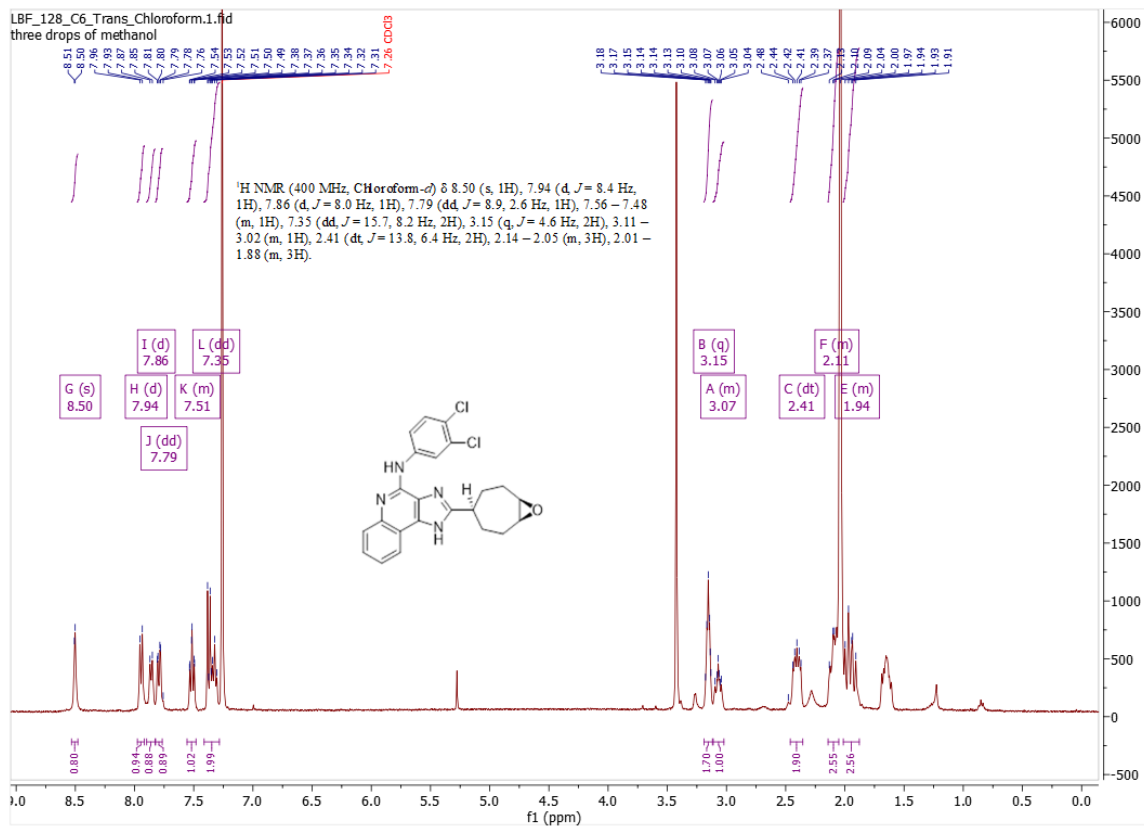
¹H NMR of 2-((1*R*,3*S*,5*S*)-bicyclo[3.3.1]nonan-3-yl)-*N*-(3,4-dichlorophenyl)-1*H*-imidazo[4,5-*c*]quinolin-4-amine – Compound **19**



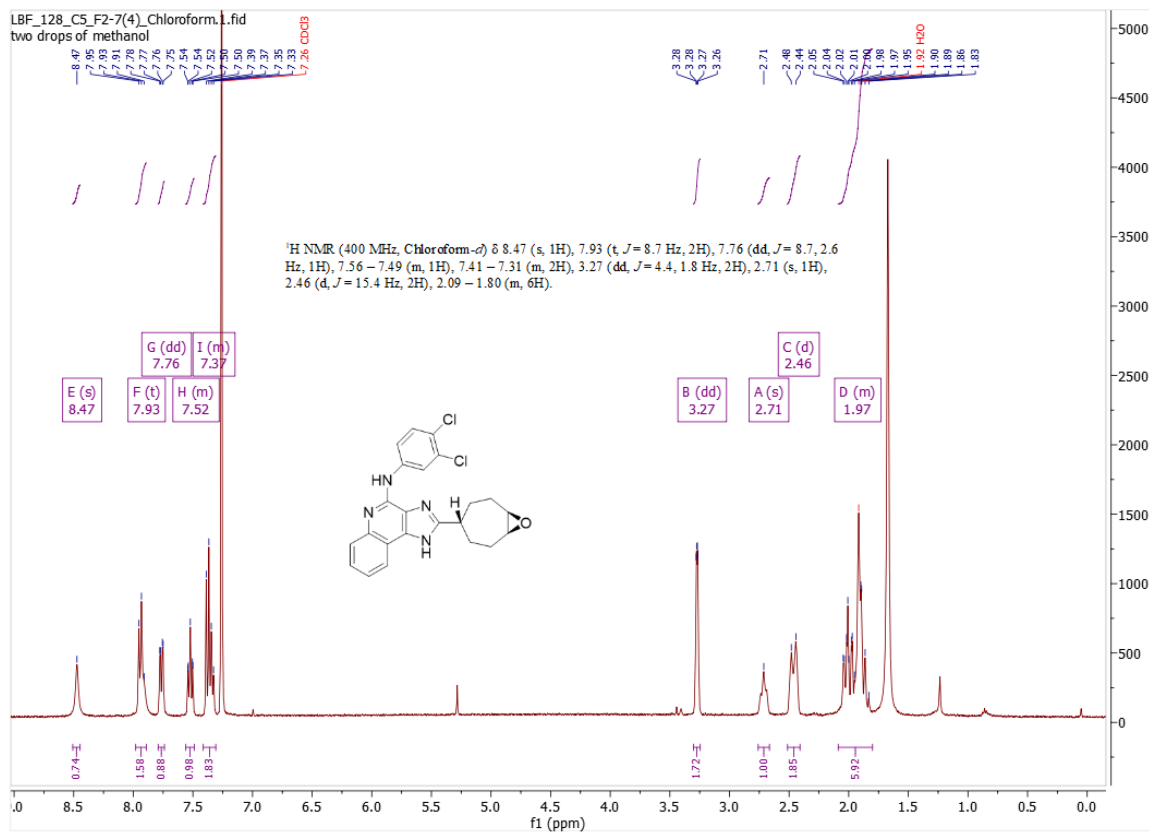
¹H NMR of 2-((1R,4r,7S)-bicyclo[5.1.0]octan-4-yl)-N-(3,4-dichlorophenyl)-1H-imidazo[4,5-c]quinolin-4-amine – Compound **20**



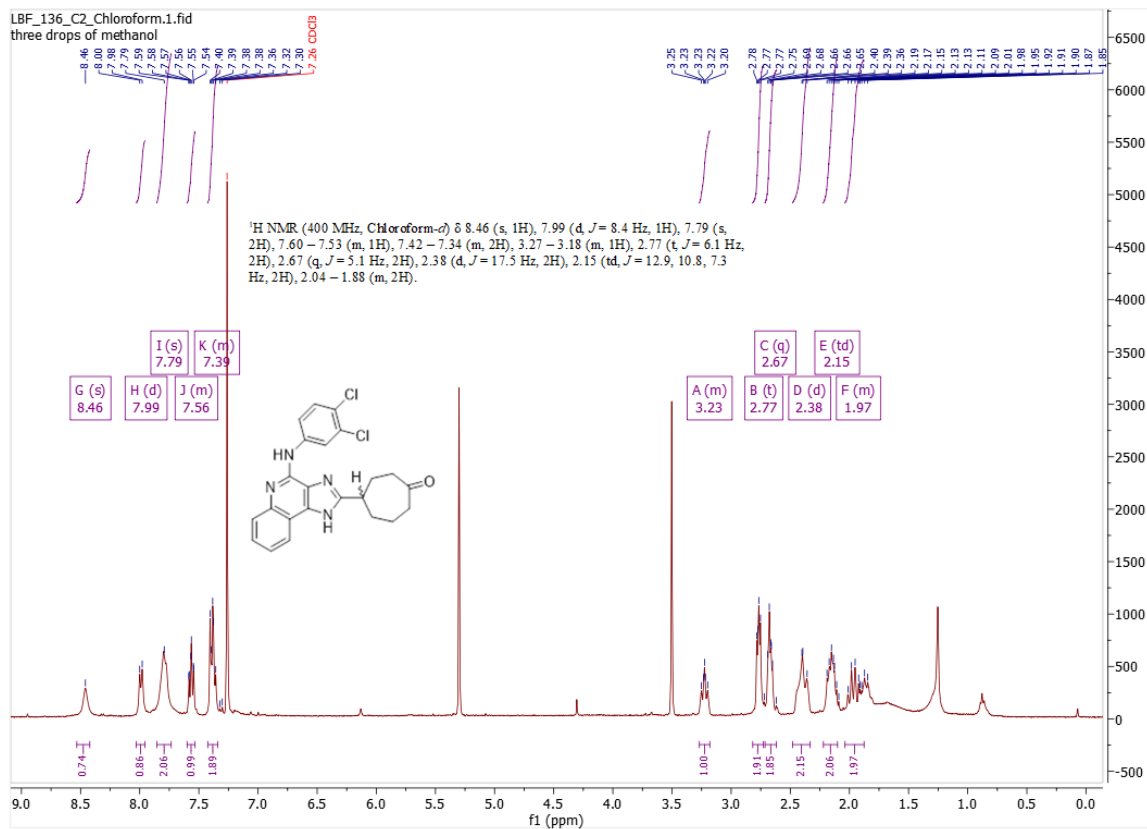
¹H NMR of 2-((1R,2R,4R) & (1S,2S,4S)-bicyclo[2.2.2]oct-5-en-2-yl)-N-(3,4-dichlorophenyl)-1H-imidazo[4,5-c]quinolin-4-amine – Compound **21**



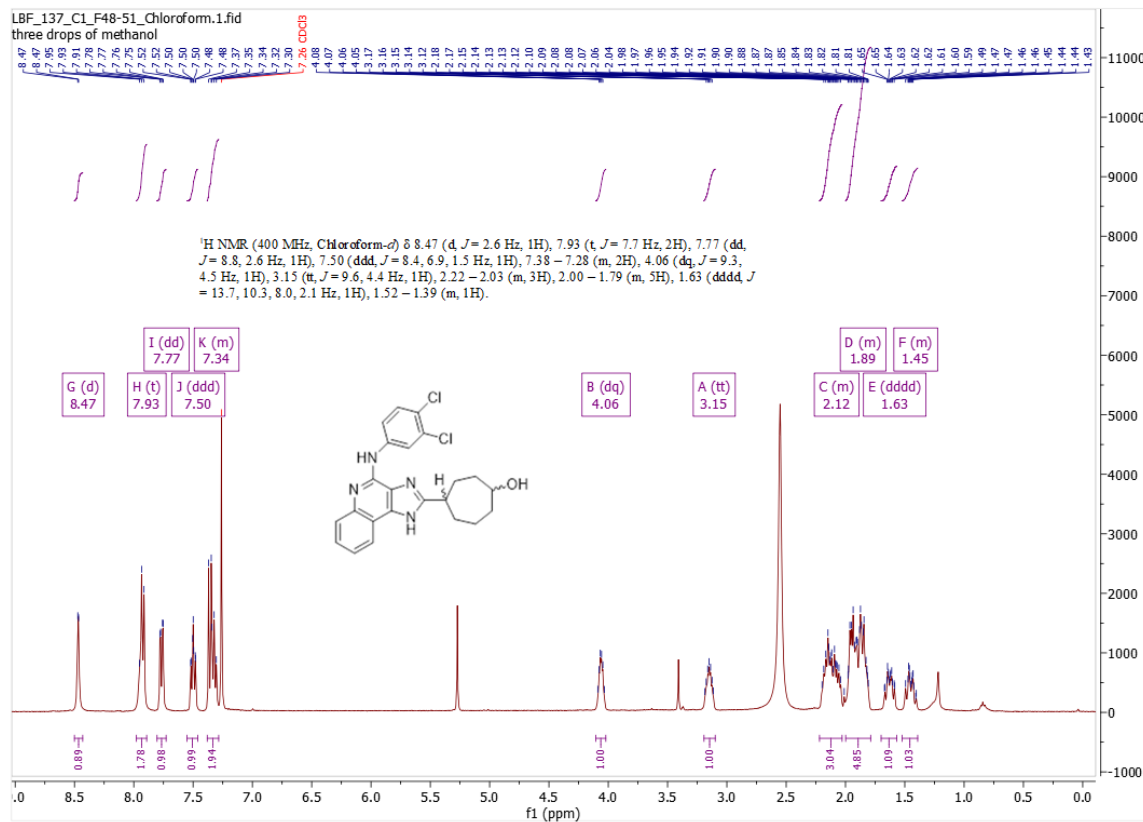
¹H NMR of 2-((1R,4r,7S)-8-oxabicyclo[5.1.0]octan-4-yl)-N-(3,4-dichlorophenyl)-1H-imidazo[4,5-c]quinolin-4-amine – Compound 22



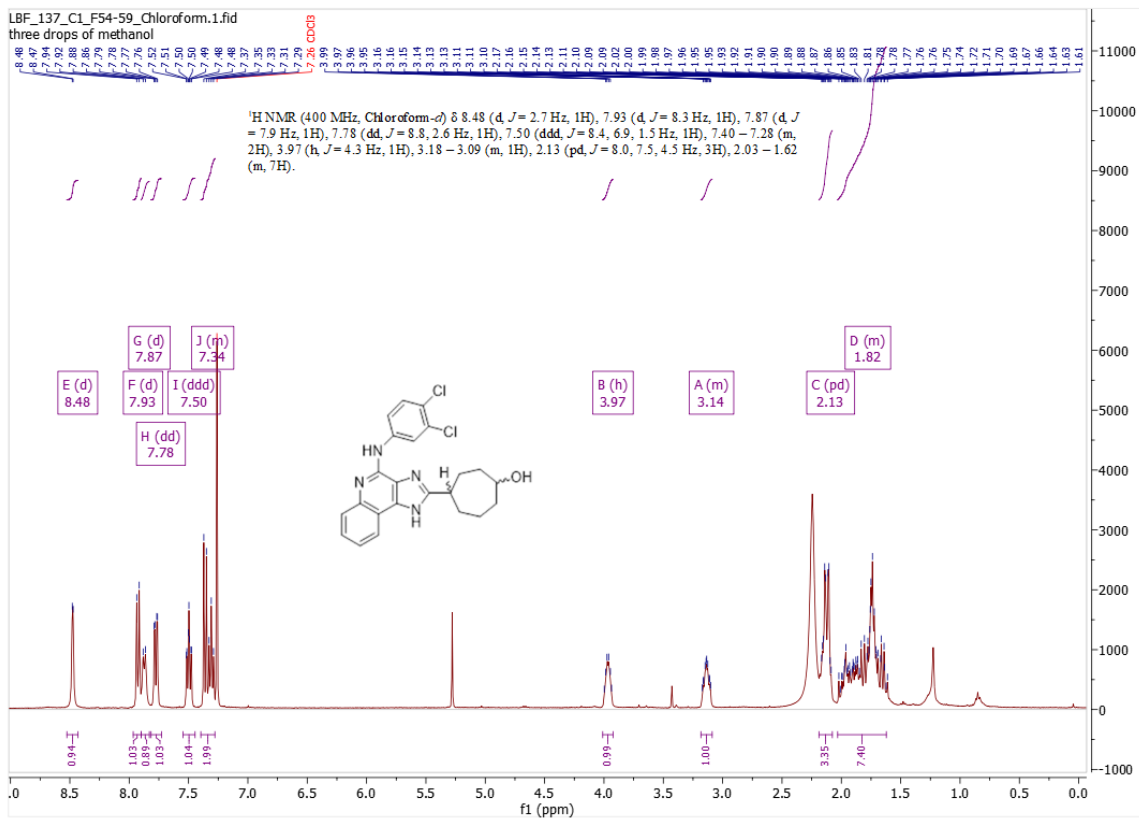
¹H NMR of 2-((1R,4S,7S)-8-oxabicyclo[5.1.0]octan-4-yl)-N-(3,4-dichlorophenyl)-1H-imidazo[4,5-c]quinolin-4-amine – Compound 23



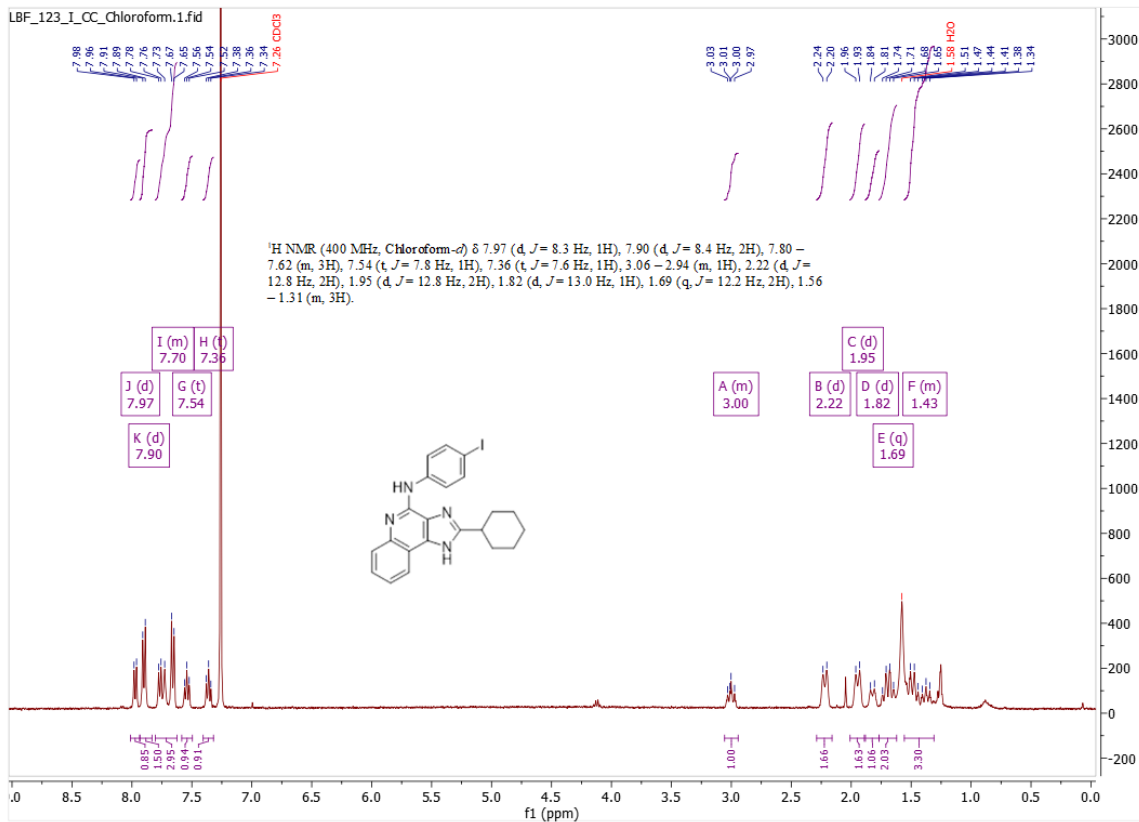
¹H NMR of (R)- & (S)-4-(4-((3,4-dichlorophenyl)amino)-1*H*-imidazo[4,5-*c*]quinolin-2-yl)cycloheptan-1-one – Compound **24**



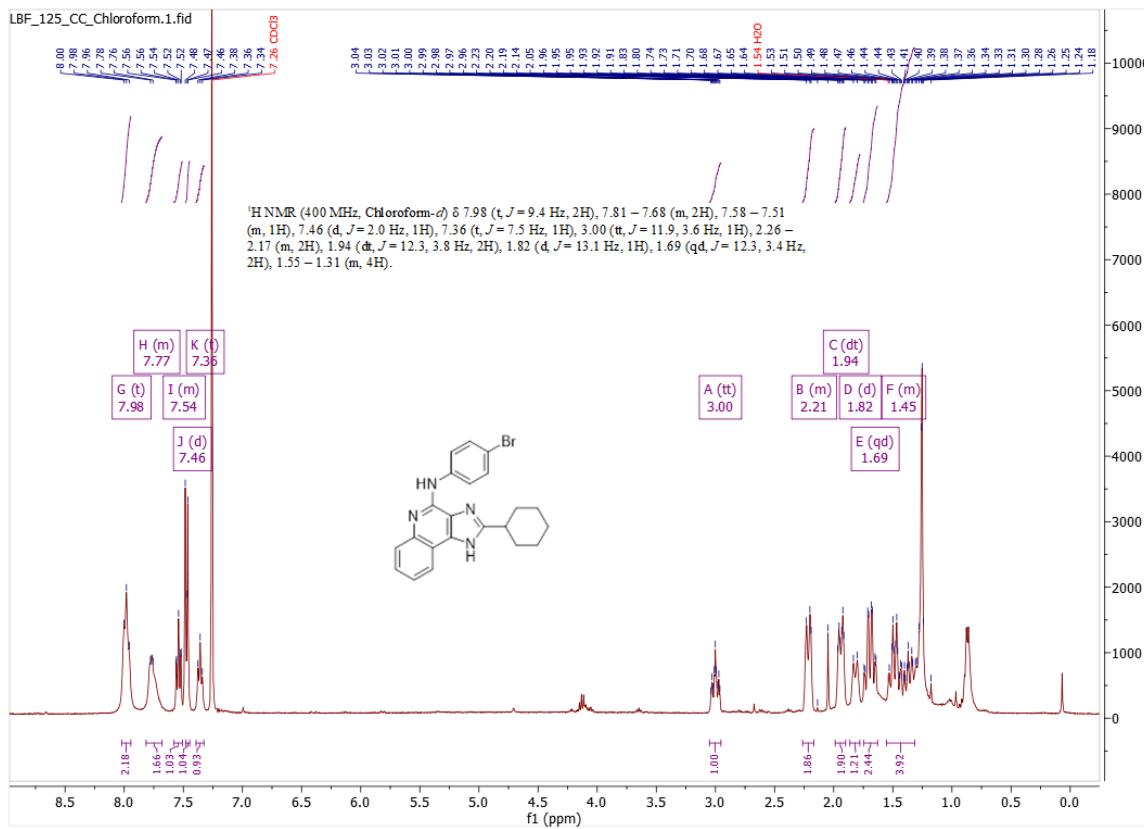
¹H NMR of (1R,4S)- & (1S,4R)-4-(4-(3,4-dichlorophenyl)amino)-1H-imidazo[4,5-c]quinolin-2-yl)cycloheptan-1-ol – Compound **25**



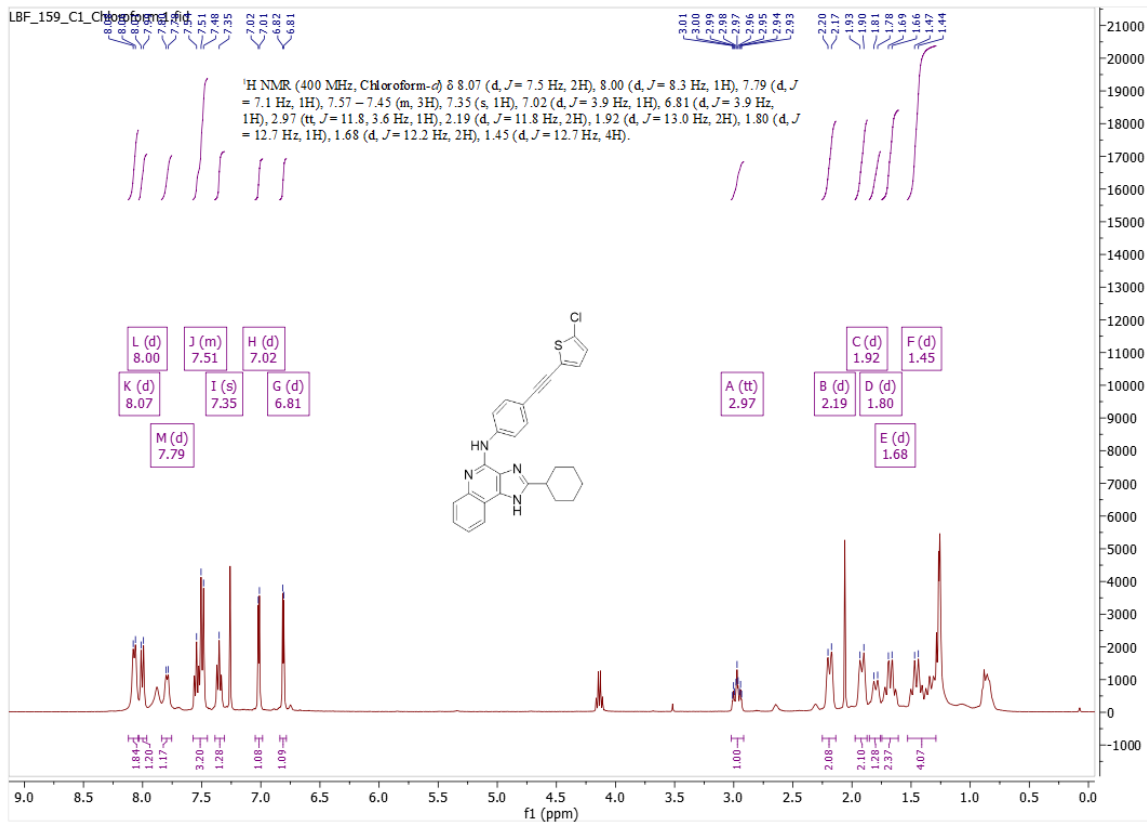
¹H NMR of (1*R*,4*R*)-, & (1*S*,4*S*)-4-(4-((3,4-dichlorophenyl)amino)-1*H*-imidazo[4,5-*c*]quinolin-2-yl)cycloheptan-1-ol – Compound **26**



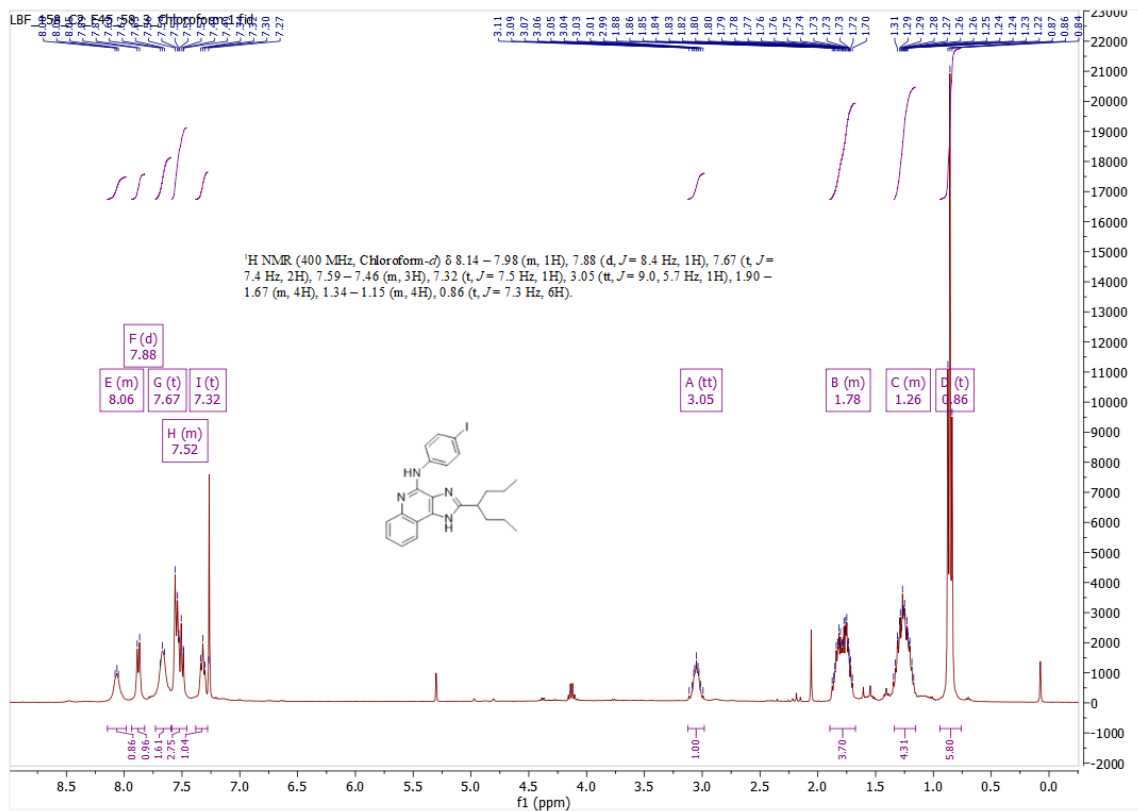
¹H NMR of 2-cyclohexyl-*N*-(4-iodophenyl)-1*H*-imidazo[4,5-*c*]quinolin-4-amine – Compound **27**



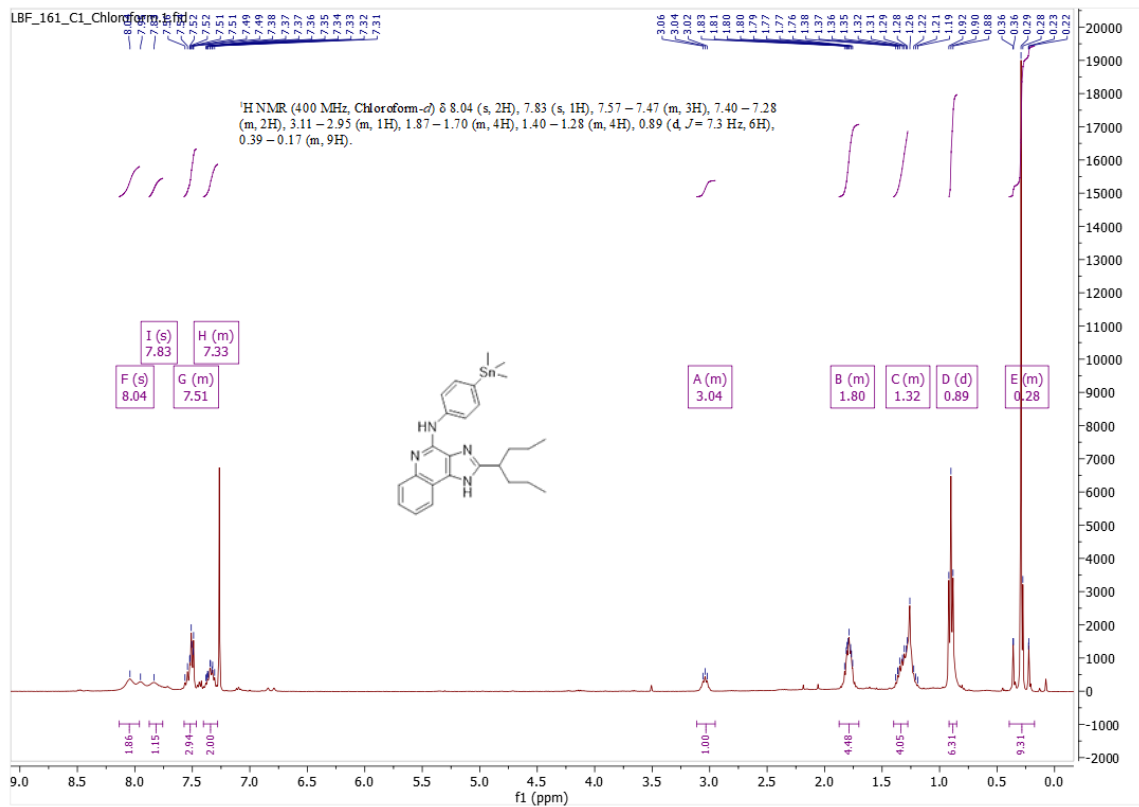
¹H NMR of 2-cyclohexyl-*N*-(4-bromophenyl)-1*H*-imidazo[4,5-*c*]quinolin-4-amine –
Compound **28**



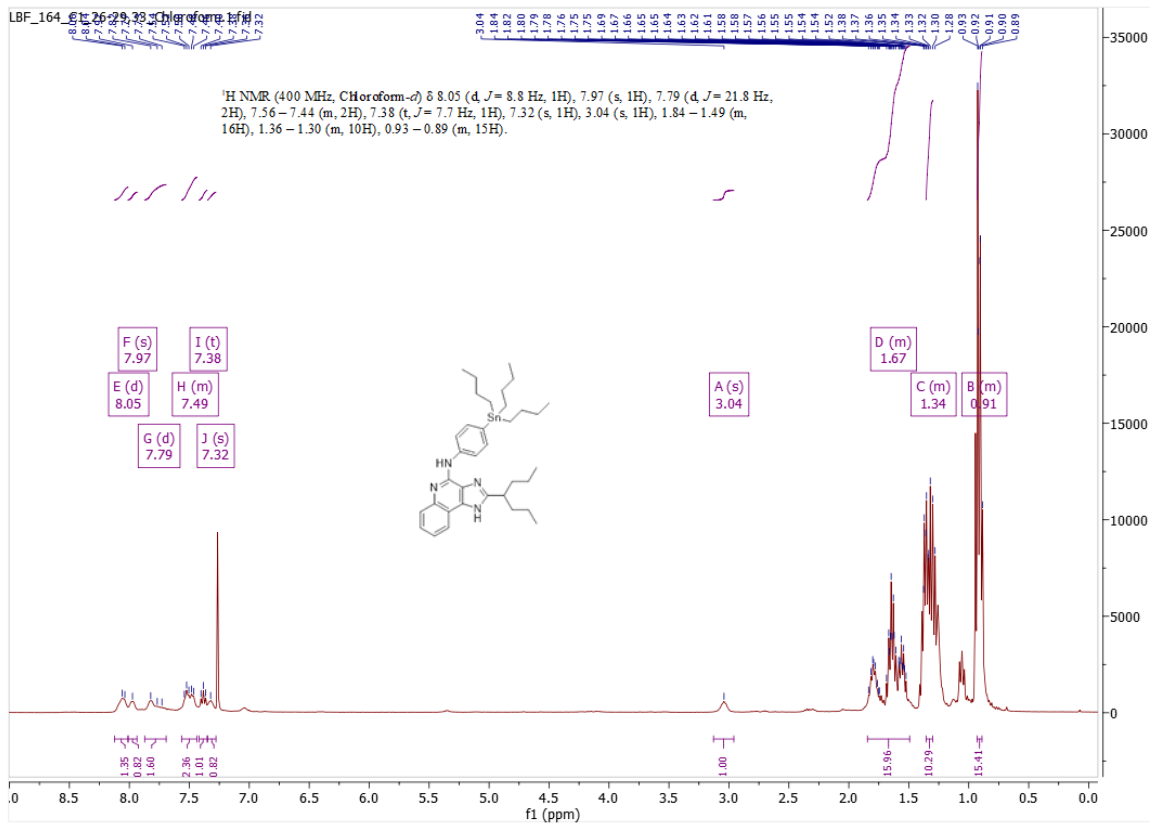
¹H NMR of 2-cyclohexyl-*N*-(4-((5-chlorothiophen-2-yl)ethynyl)phenyl)-1*H*-imidazo[4,5-*c*]quinolin-4-amine – Compound **30**



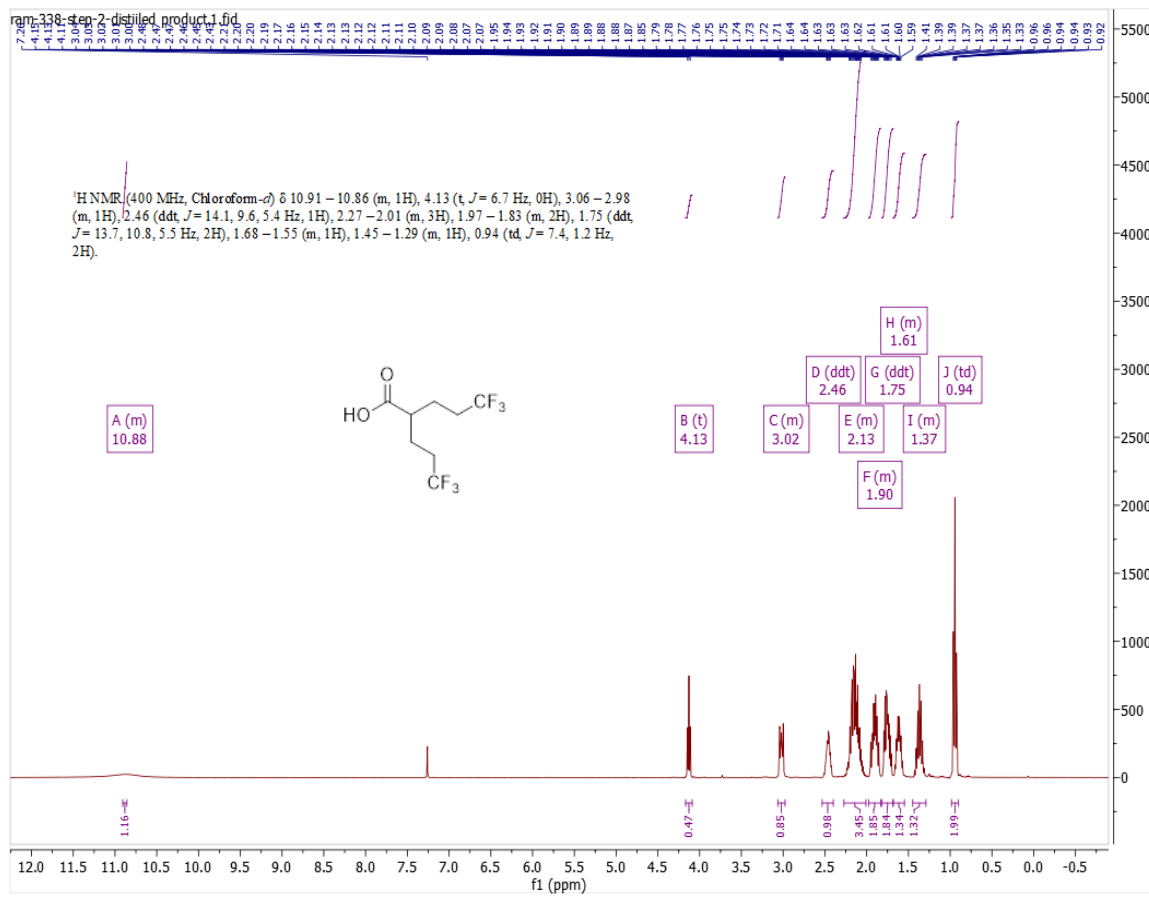
¹H NMR of 2-(heptan-4-yl)-*N*-(4-iodophenyl)-1*H*-imidazo[4,5-*c*]quinolin-4-amine –
Compound **31**



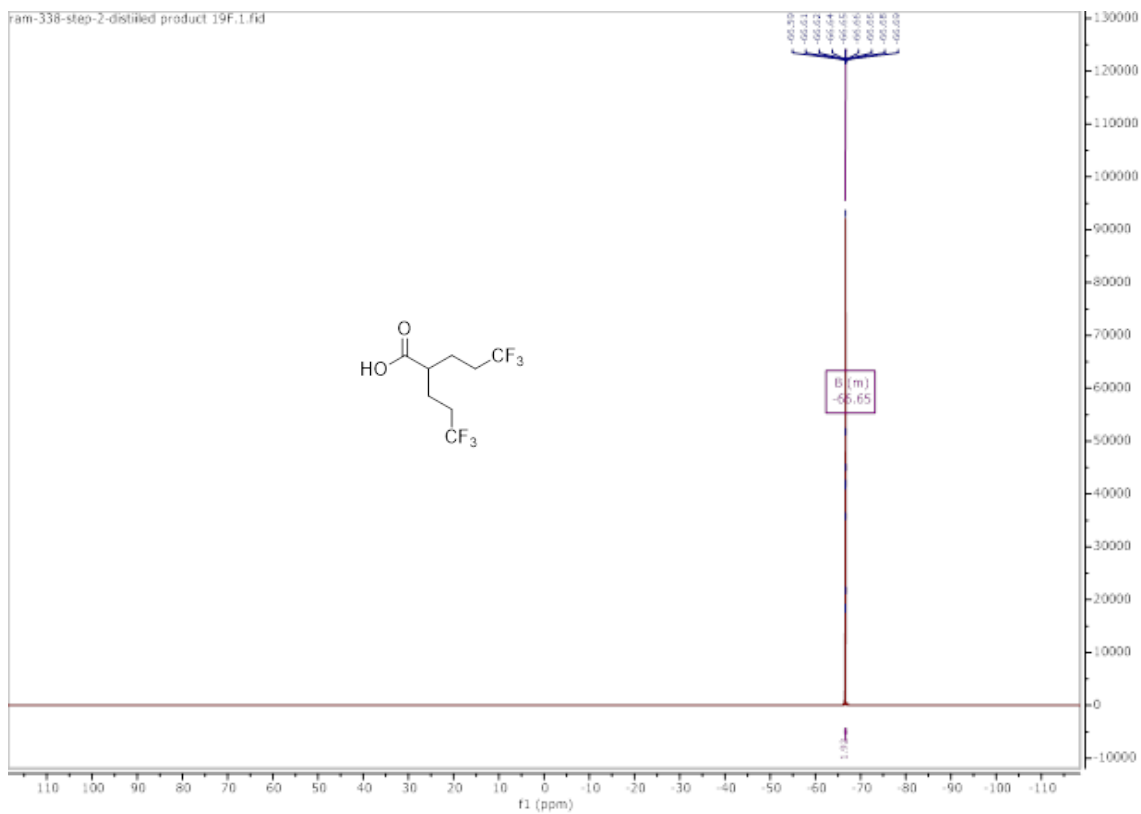
¹H NMR of 2-(heptan-4-yl)-*N*-(4-(trimethylstannyl)phenyl)-1*H*-imidazo[4,5-*c*]quinolin-4-amine – Compound **32**



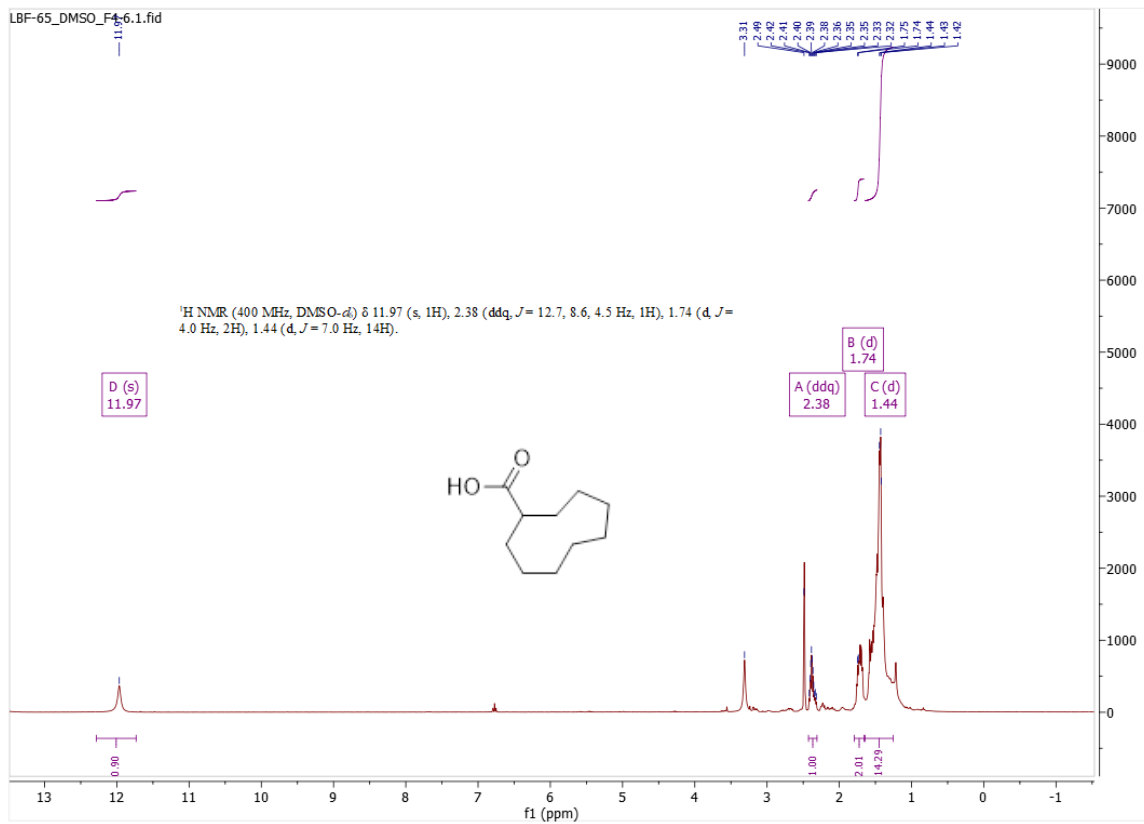
¹H NMR of 2-(heptan-4-yl)-*N*-(4-(tributylstannyl)phenyl)-1*H*-imidazo[4,5-*c*]quinolin-4-amine – Compound **33**



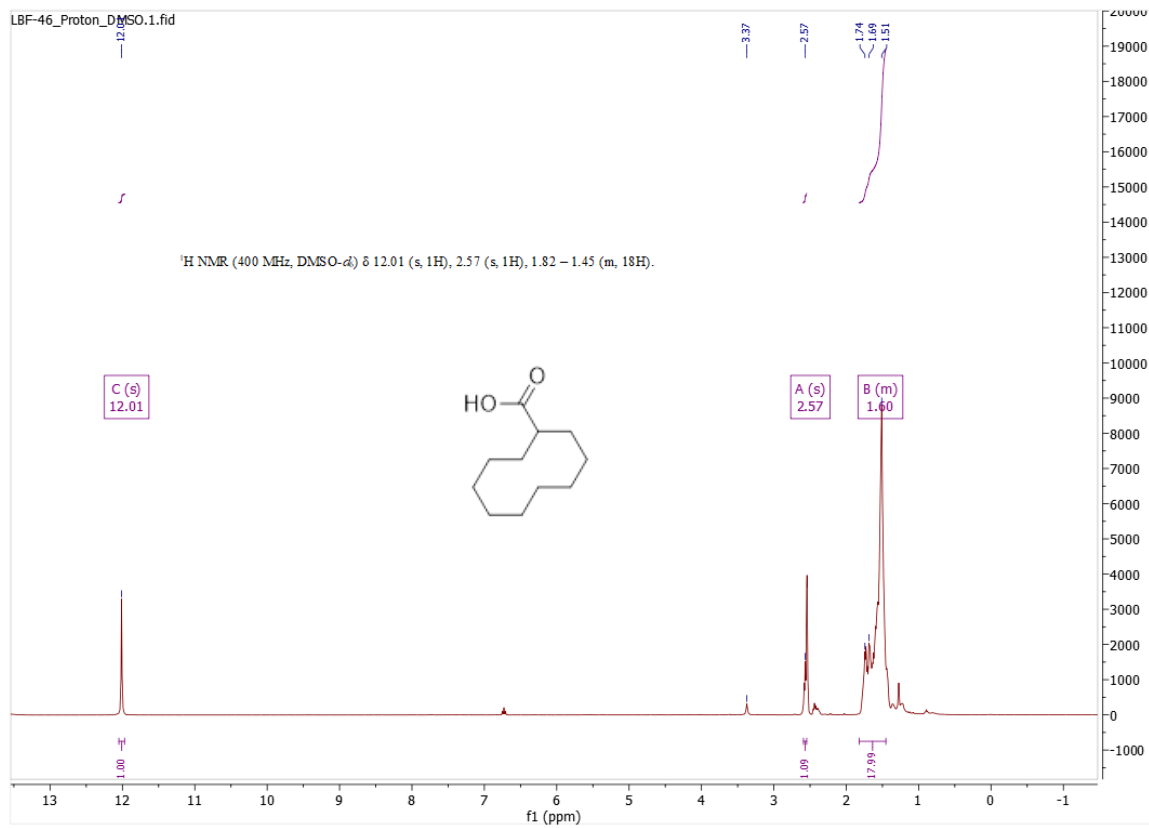
¹H NMR of 5,5,5-trifluoro-2-(3,3,3-trifluoropropyl)pentanoic acid



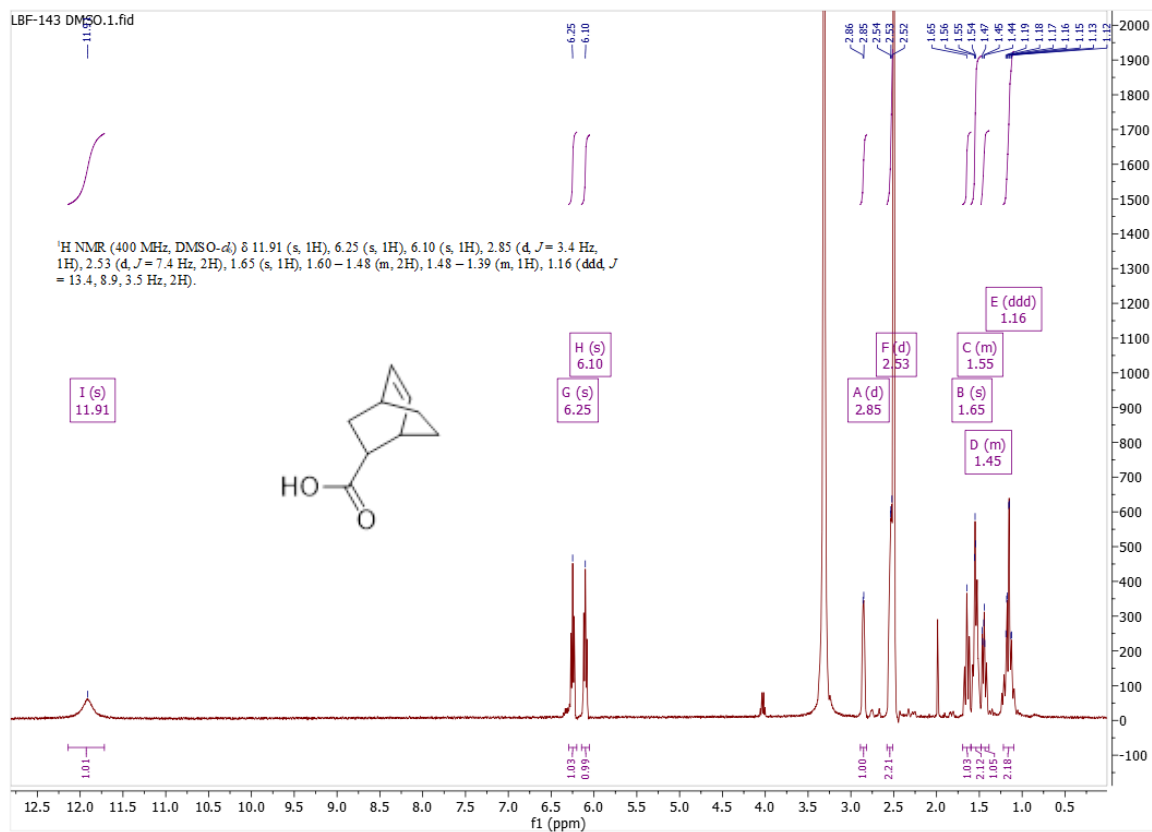
^{19}F NMR of 5,5,5-trifluoro-2-(3,3,3-trifluoropropyl)pentanoic acid



¹H NMR of cyclononanecarboxylic acid

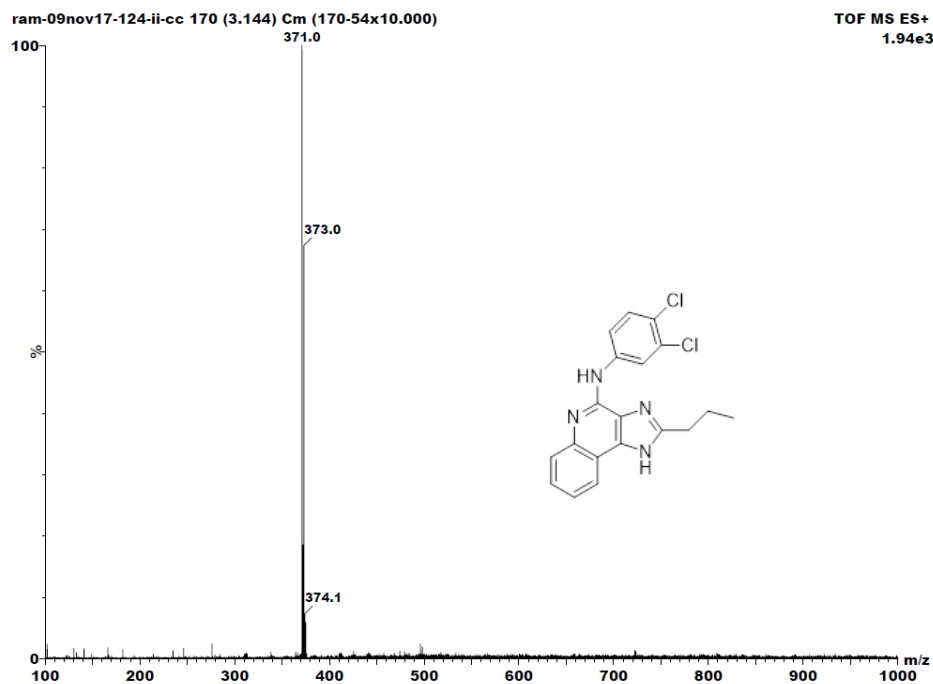


$^1\text{H NMR}$ of cyclodecanecarboxylic acid



¹H NMR of ((1R,2R,4R)- & (1S,2S,4S)-bicyclo[2.2.2]oct-5-ene carboxylic acid

Appendix B: Compound Mass Spectra and Elemental Analysis



Elemental Composition Report

Page 1

Single Mass Analysis

Tolerance = 10.0 mDa / DBE: min = -2.0, max = 1000.0

Element prediction: Off

Number of isotope peaks used for i-FIT = 3

Monoisotopic Mass, Even Electron Ions

42 formula(e) evaluated with 3 results within limits (up to 19 closest results for each mass)

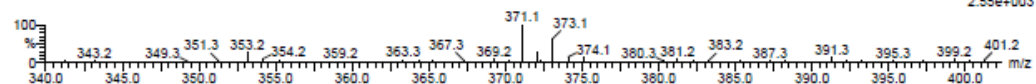
Elements Used:

C: 0-100 H: 0-200 N: 4-4 O: 0-20 35Cl: 2-2

09-Nov-2017

ram-09nov17-124-ii-cc 172 (3.181) Cn (Cen,3, 50.00, Ar); Sm (SG, 3x5.00); Sb (12,5.00)

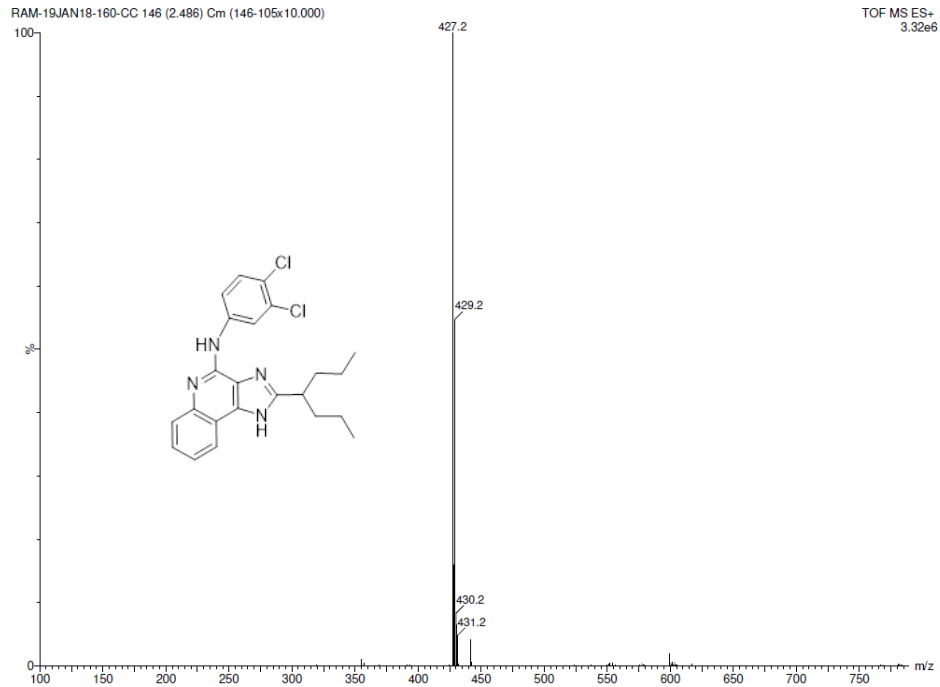
TOF MS ES+
2.55e+003



Minimum: -2.0
Maximum: 10.0 10.0 1000.0

Mass	Calc. Mass	mDa	PPM	DBE	i-FIT	Formula
371.0827	371.0890	-0.3	-0.8	12.5	758.5	C19 H17 N4 35Cl2
	371.0889	-6.2	-16.7	9.5	822.8	C12 H21 N4 O5 35Cl2
	371.0796	9.1	24.5	-0.5	978.6	C8 H21 N4 O8 35Cl2

TOF MS E+ and elemental analysis of 2-propyl-N-(3,4-dichlorophenyl)-1H-imidazo[4,5-c]quinolin-4-amine – Compound 1



Elemental Composition Report

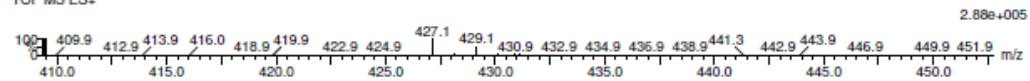
Page 1

Single Mass Analysis

Tolerance = 30.0 mDa / DBE: min = -1.5, max = 100.0
 Element prediction: Off
 Number of isotope peaks used for i-FIT = 3

Monoisotopic Mass, Even Electron Ions

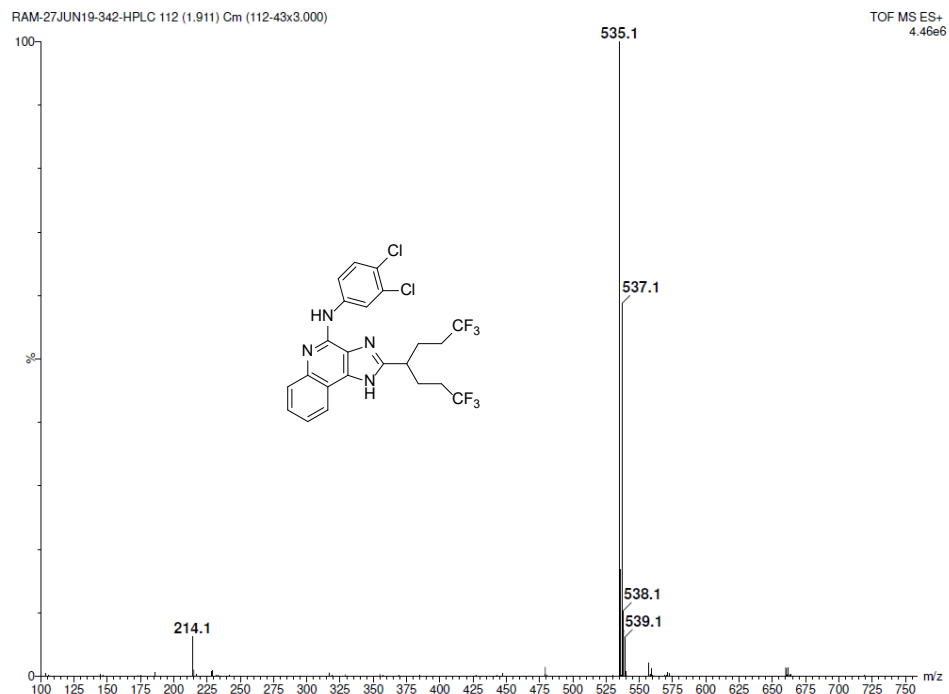
56 formula(e) evaluated with 6 results within limits (up to 50 best isotopic matches for each mass)
 Elements Used:
 C: 0-60 H: 0-200 N: 4-4 O: 0-40 35Cl: 2-2
 RAM-19JAN18-160-CC 148 (2.520) AM (Cen,5, 50.00, Ht,10000.0,0.00,0.70); Sm (SG, 1x2.00); Sb (15,10.00)
 TOF MS ES+



Minimum: -1.5
 Maximum: 100.0

Mass	Calc. Mass	mDa	PPM	DBE	i-FIT	Norm	Conf(%)	Formula
427.1462	427.1456	0.6	1.4	12.5	225.0	2.424	8.85	C23 H25 N4 35Cl2
	427.1515	-5.3	-12.4	3.5	224.3	1.721	17.89	C16 H29 N4 O5 35Cl2
	427.1362	10.0	23.4	-0.5	223.9	1.371	25.38	C12 H29 N4 O8 35Cl2
	427.1304	15.8	37.0	8.5	224.6	2.059	12.75	C19 H25 N4 O3 35Cl2
	427.1668	-20.6	-48.2	7.5	224.7	2.140	11.77	C20 H29 N4 O2 35Cl2
	427.1726	-26.4	-61.8	-1.5	224.0	1.454	23.36	C13 H33 N4 O7 35Cl2

TOF MS E+ and elemental analysis of 2-(heptan-4-yl)-N-(3,4-dichlorophenyl)-1H-imidazo[4,5-c]quinolin-4-amine – Compound 2



Elemental Composition Report

Page 1

Single Mass Analysis

Tolerance = 5.0 mDa / DBE: min = -1.5, max = 100.0

Element prediction: Off

Number of isotope peaks used for i-FIT = 3

Monoisotopic Mass, Even Electron Ions

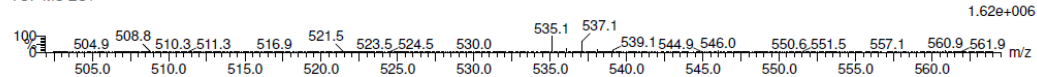
49 formula(e) evaluated with 2 results within limits (up to 50 closest results for each mass)

Elements Used:

C: 0-100 H: 0-250 N: 4-4 O: 0-60 F: 6-6 35Cl: 2-2

RAM-27JUN19-342-HPLC 115 (1.962) AM2 (Ar,25000.0,0.00,0.00); ABS

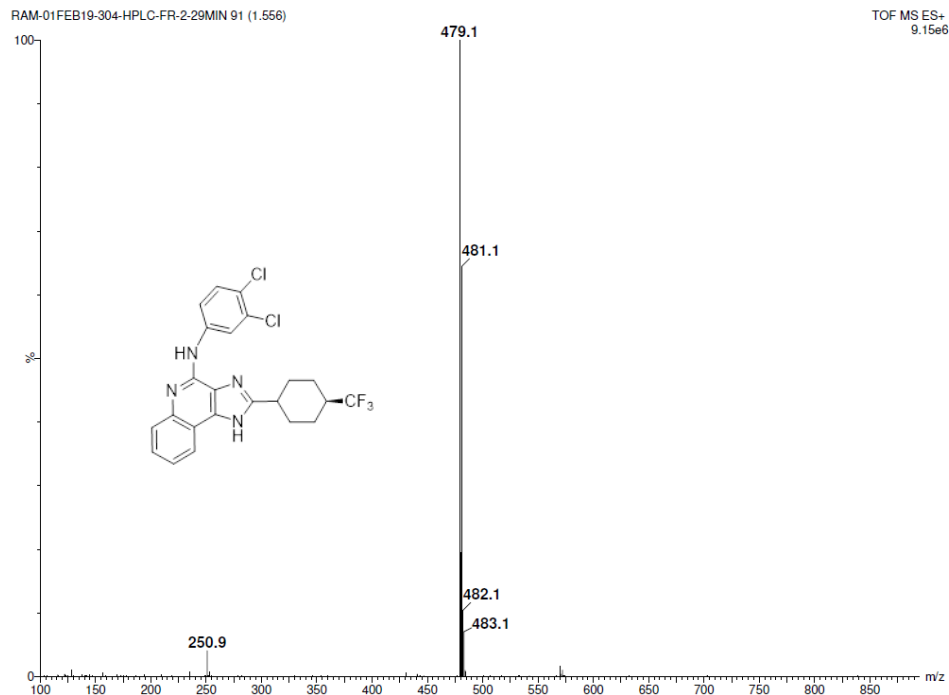
TOF MS ES+



Minimum: -1.5
Maximum: 5.0 5.0 100.0

Mass	Calc. Mass	mDa	PPM	DBE	i-FIT	Norm	Conf (%)	Formula
535.0901	535.0891	1.0	1.9	12.5	482.5	0.758	46.85	C23 H19 N4 F6 35Cl2
	535.0950	-4.9	-9.2	3.5	482.4	0.632	53.15	C16 H23 N4 O5 F6 35Cl2

TOF MS E+ and elemental analysis of 2-(1,1,1,7,7,7-hexafluoroheptan-4-yl)-N-(3,4-dichlorophenyl)-1H-imidazo[4,5-c]quinolin-4-amine – Compound 3



Elemental Composition Report

Page 1

Single Mass Analysis

Tolerance = 5.0 mDa / DBE: min = -1.5, max = 100.0

Element prediction: Off

Number of isotope peaks used for i-FIT = 3

Monoisotopic Mass, Even Electron Ions

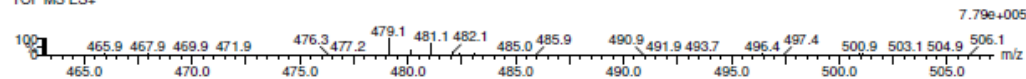
52 formula(e) evaluated with 1 results within limits (up to 50 closest results for each mass)

Elements Used:

C: 0-150 H: 0-200 N: 4-4 O: 0-60 F: 3-3 35Cl: 2-2

RAM-01FEB19-304-HPLC-FR-2-29MIN 174 (2.960) AM2 (Ar,25000.0,0.00,0.00); ABS

TOF MS ES+

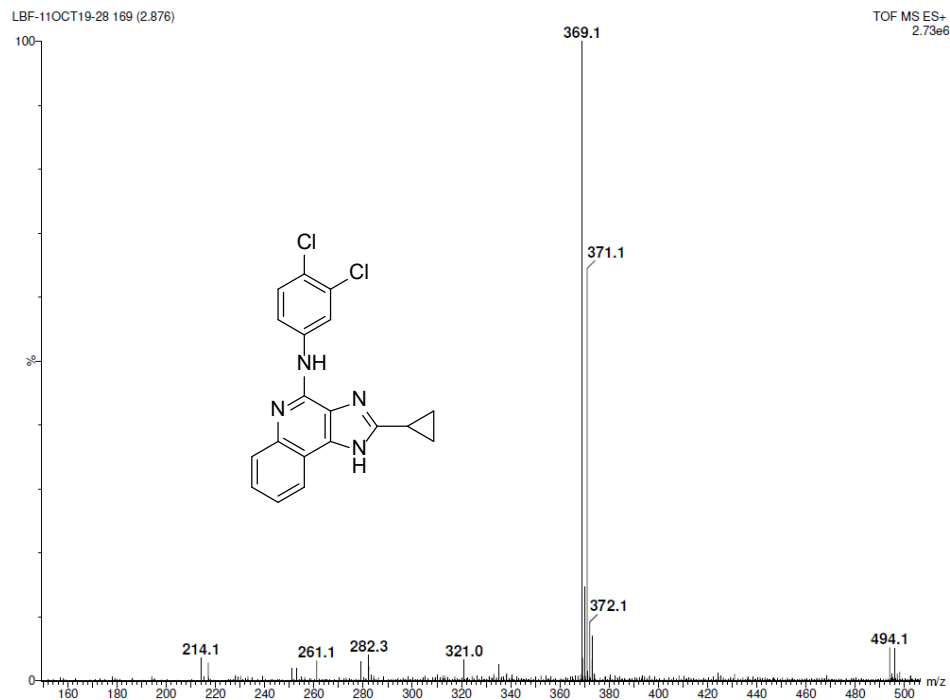


Minimum:

Maximum: 5.0 5.0 -1.5 100.0

Mass	Calc. Mass	mDa	PPM	DBE	i-FIT	Norm	Conf(%)	Formula
479.1019	479.1017	0.2	0.4	13.5	419.9	n/a	n/a	C23 H20 N4 F3 35Cl2

TOF MS E+ and elemental analysis of 2-(4-(trifluoromethyl)cyclohexyl)-N-(3,4-dichlorophenyl)-1H-imidazo[4,5-c]quinolin-4-amine – Compound 4



Elemental Composition Report

Page 1

Single Mass Analysis

Tolerance = 5.0 mDa / DBE: min = -1.5, max = 100.0

Element prediction: Off

Number of isotope peaks used for i-FIT = 3

Monoisotopic Mass, Even Electron Ions

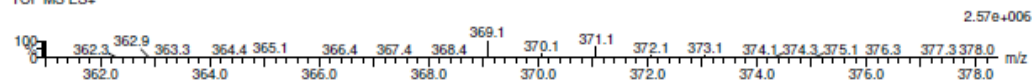
43 formula(e) evaluated with 1 results within limits (up to 50 closest results for each mass)

Elements Used:

C: 0-100 H: 0-250 N: 4-4 O: 0-60 35Cl: 2-2

LBF-11OCT19-28 171 (2.909) AM2 (Ar,25000.0,0.00,0.00); ABS

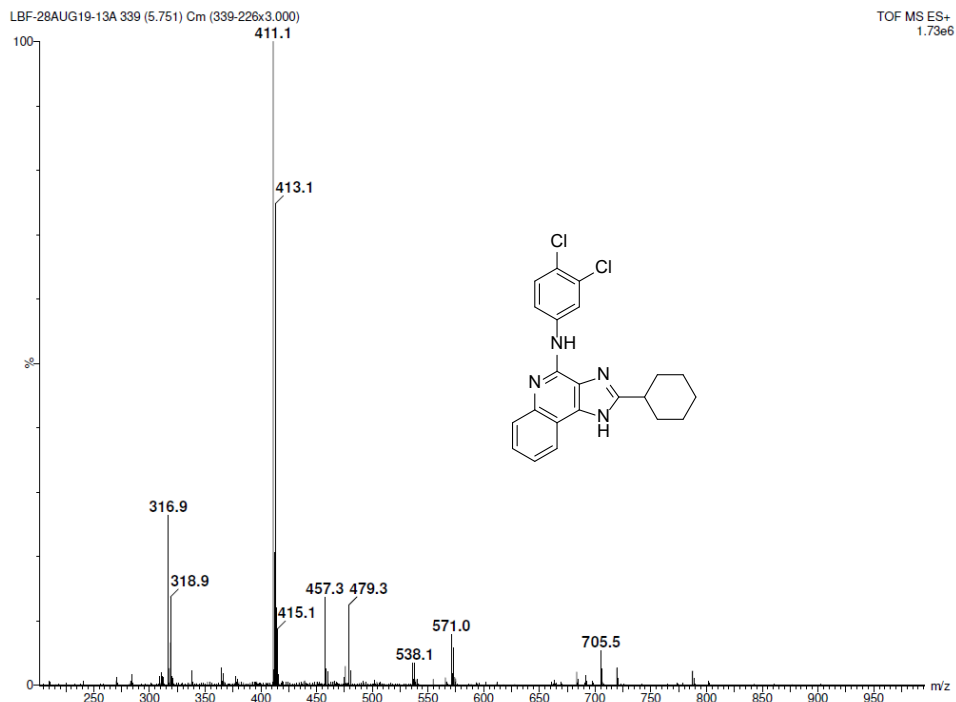
TOF MS ES+



Minimum: -1.5
Maximum: 5.0 5.0 100.0

Mass	Calc. Mass	mDa	PPM	DBE	i-FIT	Norm	Conf (%)	Formula
369.0676	369.0674	0.2	0.5	13.5	624.3	n/a	n/a	C19 H15 N4 35Cl2

TOF MS E+ and elemental analysis of 2-(cyclopropyl)-N-(3,4-dichlorophenyl)-1H-imidazo[4,5-c]quinolin-4-amine – Compound 5



Elemental Composition Report

Page 1

Single Mass Analysis

Tolerance = 5.0 mDa / DBE: min = -1.5, max = 100.0
 Element prediction: Off
 Number of isotope peaks used for i-FIT = 3

Monoisotopic Mass, Even Electron Ions

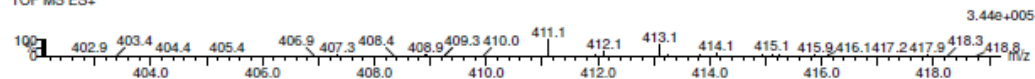
51 formula(e) evaluated with 1 results within limits (up to 50 closest results for each mass)

Elements Used:

C: 0-100 H: 0-250 N: 4-4 O: 0-60 35Cl: 2-2

LBF-27AUG19-13 329 (5.582) AM2 (Ar,25000.0,0.00,0.00); ABS

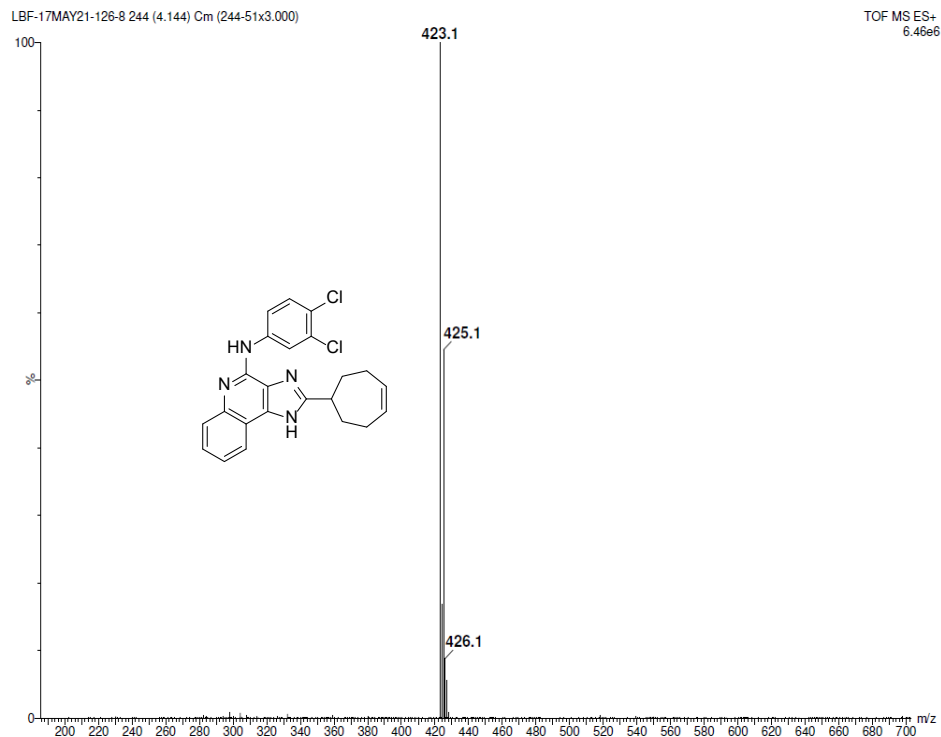
TOF MS ES+



Minimum: -1.5
 Maximum: 5.0 5.0 100.0

Mass	Calc. Mass	mDa	PPM	DBE	i-FIT	Norm	Conf(%)	Formula
411.1143	411.1143	0.0	0.0	13.5	520.2	n/a	n/a	C22 H21 N4 35Cl2

TOF MS E+ and elemental analysis of 2-(cyclohexyl)-*N*-(3,4-dichlorophenyl)-1*H*-imidazo[4,5-*c*]quinolin-4-amine – Compound **8**



Elemental Composition Report

Page 1

Single Mass Analysis

Tolerance = 5.0 mDa / DBE: min = -1.5, max = 100.0

Element prediction: Off

Number of isotope peaks used for i-FIT = 3

Monoisotopic Mass, Even Electron Ions

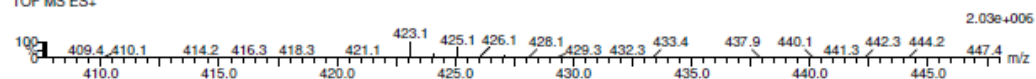
55 formula(e) evaluated with 1 results within limits (up to 50 closest results for each mass)

Elements Used:

C: 0-100 H: 0-250 N: 4-4 O: 0-50 35Cl: 2-2

LBF-17MAY21-126-8 246 (4.212) AM2 (Ar,25000.0,0.00,0.00); ABS

TOF MS ES+



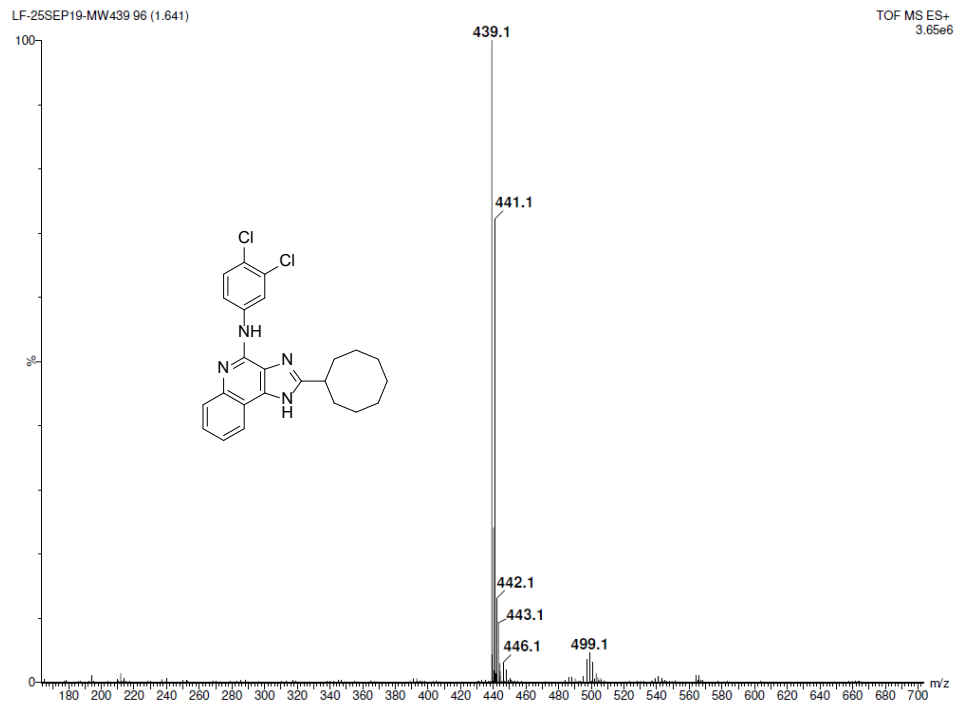
Minimum:

Maximum: 5.0 5.0 -1.5

100.0

Mass	Calc. Mass	mDa	PPM	DBE	i-FIT	Norm	Conf(%)	Formula
423.1137	423.1143	-0.6	-1.4	14.5	544.1	n/a	n/a	C23 H21 N4 35Cl2

TOF MS ES+ and elemental analysis of 2-(cyclohept-4-en-1-yl)-N-(3,4-dichlorophenyl)-1H-imidazo[4,5-c]quinolin-4-amine – Compound **10**



Elemental Composition Report

Page 1

Single Mass Analysis

Tolerance = 5.0 mDa / DBE: min = -1.5, max = 100.0
 Element prediction: Off
 Number of isotope peaks used for i-FIT = 3

Monoisotopic Mass, Even Electron Ions

5 formula(e) evaluated with 1 results within limits (up to 50 closest results for each mass)

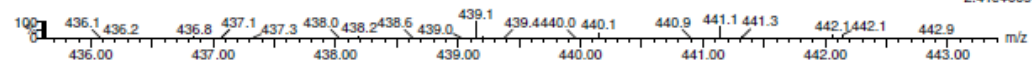
Elements Used:

C: 0-100 H: 0-250 N: 4-4 35Cl: 2-2

LF-25SEP19-MW439 155 (2.639) AM2 (Ar,25000.0,0.00,0.00); ABS

TOF MS ES+

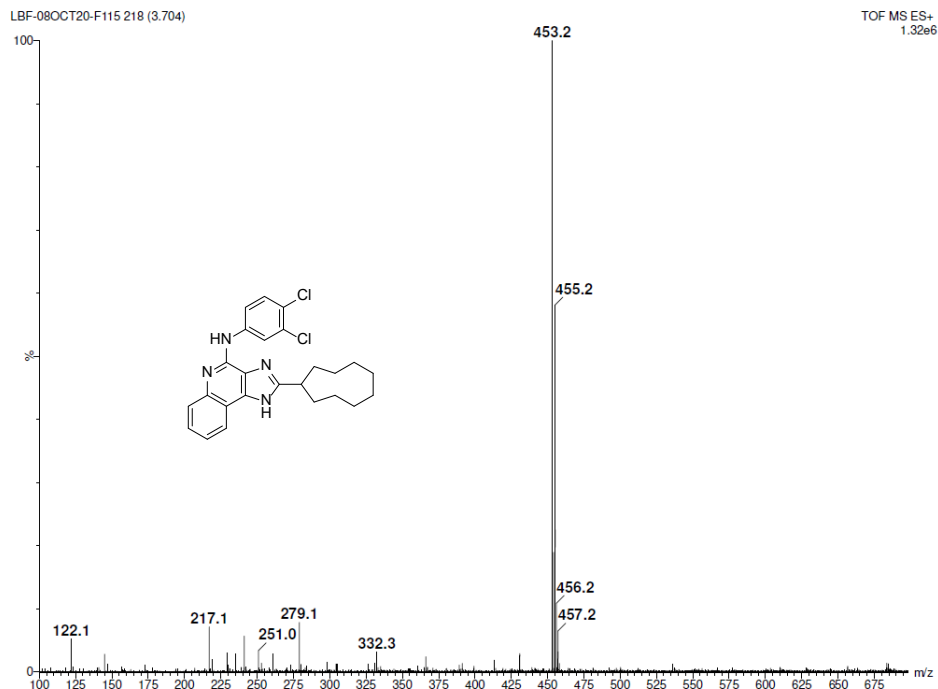
2.41e+005



Minimum: -1.5
 Maximum: 5.0 5.0 100.0

Mass	Calc. Mass	mDa	PPM	DBE	i-PIT	Norm	Conf (%)	Formula
439.1452	439.1456	-0.4	-0.9	13.5	491.0	n/a	n/a	C24 H25 N4 35Cl2

TOF MS E+ and elemental analysis of 2-(cyclooctyl)-N-(3,4-dichlorophenyl)-1H-imidazo[4,5-c]quinolin-4-amine – Compound **11**



Elemental Composition Report

Page 1

Single Mass Analysis

Tolerance = 5.0 mDa / DBE: min = -1.5, max = 100.0
 Element prediction: Off
 Number of isotope peaks used for i-FIT = 3

Monoisotopic Mass, Even Electron Ions

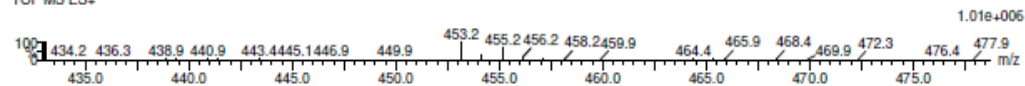
68 formula(e) evaluated with 1 results within limits (up to 50 closest results for each mass)

Elements Used:

C: 0-100 H: 0-250 N: 4-4 O: 0-50 35Cl: 2-2

LBF-08OCT20-F115 222 (3.772) AM2 (Ar,25000.0,0.00,0.00); ABS

TOF MS ES+



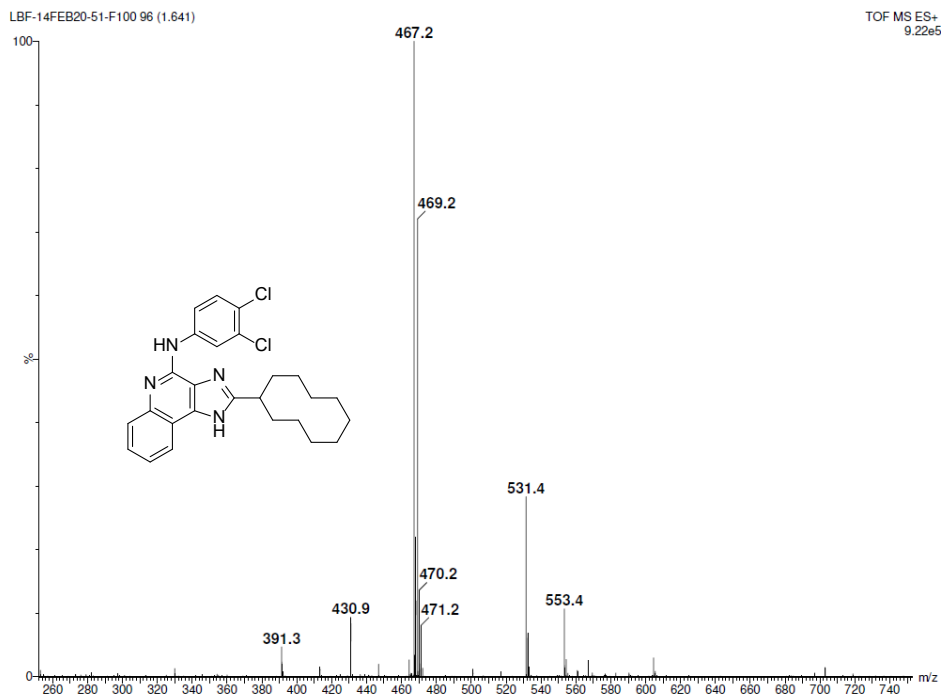
Minimum:

Maximum: 5.0 10.0 -1.5

Mass	Calc. Mass	mDa	PPM	DBE	i-FIT	Norm	Conf (%)	Formula
------	------------	-----	-----	-----	-------	------	----------	---------

453.1616	453.1613	0.3	0.7	13.5	515.0	n/a	n/a	C25 H27 N4 35Cl2
----------	----------	-----	-----	------	-------	-----	-----	------------------

TOF MS E+ and elemental analysis of 2-(cyclononyl)-*N*-(3,4-dichlorophenyl)-1*H*-imidazo[4,5-*c*]quinolin-4-amine – Compound **12**



Elemental Composition Report

Page 1

Single Mass Analysis

Tolerance = 5.0 mDa / DBE: min = -1.5, max = 100.0

Element prediction: Off

Number of isotope peaks used for i-FIT = 3

Monoisotopic Mass, Even Electron Ions

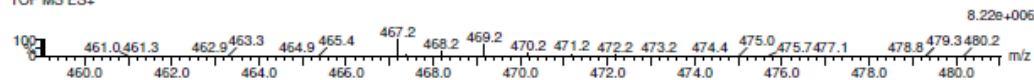
69 formula(e) evaluated with 1 results within limits (up to 50 closest results for each mass)

Elements Used:

C: 0-100 H: 0-250 N: 4-4 O: 0-60 35Cl: 2-2

LBF-14FEB20-51-F100 99 (1.691) AM2 (Ar,25000.0,0.00,0.00); ABS

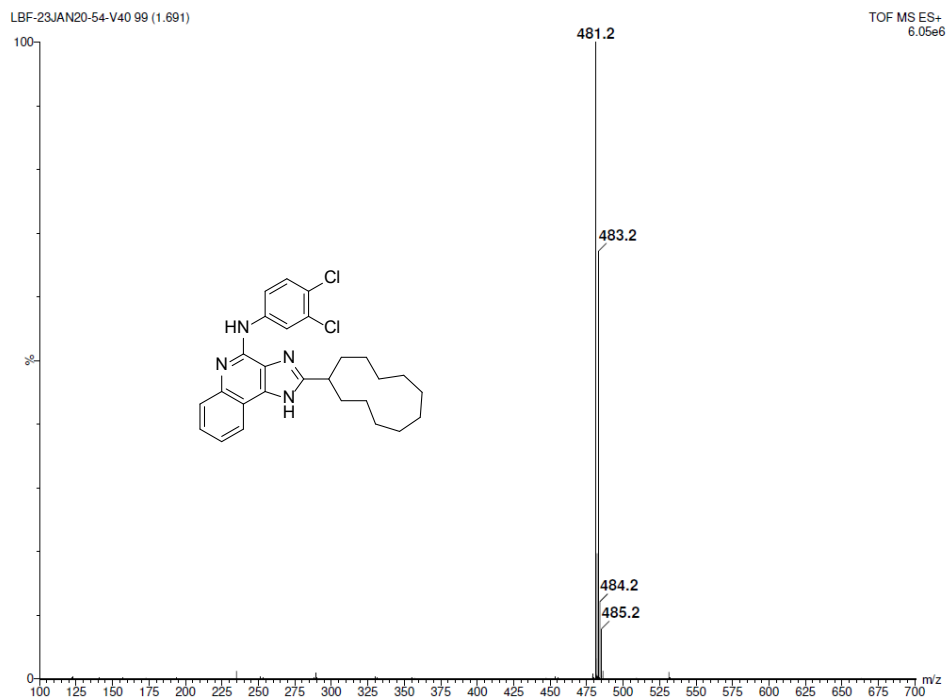
TOF MS ES+



Minimum: -1.5
Maximum: 5.0 5.0 100.0

Mass	Calc. Mass	mDa	PPM	DBE	i-FIT	Norm	Conf (%)	Formula
467.1770	467.1769	0.1	0.2	13.5	580.2	n/a	n/a	C26 H29 N4 35Cl2

TOF MS ES+ and elemental analysis of 2-(cyclodecyl)-N-(3,4-dichlorophenyl)-1H-imidazo[4,5-c]quinolin-4-amine – Compound 13



Elemental Composition Report

Page 1

Single Mass Analysis

Tolerance = 8.0 mDa / DBE: min = -1.5, max = 100.0

Element prediction: Off

Number of isotope peaks used for i-FIT = 3

Monoisotopic Mass, Even Electron Ions

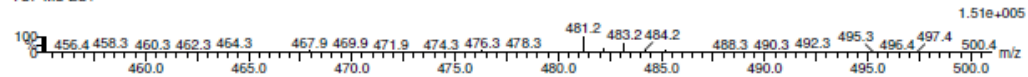
77 formula(e) evaluated with 2 results within limits (up to 50 closest results for each mass)

Elements Used:

C: 0-100 H: 0-250 N: 4-4 O: 0-60 35Cl: 2-2

LBF-23JAN20-54-V40 104 (1.776) AM2 (Ar,25000.0,0.00,0.00); ABS

TOF MS ES+

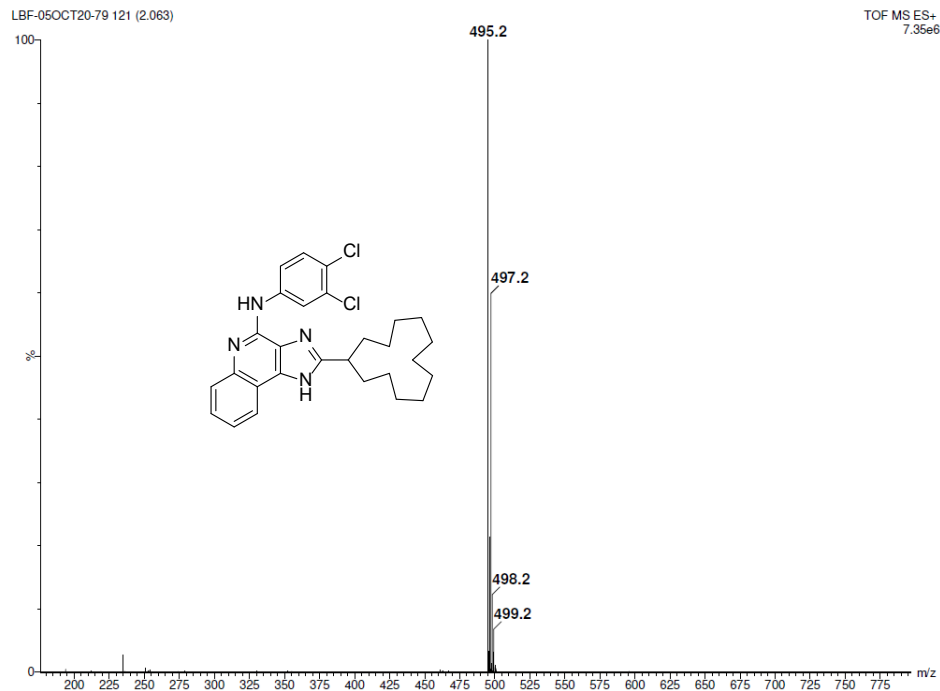


Minimum:

Maximum: 8.0 5.0 -1.5

Mass	Calc. Mass	mDa	PPM	DBE	i-FIT	Norm	Conf(%)	Formula
481.1921	481.1926	-0.5	-1.0	13.5	414.5	0.868	41.97	C27 H31 N4 35Cl2
	481.1985	-6.4	-13.3	4.5	414.2	0.544	58.03	C20 H35 N4 O5 35Cl2

TOF MS ES+ and elemental analysis of 2-(cycloundecyl)-*N*-(3,4-dichlorophenyl)-1*H*-imidazo[4,5-*c*]quinolin-4-amine – Compound **14**



Elemental Composition Report

Page 1

Single Mass Analysis

Tolerance = 5.0 mDa / DBE: min = -1.5, max = 100.0

Element prediction: Off

Number of isotope peaks used for i-FIT = 3

Monoisotopic Mass, Even Electron Ions

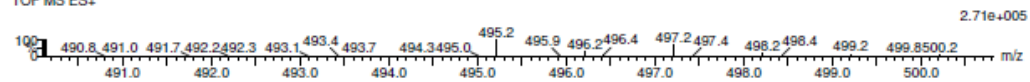
78 formula(e) evaluated with 1 results within limits (up to 50 closest results for each mass)

Elements Used:

C: 0-100 H: 0-250 N: 4-4 O: 0-50 35Cl: 2-2

LBF-05OCT20-79 126 (2.148) AM2 (Ar,25000.0,0.00,0.00); ABS

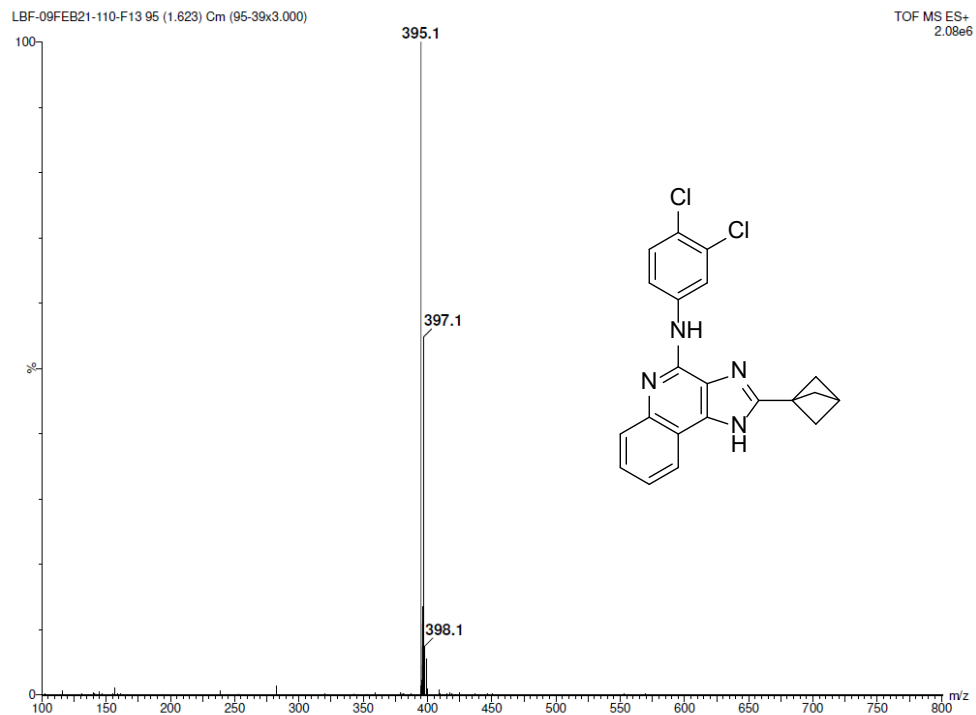
TOF MS ES+



Minimum: -1.5
Maximum: 100.0

Mass	Calc. Mass	mDa	PPM	DBE	i-FIT	Norm	Conf(%)	Formula
495.2085	495.2082	0.3	0.6	13.5	437.1	n/a	n/a	C28 H33 N4 35Cl2

TOF MS ES+ and elemental analysis of 2-(cyclododecyl)-N-(3,4-dichlorophenyl)-1H-imidazo[4,5-c]quinolin-4-amine – Compound 15



Elemental Composition Report

Page 1

Single Mass Analysis

Tolerance = 5.0 mDa / DBE: min = -1.5, max = 100.0

Element prediction: Off

Number of isotope peaks used for I-FIT = 3

Monoisotopic Mass, Even Electron Ions

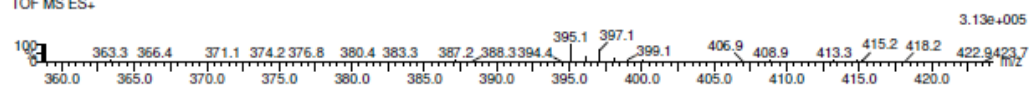
47 formula(e) evaluated with 1 results within limits (up to 50 closest results for each mass)

Elements Used:

C: 0-100 H: 0-250 N: 4-4 O: 0-50 35Cl: 2-2

LBF-09FEB21-110-F13 103 (1.759) AM2 (Ar,25000.0,0.00,0.00); ABS

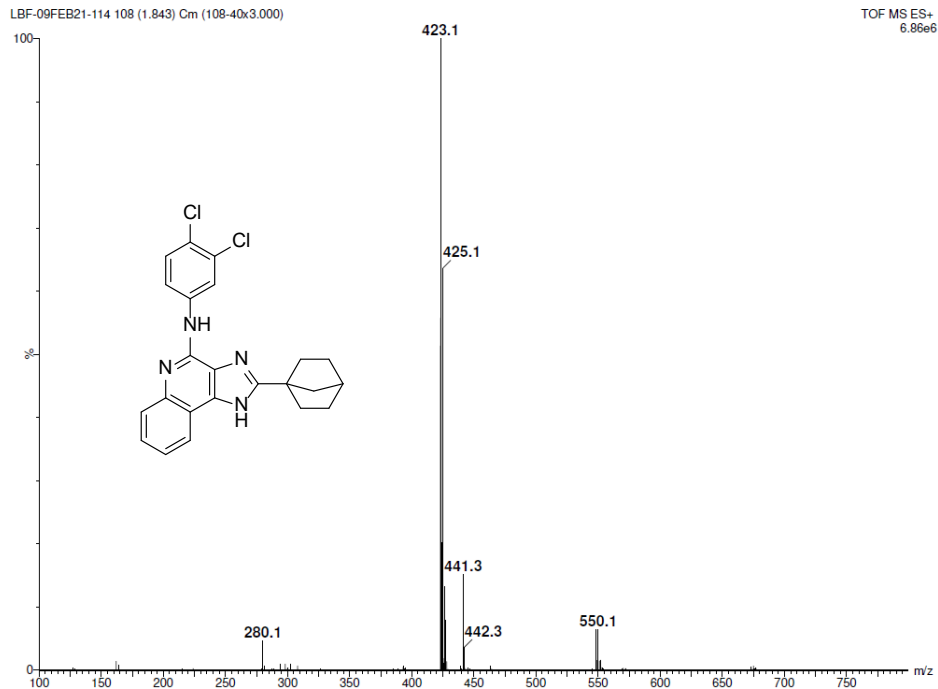
TOF MS ES+



Minimum: -1.5
Maximum: 5.0 10.0 100.0

Mass	Calc. Mass	mDa	PPM	DBE	i-FIT	Norm	Conf (%)	Formula
395.0835	395.0830	0.5	1.3	14.5	528.2	n/a	n/a	C21 H17 N4 35Cl2

TOF MS ES+ and elemental analysis of 2-(bicyclo[1.1.1]heptan-1-yl)-N-(3,4-dichlorophenyl)-1H-imidazo[4,5-c]quinolin-4-amine – Compound **16**



Elemental Composition Report

Page 1

Single Mass Analysis

Tolerance = 5.0 mDa / DBE: min = -1.5, max = 100.0

Element prediction: Off

Number of isotope peaks used for i-FIT = 3

Monoisotopic Mass, Even Electron Ions

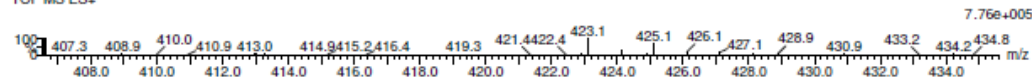
55 formula(e) evaluated with 1 results within limits (up to 50 closest results for each mass)

Elements Used:

C: 0-100 H: 0-250 N: 4-4 O: 0-50 35Cl: 2-2

LBF-09FEB21-114 117 (1.996) AM2 (Ar,25000.0,0.00,0.00); ABS

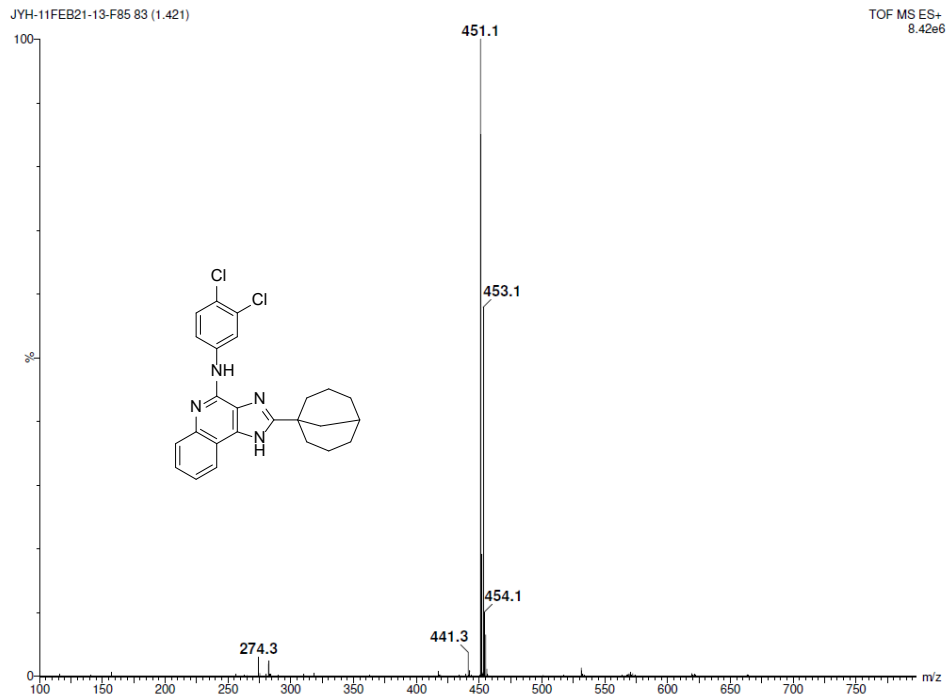
TOF MS ES+



Minimum: -1.5
Maximum: 5.0 10.0 100.0

Mass	Calc. Mass	mDa	PPM	DBE	i-FIT	Norm	Conf (%)	Formula
423.1140	423.1143	-0.3	-0.7	14.5	543.9	n/a	n/a	C23 H21 N4 35Cl2

TOF MS E+ and elemental analysis of 2-(bicyclo[2.2.1]heptan-1-yl)-N-(3,4-dichlorophenyl)-1H-imidazo[4,5-c]quinolin-4-amine – Compound 17



Elemental Composition Report

Page 1

Single Mass Analysis

Tolerance = 5.0 mDa / DBE: min = -1.5, max = 100.0

Element prediction: Off

Number of isotope peaks used for i-FIT = 3

Monoisotopic Mass, Even Electron Ions

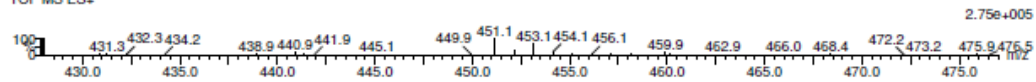
64 formula(e) evaluated with 1 results within limits (up to 50 closest results for each mass)

Elements Used:

C: 0-100 H: 0-250 N: 4-4 O: 0-50 35Cl: 2-2

JYH-11FEB21-13-F85 157 (2.672) AM2 (Ar,25000.0,0.00,0.00); ABS

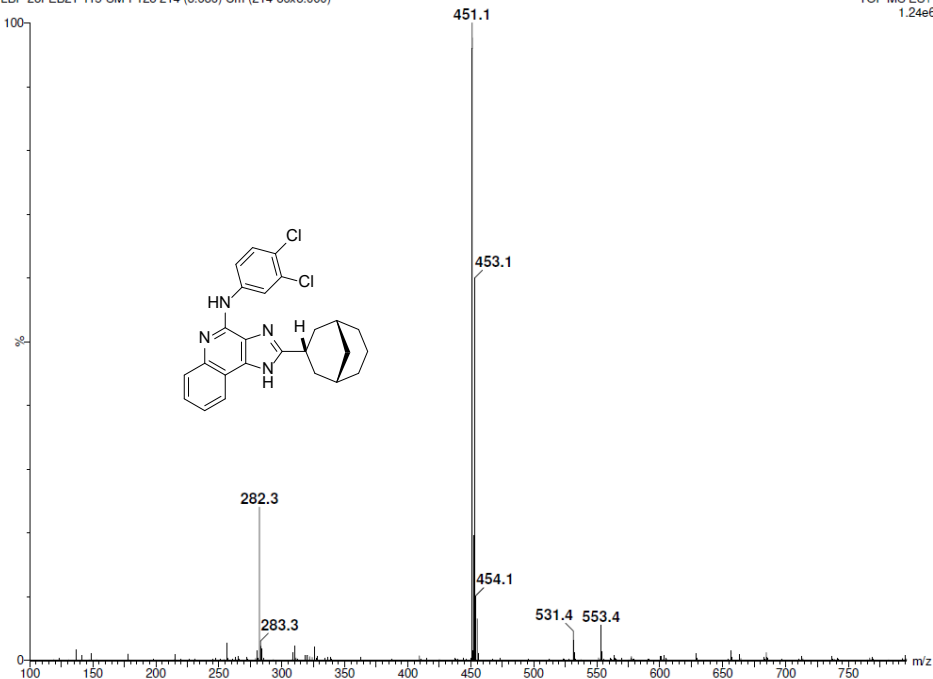
TOF MS ES+



Minimum: -1.5
Maximum: 10.0

Mass	Calc. Mass	mDa	PPM	DBE	i-FIT	Norm	Conf (%)	Formula
451.1452	451.1456	-0.4	-0.9	14.5	428.8	n/a	n/a	C25 H25 N4 35Cl2

TOF MS ES+ and elemental analysis of 2-(bicyclo[3.3.1]nonan-1-yl)-N-(3,4-dichlorophenyl)-1H-imidazo[4,5-c]quinolin-4-amine – Compound **18**



Elemental Composition Report

Page 1

Single Mass Analysis

Tolerance = 5.0 mDa / DBE: min = -1.5, max = 100.0

Element prediction: Off

Number of isotope peaks used for i-FIT = 3

Monoisotopic Mass, Even Electron Ions

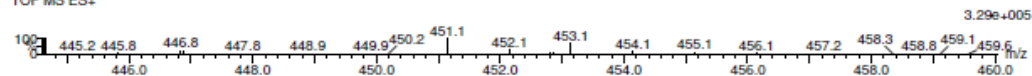
64 formula(e) evaluated with 1 results within limits (up to 50 closest results for each mass)

Elements Used:

C: 0-100 H: 0-250 N: 4-4 O: 0-50 35Cl: 2-2

LBF-23FEB21-115-SM-F123 226 (3.839) AM2 (Ar,25000,0,0,00,0,00): ABS

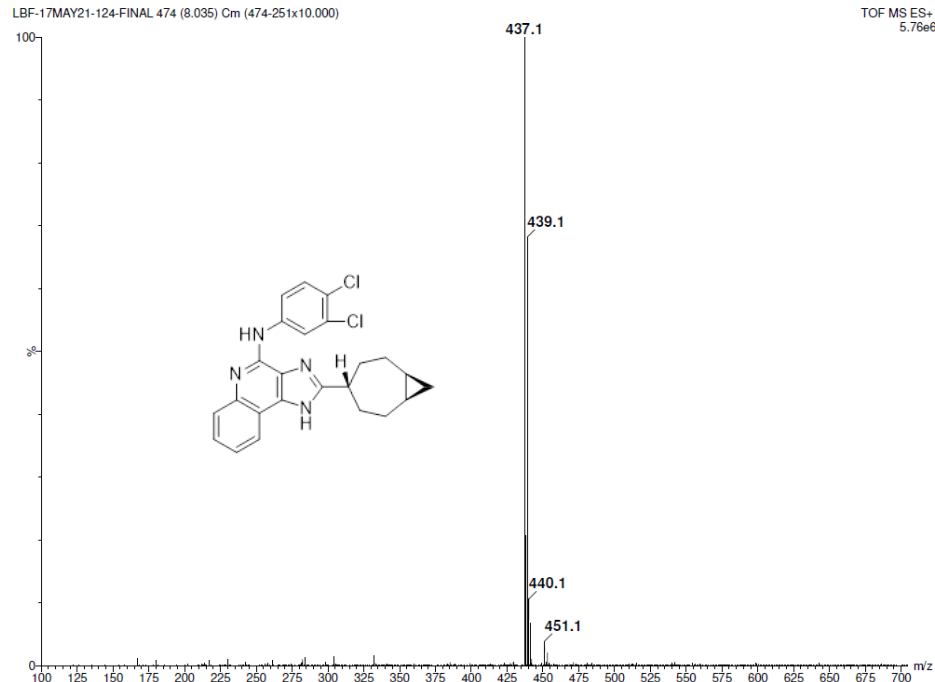
TOF MS ES+



Minimum: -1.5
Maximum: 5.0 10.0 100.0

Mass	Calc. Mass	mDa	PPM	DBE	i-FIT	Norm	Conf (%)	Formula
451.1460	451.1456	0.4	0.9	14.5	474.5	n/a	n/a	C25 H25 N4 35Cl2

TOF MS ES+ and elemental analysis of 2-((1R,3s,5S)-bicyclo[3.3.1]nonan-3-yl)-N-(3,4-dichlorophenyl)-1H-imidazo[4,5-c]quinolin-4-amine – Compound **19**



Elemental Composition Report

Page 1

Single Mass Analysis

Tolerance = 5.0 mDa / DBE: min = -1.5, max = 100.0
 Element prediction: Off
 Number of isotope peaks used for i-FIT = 3

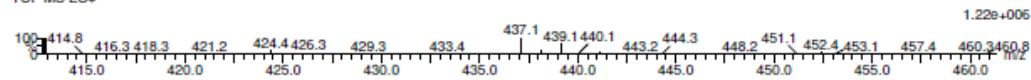
Monoisotopic Mass, Even Electron Ions

63 formula(e) evaluated with 1 results within limits (up to 50 closest results for each mass)

Elements Used:

C: 0-100 H: 0-250 N: 4-4 O: 0-50 35Cl: 2-2

LBF-17MAY21-124-FINAL 479 (8.119) AM2 (Ar,25000.0,0.00,0.00); ABS
 TOF MS ES+

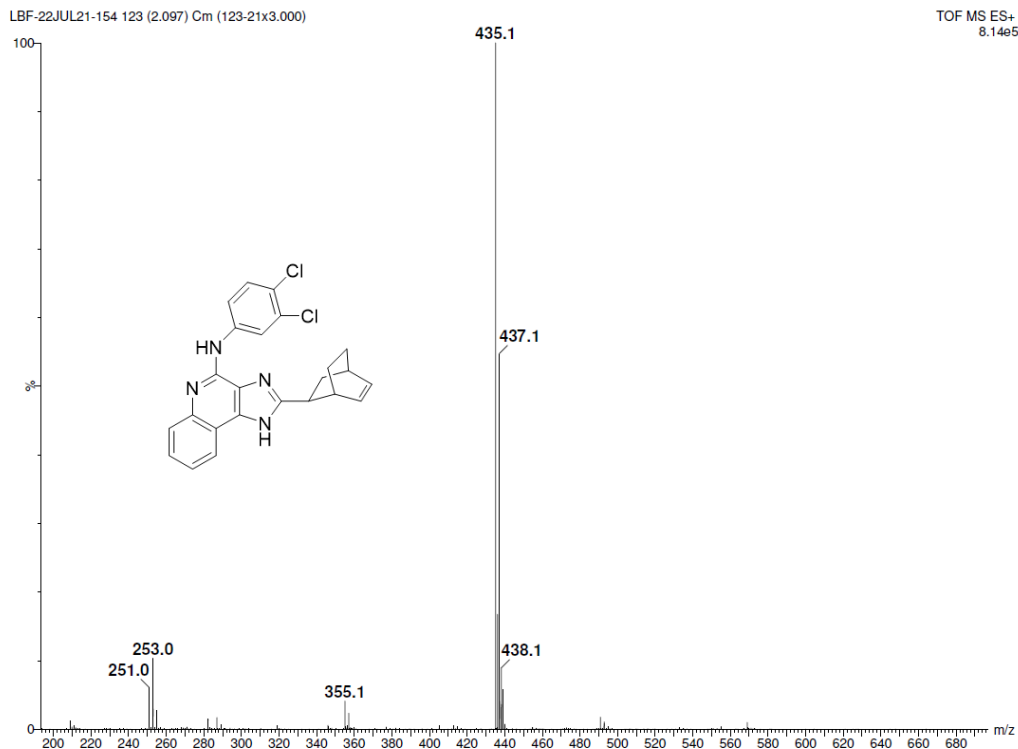


Minimum:

Maximum: 5.0 5.0 -1.5 100.0

Mass	Calc. Mass	mDa	PPM	DBE	i-FIT	Norm	Conf (%)	Formula
437.1304	437.1300	0.4	0.9	14.5	476.3	n/a	n/a	C24 H23 N4 35Cl2

TOF MS ES+ and elemental analysis of 2-((1R,4r,7S)-bicyclo[5.1.0]octan-4-yl)-N-(3,4-dichlorophenyl)-1H-imidazo[4,5-c]quinolin-4-amine – Compound 20



Elemental Composition Report

Page 1

Single Mass Analysis

Tolerance = 5.0 mDa / DBE: min = -1.5, max = 100.0

Element prediction: Off

Number of isotope peaks used for i-FIT = 3

Monoisotopic Mass, Even Electron Ions

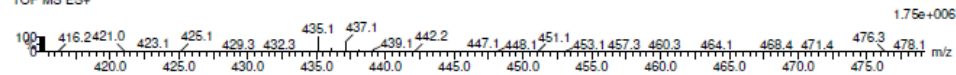
59 formula(e) evaluated with 1 results within limits (up to 50 closest results for each mass)

Elements Used:

C: 0-100 H: 0-250 N: 4-4 O: 0-20 35Cl: 2-2

LBF-22JUL21-154 116 (1.979) AM2 (Ar,25000.0,0.00,0.00); ABS

TOF MS ES+

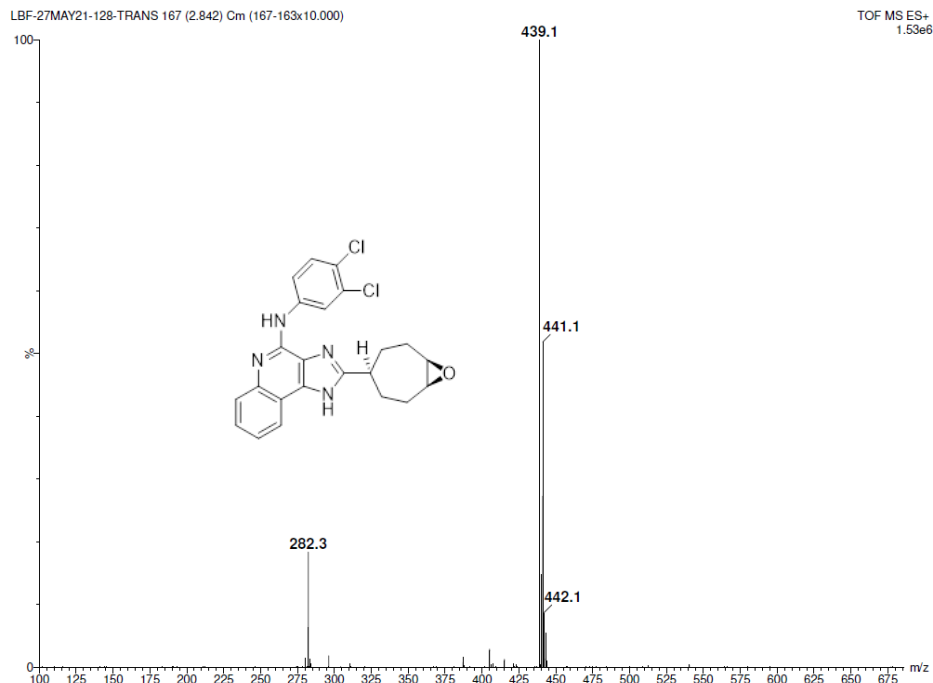


Minimum: -1.5

Maximum: 100.0

Mass	Calc. Mass	mDa	PPM	DBE	1-FIT	Norm	Conf (%)	Formula
435.1136	435.1143	-0.7	-1.6	15.5	509.0	n/a	n/a	C ₂₄ H ₂₁ N ₄ Cl ₂

TOF MS ES+ and elemental analysis of 2-((1R,2R,4R) & (1S,2S,4S)-bicyclo[2.2.2]oct-5-en-2-yl)-N-(3,4-dichlorophenyl)-1H-imidazo[4,5-c]quinolin-4-amine – Compound **21**



Elemental Composition Report

Page 1

Single Mass Analysis

Tolerance = 5.0 mDa / DBE: min = -1.5, max = 100.0

Element prediction: Off

Number of isotope peaks used for i-FIT = 3

Monoisotopic Mass, Even Electron Ions

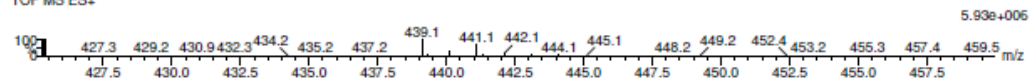
60 formula(e) evaluated with 1 results within limits (up to 50 closest results for each mass)

Elements Used:

C: 0-100 H: 0-250 N: 4-4 O: 0-50 35Cl: 2-2

LBF-27MAY21-128-TRANS 166 (2.825) AM2 (Ar,25000.0,0.00,0.00); ABS

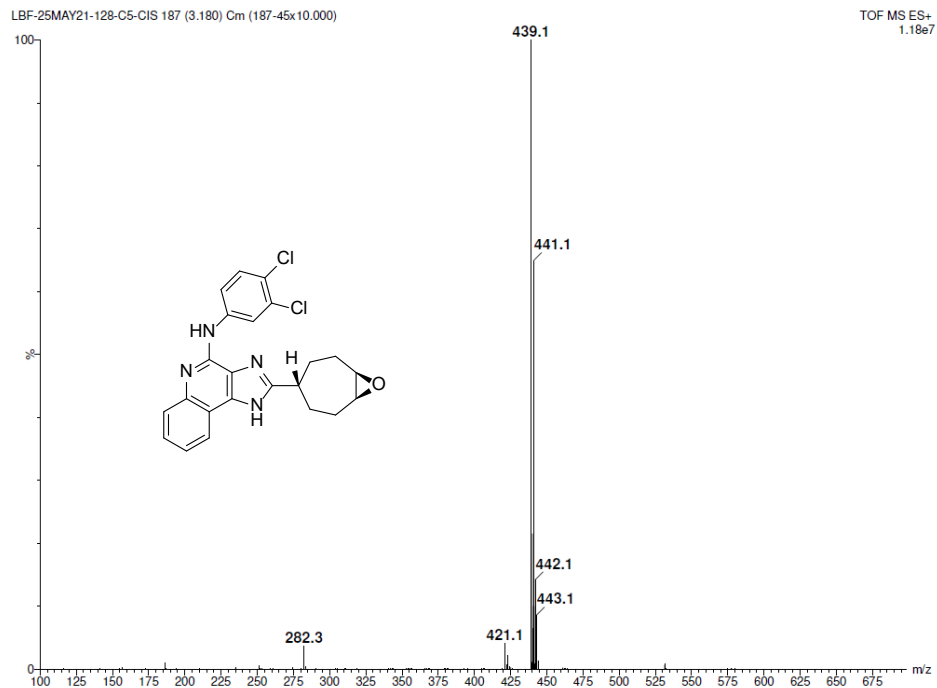
TOF MS ES+



Minimum: -1.5
Maximum: 5.0 5.0 100.0

Mass	Calc. Mass	mDa	PPM	DBE	i-FIT	Norm	Conf(%)	Formula
439.1093	439.1092	0.1	0.2	14.5	716.2	n/a	n/a	C23 H21 N4 O 35Cl2

TOF MS ES+ and elemental analysis of 2-((1R,4r,7S)-8-oxabicyclo[5.1.0]octan-4-yl)-N-(3,4-dichlorophenyl)-1H-imidazo[4,5-c]quinolin-4-amine – Compound **22**



Elemental Composition Report

Page 1

Single Mass Analysis

Tolerance = 5.0 mDa / DBE: min = -1.5, max = 100.0

Element prediction: Off

Number of isotope peaks used for i-FIT = 3

Monoisotopic Mass, Even Electron Ions

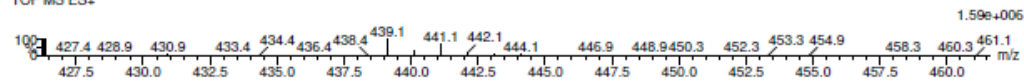
60 formula(e) evaluated with 1 results within limits (up to 50 closest results for each mass)

Elements Used:

C: 0-100 H: 0-250 N: 4-4 O: 0-50 35Cl: 2-2

LBF-25MAY21-128-C5-CIS 191 (3.248) AM2 (Ar,25000.0.0.00.0.00); ABS

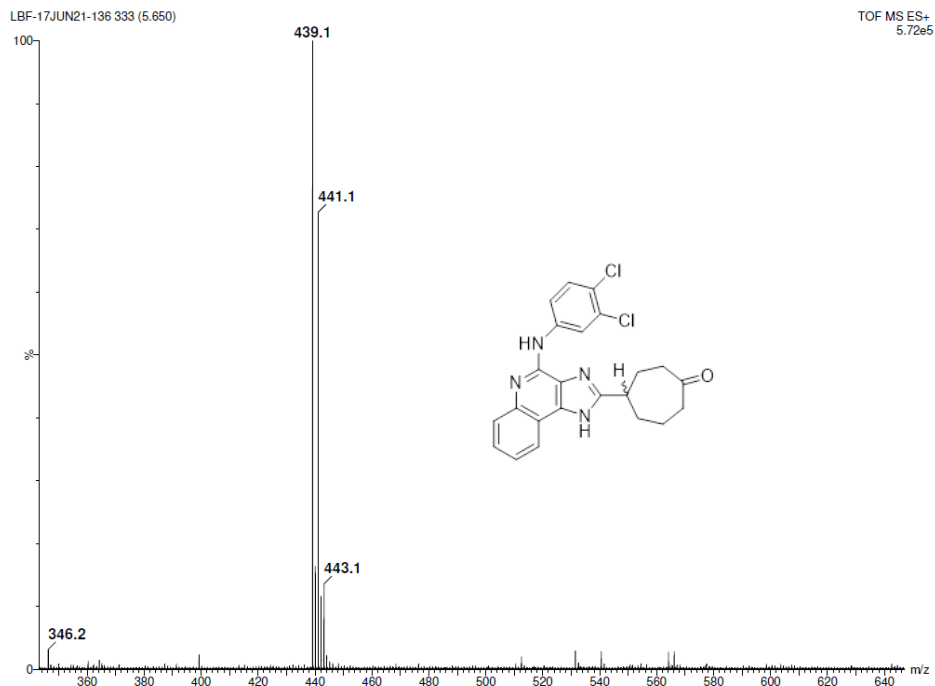
TOF MS ES+



Minimum: -1.5
Maximum: 5.0 5.0 100.0

Mass	Calc. Mass	mDa	PPM	DBE	i-FIT	Norm	Conf(%)	Formula
439.1090	439.1092	-0.2	-0.5	14.5	481.6	n/a	n/a	C23 H21 N4 O 35Cl2

TOF MS ES+ and elemental analysis of 2-((1R,4s,7S)-8-oxabicyclo[5.1.0]octan-4-yl)-N-(3,4-dichlorophenyl)-1H-imidazo[4,5-c]quinolin-4-amine – Compound **23**



Elemental Composition Report

Page 1

Single Mass Analysis

Tolerance = 5.0 mDa / DBE: min = -1.5, max = 100.0

Element prediction: Off

Number of isotope peaks used for i-FIT = 3

Monoisotopic Mass, Even Electron Ions

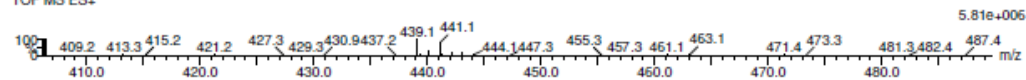
60 formula(e) evaluated with 1 results within limits (up to 50 closest results for each mass)

Elements Used:

C: 0-100 H: 0-250 N: 4-4 O: 0-50 35Cl: 2-2

LBF-17JUN21-136 329 (5.582) AM2 (Ar,25000.0,0.00,0.00); ABS

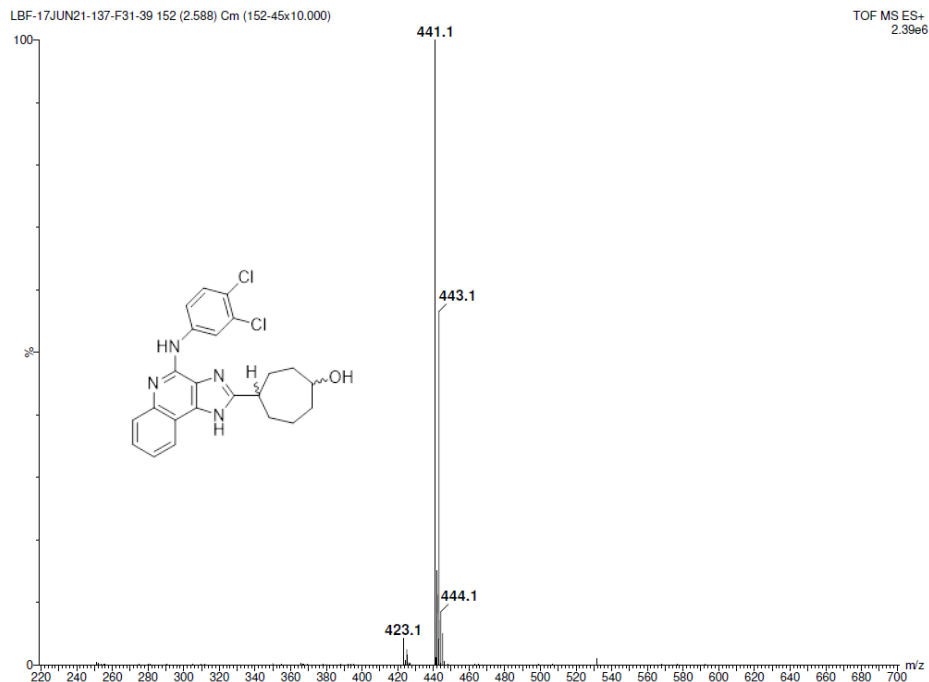
TOF MS ES+



Minimum: -1.5
Maximum: 5.0 5.0 100.0

Mass	Calc. Mass	mDa	PPM	DBE	i-PIT	Norm	Conf(%)	Formula
439.1100	439.1092	0.8	1.8	14.5	626.8	n/a	n/a	C23 H21 N4 O 35Cl2

TOF MS ES+ and elemental analysis of (R)- & (S)-4-(4-((3,4-dichlorophenyl)amino)-1H-imidazo[4,5-c]quinolin-2-yl)cycloheptan-1-one – Compound **24**



Elemental Composition Report

Page 1

Single Mass Analysis

Tolerance = 5.0 mDa / DBE: min = -1.5, max = 100.0

Element prediction: Off

Number of isotope peaks used for i-FIT = 3

Monoisotopic Mass, Even Electron Ions

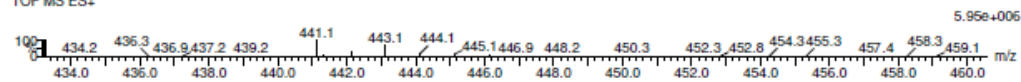
64 formula(e) evaluated with 1 results within limits (up to 50 closest results for each mass)

Elements Used:

C: 0-100 H: 0-250 N: 4-4 O: 0-50 35Cl: 2-2

LBF-17JUN21-137-F31-39 152 (2.588) AM2 (Ar,25000.0,0.00,0.00); ABS

TOF MS ES+

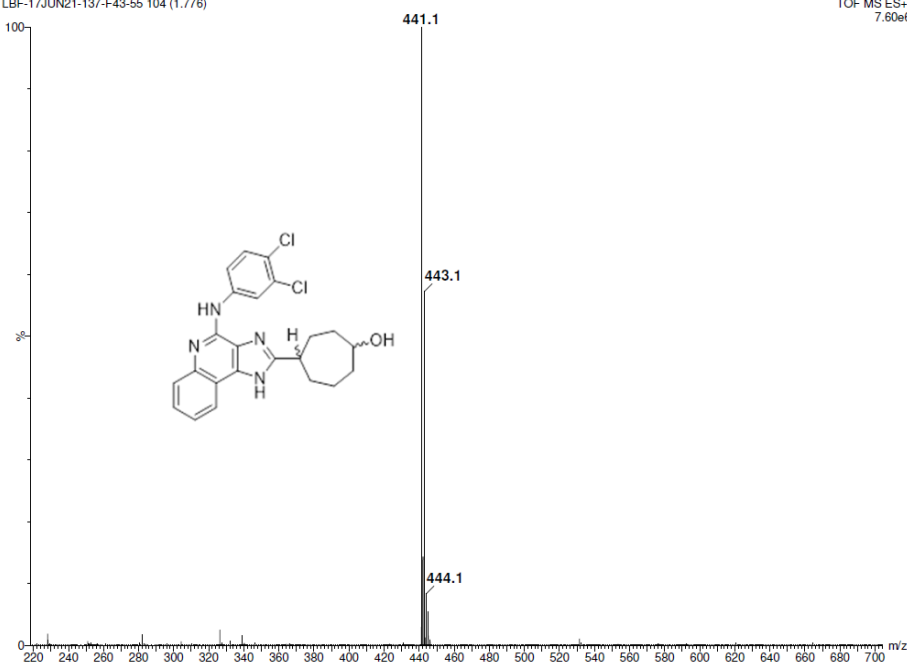


Minimum: -1.5
Maximum: 5.0 5.0 100.0

Mass	Calc. Mass	mDa	PPM	DBE	i-FIT	Norm	Conf(%)	Formula
441.1247	441.1249	-0.2	-0.5	13.5	577.2	n/a	n/a	C23 H23 N4 O 35Cl2

TOF MS ES+ and elemental analysis (1R,4S)- & (1S,4R)-4-(4-((3,4-dichlorophenyl)amino)-1H-imidazo[4,5-c]quinolin-2-yl)cycloheptan-1-ol – Compound

25



Elemental Composition Report

Page 1

Single Mass Analysis

Tolerance = 5.0 mDa / DBE: min = -1.5, max = 100.0

Element prediction: Off

Number of isotope peaks used for i-FIT = 3

Monoisotopic Mass, Even Electron Ions

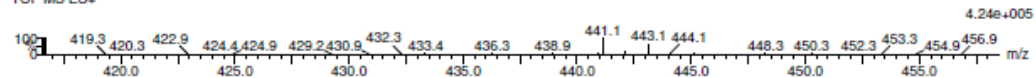
64 formula(e) evaluated with 1 results within limits (up to 50 closest results for each mass)

Elements Used:

C: 0-100 H: 0-250 N: 4-4 O: 0-50 35Cl: 2-2

LBF-17JUN21-137-F43-55 116 (1.979) AM2 (Ar,25000.0,0.00,0.00):ABS

TOF MS ES+

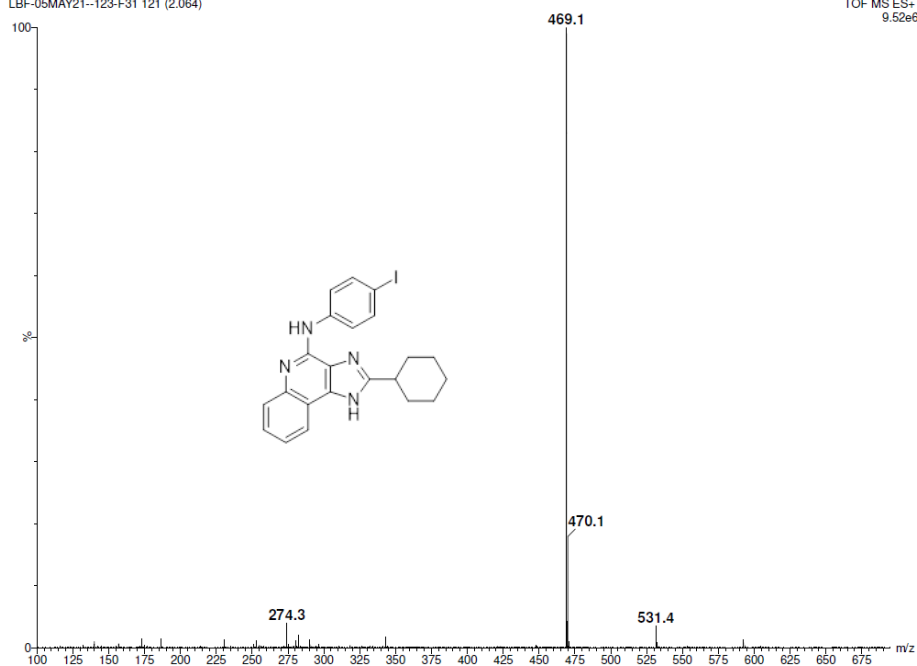


Minimum: -1.5
Maximum: 5.0 5.0 100.0

Mass	Calc. Mass	mDa	PPM	DBE	i-FIT	Norm	Conf(%)	Formula
441.1252	441.1249	0.3	0.7	13.5	430.9	n/a	n/a	C23 H23 N4 O 35Cl2

TOF MS ES+ and elemental analysis of (1R,4R)-, & (1S,4S)-4-(4-((3,4-dichlorophenyl)amino)-1H-imidazo[4,5-c]quinolin-2-yl)cycloheptan-1-ol – Compound

26



Elemental Composition Report

Page 1

Single Mass Analysis

Tolerance = 5.0 mDa / DBE: min = -1.5, max = 100.0

Element prediction: Off

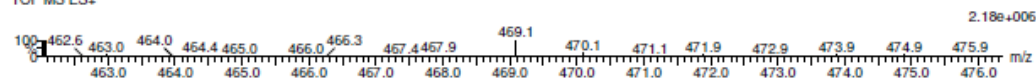
Number of isotope peaks used for i-FIT = 3

Monoisotopic Mass, Even Electron Ions

51 formula(e) evaluated with 2 results within limits (up to 50 closest results for each mass)

Elements Used:

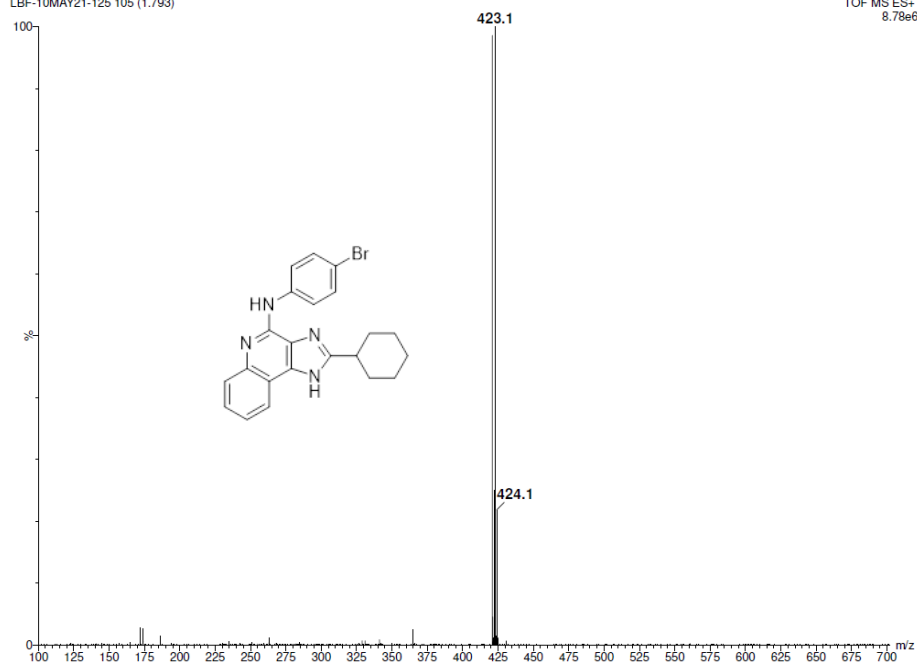
C: 0-100 H: 0-250 N: 4-4 O: 0-50 I: 1-1

LBF-05MAY21--123-F31 131 (2.233) AM2 (Ar,25000.0,0.00,0.00); ABS; Cm (131:140)
TOF MS ES+

Minimum: -1.5
Maximum: 5.0 5.0 100.0

Mass	Calc. Mass	mDa	PPM	DBE	i-FIT	Norm	Conf (%)	Formula
469.0898	469.0889	0.9	1.9	13.5	354.4	0.434	64.76	C22 H22 N4 I
	469.0948	-5.0	-10.7	4.5	355.1	1.043	35.24	C15 H26 N4 O5 I

TOF MS ES+ and elemental analysis of 2-cyclohexyl-N-(4-iodophenyl)-1H-imidazo[4,5-c]quinolin-4-amine – Compound 27



Elemental Composition Report

Page 1

Single Mass Analysis

Tolerance = 5.0 mDa / DBE: min = -1.5, max = 100.0

Element prediction: Off

Number of isotope peaks used for i-FIT = 3

Monoisotopic Mass, Even Electron Ions

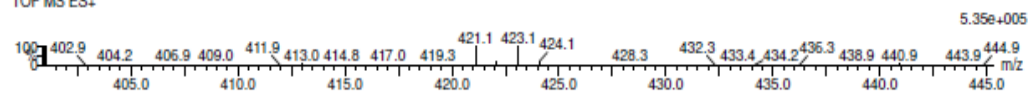
51 formula(e) evaluated with 1 results within limits (up to 50 closest results for each mass)

Elements Used:

C: 0-100 H: 0-250 N: 4-4 O: 0-50 79Br: 1-1

LBF-10MAY21-125 121 (2.064) AM2 (Ar,25000.0,0.00,0.00); ABS

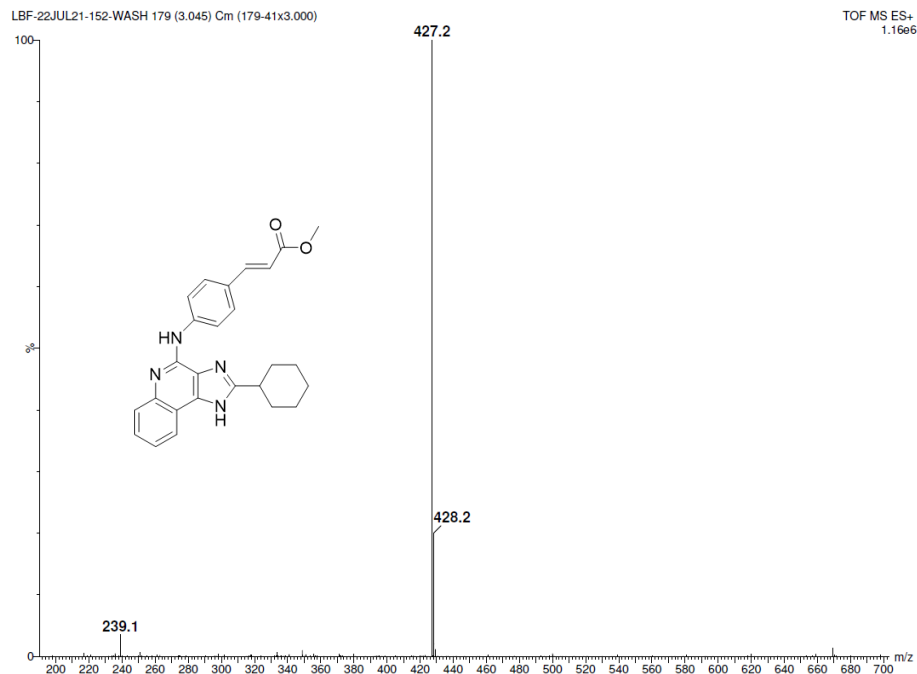
TOF MS ES+



Minimum: -1.5
Maximum: 5.0 5.0 100.0

Mass	Calc. Mass	mDa	PPM	DBE	i-FIT	Norm	Conf(%)	Formula
421.1029	421.1028	0.1	0.2	13.5	418.9	n/a	n/a	C22 H22 N4 79Br

TOF MS ES+ and elemental analysis of 2-cyclohexyl-N-(4-bromophenyl)-1H-imidazo[4,5-c]quinolin-4-amine – Compound **28**



Elemental Composition Report

Page 1

Single Mass Analysis

Tolerance = 5.0 mDa / DBE: min = -1.5, max = 100.0

Element prediction: Off

Number of isotope peaks used for i-FIT = 3

Monoisotopic Mass, Even Electron Ions

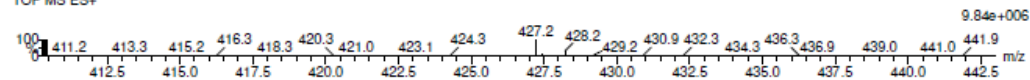
82 formula(e) evaluated with 1 results within limits (up to 50 closest results for each mass)

Elements Used:

C: 0-100 H: 0-250 N: 4-4 O: 0-20

LBF-22JUL21-152-WASH 176 (2.994) AM2 (Ar,25000.0,0.00,0.00); ABS

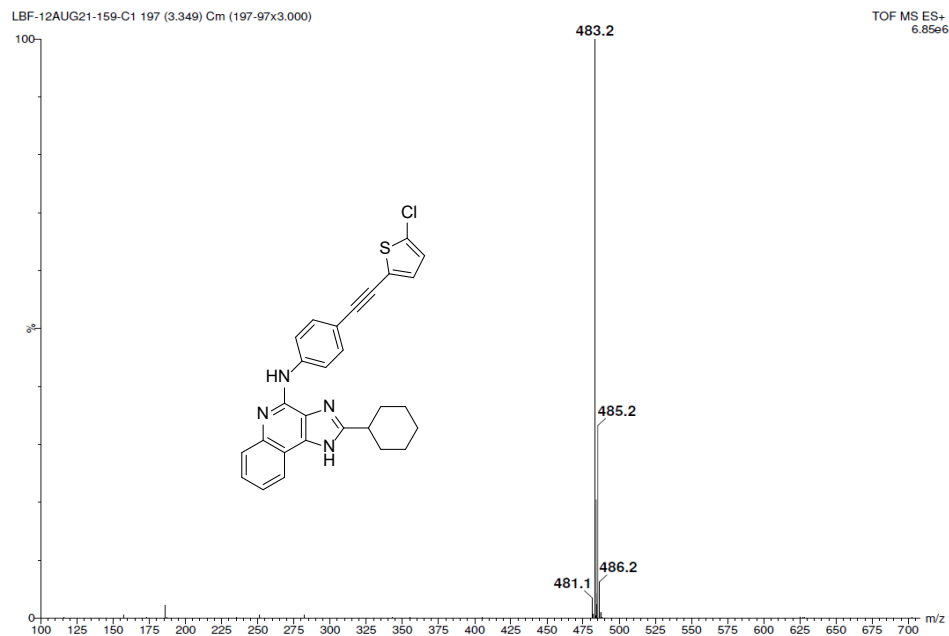
TOF MS ES+



Minimum: -1.5
Maximum: 5.0 5.0 100.0

Mass	Calc. Mass	mDa	PPM	DBE	1-FIT	Norm	Conf (%)	Formula
427.2133	427.2134	-0.1	-0.2	15.5	492.6	n/a	n/a	C26 H27 N4 O2

TOF MS ES+ and elemental analysis of methyl (E)- & (Z)-3-(4-((2-cyclohexyl-1H-imidazo[4,5-c]quinolin-4-yl)amino)phenyl)acrylate – Compound **29**



Elemental Composition Report

Page 1

Single Mass Analysis

Tolerance = 5.0 mDa / DBE: min = -1.5, max = 100.0

Element prediction: Off

Number of isotope peaks used for i-FIT = 3

Monoisotopic Mass, Even Electron Ions

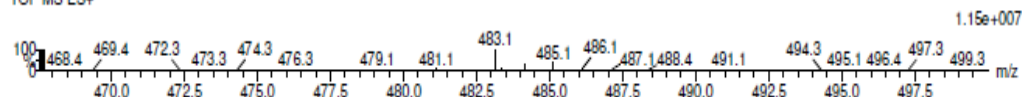
76 formula(e) evaluated with 1 results within limits (up to 50 closest results for each mass)

Elements Used:

C: 0-100 H: 0-250 N: 4-4 O: 0-20 32S: 1-1 35Cl: 1-1

LBF-12AUG21-159-C1 193 (3.281) AM2 (Ar,25000.0,0.00,0.00); ABS

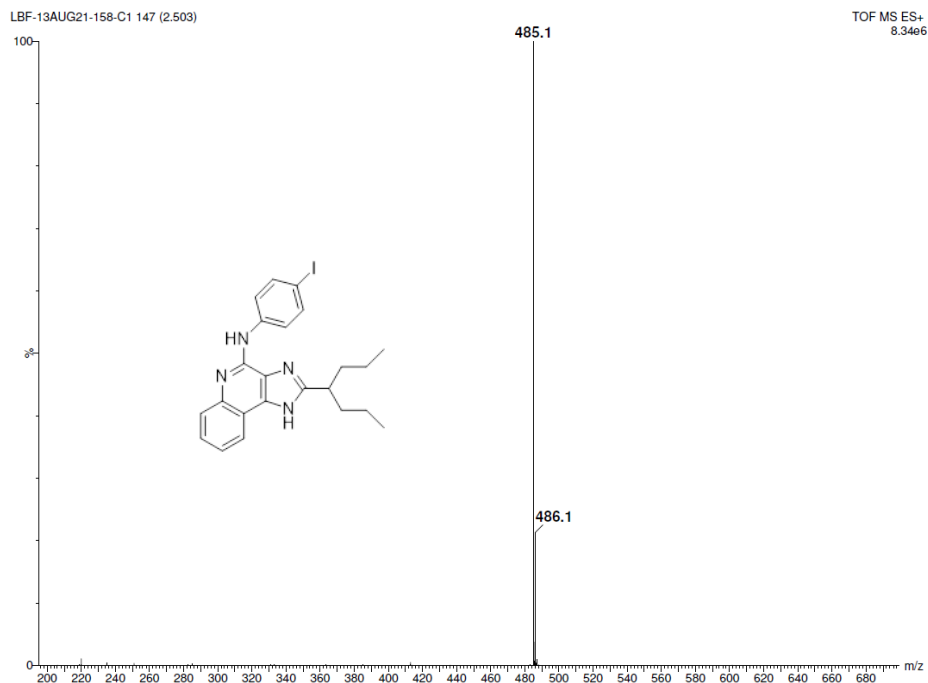
TOF MS ES+



Minimum: -1.5
Maximum: 5.0 5.0 100.0

Mass	Calc. Mass	mDa	PPM	DBE	i-FIT	Norm	Conf(%)	Formula
483.1412	483.1410	0.2	0.4	18.5	516.3	n/a	n/a	C ₂₈ H ₂₄ N ₄ S ₂ Cl

TOF MS ES+ and elemental analysis of 2-cyclohexyl-*N*-(4-((5-chlorothiophen-2-yl)ethynyl)phenyl)-1*H*-imidazo[4,5-*c*]quinolin-4-amine – Compound **30**



Elemental Composition Report

Page 1

Single Mass Analysis

Tolerance = 5.0 mDa / DBE: min = -1.5, max = 100.0

Element prediction: Off

Number of isotope peaks used for i-FIT = 3

Monoisotopic Mass, Even Electron Ions

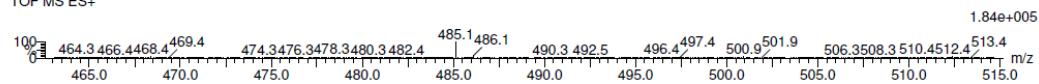
56 formula(e) evaluated with 1 results within limits (up to 50 closest results for each mass)

Elements Used:

C: 0-100 H: 0-250 N: 4-4 O: 0-20 I: 1-1

LBF-13AUG21-158-C1 151 (2.571) AM2 (Ar,25000.0,0.00,0.00); ABS

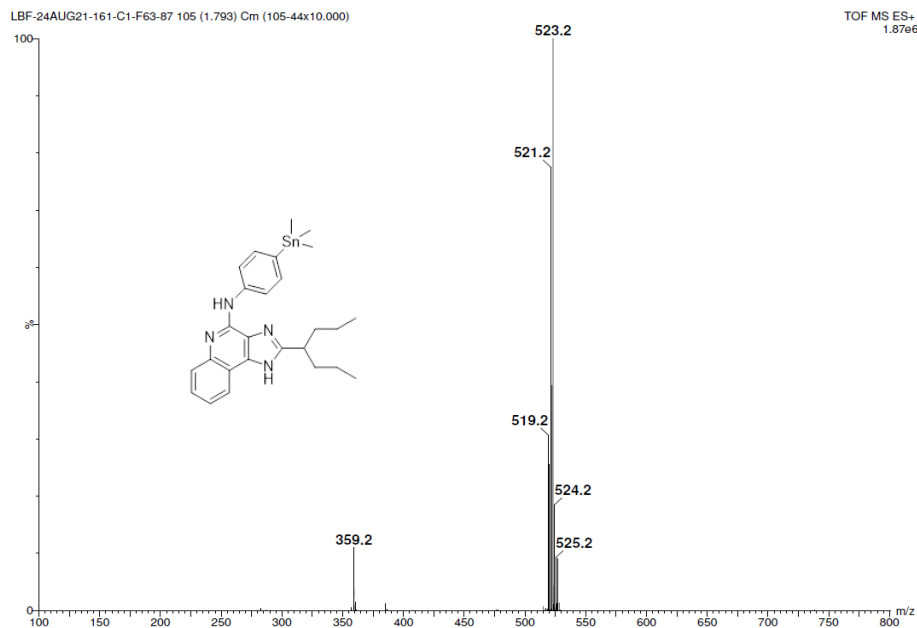
TOF MS ES+



Minimum: -1.5
Maximum: 100.0

Mass	Calc. Mass	mDa	PPM	DBE	i-FIT	Norm	Conf(%)	Formula
485.1200	485.1202	-0.2	-0.4	12.5	329.6	n/a	n/a	C23 H26 N4 I

TOF MS ES+ and elemental analysis of 2-(heptan-4-yl)-N-(4-iodophenyl)-1H-imidazo[4,5-c]quinolin-4-amine – Compound **31**



Elemental Composition Report

Page 1

Single Mass Analysis

Tolerance = 5.0 mDa / DBE: min = -1.5, max = 100.0

Element prediction: Off

Number of isotope peaks used for i-FIT = 3

Monoisotopic Mass, Even Electron Ions

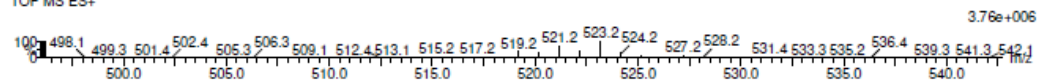
149 formula(e) evaluated with 3 results within limits (up to 50 closest results for each mass)

Elements Used:

C: 0-100 H: 0-250 N: 4-4 O: 0-20 Na: 0-1 120Sn: 1-1

LBF-24AUG21-161-C1-F63-87 101 (1.725) AM2 (Ar,25000.0.0.00.00); ABS

TOF MS ES+

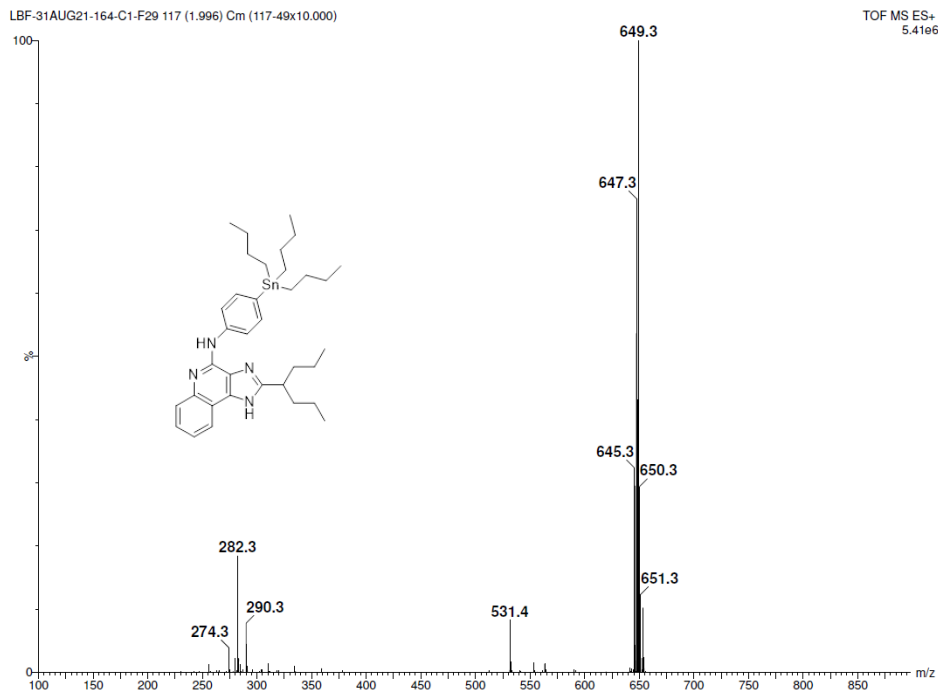


Minimum:

Maximum: 5.0 5.0 -1.5

Mass	Calc. Mass	mDa	PPM	DBE	1-FIT	Norm	Conf (%)	Formula
523.1882	523.1884	-0.2	-0.4	12.5	498.6	1.117	32.72	C26 H35 N4 120Sn
	523.1860	2.2	4.2	9.5	498.6	1.140	31.98	C24 H36 N4 Na 120Sn
	523.1918	-3.6	-6.9	0.5	498.5	1.041	35.30	C17 H40 N4 O5 Na 120Sn

TOF MS ES+ and elemental analysis of 2-(heptan-4-yl)-N-(4-(trimethylstannyl)phenyl)-1H-imidazo[4,5-c]quinolin-4-amine – Compound **32**



Elemental Composition Report

Page 1

Single Mass Analysis

Tolerance = 5.0 mDa / DBE: min = -1.5, max = 100.0

Element prediction: Off

Number of isotope peaks used for i-FIT = 3

Monoisotopic Mass, Even Electron Ions

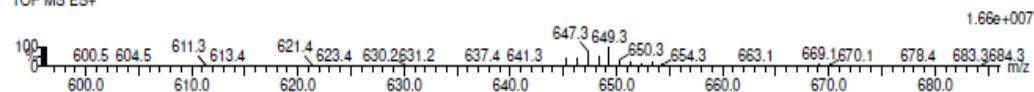
107 formula(e) evaluated with 1 results within limits (up to 50 closest results for each mass)

Elements Used:

C: 0-100 H: 0-250 N: 4-4 O: 0-20 120Sn: 1-1

LBF-31AUG21-164-C1-F29 111 (1.894)AM2 (Ar,25000.0.0.00.0.00); ABS

TOF MS ES+



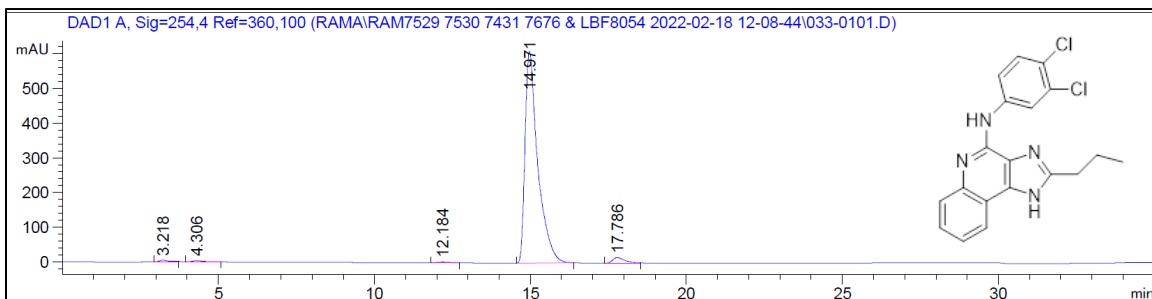
Minimum: -1.5
Maximum: 5.0 5.0 100.0

Mass	Calc. Mass	mDa	PPM	DBE	1-FIT	Norm	Conf(%)	Formula
649.3293	649.3292	0.1	0.2	12.5	420.8	n/a	n/a	C35 H53 N4 120Sn

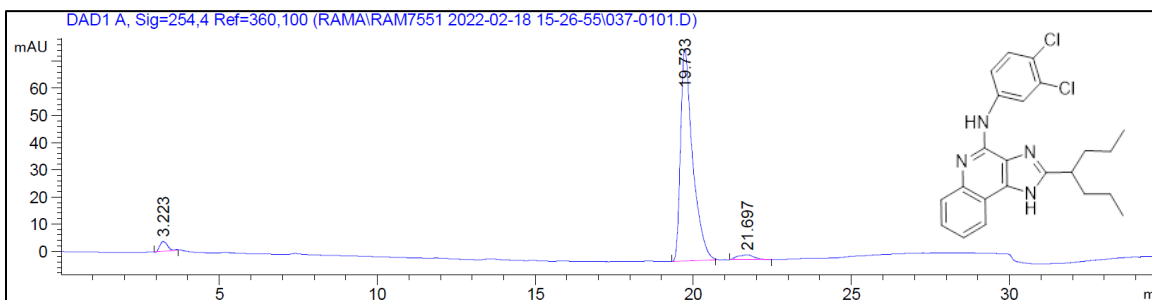
TOF MS ES+ and elemental analysis of 2-(heptan-4-yl)-N-(4-(tributylstannyl)phenyl)-1H-imidazo[4,5-c]quinolin-4-amine – Compound **33**

Appendix C: Compound HPLC Purity

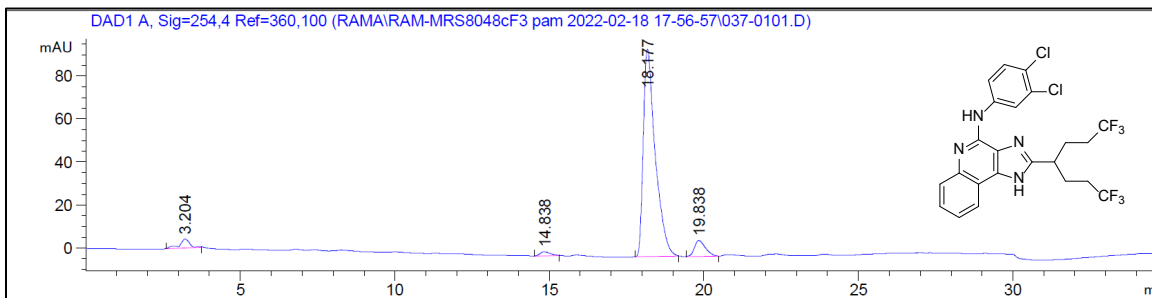
1 – HPLC Purity 97% ($R_t = 14.9$ min)



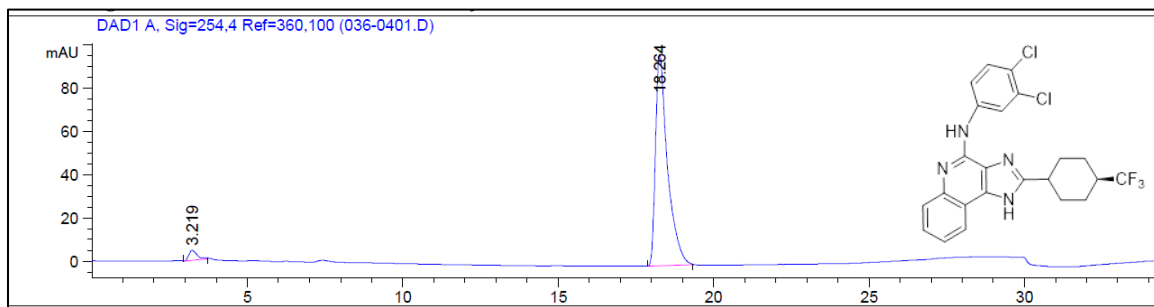
2 – HPLC Purity 97% ($R_t = 19.7$ min)



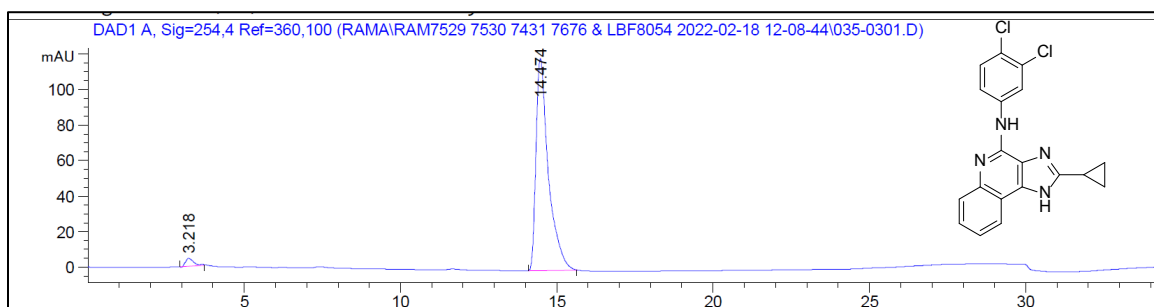
3 – HPLC Purity 91% ($R_t = 18.1$ min)



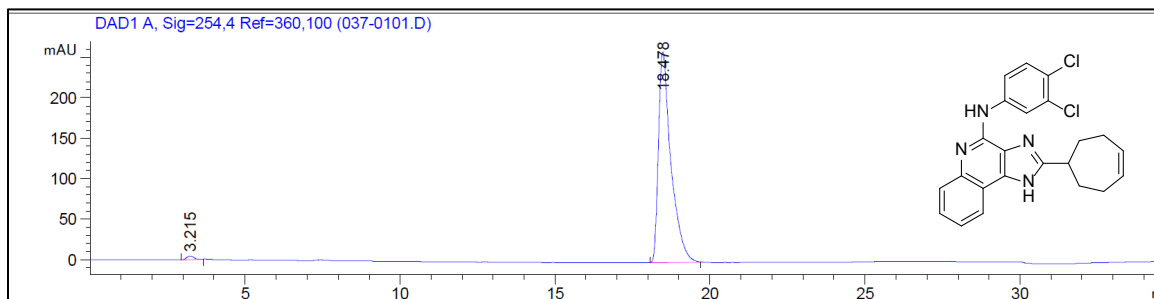
4 – HPLC Purity 99% ($R_t = 18.2$ min)



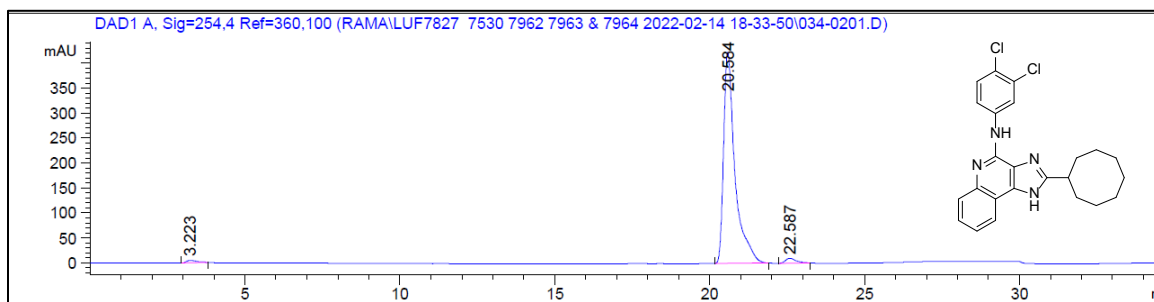
5 – HPLC Purity 99% ($R_t = 14.4$ min)



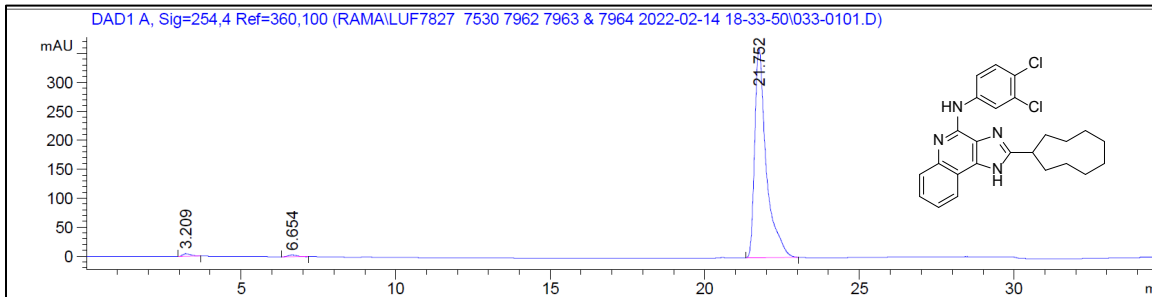
10 – HPLC Purity 99% ($R_t = 18.4$ min)



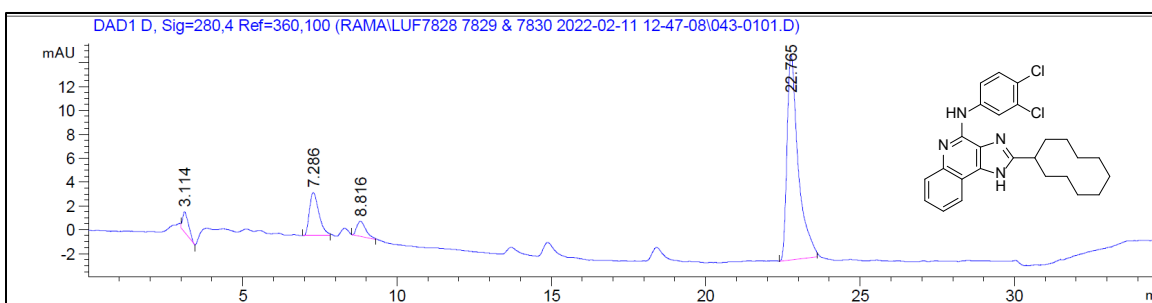
11 – HPLC Purity 98% ($R_t = 20.5$ min)



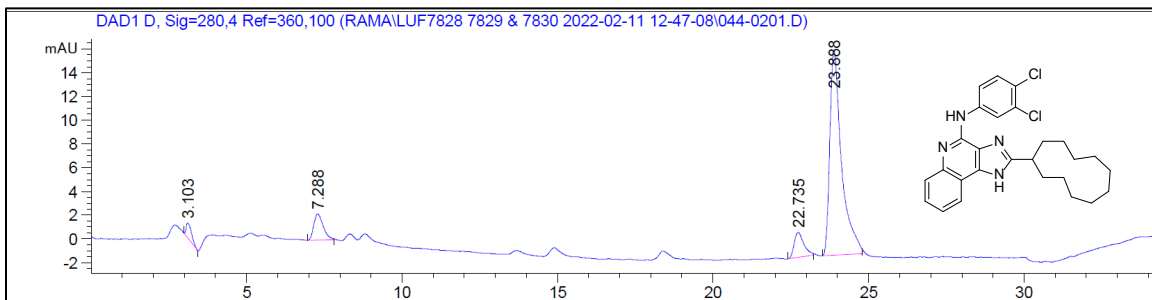
12 – HPLC Purity 99% ($R_t = 21.7$ min)



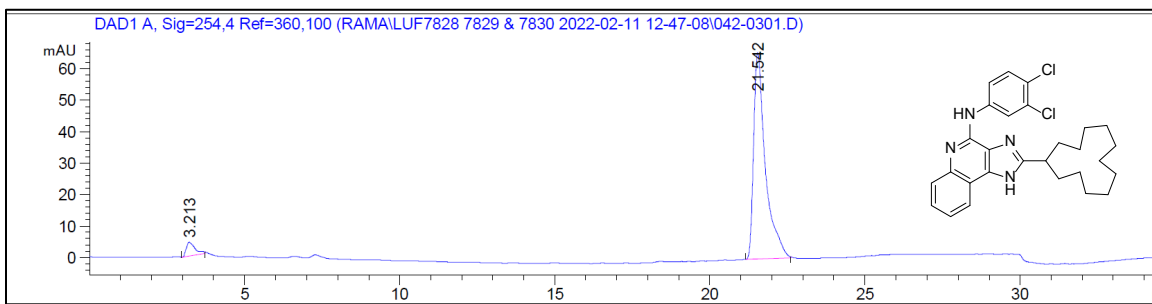
13 – HPLC Purity 77% ($R_t = 23.8$ min)



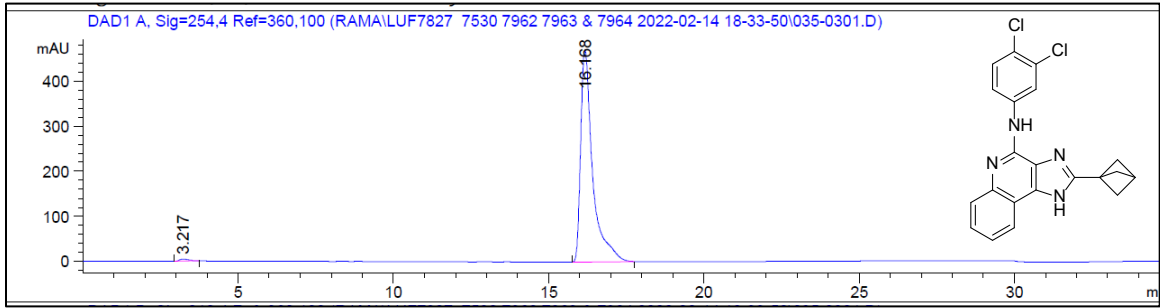
14 – HPLC Purity 80% ($R_t = 22.7$ min)



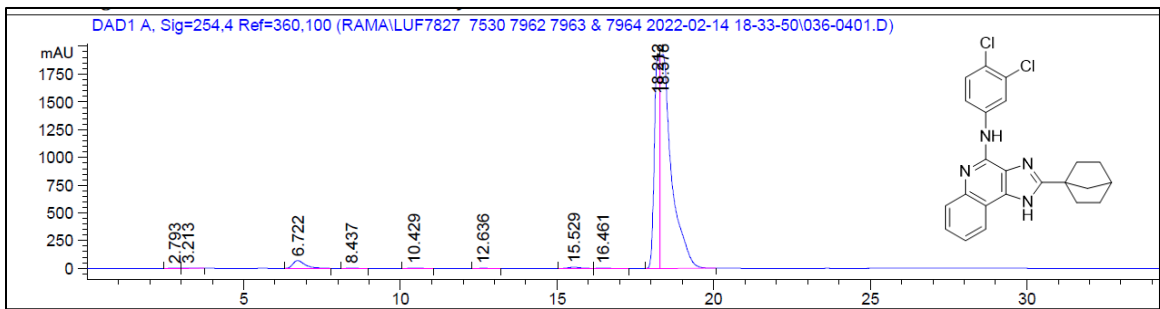
15 – HPLC Purity 95% ($R_t = 21.6$ min)



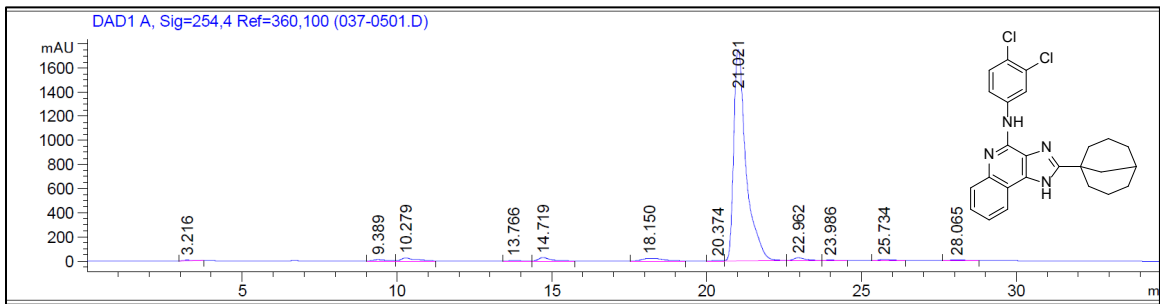
16 – HPLC Purity 99% ($R_t = 16.1$ min)



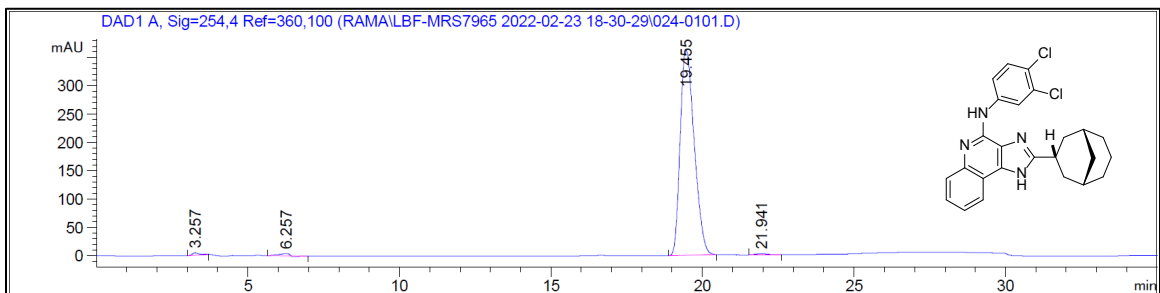
17 – HPLC Purity 96% ($R_t = 18.3$ min)



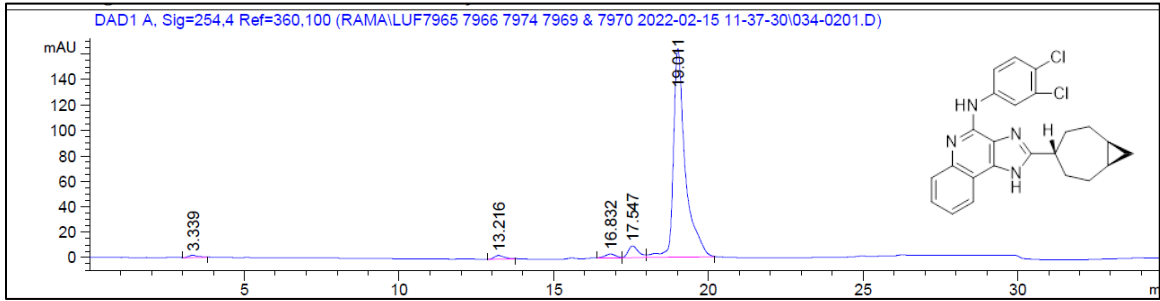
18 – HPLC Purity 95% ($R_t = 21.0$ min)



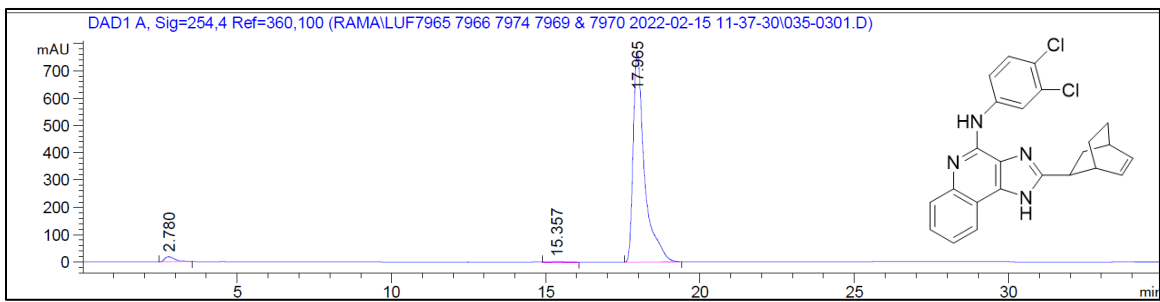
19 – HPLC Purity 98% ($R_t = 19.4$ min)



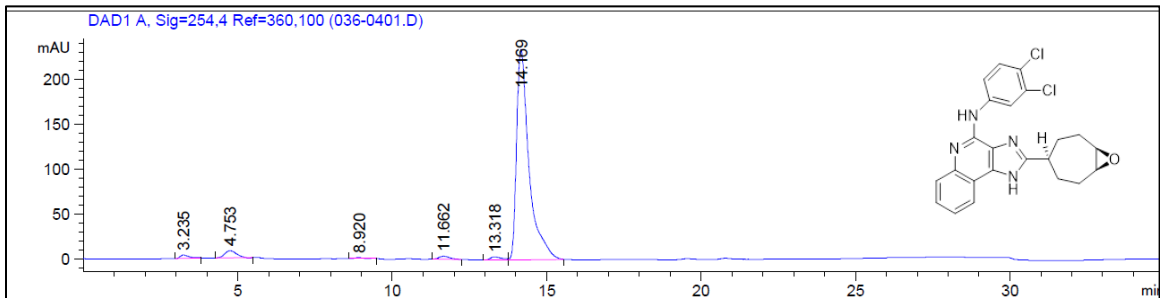
20 – HPLC Purity 95% ($R_t = 19.0$ min)



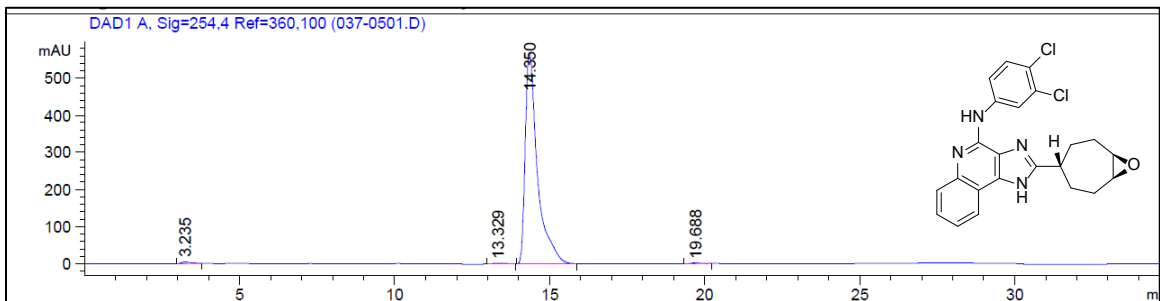
21 – HPLC Purity 99% ($R_t = 17.9$ min)



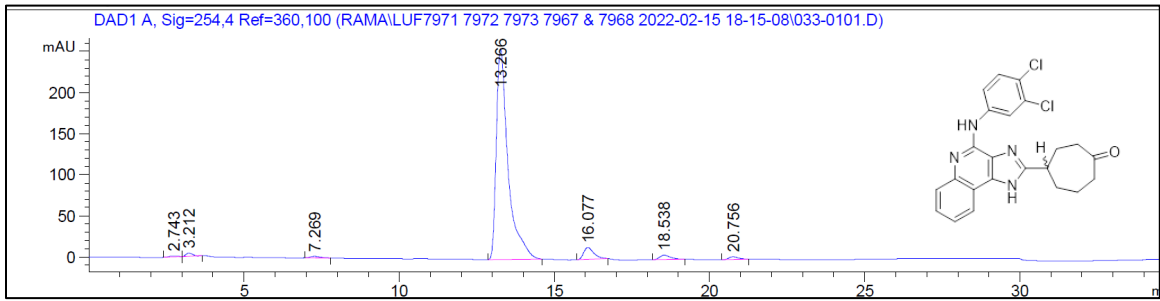
22 – HPLC Purity 96% ($R_t = 14.1$ min)



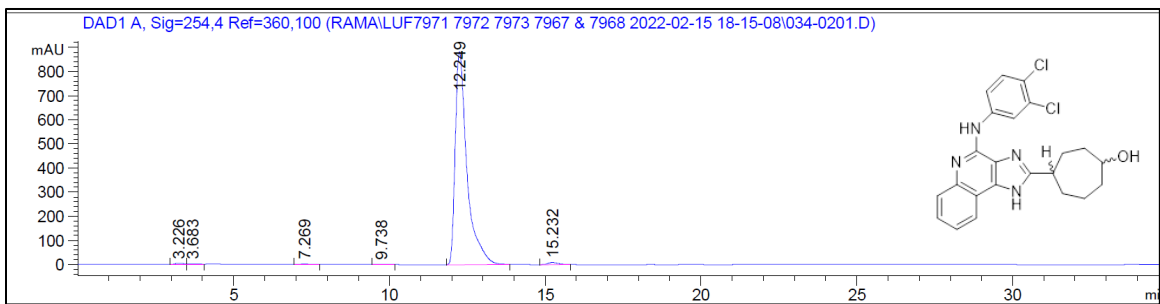
23 – HPLC Purity 99% ($R_t = 14.3$ min)



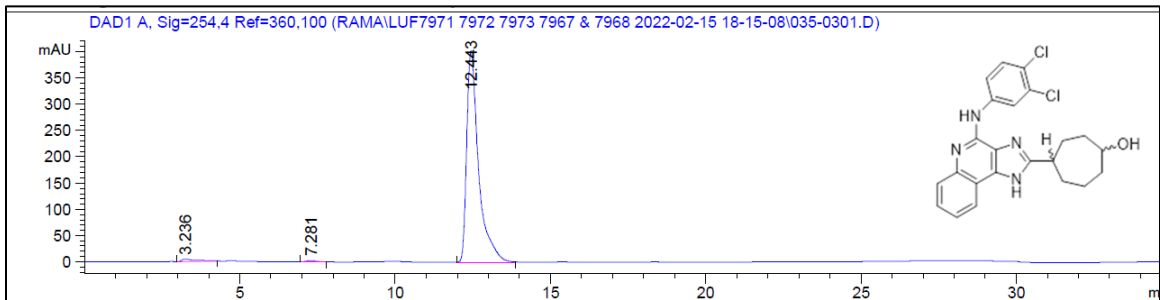
24 – HPLC Purity 95% ($R_t = 13.2$ min)



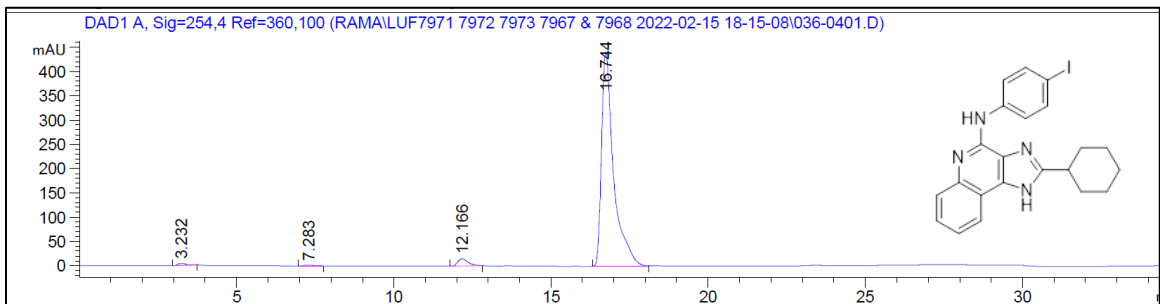
25 – HPLC Purity 95% ($R_t = 12.2$ min)



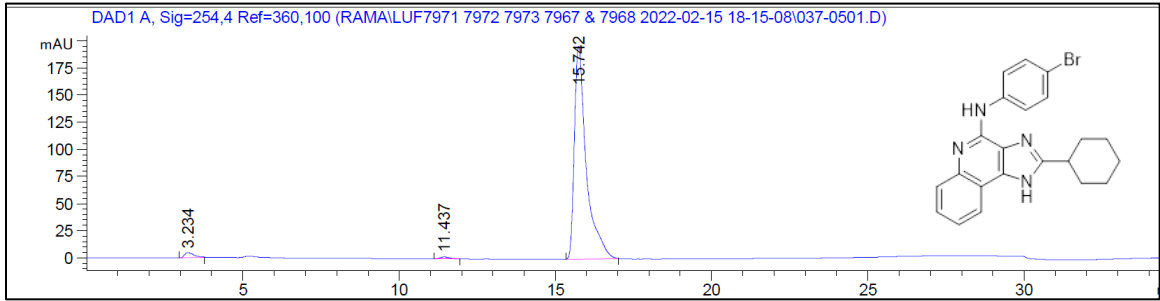
26 – HPLC Purity 98% ($R_t = 12.4$ min)



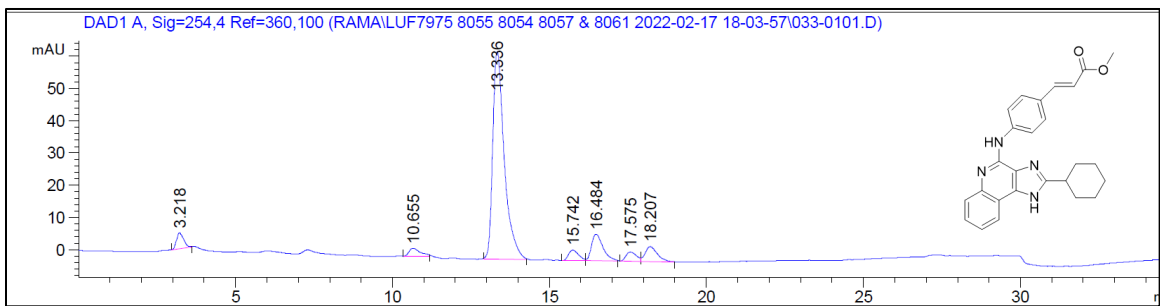
27 – HPLC Purity 96% ($R_t = 16.7$ min)



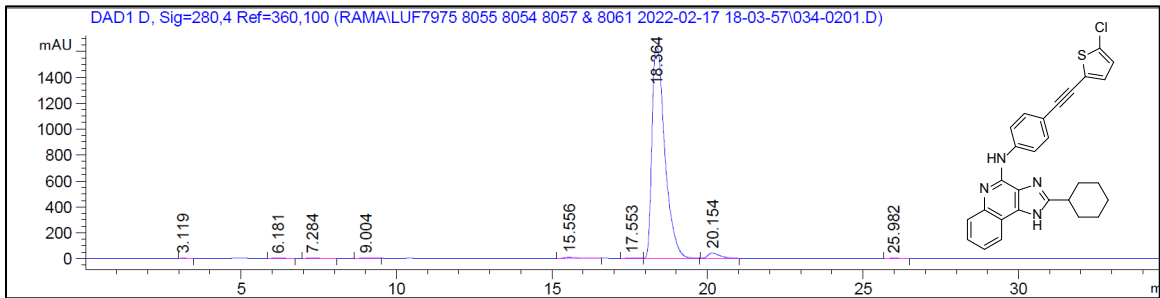
28 – HPLC Purity 98% ($R_t = 15.7$ min)



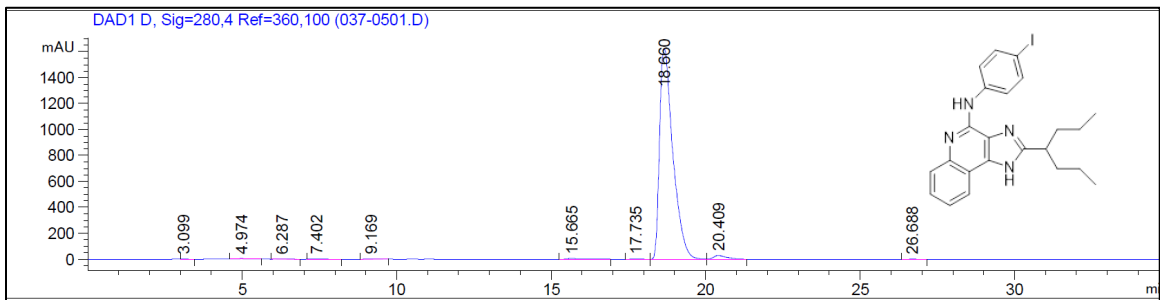
29 – HPLC Purity 76% ($R_t = 13.3$ min)



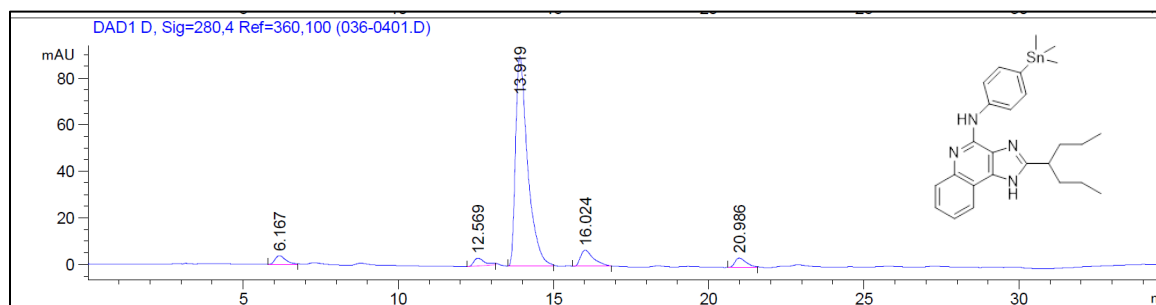
30 – HPLC Purity 96% ($R_t = 16.3$ min)



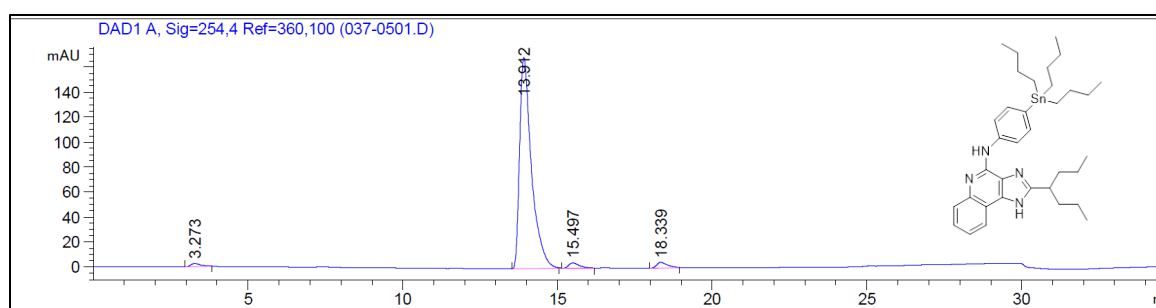
31 – HPLC Purity 97% ($R_t = 18.6$ min)



32 – HPLC Purity 86% ($R_t = 13.9$ min)



33 – HPLC Purity 95% ($R_t = 13.9$ min)



Appendix D: Kinetic Binding Assay Methods

HEK 293 CELL LINE MAINTENANCE

HEK 293 cell lines expressing recombinant human, mouse, or chimeric A₃AR were cultured (37°C with 5% CO₂) and maintained in Dulbecco's modified eagle medium (DMEM) and 10% fetal bovine serum, 1% penicillin/streptomycin, and 0.6 mg/mL G418.

MEMBRANE PREPARATION

HEK 293 cells stably expressing recombinant human, mouse, or chimeric A₃ARs were washed in PBS followed by homogenization in hypotonic lysis buffer containing Tris-HCl buffer (50 mM, pH 7.4) containing 1 mM EDTA and 5 mM MgCl₂ and then centrifuged at 27,000×g for 30 min at 4 °C. Cell pellets were subsequently washed in Tris-HCl buffer (50 mM, pH 7.4) containing 10 mM EDTA and 5 mM MgCl₂, after which the resultant pellets were re-suspended in Tris-HCl buffer (50 mM, pH 7.4) containing 10 mM EDTA, 5 mM MgCl₂, 10% sucrose and stored at -80°C. Because the modulators failed to increase [³⁵S]GTPγS binding in preliminary studies with the mouse A₃AR using crude P1 preparations, for some studies, plasma membranes were enriched by preparing P2 pellets. Cells were homogenized in lysis buffer containing 10% sucrose and centrifuged at 500×g for 10 min to remove nuclear and other cellular debris. The pellets were re-suspended in sucrose buffer (10 mM HEPES sodium salt, 1 mM EDTA, 1mM benzamidine, and 10% sucrose) and centrifuged again at 500×g. The pooled supernatants were diluted threefold, pelleted, and washed twice by centrifugation at 27,000×g for 30 min in 50 mM Tris-HCl buffer (pH 7.4). The resultant pellets were re-suspended and frozen in sucrose buffer.

SINGLE-POINT DISSOCIATION BINDING ASSAYS

~0.3 nM of [¹²⁵I]I-AB-MECA was incubated with 50 µg of HEK 293 cell membranes expressing A₃ARs for 2 h at rt in 100 µL of binding buffer. The assay was started by adding 100 µM of a nonselective agonist, NECA, and 10 µM of the PAM or vehicle (DMSO). After 60 min, the amount of [¹²⁵I]I-AB-MECA receptor-bound was measured by a gamma counter after rapid filtration using GF/C glass fiber filters. Data are expressed as the amount of radioligand left remaining after 60 min as a percent of the vehicle. Non-specific binding was determined for all assays by incubation in the presence of 100 µM NECA. All experiments were performed in technical and biological triplicate. Binding data of agonists influenced by modulators were statistically compared to the control using a two-tailed paired student's t-test.

SINGLE-POINT EQUILIBRIUM BINDING ASSAYS

HEK 293 membranes (50 µg) were incubated at room temperature with ~0.3 nM [¹²⁵I]I-AB-MECA and 10 µM modulator or vehicle (DMSO) for 18 h at which point the amount of radioligand receptor-bound was measured a gamma counter after rapid filtration using GF/C glass fiber filters. Data are expressed as the amount of specific binding as a fold change from vehicle (specific binding modulator/specific binding vehicle). Non-specific binding was determined for all assays by incubation in the presence of 100 µM NECA. All experiments were performed in technical and biological triplicate. Binding data of agonists influenced by modulators were statistically compared to the control using a two-tailed paired student's t-test.

Appendix E: GTP γ S Binding Method for Measuring Receptor Activation

HEK 293 cell line maintenance and membrane preparation were conducted similarly as described in Appendix D.

[³⁵S]GTP γ S BINDING ASSAYS

[³⁵S]GTP γ S binding assays were conducted to assess the direct effects of modulators on receptor activation. 5 μ g membranes overexpressing the hA₃AR in a 96-well large-volume (1mL) polypropylene assay plate was treated with agonists and modulators and allowed to incubate for 2 h at room temperature. To block other AR subtypes expressed on HEK 293 cells, 1 μ M each of the A_{2B}AR antagonists, PSB-603 and ZM-241385, were included (A_{2B}AR are endogenously expressed by HEK 293 cells). Any endogenous adenosine that might have been present was broken down with the addition of 1 μ L/mL of ADA. After the reactions were stopped, the membranes were harvested by rapid filtration through Whatman GF/B filters using a Brandel cell harvester. Liquid scintillation counting measured the radioactivity trapped in the filters. Non-specific binding of [³⁵S]GTP γ S was measured in the presence of 10 μ M unlabeled GTP γ S. Cl-IB-MECA potency and maximal efficacy were measured using 0.1 μ M, 1.0 μ M, and 10 μ M of PAM. Statistical significance was determined by one-way ANOVA with Bonferroni post-hoc multiple comparisons (n=3; * denotes p < 0.05). Data are presented as mean \pm SEM.

Appendix F: Chimeric Receptor Methods

HEK 293 cell line maintenance and membrane preparation were conducted similarly as described in Appendix D.

CREATION OF STABLE HEK 293 CELL LINES EXPRESSING WT AND CHIMERIC A₃ARS

The cDNA resource center provided the full-length mouse A₃AR cDNA subcloned into the mammalian expression vector pCDNA3.1. The hA₃AR cDNA in pCDNA3.1 was acquired from the cDNA Resource Center (www.cdna.org). After amplification in *Escherichia coli*, plasmids were purified using Qiagen (Valencia, CA) purification kits and sequenced through the entire coding region to make certain inadvertent mutations potentially generated during the amplification step did not exist.

Gene syntheses created chimeras at TopGene Technologies (St-Laurent, Quebec). The plasmids were transfected into human HEK 293 cells using Lipofectamine 2000 reagent (Invitrogen), and cells were selected with 2 mg/mL of G418 in cell culture media. Cell lines resulting from individual clones were maintained in cell culture media (Dulbecco's modified Eagle's medium with 10% fetal bovine serum and antibiotics) containing 0.6 mg/mL G418. The level of expression of the receptors in each cell line was equivalent (~1,000 fmol/mg) based on saturation radioligand binding analyses.

CHIMERIC RECEPTOR SEQUENCES

human_{Out}/mouse_{In} A₃AR Chimera

```
ATGCCCAACAACAGCACTGCTCTGTCATTGGCCAATGTTACCTACATCACCATGGAA
ATTTTCATTGGACTCTGCGCCATAGTGGGCAACATGCTGGTCATCTGGGTGGTCAAGC
TGAACCCCACTCTGAGGACCACCAGTTCTATTTTCATTGTCTCCCTAGCACTGGCTGACA
TTGCTGTTGGGGTGCTGGTCATGCCTTTGGCCATTGTTGTCAGCCTGGGCATCACAA
TCCACTTCTACAGCTGCCTTTTTATGACTTGCCTACTGCTTATCTTTACCCACGCCTC
CATCATGTCTTGCTGGCCATCGCTGTGGACCGATACCTGCGGGTCAAGCTGACAGTC
```

AGATATAGAACGGTTACCACTCAAAGAAGAATATGGCTATTCTTGGGCCTTTGCTGGCT
GGTGTCAATTCCTGGTGGGATTGACCCCATGTTTGGCTGGAACATGAAACTGACCTC
AGAGTACCACAGAAATGTCACCTTCCTTTCATGCCAATTTGTTTCCGTCATGAGAAT
GGACTACATGGTATACTTCAGCTTCCTCACCTGGATTTTCATCCCCCTGGTTGTCATG
TGTGTCATCTACCTAGACATCTTCTACATCATCCGAAATAAGCTCAGTCAAAACCTGTCT
GGCTTCAGAGAGACGCGTGCATTTTATGGACGGGAGTTCAAGACAGCTAAGTCCCTGTTT
CTGGTTCTCTTCTTGTGGCGCTGTGCTGGCTGCCTTTATCTATCATCAACTGCATCAT
CTACTTTAATGGTGAGGTACCACAGCTTGTGCTGTACATGGGCATCCTGCTGTCCCA
TGCCAACTCCATGATGAACCCTATTGTCTACGCCTGCAAAAATAAAAAAGTTCAAAGAG
ACCTACTTTCTGATCCTCAGAGCTCTCAGGCTCTGTCAGACCTCAGATTCTTTGGACTCA
AACATGGAACAGACTACTGAATAG

mouse_{Out}/human_{In} A₃AR Chimera

ATGGAAGCCGACAACACCACGGAGACGGACTGGCTGAACATCACCTACATCACCATG
GAGGCTGCCATCGGGCTCTGTGCCGTTGTGGGCAACGTGCTGGTCATCTGCGTGGTCA
AGCTGAACCCAGCCTGCAGACCACCACCTTCTATTTTCATTGTCTCTCTAGCCCTGGCTG
ACATTGCCGTTGGGGTGTGGTCACACCTTTGGCCATTGCTGTCAGCCTGCAAGTCA
AGATGCACTTCTATGCCTGCCTTTTCATGTCCTGTGTGCTGCTGATCTTCACCCATG
CTTCCATCATGTCCTTGTGGCCATTGCTGTAGACCGATACTTGCGGGTCAAGCTTAC
CGTCAGATACAAGAGGGTCACCACTCACAGAAGAATATGGCTGGCCCTGGGCCTTTGCTG
GCTAGTTTCCTTTCTGGTGGGGCTGACCCCATGTTTGGCTGGAATAGAAAAGCAAC
CTTAGCGAGCTCTCAAAATAGCAGCACTCTTTTGTGCCACTTCCGTTCCGTGGTCCAG
TTTGGATTACATGGTCTTCTTCAGCTTCGTCACCTGGATCCTCGTCCCCCTGGTTGTC
ATGTGCGCCATCTATCTTGACATCTTTTACATCATTCGGAACAAACTCAGTCTGAACTTA
TCTAACTCCAAAGAGACAGGTGCATTTTATGGACGGGAGTTCAAGACGGCTAAGTCCCT
GTTTCTGGTTCTTTTCTTGTGGTCTGTCATGGCTGCCTTTGTCCATCATCAATTTG
TTTCTATTTTGTATGTAAGATACCAGATGTCGCAATGTGCCTGGGGATCCTGTTG
TCCACGCGAACTCCATGATGAACCCTATCGTCTATGCCTATAAAAATAAAGAAGTTCAA
GGAAACCTACCTTTTGTATCCTCAAAGCCTGTGTGGTCTGCCATCCCTCTGATTCTTTGGA
CACAAGCATTGAGAAGAATTCTGAATAG

CHIMERA RECEPTOR [³⁵S]GTP γ S BINDING ASSAYS

Chimera receptor [³⁵S]GTP γ S binding assays were conducted similarly to the [³⁵S]GTP γ S binding assays described in Appendix E. Cl-IB-MECA potency and maximal efficacy were measured using 0.1 μ M, 1.0 μ M, and 10 μ M of PAM. Statistical significance was determined by one-way ANOVA with Bonferroni post-hoc multiple comparisons (n=3; * denotes $p < 0.05$). Data are presented as mean \pm SEM.

Appendix G: ADMET Methods

***IN VIVO* EXPERIMENTS TO MEASURE DRUG METABOLISM AND PHARMACOKINETIC PROPERTIES**

The animal breeding facility, Jai Research Foundation, provided healthy adult male rats (*Rattus norvegicus*) of Wistar strain (RccHan:WIST). Rats were 6 to 10 weeks old at the start of acclimation. The weight variation of rats was $\pm 20\%$ of mean body weight (b. wt.) at the beginning of acclimation (114). Table 10 shows the experimental outline for the *in vivo* study of pharmacokinetics using rats.

Table 10. *In vivo* experimental outline using Wistar rats

Groups	G1	G2	G3	G4
Species of Strain	Rat and RccHan:WIST			
N⁰	3	3	3	3
Routes	Intravenous	Oral		
Feeding Condition	Fed	Fasting overnight, feed 4 h post-dosing		
Dose Volume (mg/kg b. wt.)	5			
Concentration (mg/mL)	0.1	0.2	0.6	2
Vehicles	DMSO: 20% HPBCD (10:90)	DMSO: Kolliphor EL: PBS (15:15:70)		
Blood Collection Site	Jugular vein through catheter			
Anticoagulant	Heparin (20 IU/mL)			
Time Points (h)	0.083, 0.25, 0.5, 1, 2, 4, 8, 12, 24	0.25, 0.5, 1, 2, 4, 8, 12, 24		

Two routes of administration, intravenous and oral, were used to determine A₃AR PAM bioavailability. The dose level for the G₁ intravenous route was 0.5 mg/kg. b. wt. and the dose levels for the G₂₋₄ oral route were 1, 3, and 10 mg/kg. b. wt. For the intravenous administration, the A₃AR PAM-DMSO solution was diluted with an aqueous

solution of 20% HPBCD, creating a final volume ratio of DMSO to HPBCD, 10:90. An equal volume of Kolliphor EL (polyoxyl castor oil) was added to the A₃AR PAM-DMSO solution for oral administration, followed by phosphate buffer saline (PBS). The final volume ratio of DMSO:Kolliphor:PBS for the oral administration was 15:15:70 (114).

200 µL of blood was collected from the jugular vein from each rat group on the day of dosing at 0.083, 0.25, 0.5, 1, 2, 4, 8, 12, and 24 h post-dosing to assess the A₃AR PAM PK profile through intravenous administration. Blood samples were collected in pre-labeled—(having research N^o, group N^o, sex, rat N^o, and time point)—microcentrifuge tubes with the anticoagulant heparin (20 IU/mL of blood). After collection, samples were inverted 4 to 5 times, placed on ice, and centrifuged at 9000 rpm for 10 min. Plasma was frozen at -70 °C (114).

Pharmacokinetic analysis of the frozen plasma concentration-time data was performed using the noncompartmental model of the WinNonlin® software. Estimated parameters were the maximum plasma concentration (C_{max}), the time to achieve peak plasma concentration (T_{max}), the area under the plasma concentration-time curve until the last measured time point (AUC_{0-last}), the area under the plasma concentration-time curve extrapolated to infinity ($AUC_{0-\infty}$), the terminal elimination half-life ($T_{1/2}$), the mean residence time (MRT), volume of distribution (V_d), the elimination rate constant (k_{el}), the bioavailability (%F), and the clearance (Cl).

***IN VITRO* ASSAYS TO MEASURE DRUG METABOLISM AND PHARMACOKINETIC PROPERTIES**

Plasma Stability

This assay measured the degradation of A₃AR in the plasma. To investigate species differences of the A₃AR PAM, plasma stability was measured in three species:

human, rat, and mouse at 0 to 120 min by liquid chromatography mass spectrometry – mass spectrometry (LCMS-MS). % A₃AR PAM remaining was provided at 120 min and t_{1/2} (min).

$$\% \text{ A}_3\text{AR PAM remaining} = \frac{\text{Peak area ratio at time (120 min)}}{\text{Peak area ratio at time(0 min)}} * 100$$

HepG2 Cytotoxicity

HepG2 cytotoxicity was measured using the CellTiter-Glo Luminescent Cell Viability assay. This assay determined the number of live cells in culture by measuring the ATP metabolism of active cells. 10 to 40 K cells were placed in a 96-well. The A₃AR PAMs were incubated with live cells for 48 h. 8 dilutions were made with varying concentrations of A₃AR PAM ranging from 30 μM-0.2 μM and incubated. Verapamil/Rifampicin were used as a reference compound. Analysis was done via luminometry. Data was reported as an IC₅₀ value, the concentration of A₃AR PAM that reduces cell viability by 50% (ATP measurement).

Human Ether-a-go-go Related Gene (hERG)

hERG potassium channels are involved in cardiac action potential repolarization. hERG assay measures the % inhibition of the potassium channels by the A₃AR PAM. The assay used HEK 293 cells stably transfected with the hERG potassium channel. A₃AR PAM concentrations were prepared using serial half-log dilutions, starting at 30 μM. A₃AR PAMs were incubated with the hERG cells for 2 h. A₃AR PAMs bound to the hERG ion channel were identified by their ability to displace the tracer (Predictor™ hERG Tracer Red), which resulted in lower fluorescence polarization, as assessed using a TAMRA fluorescent polarization filter. E-4031 is a reference compound. The %

inhibition was reported as the ratio of a half-maximum inhibitory concentration of the hERG channel (hERG IC₅₀, μM) to the peak serum concentration of unbound drug (C_{max}).

CYP Inhibition

CYP inhibition was conducted by way of a cocktail approach, A₃AR PAMs—six concentrations in duplicate (30 μM – 0.12 μM)—were incubated with liver microsomes (human, rat, mice) containing the CYP panel (1A2 – phenacetin (10 μM), 2C9 – diclofenac (5 μM), 2C19 – omeprazole (5 μM), 2D6 – dextromethorphan (5 μM), 3A4 – midazolam (2 μM)), 1mM of NADPH co-factor, 1 μM miconazole (pan inhibitor) in plasma. Analysis of substrates was done by LC-MS/MS. This approach reported A₃AR PAM concentrations which produced 50% inhibition of cytochrome isozymes (IC₅₀ value, μM). LCMS-MS quantified metabolites by area ratio: acetaminophen (1A2), 4-OH-diclofenac (2C9), 5-OH-omeprazole (2C19), dextrorphan (2D6), and 1-OH-midazolam (3A4).

Microsomal Stability Assays

Microsomal stability assays were done using human, rat, and mouse liver microsomes containing the following enzymes: Cytochrome P450s (CYPs), flavin monooxygenases, carboxylesterases, and epoxide hydrolase. A₃AR PAMs were in 3 μM concentrations duplicates and mixed with 1 mM NADPH and 0.5 g/mL of human, rat, or mouse liver microsomes. Samples were taken from five time periods (0.5, 15, 30, 60, 90, 120 min) and analyzed by LC-MS/MS. The average half-life (min) and % remaining at 120 min was reported.

Caco-2 Permeability Assay

Caco-2 permeability assay measured the rate of transport of a compound across the Caco-2 cell line (21-day process consisting of bidirectional monitoring of absorptive (A-B) and secretory (B-A) fluxes). The Caco-2 cell line originated from a human colon carcinoma, having a polarized monolayer, an apical surface, and intercellular junctions. 10 μ M of the A₃AR PAMs were exposed to the cells in an HBSS buffer with 2% BSA. Samples were gathered at 0- and 120-min. Samples were analyzed by LCMS-MS. Positive controls were atenolol, digoxin, and propranolol. Apparent permeability (P_{app} – 10^6 cm/sec), efflux ratio, and % recovery were reported.

pION Solubility

pION solubility of each A₃AR PAM at pH 7.4 was measured using the pION buffer method. 500 μ M of the A₃AR PAM was exposed to the pION buffer. Sampling was done at 18 h. Positive controls were albendazole and flurbiprofen. Solubility was reported for each A₃AR PAM as mean solubility (μ g/mL).

Plasma Protein Binding

Plasma protein binding measured the % unbound A₃AR PAM in the plasma of three species (rat, mice, and human). Cellulose membranes in potassium phosphate buffer (100 mM, pH 7.4) were exposed to 10 μ M of A₃AR PAM and 500 μ L of plasma. Samples were loaded into dialysis cells and maintained in an incubator at 37 °C at 100 rpm. Samples were collected into prelabelled microfuge tubes at 0 and 5 h. The samples were vortexed and centrifuged. Supernatants were analyzed by LC-MS/MS. % binding reported: 1-40% low bound, 41-70% medium bound, 71-100% highly bound.

$$\% \text{ Unbound} = \frac{c_b}{c_{pe}} * 100$$

C_{pe} = Concentration of test compound in plasma at equilibrium (Donor)

C_b = Concentration of test compound in buffer at equilibrium (Receiver)

Stability in Gastrointestinal Tract (GIT)

Stability in GIT determined whether A₃AR PAMs have low bioavailability as they are broken down in the stomach at low pH 1-2 or in the intestine pH 6-8. 5 μM of A₃AR PAMs were subjected to simulated gastric fluid (SGF) and simulated intestinal fluid (SIF). Sampling was done at 0- and 120-min time points. The method of analysis was LC-MS/MS by area ratio. % A₃AR PAM at 120 min was reported.

$$\% \text{ remaining} = \frac{\text{Peak area ratio at time (120 min)}}{\text{Peak area ratio at time(0 min)}} * 100$$

Appendix H: Results Chapter Tables

Table 11. Effect of PAM derivatives (10 μ M) on dissociation of [125 I]-AB-MECA (0.3 nM) using hA₃ARs. Statistical significance was determined by two-tailed paired student's t-test (n=3; * denotes P < 0.05). Data are presented as mean \pm SEM.

Compound ID		% Remaining	SEM	P-value
1	MRS7529	24.6	1.8	0.760
2	MRS7551	71.2	2.7*	0.001
3	MRS8048	45.2	5.1	0.056
4	MRS7676	25.9	4.4	0.958
5	MRS7431	33.3	2.4	0.271
6	MRS3720	36.2	3.8	0.187
7	MRS3557	43.4	5.2	0.075
8	LUF6000	54.4	3.4*	0.009
9	MRS3718	52.2	6.1*	0.030
10	MRS7788	54.1	3.4*	0.001
11	MRS7530	44.5	4.1*	0.046
12	MRS7827	37.1	4.7	0.188
13	MRS7828	24.6	3.1	0.786
14	MRS7829	24.5	4.6	0.808
15	MRS7830	23.9	4.5	0.735
16	MRS7962	45.6	3.8*	0.036
17	MRS7963	44.5	4.0*	0.046
18	MRS7964	52.1	3.1*	0.011
19	MRS7965	46.1	4.4*	0.040
20	MRS7966	45.7	4.9*	0.048
21	MRS7974	42.1	5.6	0.100
22	MRS7969	33.2	4.3	0.350
23	MRS7970	39.4	3.6	0.098
24	MRS7971	33.1	3.7	0.328
25	MRS7972	33.0	3.7	0.340
26	MRS7973	34.9	3.0	0.210
27	MRS7967	57.8	4.8*	0.010
28	MRS7978	55.8	5.2*	0.015
29	MRS7975	49.6	7.0	0.052
30	MRS8055	32.5	5.5	0.450
31	MRS8054	65.3	4.0*	0.003

Table 12. Effect of PAM derivatives (10 μ M) on equilibrium binding of [125 I]-AB-MECA (0.3 nM) at the hA₃AR. Statistical significance was determined by two-tailed paired student's t-test (n=3; * denotes P < 0.05). Data are presented as mean \pm SEM.

Compound ID		% Change From Vehicle	SEM	P-value
1	MRS7529	-45.2	1.6*	0.002
2	MRS7551	70.2	9.3*	0.020
3	MRS8048	18.4	5.3*	0.035
4	MRS7676	-4.5	2.2	0.171
5	MRS7431	-70.9	2.3*	0.006
6	MRS3720	-23.3	3.0*	0.028
7	MRS3557	1.9	4.3	0.662
8	LUF6000	24.9	6.8*	0.031
9	MRS3718	0.3	0.1	0.052
10	MRS7788	-11.8	1.6*	0.026
11	MRS7530	41.3	4.7*	0.019
12	MRS7827	27.8	3.2*	0.007
13	MRS7828	17.5	5.0	0.084
14	MRS7829	15.7	5.6	0.083
15	MRS7830	6.9	2.2	0.070
16	MRS7962	-5	1.8	0.135
17	MRS7963	-6.7	3.3	0.204
18	MRS7964	38.3	4.6*	0.012
19	MRS7965	41	4.9*	0.0069
20	MRS7966	-36.6	5.9	0.0561
21	MRS7974	-20.5	2.5*	0.032
22	MRS7969	-21.3	3.0	0.050*
23	MRS7970	-24.1	2.8	0.040*
24	MRS7971	-19.1	2.6	0.050*
25	MRS7972	-35.8	2.1	0.023*
26	MRS7973	-31.3	3.1	0.037*
27	MRS7967	-31.1	3.5	0.040*
28	MRS7978	-48.9	5.5	0.036*
29	MRS7975	14.6	4.0	0.011*
30	MRS8055	19.5	6.4	0.055
31	MRS8054	22.9	10.2	0.125

Table 13. Effect of alkyl and cycloalkyl PAM derivatives on [³⁵S]GTP γ S binding induced by CI-IB-MECA using WT hA₃ARs. Statistical significance was determined by one-way ANOVA with Bonferroni post-hoc multiple comparisons (n=3; * denotes P < 0.05). Data are presented as mean \pm SEM.

Structural Specifications				DMSO		0.1 μ M Compound			1 μ M Compound			10 μ M Compound				
# ID	Compound ID	R ¹	EC ₅₀ (nM)	E _{max} (%)	EC ₅₀ (nM)	P-value	E _{max} (%)	P-value	EC ₅₀ (nM)	P-value	E _{max} (%)	P-value	EC ₅₀ (nM)	P-value	E _{max} (%)	P-value
1	MRS7529	propan-4-yl	22 \pm 4	100 \pm 2	167 \pm 46	0.531	128 \pm 11	0.068	622 \pm 129*	0.001	150 \pm 15*	0.005	311 \pm 20	0.055	130 \pm 9	0.0773
2	MRS7551	heptan-4-yl	47 \pm 20	100 \pm 6	23 \pm 9	0.562	171 \pm 9*	0.002	17 \pm 3	0.327	216 \pm 12*	<0.0001	25 \pm 8	0.668	216 \pm 9*	<0.0001
3	MRS8048	trifluoroheptan-4-yl	48 \pm 17	99 \pm 5	43 \pm 22	>0.999	118 \pm 7	0.534	52 \pm 25	>0.999	159 \pm 13*	0.004	47 \pm 18	>0.999	185 \pm 10*	0.0004
4	MRS7676	trifluoromethylcyclohexyl	23 \pm 9	99 \pm 5	23 \pm 5	>0.999	120 \pm 4*	0.041	23 \pm 8	>0.999	150 \pm 5*	0.0002	125 \pm 24*	0.002	174 \pm 6*	<0.0001
5	MRS7431	cyclopropyl	27 \pm 2	100 \pm 2	35 \pm 8	>0.999	118 \pm 8	>0.999	191 \pm 36	>0.999	111 \pm 16	>0.999	789 \pm 307*	0.025	90 \pm 20	>0.999
6	MRS3720	cyclobutyl	28 \pm 7	100 \pm 3	48 \pm 5	0.569	113 \pm 4	0.290	78 \pm 17*	0.021	109 \pm 4	0.737	259 \pm 5*	<0.0001	136 \pm 8*	0.003
7	MRS3557	cyclopropyl	13 \pm 3	100 \pm 3	25 \pm 7	>0.999	110 \pm 4	0.626	38 \pm 2	0.820	142 \pm 5*	0.001	147 \pm 29*	0.001	201 \pm 7*	<0.0001
8	LUF6000	cyclohexyl	27 \pm 4	100 \pm 5	20 \pm 2	>0.999	154 \pm 9*	0.030	24 \pm 3	>0.999	225 \pm 10*	0.0002	71 \pm 25	0.123	241 \pm 18*	<0.0001
9	MRS3718	cycloheptyl	19 \pm 4	100 \pm 3	13 \pm 2	0.970	120 \pm 4*	0.018	16 \pm 3	>0.999	175 \pm 3*	<0.0001	62 \pm 6*	0.0002	218 \pm 6*	<0.0001
10	MRS7788	cyclohept-4-enyl	37 \pm 9	100 \pm 3	26 \pm 2	0.943	147 \pm 7*	0.011	16 \pm 2	0.224	241 \pm 9*	<0.0001	81 \pm 11*	0.008	287 \pm 11*	<0.0001
11	MRS7530	cyclooctyl	40 \pm 6	100 \pm 3	27 \pm 2	0.156	107 \pm 3	0.356	26 \pm 3	0.119	147 \pm 2*	<0.0001	24 \pm 4	0.069	164 \pm 4*	<0.0001
12	MRS7827	cyclononyl	41 \pm 2	100 \pm 3	26 \pm 3	0.051	143 \pm 6*	0.046	20 \pm 1*	0.009	242 \pm 12*	<0.0001	29 \pm 6	0.130	259 \pm 14*	<0.0001
13	MRS7828	cyclodecyl	25 \pm 2	100 \pm 3	19 \pm 2	>0.999	109 \pm 6	>0.999	34 \pm 11	0.931	135 \pm 7*	0.018	17 \pm 3	>0.999	194 \pm 10*	<0.0001
14	MRS7829	cycloundecyl	24 \pm 1	100 \pm 3	37 \pm 6	0.1734	118 \pm 4	0.121	25 \pm 4	>0.999	123 \pm 6	0.053	17 \pm 4	0.803	166 \pm 8*	<0.0001
15	MRS7830	cyclododecyl	32 \pm 9	100 \pm 7	14 \pm 3	0.0992	99 \pm 3	>0.999	14 \pm 2	0.099	101 \pm 3	>0.999	17 \pm 2	0.194	116 \pm 5	0.108

Table 14. Effect of bridged PAM derivatives on [³⁵S]GTP γ S binding induced by CI-IB-MECA using WT hA₃ARs. Statistical significance was determined by one-way ANOVA with Bonferroni post-hoc multiple comparisons (n=3; * denotes P < 0.05). Data are presented as mean \pm SEM.

Structural Specifications				DMSO		0.1 μ M Compound			1 μ M Compound			10 μ M Compound				
# ID	Compound ID	R ¹	EC ₅₀ (nM)	E _{max} (%)	EC ₅₀ (nM)	P-value	E _{max} (%)	P-value	EC ₅₀ (nM)	P-value	E _{max} (%)	P-value	EC ₅₀ (nM)	P-value	E _{max} (%)	P-value
16	MRS7962	bicyclo[1.1.1]pent-1-yl	31 \pm 4	100 \pm 5	34 \pm 15	>0.999	141 \pm 9	0.217	50 \pm 19	>0.999	187 \pm 14*	0.007	306 \pm 53*	0.0005	195 \pm 22*	0.004
17	MRS7963	bicyclo[2.2.1]hept-1-yl	19 \pm 7	100 \pm 5	39 \pm 13	>0.999	120 \pm 6	0.320	82 \pm 18*	0.049	170 \pm 6*	0.001	174 \pm 18*	0.0002	180 \pm 12*	0.0003
18	MRS7964	bicyclo[3.3.1]nonan-1-yl	32 \pm 20	97 \pm 5	19 \pm 10	>0.999	147 \pm 9	0.080	43 \pm 23	>0.999	219 \pm 16*	0.001	70 \pm 10	0.445	216 \pm 17*	0.0006
19	MRS7965	2-((1R,3S,5S)-bicyclo[3.3.1]nonan-3-yl)-	40 \pm 21	98 \pm 5	31 \pm 11	>0.999	141 \pm 9*	0.014	20 \pm 5	0.978	187 \pm 8*	0.0001	46 \pm 12	>0.999	182 \pm 8*	0.0002
20	MRS7966	(1R,4S)-bicyclo[5.1.0]octan-4-yl	38 \pm 13	100 \pm 5	62 \pm 24	>0.999	143 \pm 14	0.110	104 \pm 50	0.523	180 \pm 14*	0.005	121 \pm 26	0.293	154 \pm 14*	0.041
21	MRS7974	2-((1R,2R,4R)- & (1S,2S,4S)-bicyclo[2.2.2]oct-5-en-2-yl)	39 \pm 13	98 \pm 5	35 \pm 0	>0.999	129 \pm 9	0.179	158 \pm 70	0.631	167 \pm 12*	0.0001	458 \pm 101*	0.004	182 \pm 13*	0.001

Table 15. Effect of PAM derivatives with hydrophilic substitutions on [³⁵S]GTP γ S binding induced by CI-IB-MECA using WT hA₃ARs. Statistical significance was determined by one-way ANOVA with Bonferroni post-hoc multiple comparisons (n=3; * denotes P < 0.05). Data are presented as mean \pm SEM.

Structural Specifications				DMSO		0.1 μ M Compound			1 μ M Compound			10 μ M Compound				
# ID	Compound ID	R ¹	EC ₅₀ (nM)	E _{max} (%)	EC ₅₀ (nM)	P-value	E _{max} (%)	P-value	EC ₅₀ (nM)	P-value	E _{max} (%)	P-value	EC ₅₀ (nM)	P-value	E _{max} (%)	P-value
22	MRS7969	(1R,4S)-8-oxabicyclo[5.1.0]octan-4-yl	55 \pm 0	99 \pm 7	118 \pm 15	0.310	131 \pm 11	0.282	63 \pm 19	>0.999	136 \pm 11	0.167	155 \pm 42	0.058	145 \pm 16	0.073
23	MRS7970	(1R,4S)-8-oxabicyclo[5.1.0]octan-4-yl	42 \pm 19	98 \pm 5	16 \pm 4	0.764	119 \pm 5	0.500	44 \pm 11	>0.999	173 \pm 14*	0.002	72 \pm 20	0.584	174 \pm 12*	0.002
24	MRS7971	cycloheptan-1-one	40 \pm 24	100 \pm 6	40 \pm 0	>0.999	108 \pm 9	>0.999	81 \pm 17	>0.999	167 \pm 24*	0.027	340 \pm 136*	0.230	166 \pm 23	0.059
25	MRS7972	(1S,4R)- & (1R,4S)-cycloheptan-1-ol	53 \pm 9	100 \pm 12	119 \pm 28	0.579	156 \pm 8*	0.168	31 \pm 9	>0.999	99 \pm 12	0.712	594 \pm 58*	<0.0001	132 \pm 16	0.434
26	MRS7973	(1R,4R)- & (1S,4S)-cycloheptan-1-ol	40 \pm 17	100 \pm 8	67 \pm 15	>0.999	160 \pm 13*	0.185	228 \pm 46	0.213	186 \pm 14*	0.022	847 \pm 117*	<0.0001	142 \pm 19	>0.999

Table 16. Effect of *para*-phenylamino substituted PAM derivatives on [³⁵S]GTPγS binding induced by CI-IB-MECA using WT hA₃ARs. Statistical significance was determined by one-way ANOVA with Bonferroni post-hoc multiple comparisons (n=3; * denotes P < 0.05). Data are presented as mean ± SEM.

# ID	Structural Specifications			DMSO		0.1 μM Compound			1 μM Compound			10 μM Compound					
	Compound ID	R ²		EC ₅₀ (nM)	E _{max} (%)	EC ₅₀ (nM)	P-value	E _{max} (%)	P-value	EC ₅₀ (nM)	P-value	E _{max} (%)	P-value	EC ₅₀ (nM)	P-value	E _{max} (%)	P-value
27	MRS7967	4-iodophenyl		34 ± 4	100 ± 6	42 ± 15	>0.999	136 ± 8	0.102	39 ± 10	>0.999	184 ± 9*	0.001	111 ± 11*	0.003	206 ± 15*	0.0002
28	MRS7978	4-bromophenyl		34 ± 22	102 ± 6	56 ± 40	>0.999	162 ± 16	0.069	117 ± 35	0.289	207 ± 17*	0.004	273 ± 24*	0.002	212 ± 19*	0.003
29	MRS7975	methyl (E)- & (Z)-3-(4-phenylacrylate)		21 ± 5	100 ± 6	48 ± 27	0.659	133 ± 6*	0.044	32 ± 8	>0.999	164 ± 10*	0.0009	25 ± 2	>0.999	193 ± 8*	<0.0001
30	MRS8055	4-((5-chlorothiophen-2-yl)ethynyl)phenyl		39 ± 5	97 ± 7	61 ± 11	>0.999	131 ± 8	0.081	108 ± 258	>0.999	170 ± 12*	0.0012	40 ± 9	>0.999	203 ± 8*	<0.0001

Table 17. Effect of compound 31 (R² = I) on [³⁵S]GTPγS binding induced by CI-IB-MECA using WT hA₃ARs. Statistical significance was determined by one-way ANOVA with Bonferroni post-hoc multiple comparisons (n=3; * denotes P < 0.05). Data are presented as mean ± SEM.

# ID	Structural Specifications				DMSO		0.1 μM Compound			1 μM Compound			10 μM Compound					
	Compound ID	R ¹	R ²		EC ₅₀ (nM)	E _{max} (%)	EC ₅₀ (nM)	P-value	E _{max} (%)	P-value	EC ₅₀ (nM)	P-value	E _{max} (%)	P-value	EC ₅₀ (nM)	P-value	E _{max} (%)	P-value
31	MRS8054	2-heptan-4-yl / 4-iodophenyl			67 ± 17	99 ± 6	45 ± 36	>0.999	158 ± 8*	0.002	45 ± 10	>0.999	223 ± 10*	<0.0001	41 ± 14	>0.999	215 ± 8*	0.0001

Table 18. Effect of compound 8 on dissociation rate of [¹²⁵I]I-AB-MECA using WT and chimeric A₃ARs (n=3)

Receptor	DMSO	10 μM Compound 8
	t _{1/2} (Min)	t _{1/2} (Min)
WT Human	39.8	97.6
WT Mouse	101	88.1
Mouse _{Out} /Human _{In}	98.6	208
Human _{Out} /Mouse _{In}	72.7	70.9

Table 19. Effect of compound 5 on [³⁵S]GTPγS binding induced by CI-IB-MECA using WT and chimeric A₃ARs. Statistical significance was determined by one-way ANOVA with Bonferroni post-hoc multiple comparisons (n=3; * denotes P < 0.05). Data are presented as mean ± SEM.

Receptor	DMSO		0.1 μM of Compound 5			1.0 μM of Compound 5			10 μM of Compound 5					
	EC ₅₀ (nM)	E _{max} (%)	EC ₅₀ (nM)	P-value	E _{max} (%)	P-value	EC ₅₀ (nM)	P-value	E _{max} (%)	P-value	EC ₅₀ (nM)	P-value	E _{max} (%)	P-value
WT Human	27.1 ± 1.6	99.8 ± 2.0	35.1 ± 8.2	>0.999	117 ± 8	>0.999	191 ± 36	>0.999	111 ± 16	>0.999	789 ± 307*	0.025	89.7 ± 20.0	>0.999
WT Mouse	2.68 ± 0.81	99.2 ± 2.6	1.73 ± 0.67	>0.999	97.9 ± 3.7	>0.999	2.78 ± 1.27	>0.999	93.9 ± 3.4	>0.999	2.17 ± 0.09	>0.999	97.9 ± 5.2	>0.999
Mouse _{Out} /Human _{In}	5.73 ± 2.78	99.9 ± 3.8	8.93 ± 5.29	>0.999	97.4 ± 5.2	>0.999	9.93 ± 4.89	>0.999	103 ± 7	>0.999	7.67 ± 2.29	>0.999	96.0 ± 4.2	>0.999
Human _{Out} /Mouse _{In}	27.6 ± 17.2	99.9 ± 7.5	77.5 ± 37.9	>0.999	115 ± 18	0.439	331 ± 175	0.970	85.9 ± 5.3	0.152	1250 ± 370*	0.009	80.9 ± 5.4	>0.999

Table 20. Effect of compound 8 on [³⁵S]GTPγS binding induced by CI-IB-MECA using WT and chimeric A₃ARs. Statistical significance was determined by one-way ANOVA with Bonferroni post-hoc multiple comparisons (n=3; * denotes P < 0.05). Data are presented as mean ± SEM.

Receptor	DMSO		0.1 μM of Compound 8				1.0 μM of Compound 8				10 μM of Compound 8			
	EC ₅₀ (nM)	E _{max} (%)	EC ₅₀ (nM)	P-value	E _{max} (%)	P-value	EC ₅₀ (nM)	P-value	E _{max} (%)	P-value	EC ₅₀ (nM)	P-value	E _{max} (%)	P-value
WT Human	26.9 ± 3.5	100 ± 5	20.1 ± 1.7	>0.999	154 ± 9*	0.030	24.4 ± 3.4	>0.999	225 ± 10*	0.0002	70.6 ± 25.4	0.132	241 ± 18*	<0.0001
WT Mouse	0.97 ± 0.23	99.7 ± 2.4	1.65 ± 0.45	>0.999	111 ± 3	>0.999	26.2 ± 14.3	0.134	123 ± 2	0.169	7.24 ± 4.55	>0.999	151 ± 4*	0.027
Mouse _{out} / Human _{in}	10.3 ± 0.7	100 ± 4	9.03 ± 2.73	>0.999	150 ± 6*	0.003	0.597 ± 0.185*	0.004	178 ± 8*	0.0002	0.723 ± 0.285*	0.004	195 ± 9*	<0.0001
Human _{out} / Mouse _{in}	13.4 ± 1.4	100 ± 4	28.6 ± 10.1	0.725	119 ± 6	0.176	32.8 ± 11.1	0.433	121 ± 6	0.118	98.5 ± 7.7*	0.0003	132 ± 8*	0.016

REFERENCES

1. Abbracchio MP, Brambilla R, Ceruti S, Kim HO, von Lubitz DK, et al. 1995. G protein-dependent activation of phospholipase C by adenosine A3 receptors in rat brain. *Mol Pharmacol* 48:1038-45
2. Aderibigbe BA, Naki T. 2018. Design and efficacy of nanogels formulations for intranasal administration. *Molecules* 23:1241
3. Appendino G, Spagliardi P, Sterner O, Milligan S. 2004. Structure–activity relationships of the estrogenic sesquiterpene ester ferutinin. Modification of the Terpenoid Core. *Journal of Natural Products* 67:1557-64
4. Atkinson MR, Townsend-Nicholson A, Nicholl JK, Sutherland GR, Schofield PR. 1997. Cloning, characterisation and chromosomal assignment of the human adenosine A3 receptor (ADORA3) gene | GenBank™ accession numbers: L77729 and L77730.1. *Neuroscience Research* 29:73-9
5. Auchampach JA, Gizewski ET, Wan TC, de Castro S, Brown GG, Jr., Jacobson KA. 2010. Synthesis and pharmacological characterization of [(125)I]MRS5127, a high affinity, selective agonist radioligand for the A3 adenosine receptor. *Biochem Pharmacol* 79:967-73
6. Auchampach JA, Jin X, Wan TC, Caughey GH, Linden J. 1997. Canine mast cell adenosine receptors: Cloning and expression of the A3 receptor and evidence that degranulation is mediated by the A2B receptor. *Molecular Pharmacology* 52:846-60
7. Bajracharya R, Song JG, Back SY, Han H-K. 2019. Recent advancements in non-invasive formulations for protein drug delivery. *Comput Struct Biotechnol J* 17:1290-308
8. Bar-Yehuda S, Stemmer SM, Madi L, Castel D, Ochaion A, et al. 2008. The A3 adenosine receptor agonist CF102 induces apoptosis of hepatocellular carcinoma via de-regulation of the Wnt and NF-kappaB signal transduction pathways. *Int J Oncol* 33:287-95
9. Beghetto V, Scrivanti A, Bertoldini M, Aversa M, Zancanaro A, Matteoli U. 2015. A Practical, enantioselective synthesis of the fragrances canthoxal and silvial®, and evaluation of their olfactory activity. *Synthesis* 47:272-88
10. Bennett GJ, Xie YK. 1988. A peripheral mononeuropathy in rat that produces disorders of pain sensation like those seen in man. *Pain* 33:87-107
11. Besnard J, Ruda GF, Setola V, Abecassis K, Rodriguiz RM, et al. 2012. Automated design of ligands to polypharmacological profiles. *Nature* 492:215-20
12. Beutner GL, Young IS, Davies ML, Hickey MR, Park H, et al. 2018. TCFH–NMI: Direct access to N-acyl imidazoliums for challenging amide bond formations. *Organic Letters* 20:4218-22
13. Bhattacharjee AK, Lang L, Jacobson O, Shinkre B, Ma Y, et al. 2011. Striatal adenosine A(2A) receptor-mediated positron emission tomographic imaging in 6-hydroxydopamine-lesioned rats using [(18)F]-MRS5425. *Nucl Med Biol* 38:897-906
14. Borea PA, Gessi S, Merighi S, Vincenzi F, Varani K. 2018. Pharmacology of adenosine receptors: The state of the art. *Physiological Reviews* 98:1591-625

15. Borea PA, Varani K, Vincenzi F, Baraldi PG, Tabrizi MA, et al. 2015. The A₃ adenosine receptor: History and perspectives. *Pharmacological Reviews* 67:74
16. Changeux J-P, Edelstein SJ. 2005. Allosteric mechanisms of signal transduction. *Science* 308:1424-8
17. Christopoulos A. 2002. Allosteric binding sites on cell-surface receptors: novel targets for drug discovery. *Nature Reviews Drug Discovery* 1:198-210
18. Christopoulos A. 2014. Advances in G protein-coupled receptor allostery: from function to structure. *Mol Pharmacol* 86:463-78
19. Christopoulos A, Changeux JP, Catterall WA, Fabbro D, Burris TP, et al. 2014. International Union of Basic and Clinical Pharmacology. XC. multisite pharmacology: recommendations for the nomenclature of receptor allostery and allosteric ligands. *Pharmacol Rev* 66:918-47
20. Ciancetta A, Jacobson KA. 2017. Structural probing and molecular modeling of the A₃ adenosine receptor: A Focus on Agonist Binding. *Molecules* 22
21. Cohen S, Barer F, Bar-Yehuda S, AP IJ, Jacobson KA, Fishman P. 2014. A₃ adenosine receptor allosteric modulator induces an anti-inflammatory effect: in vivo studies and molecular mechanism of action. *Mediators Inflamm*:708746
22. Cohen S, Fishman P. 2019. Targeting the A(3) adenosine receptor to treat cytokine release syndrome in cancer immunotherapy. *Drug Des Devel Ther* 13:491-7
23. Conn PJ, Christopoulos A, Lindsley CW. 2009. Allosteric modulators of GPCRs: a novel approach for the treatment of CNS disorders. *Nat Rev Drug Discov* 8:41-54
24. Dengale SJ, Grohgan H, Rades T, Löbmann K. 2016. Recent advances in co-amorphous drug formulations. *Advanced Drug Delivery Reviews* 100:116-25
25. Denmark SE, Edwards JP. 1991. A comparison of (chloromethyl)- and (iodomethyl)zinc cyclopropanation reagents. *The Journal of Organic Chemistry* 56:6974-81
26. DeWire SM, Ahn S, Lefkowitz RJ, Shenoy SK. 2007. Beta-arrestins and cell signaling. *Annu Rev Physiol* 69:483-510
27. Dikošová L, Laceková J, Záborský O, Fischer R. 2020. Synthesis of 3-substituted isoxazolidin-4-ols using hydroboration–oxidation reactions of 4,5-unsubstituted 2,3-dihydroisoxazoles. *Beilstein Journal of Organic Chemistry* 16:1313-9
28. Draper-Joyce CJ, Bhola R, Wang J, Bhattarai A, Nguyen ATN, et al. 2021. Positive allosteric mechanisms of adenosine A₁ receptor-mediated analgesia. *Nature* 597:571-6
29. Du L, Gao Z-G, Nithipatikom K, Ijzerman AP, van Veldhoven JPD, et al. 2012. Protection from myocardial ischemia/reperfusion injury by a positive allosteric modulator of the A₃ adenosine receptor. *Journal of Pharmacology and Experimental Therapeutics* 340:210
30. Du L, Gao Z-G, Paoletta S, Wan TC, Gizewski ET, et al. 2018. Species differences and mechanism of action of A₃ adenosine receptor allosteric modulators. *Purinergic Signalling* 14:59-71
31. Duan X, Mao S. 2010. New strategies to improve the intranasal absorption of insulin. *Drug Discov Today* 15:416-27

32. Effendi WI, Nagano T, Kobayashi K, Nishimura Y. 2020. Focusing on adenosine receptors as a potential targeted therapy in human diseases. *Cells* 9:785
33. Englert M, Quitterer U, Klotz KN. 2002. Effector coupling of stably transfected human A3 adenosine receptors in CHO cells. *Biochem Pharmacol* 64:61-5
34. Fishman P, Bar-Yehuda S, Barer F, Madi L, Multani AS, Pathak S. 2001. The A3 adenosine receptor as a new target for cancer therapy and chemoprotection. *Experimental Cell Research* 269:230-6
35. Fishman P, Bar-Yehuda S, Ohana G, Barer F, Ochaion A, et al. 2004. An agonist to the A3 adenosine receptor inhibits colon carcinoma growth in mice via modulation of GSK-3 beta and NF-kappa B. *Oncogene* 23:2465-71
36. Fishman P, Cohen S. 2016. The A3 adenosine receptor (A3AR): therapeutic target and predictive biological marker in rheumatoid arthritis. *Clin Rheumatol* 35:2359-62
37. Fishman P, Salhab A, Cohen S, Amer J, Itzhak I, et al. 2018. THU-487 - The anti-inflammatory and anto-fibrogenic effects of namodenoson in NAFLD/NASH animal models. *Journal of Hepatology* 68:S349-S50
38. Fors BP, Krattiger P, Strieter E, Buchwald SL. 2008. Water-mediated catalyst preactivation: An efficient protocol for C–N cross-coupling reactions. *Organic Letters* 10:3505-8
39. Foster DJ, Conn PJ. 2017. Allosteric modulation of GPCRs: New insights and potential utility for treatment of schizophrenia and other CNS disorders. *Neuron* 94:431-46
40. Fredholm BB, Ijzerman AP, Jacobson KA, Klotz K-N, Linden J. 2001. International union of pharmacology. XXV. Nomenclature and classification of adenosine receptors. *Pharmacological Reviews* 53:527
41. Fredholm BB, Ijzerman AP, Jacobson KA, Linden J, Müller CE. 2011. International union of basic and clinical pharmacology. LXXXI. Nomenclature and classification of adenosine receptors--an update. *Pharmacological reviews* 63:1-34
42. Gao D, Xiao Q, Zhang M, Li Y. 2016. Design, synthesis and biological evaluation of benzyloxyphenyl-methylaminophenol derivatives as STAT3 signaling pathway inhibitors. *Bioorganic & Medicinal Chemistry* 24:2549-58
43. Gao Z-G, Chen A, Barak D, Kim S-K, Müller CE, Jacobson KA. 2002. Identification by site-directed mutagenesis of residues involved in ligand recognition and activation of the human A3 adenosine receptor. *J Biol Chem* 277:19056-63
44. Gao Z-G, Ijzerman AP. 2000. Allosteric modulation of A2A adenosine receptors by amiloride analogues and sodium ions. *Biochem Pharmacol* 60:669-76
45. Gao Z-G, Kim S-K, Gross AS, Chen A, Blaustein JB, Jacobson KA. 2003. Identification of essential residues involved in the allosteric modulation of the human A(3) adenosine receptor. *Molecular pharmacology* 63:1021-31
46. Gao Z-G, Kim S-K, Ijzerman AP, Jacobson KA. 2005. Allosteric modulation of the adenosine family of receptors. *Mini Rev Med Chem* 5:545-53
47. Gao Z-G, Kim SG, Soltysiak KA, Melman N, Ijzerman AP, Jacobson KA. 2002. Selective allosteric enhancement of agonist binding and function at human A3

- adenosine receptors by a series of imidazoquinoline derivatives. *Molecular pharmacology* 62:81-9
48. Gao Z-G, Melman N, Erdmann A, Kim SG, Müller CE, et al. 2003. Differential allosteric modulation by amiloride analogues of agonist and antagonist binding at A1 and A3 adenosine receptors. *Biochem Pharmacol* 65:525-34
 49. Gao Z-G, Van Muijlwijk-Koezen JE, Chen A, Müller CE, Ijzerman AP, Jacobson KA. 2001. Allosteric modulation of A3 adenosine receptors by a series of 3-(2-pyridinyl)isoquinoline derivatives. *Molecular Pharmacology* 60:1057
 50. Gao Z-G, Verzijl D, Zweemer A, Ye K, Göblyös A, et al. 2011. Functionally biased modulation of A(3) adenosine receptor agonist efficacy and potency by imidazoquinolinamine allosteric enhancers. *Biochem Pharmacol* 82:658-68
 51. Gao Z, Li B-S, Day Y-J, Linden J. 2001. Adenosine receptor activation triggers phosphorylation of protein kinase B and protects rat basophilic leukemia 2H3 mast cells from apoptosis. *Molecular Pharmacology* 59:76
 52. Gao ZG, Van Muijlwijk-Koezen JE, Chen A, Müller CE, Ijzerman AP, Jacobson KA. 2001. Allosteric modulation of A(3) adenosine receptors by a series of 3-(2-pyridinyl)isoquinoline derivatives. *Molecular pharmacology* 60:1057-63
 53. Gessi S, Merighi S, Varani K, Leung E, Mac Lennan S, Borea PA. 2008. The A3 adenosine receptor: An enigmatic player in cell biology. *Pharmacology & Therapeutics* 117:123-40
 54. Gessi S, Sacchetto V, Fogli E, Merighi S, Varani K, et al. 2010. Modulation of metalloproteinase-9 in U87MG glioblastoma cells by A3 adenosine receptors. *Biochem Pharmacol* 79:1483-95
 55. Ghodke PP, Pradeepkumar PI. 2018. Chapter 10 - Nucleoside Modification Using Buchwald-Hartwig Amination Reactions. In *Palladium-Catalyzed Modification of Nucleosides, Nucleotides and Oligonucleotides*, ed. AR Kapdi, D Maiti, YS Sanghvi, pp. 295-333. Elsevier.
 56. Göblyös A, Gao Z-G, Brussee J, Connestari R, Santiago SN, et al. 2006. Structure–activity relationships of new 1H-imidazo[4,5-c]quinolin-4-amine derivatives as allosteric enhancers of the A3 adenosine receptor. *J Med Chem* 49:3354-61
 57. Hammarberg C, Fredholm BB, Schulte G. 2004. Adenosine A3 receptor-mediated regulation of p38 and extracellular-regulated kinase ERK1/2 via phosphatidylinositol-3'-kinase. *Biochem Pharmacol* 67:129-34
 58. Harpaz Z. 2021. *Piclidenoson for Treatment of COVID-19*. <https://www.clinicaltrials.gov/ct2/show/NCT04333472>
 59. Hauser AS, Attwood MM, Rask-Andersen M, Schiöth HB, Gloriam DE. 2017. Trends in GPCR drug discovery: new agents, targets and indications. *Nature Reviews Drug Discovery* 16:829-42
 60. Heitman LH, Göblyös A, Zweemer AM, Bakker R, Mulder-Krieger T, et al. 2009. A series of 2,4-disubstituted quinolines as a new class of allosteric enhancers of the adenosine A3 receptor. *J Med Chem* 52:926-31
 61. Ingoglia BT, Wagen CC, Buchwald SL. 2019. Biaryl monophosphine ligands in palladium-catalyzed C–N coupling: An updated User's guide. *Tetrahedron* 75:4199-211

62. Jacobson K, Gao Z-G. 2006. Jacobson KA, Gao ZG.. Adenosine receptors as therapeutic targets. *Nat Rev Drug Discov* 5: 247-264. *Nat Rev Drug Discov* 5:247-64
63. Jacobson KA, Gao Z-G. 2017. Chapter 11 Allosteric Modulators of Adenosine, P2Y and P2X Receptors. In *Allosterism in Drug Discovery*. pp. 247-70. Washington D.C.: The Royal Society of Chemistry
64. Jacobson KA, Giancotti LA, Lauro F, Mufti F, Salvemini D. 2020. Treatment of chronic neuropathic pain: purine receptor modulation. *Pain* 161:1425-41
65. Jin X, Shepherd RK, Duling BR, Linden J. 1997. Inosine binds to A3 adenosine receptors and stimulates mast cell degranulation. *J Clin Invest* 100:2849-57
66. Kamal M, Jockers R. 2009. Bitopic ligands: all-in-one orthosteric and allosteric. *F1000 biology reports* 1:77-
67. Kende AS. 2011. The Favorskiï rearrangement of haloketones. *Organic Reactions*:261-316
68. Kim Y, de Castro S, Gao Z-G, Ijzerman AP, Jacobson KA. 2009. Novel 2- and 4-substituted 1H-imidazo[4,5-c]quinolin-4-amine derivatives as allosteric modulators of the A3 adenosine receptor. *J Med Chem* 52:2098-108
69. Klotz K-N. 2010. Pharmacology and Molecular Biology of A3 Adenosine Receptors. In *A3 Adenosine Receptors from Cell Biology to Pharmacology and Therapeutics*, ed. PA Borea, pp. 49-58. Dordrecht, Netherlands: Springer
70. Kumar S, Gupta S. 2013. Pharmaceutical solid dispersion technology: A strategy to improve dissolution of poorly water-soluble drugs. *Recent patents on drug delivery & formulation* 7
71. Linden J. 2005. Adenosine in tissue protection and tissue regeneration. *Molecular Pharmacology* 67:1385
72. Liston TE, Hinz S, Müller CE, Holstein DM, Wendling J, et al. 2020. Nucleotide P2Y(1) receptor agonists are in vitro and in vivo prodrugs of A(1)/A(3) adenosine receptor agonists: implications for roles of P2Y(1) and A(1)/A(3) receptors in physiology and pathology. *Purinergic Signal* 16:543-59
73. Madi L, Bar-Yehuda S, Barer F, Ardon E, Ochaion A, Fishman P. 2003. A3 adenosine receptor activation in melanoma cells: association between receptor fate and tumor growth inhibition. *J Biol Chem* 278:42121-30
74. Martins S, Sarmiento B, Ferreira DC, Souto EB. 2007. Lipid-based colloidal carriers for peptide and protein delivery--liposomes versus lipid nanoparticles. *Int J Nanomedicine* 2:595-607
75. May LT, Leach K, Sexton PM, Christopoulos A. 2007. Allosteric modulation of G protein-coupled receptors. *Annual Review of Pharmacology and Toxicology* 47:1-51
76. Meanwell NA. 2018. Fluorine and fluorinated motifs in the design and application of bioisosteres for drug design. *J Med Chem* 61:5822-80
77. Merighi S, Benini A, Mirandola P, Gessi S, Varani K, et al. 2006. Adenosine modulates vascular endothelial growth factor expression via hypoxia-inducible factor-1 in human glioblastoma cells. *Biochem Pharmacol* 72:19-31
78. Merighi S, Simioni C, Lane R, Ijzerman AP. 2010. Regulation of Second Messenger Systems and Intracellular Pathways. In *A3 Adenosine Receptors from*

- Cell Biology to Pharmacology and Therapeutics*, ed. PA Borea, pp. 61-73. Dordrecht, Netherlands: Springer
79. Miller MA, Sletten EM. 2018. A general approach to biocompatible branched fluorinated tags for increased solubility in perfluorocarbon solvents. *Organic Letters* 20:6850-4
 80. Mozzicato S, Joshi BV, Jacobson KA, Liang BT. 2004. Role of direct RhoA-phospholipase D1 interaction in mediating adenosine-induced protection from cardiac ischemia. *FASEB J* 18:406-8
 81. Munk C, Mutt E, Isberg V, Nikolajsen LF, Bibbe JM, et al. 2019. An online resource for GPCR structure determination and analysis. *Nature Methods* 16:151-62
 82. Murrison EM, Goodson SJ, Edbrooke MR, Harris CA. 1996. Cloning and characterisation of the human adenosine A3 receptor gene. *FEBS Letters* 384:243-6
 83. Muse D. 2017. *A Dental Pain Study to Test the Effectiveness of a New Pain Reliever Medicine*. www.clinicaltrials.gov/ct2/show/NCT02209181
 84. Neary JT, McCarthy M, Kang Y, Zuniga S. 1998. Mitogenic signaling from P1 and P2 purinergic receptors to mitogen-activated protein kinase in human fetal astrocyte cultures. *Neuroscience Letters* 242:159-62
 85. Ouvry G. 2022. Recent applications of seven-membered rings in drug design. *Bioorganic & Medicinal Chemistry* 57:116650
 86. Palmer TM, Stiles GL. 2000. Identification of threonine residues controlling the agonist-dependent phosphorylation and desensitization of the rat A3 adenosine receptor. *Molecular Pharmacology* 57:539
 87. Pándy-Szekeres G, Esguerra M, Hauser AS, Caroli J, Munk C, et al. 2021. The G protein database, GproteinDb. *Nucleic Acids Research* 50:D518-D25
 88. Park C-W, Han C-T, Sakaguchi Y, Youn H-Y. 2020. Safety evaluation of FM101, an A3 adenosine receptor modulator, in rat, for developing as therapeutics of glaucoma and hepatitis. *EXCLI journal* 19:187-200
 89. Puri A, Loomis K, Smith B, Lee JH, Yavlovich A, et al. 2009. Lipid-based nanoparticles as pharmaceutical drug carriers: from concepts to clinic. *Crit Rev Ther Drug Carrier Syst* 26:523-80
 90. Qadir M, Möchel T, Hii KK. 2000. Examination of ligand effects in the Heck arylation reaction. *Tetrahedron* 56:7975-9
 91. Ramkumar V, Stiles GL, Beaven MA, Ali H. 1993. The A3 adenosine receptor is the unique adenosine receptor which facilitates release of allergic mediators in mast cells. *Journal of Biological Chemistry* 268:16887-90
 92. Rautio J, Meanwell NA, Di L, Hageman MJ. 2018. The expanding role of prodrugs in contemporary drug design and development. *Nat Rev Drug Discov* 17:559-87
 93. Ruiz-Castillo P, Buchwald SL. 2016. Applications of palladium-catalyzed C–N cross-coupling reactions. *Chemical Reviews* 116:12564-649
 94. Sandri G, Bonferoni MC, Rossi S, Ferrari F, Boselli C, Caramella C. 2010. Insulin-loaded nanoparticles based on N-trimethyl chitosan: In vitro (caco-2 model) and ex vivo (excised rat jejunum, duodenum, and ileum) evaluation of penetration enhancement properties. *AAPS PharmSciTech* 11:362-71

95. Sato J, Makita N, Iiri T. 2016. Inverse agonism: the classic concept of GPCRs revisited [Review]. *Endocr J* 63:507-14
96. Schaddelee MP, Read KD, Cleypool CG, Ijzerman AP, Danhof M, de Boer AG. 2005. Brain penetration of synthetic adenosine A1 receptor agonists in situ: role of the rENT1 nucleoside transporter and binding to blood constituents. *Eur J Pharm Sci* 24:59-66
97. Schulte G, Fredholm BB. 2002. Signaling pathway from the human adenosine A(3) receptor expressed in Chinese hamster ovary cells to the extracellular signal-regulated kinase 1/2. *Mol Pharmacol* 62:1137-46
98. Sekhar T, Thriveni P, Venkateswarlu A, Daveedu T, Peddanna K, Sainath SB. 2020. One-pot synthesis of thiazolo[3,2-a]pyrimidine derivatives, their cytotoxic evaluation and molecular docking studies. *Spectrochimica Acta Part A: Molecular and Biomolecular Spectroscopy* 231:118056
99. Singh A, Van den Mooter G. 2016. Spray drying formulation of amorphous solid dispersions. *Advanced Drug Delivery Reviews* 100:27-50
100. Singh V, Pal S, Tosh DK, Mobin SM. 2007. Molecular complexity from aromatics. Cycloaddition of cyclohexa-2,4-dienones, sigmatropic 1,2-acyl shift and ring-closing metathesis: a new, efficient, and stereoselective synthesis of (±)-hirsutic acid C and medium ring carbocycles. *Tetrahedron* 63:2446-54
101. Singh V, Tosh DK, Mobin SM. 2004. Synthesis of embellished bicyclo[2.2.2]octenones and a sigmatropic 1,2-acyl shift in an excited state: a novel and stereoselective route to (±)-hirsutic acid C and complicatic acid. *Tetrahedron Letters* 45:1729-32
102. SL P. 2020. *Study to Assess the Safety and Tolerability of PBF-1650 in Healthy Volunteers. (ADENOIMMUNE)*.
103. SL P. 2022. *Safety and Efficacy of PBF-677 in Ulcerative Colitis Patients (ADENOIBD)*. www.clinicaltrials.gov/ct2/show/NCT03773952
104. Sloan NL, Luthra SK, McRobbie G, Pimlott SL, Sutherland A. 2017. A one-pot radioiodination of aryl amines via stable diazonium salts: preparation of 125I-imaging agents. *Chemical Communications* 53:11008-11
105. Soni KS, Desale SS, Bronich TK. 2016. Nanogels: An overview of properties, biomedical applications and obstacles to clinical translation. *Journal of Controlled Release* 240:109-26
106. Sonogashira K. 2002. Development of Pd–Cu catalyzed cross-coupling of terminal acetylenes with sp²-carbon halides. *Journal of Organometallic Chemistry* 653:46-9
107. Stemmer SM, Benjaminov O, Medalia G, Ciuraru NB, Silverman MH, et al. 2013. CF102 for the treatment of hepatocellular carcinoma: a phase I/II, open-label, dose-escalation study. *Oncologist* 18:25-6
108. Suresh RR, Jain S, Chen Z, Tosh DK, Ma Y, et al. 2020. Design and in vivo activity of A(3) adenosine receptor agonist prodrugs. *Purinergic Signal* 16:367-77
109. Surry DS, Buchwald SL. 2008. Biaryl phosphane ligands in palladium-catalyzed amination. *Angew Chem Int Ed Engl* 47:6338-61
110. Talele TT. 2016. The “cyclopropyl fragment” is a versatile player that frequently appears in preclinical/clinical drug molecules. *J Med Chem* 59:8712-56

111. Thal DM, Glukhova A, Sexton PM, Christopoulos A. 2018. Structural insights into G-protein-coupled receptor allostery. *Nature* 559:45-53
112. Thorand S, Krause N. 1998. Improved procedures for the palladium-catalyzed coupling of terminal alkynes with aryl bromides (Sonogashira Coupling). *The Journal of Organic Chemistry* 63:8551-3
113. Tiessen R. 2020. *A SAD, MAD, and FE Study to Evaluate the Safety, Tolerability, and Pharmacokinetic Profile of FM101 in Healthy Volunteers.*
114. Tosh DK, Salmaso V, Campbell RG, Rao H, Bitant A, et al. 2022. A(3) adenosine receptor agonists containing dopamine moieties for enhanced interspecies affinity. *Eur J Med Chem* 228:113983
115. Tränkle C, Weyand O, Voigtländer U, Mynett A, Lazareno S, et al. 2003. Interactions of orthosteric and allosteric ligands with [3H]dimethyl-W84 at the common allosteric site of muscarinic M2 receptors. *Mol Pharmacol* 64:180-90
116. Tsuchida N, Yamazaki S, Yamabe S. 2008. A new mechanism for the Favorskii rearrangement. *Organic & Biomolecular Chemistry* 6:3109-17
117. Valant C, May LT, Aurelio L, Chuo CH, White PJ, et al. 2014. Separation of on-target efficacy from adverse effects through rational design of a bitopic adenosine receptor agonist. *Proceedings of the National Academy of Sciences* 111:4614-9
118. Van Galen PJM, Nissen P, Van Wijngaarden I, Ijzerman AP, Soudijn W. 1991. 1H-Imidazo[4,5-c]quinolin-4-amines: novel non-xanthine adenosine antagonists. *J Med Chem* 34:1202-6
119. Wold EA, Chen J, Cunningham KA, Zhou J. 2019. Allosteric modulation of class A GPCRs: Targets, agents, and emerging concepts. *J Med Chem* 62:88-127
120. Xiang SY, Vanhoutte D, Del Re DP, Purcell NH, Ling H, et al. 2011. RhoA protects the mouse heart against ischemia/reperfusion injury. *J Clin Invest* 121:3269-76
121. Xiao P, Yan W, Gou L, Zhong Y-N, Kong L, et al. 2021. Ligand recognition and allosteric regulation of DRD1-Gs signaling complexes. *Cell* 184:943-56.e18
122. Yamano K, Inoue M, Masaki S, Saki M, Ichimura M, Satoh M. 2005. Human adenosine A(3) receptor leads to intracellular Ca(2+) mobilization but is insufficient to activate the signaling pathway via phosphoinositide 3-kinase gamma in mice. *Biochem Pharmacol* 70:1487-96
123. Yamano K, Inoue M, Masaki S, Saki M, Ichimura M, Satoh M. 2006. Generation of adenosine A3 receptor functionally humanized mice for the evaluation of the human antagonists. *Biochem Pharmacol* 71:294-306
124. Zhong H, Shlykov SG, Molina JG, Sanborn BM, Jacobson MA, et al. 2003. Activation of murine lung mast cells by the adenosine A3 receptor. *J Immunol* 171:338-45
125. Zhou QY, Li C, Olah ME, Johnson RA, Stiles GL, Civelli O. 1992. Molecular cloning and characterization of an adenosine receptor: the A3 adenosine receptor. *Proc Natl Acad Sci U S A* 89:7432-6